THE UNIVERSITY
of EDINBURGH

This thesis has been submitted in fulfilment of the requirements for a postgraduate degree (e.g. PhD, MPhil, DClinPsychol) at the University of Edinburgh. Please note the following terms and conditions of use:

Synchrophasor-based Predictive Control considering Optimal Phasor Measurement Unit Placements Methods

Dahunsi John OKEKUNLE

A thesis submitted in fulfilment of the requirements for the degree of
Doctor of Philosophy

May 6, 2020

Declaration of Authorship

I declare that this thesis has been composed solely by myself and that it has not been submitted, either in whole, or in part, in any previous application for a degree. Except where otherwise acknowledged, the work presented is entirely my own.

Dahunsi John Okekunle

"A little learning is a dangerous thing. Drink deep, or taste not the Pierian Spring; Their shallow draughts intoxicate the brain, and drinking largely sobers us again."

Alexander Pope

Abstract

A blackout is the total collapse of an electric power grid, due to the inability to balance load demand and power generation. Blackouts generally develop from a series of unattended voltage stability problems, stemming from a combination of human and operational errors, and may have fatal consequences. The report on the blackout incident of August 14 2003, which affected parts of the United States and Canada, particularly emphasised the need for improved wide area monitoring of the grid. In the United Kingdom, the recent blackout of August 9 2019 has reinforced the need for increased grid visibility and data recording. These have led to an ever-increasing interest in a family of measurement devices known as Wide Area Monitoring Systems (WAMS). The most popular device in this family is the Phasor Measurement Unit (PMU), which report voltage and current phasors at rates up to 60 samples/second. PMUs may be used to monitor all or part of the grid to prevent future blackouts with timely control actions. The goal is to *'See it fast: Keep it calm'*.

Wide-area monitoring enhances the possibility of visualising the electric grid as a single system. This has led to the extension of the application of WAMS from mainly monitoring to wide-area control in relatively recent research efforts. This work explores how predictive control technique may be used to automate the control of power systems voltages at secondary level using an array of synchrophasors. The intuition is to develop a model-free (or synchrophasor-based) control algorithm, which reduces, as much as possible, the need for human interventions in the mitigation of voltage problems, and is fast enough to be applied online in real-time. Although model-based techniques can be applied online, they may not be fast enough for real-time applications. In addition, this method may depend on components' parameters, which may not be available in practice.

The work is split into two parts. First, novel WAMS deployment algorithms —using multivariable, multi-objective optimisation set-ups, which return optimal placement solutions —are presented. Formulations are described for multi-stage deployments given a limited budget and for application-focused cases. Practical issues which may develop are anticipated and addressed. The formulations were shown to return optimal solutions with qualitative placement specifications. In the second part, methods of realising models from input-output relationships are developed and described. The first involved a method numerical derivatives based on data that are sampled at PMU rate. This may be seen as a viable alternative to the use of trajectory sensitivity, especially for real-time control design. In the second, subspace algorithm are used to realise models. The process is comprehensively described for secondary voltage regulation in normal and emergency situations. The approach is demonstrated on a number of IEEE test cases and the controller's performance were found to be satisfactory for non-viable voltage regulations.

This research work is particularly relevant in a number of ways. Chief among these is that voltage control problems may be handled in real-time without a knowledge of the model parameters. The model-free approach particularly desired since increasing integration of renewable energy sources means that the electric grid is becoming increasingly complex. Another is that the placement algorithms describe all various practical issues around the measurement-based design, which utilities may found useful, especially when they wish to address budget limitation and device compatibility issues.

Acknowledgements

My very special gratitude goes to my parents, Mr and Mrs. Okekunle, who started all and gave all, at great cost to themselves.

I am grateful to the Federal Government of Nigeria and all members of staff of the National Universities Commission (NUC) and of the Petroleum Technology Development Fund (PTDF) for the opportunity to study at this great citadel.

My sincere gratitude goes to Dr. Aristides Kiprakis, my supervisor, for his advice, support and encouragement, and for reading through drafts upon drafts of this thesis.

I thank all recipients of the 'Peffermill Wednesday Football' emails, past and present, for the chance to give the body a break, every now and then, from the rigours and pressures of work.

Many thanks to all members of Room A.110, past and present, and to Kaswar, my faithful gym companion, in the times before this time.

I am grateful to Mr. Douglas Carmichal and Mr. Jamie Graham for their support in the laboratory.

A very special mention to Dr. Jagadeesh Gunda, for many occasions of stimulating discussions. And to Obinna, good fellow.

I would like to thank my external examiner, Dr. David Laverty, and internals, Dr. Micheal Merlin and Dr. Harry van der Weijde for taking the time to read this thesis and for their very helpful feedbacks.

To the members of the North Edinburgh Small Group, for making Edinburgh feel like a home away from home. And especially to Mr and Mrs Pembroke, for their prayers and pastoral care.

I should not forget to mention Emmanuel Oni, Gani and Temi Otunbade, Bukola Adeola, and Helen Omotowa, who made me forget how to cook, in the times before this time.

And finally to my wife, Oluwadolapo, without whom the final months would have been nigh impossible. And to Rerelolu, whose smile made it all worth it.

Contents

List of Figures

List of Tables

List of Abbreviations

AVR	**Automatic Voltage Regulator**
CI	**Communication Infrastructure**
CVA	**Canonical Variate Analysis**
DAQ	**Data Acquisition**
DULR	**Dual Use Line Relay**
DULR	**Electricity System Operator**
ILP	**Integer Linear Programming**
EMS	**Energy Management Systems**
FE	**Frequency Error**
ERA	**Eigensystem Realization Algorithm**
GPS	**Global Positioning System**
FDR	**Frequency Disturbance Recorder**
LMPC	**Linear Model Predictive Control**
LTI	**Linear Time-Invariant**
LTI	**Low Frequency Demand Disconnection**
MPC	**Model Predictive Control**
MOESP	**Multivariable Output-Error State SPace**
N4SID	**Numerical Algoirthm for Subspace State Space IDentification**
PDC	**Phasor Data Concentrator**
PMU	**Phasor Measurement Unit**
PPP	**PMU Placement Problem**
PSS	**Power Systems Stabiliser**
PVR	**Primary Voltage Regulation**
RC	**Reliability Coordinator**
RFE	**Rate of change of Frequency Error**
RES	**Renewable Energy Sources**
RTU	**Remote Terminal Unit**
ROCOF	**Rate Of Change Of Frequency**
ROCOA	**Rate Of Change Of Angle**
RT-HIL	**Real Time Hardware In (the) Loop.**
SVR	**Secondary Voltage Regulation**
SSARX	**State-Space Auto-regressive with eXogenous inputs**
SCADA	**Supervisory Control And Data Acquisition**
SBPVC	**Subspace Based Predictive Voltage Control**
STATCOM	**STATic (synchronous) COMpensator**
SIL	**Software In (the) Loop**
SVC	**STATic (VAR) COMpensator**

TVR	**Tertiary Voltage Regulation**
TCR	**Thyristor Controlled Reactor**
TSC	**Thyristor Switched Capacitor**
TSO	**Transmission System Operator**
V-WAR	**Voltage- Wide Area Regulation**
VSI	**Voltage Stability Indicator**
WMU	**Waveform Measurement Unit**
WAMPAC	**Wide Area Monitoring, Protection, And Control**
WAMS	**Wide Area Monitoring Systems**

—

List of Symbols

Chapter 3

i, j	Bus indices
I	Set of buses
$\boldsymbol{L}_i$	Aggregated Loads
$\bar{r}_{ij}, \bar{x}_{ij}$	Resistance and reactance of line i, j
$\bar{V}_{ij} \angle \theta_{ij}$	voltage phasor across line ij
$\bar{I}_{ij} \angle \delta_{ij}$	current phasor across line ij
$\Delta(e), \delta(e)$	maximum, minimum number of branches in a network
e_j	Number of branches connected to a bus j
l, L	Current channel capacity, Maximum current channel capacity (of a PMU)
r	Branch subset index
S_{jl}	Sets of similar current channel capacities
r_{jl}	Number of subsets in S_{jl}
r^T	Total number of subsets of all r_j
r^s	Maximum number of Subsets in S_{jl}.
S_{jlr}	Subsets of the subset S_{jl}.
C_{jlr}^{IT}	Cost of installing Instrument transformers on a bus j
	for the purpose of installing a PMU of channel l on the r-th subset of S_{jlr}.
d, v	indices of buses, PDCs, and vendors respectively.
n, D, V	Total number of buses, PDCs, and vendors respectively.
a_{ij}	Connectivity matrix.
$b, \boldsymbol{B}$	Containment parameter, matrix.
$R_i, \mathbf{R}_b$	element, array specifying bus redundancy level(s)
$\bar{R}$	PMU reliability.
$x, \boldsymbol{X}$	decision variable, vector of variables.
$R_{\min}$	Minimum system reliability.
$\mathbf{E}$	Bus maximum placement selection matrix.
$\mathbf{E}_{\max}$	Vector of maximum allowable placement.
$\mathbf{F}$	Pre-existing measurements selection matrix.
$\mathbf{M}^F$	$n \times 1$ vector specifying the locations of pre-existing measurements.
$\mathbf{G}$	Prohibited buses 6-D selection matrix.
$\mathbf{M}^G$	$n \times 1$ vector specifying the locations of prohibited buses.

Chapter 4

k	Stage index
$\boldsymbol{x}^*, \boldsymbol{x}_{\mathrm{sol}}^*$	general optimal solution, optimal solution(only 1 at candidate buses).

$N_{\text{pmu}}^{\text{fo}}$	Number of PMUs required for full observability.
$C_{\text{pmu}}^{\text{fo}}$	Costs of PMUs required for full observability (monetary units).
$C_{\text{pmu}}^{\text{STG},k}$	Costs of PMUs required at Stage k (monetary units).
u_i	binary observability variable of Bus i.
$M_{ijlr}^{dv,k,\text{full}}$	The full candidate solution selection parameter.
$\tilde{M}_{ijlr}^{dv,k}$	Already-deployed candidate buses selection parameter
$.\,\hat{M}_{ijlr}^{dv,k}$	Undeployed candidate buses selection parameter.
$M_{ijlr}^{dv,k}$	Prohibited from deployment selection parameter.
B_{phase}^{k}	Budget assigned for placements at Stage k.
$\bar{R}_{\text{min}}^{k}$	Stage k reliability threshold.
$N_{\text{pmu}}^{\text{STG},k}$	Number of PMUs deployed at Stage k
$S^{\text{STG},1}$	Set of PMUs at Stage k.
S^{fo}	Superset of PMUs required for full observability over all stages
$\bar{W}_i$	Priority of a Bus i.
$B_{\text{phase}}^{k,\text{carry}}$	Unspent budget from Stage k.
MC^k	Maintenance cost of already-installed devices at Stage k.
RC^k	Repair costs of already-installed devices at Stage k.
RMC^k	Total costs of maintenance and repair of already-installed devices at Stage k
h	the inflation rate at the stage $k+1$.
Chapter 5	(excluding those already defined for Chapter 4
κ	Selective placements redundancy.
B	Budget
ϱ	Add-on application capability.
$\bar{B}_\varrho$	Benefit of application ϱ.
$\bar{B}$	Total benefit of all applications.
$\mu_{\varrho,v}^{l}$	binary parameter indicating whether or not a particular application is offered as an add-on.
n_{app}	Total number of applications ϱ under consideration.
Chapter 6	
$\Delta P, \Delta Q$	Change in real, reactive power [at a bus].
$\Delta P_{ik}, \Delta Q_{ik}$	Change in real, reactive power along a line ik.
$S_{\Delta v}$	Sensitivity of machine angle to a small change in bus voltage.
$V_i(\Delta V_i)$	Voltage magnitude (change in voltage magnitude) at a bus i.
$\theta_i(\Delta\theta_i)$	Voltage angle (change in voltage angle) at a bus i.
V_g^{ref}	Voltage references of generators.
$V_{\text{svc}}^{\text{ref}}$	Voltage references of SVCs
λ	Load shedding.
S_{vg}^{ir}	Sensitivity of the i-th bus voltage magnitude to a small change in the r-th generator voltage reference.
S_{vs}^{c}	Sensitivity of the i-th bus voltage magnitude to a small change in the c-th SVC voltage reference.

S_{vu}	Sensitivity (of bus voltages to a set of inputs) block matrix.
$S_{\mathrm{v}\lambda}^{il}$	Sensitivity of the i-th bus voltage magnitude to a small change in the l-th load magnitude.
$\Delta Q_{\mathrm{g}}^i, \Delta Q_{\mathrm{s}}^i, \Delta Q_{\lambda}^i$	Change in reactive power at generator, SVC, and load respectively.
S_{Qg}^{ir}	Sensitivity of the r-th generator reactive power output to a small change in the r-th generator voltage reference at the i-th generator bus.
S_{Qs}^{ic}	Sensitivity of the c-th SVC reactive power output to a small change in the c-th SVC voltage reference at the i-th SVC bus.
S_{Qs}^{ic}	Sensitivity of the l-th load reactive power to a small change in the l-th load at the i-th load bus.
ΔV_p	Change in the p-th pilot bus voltage.
$S_{\mathrm{vu}}^{\mathrm{t}}, S_{\mathrm{vu}}^{\mathrm{s}}$	The matrix and vector bus voltage sensitivities of all buses respectively.
S_{vQu}	Combined matrix of voltage and Q sensitivities.
$\Delta \boldsymbol{X}$	Stacked vector of bus voltage and generator bus reactive power.
$\Delta \boldsymbol{U}$	Stacked vector of inputs.
f_R	Reporting rate.
t_R	Time interval between reports.
G_y	Output on Gain.
$k, \Delta k_a$	Present time instant, change in time instant.
$\Delta V_i(f)$	Change in bus i voltage at instant f of time interval Δk_a.
$S_{\mathrm{vu}}^{\mathrm{new}}, S_{\mathrm{vu}}^{\mathrm{old}}$	New, old values of the sensitivities measured at current and previous time instants.
N_p, N_c	Prediction, control horizon.
$\boldsymbol{V}^{\mathrm{ref}}, \boldsymbol{V}$	Vectors of bus voltage reference and bus voltage respectively.
$\underline{\boldsymbol{X}}, \overline{\boldsymbol{X}}$	Vectors of lower, upper limits of stacked vector of $\Delta \boldsymbol{X}$.
$\underline{\Delta \boldsymbol{U}}, \overline{\Delta \boldsymbol{U}}$	Vectors of lower, upper limits on $\Delta \boldsymbol{U}$.
$\boldsymbol{Y_1}, \boldsymbol{Y_2}$	Vectors of slack variables on [pilot] bus voltage, generator buses reactive power (as outputs).
$\boldsymbol{Y}$	Stacked vector of slack variables.
$\underline{\boldsymbol{Y}}, \overline{\boldsymbol{Y}}$	Vectors of lower, upper limits on $\boldsymbol{Y}$.
$\underline{\boldsymbol{Q_G}}, \overline{\boldsymbol{Q_G}}$	Vectors of lower, upper limits on vector of generator reactive power, $\boldsymbol{Q_G}$.

————————————————— —————————————————

$\boldsymbol{x}, \boldsymbol{y}$	Vectors of states, outputs
$\boldsymbol{A}, \boldsymbol{B}, \boldsymbol{C}, \boldsymbol{D}$	State, input, output, and transition matrices respectively.
n, m, p	Numbers of states, inputs, and outputs respectively
$\boldsymbol{w}, \boldsymbol{v}$	[usually unmeasurable] disturbance, noise quantities
$\boldsymbol{Y}_p, \boldsymbol{U}_p$	Matrices of past outputs and inputs respectively.
$\boldsymbol{Y}_f, \boldsymbol{U}_f$	Matrices of future outputs and inputs respectively.
$\bar{V}^{\mathrm{p,pmu}},$	PMU-measured voltage magnitude.
$\bar{V}^{\mathrm{p,mod}}$	Synthesised model output response.
N	Length of measured data.
y_i^{nom}	Nominal output value determined by a power-flow steady-state solution
T_s	[Fixed] sampling time.
F_s	[Fixed] sampling frequency.

$\lvert \rho(A) \rvert$	Magnitudes of the eigenvalues of a state matrix, A
Θ, Π	Observability, controllability matrices
$f[k], f[k-1]$	Frequencies at step $k, k-1$
$\boldsymbol{R}, \boldsymbol{R}_\Delta, \boldsymbol{Q}$	positive semi-definite diagonal penalty matrices on control variables, rates of change of control variables, and outputs respectively.

Dedicated to Moses and Modupeola, dearest parents, to Oluwadolapo, beloved wife, and to Rerelolu, beautiful daughter.

Chapter 1

Introduction

1.1 The need for voltage control in power systems

The electric power grid is a complex interconnected network of static and dynamic components. Traditionally, the power system is composed consists of generation, transmission, sub-transmission, and distribution subsystems at various voltage levels. The output voltage at generation substations, where electric power is generated is usually between 11kV-35kV. The function of the transmission system is to *wheel* electric power from the generation stations to the load centres at sub-transmission and distribution systems. In order to minimise power losses along the transmission lines linking the generation substations to distribution subsystems, electric power is transmitted at stepped-up voltages of 230 kV or greater. Electric power may also be transmitted to neighbouring power systems The sub-transmission voltage levels are usually between 69kV-138kV [1]. Industrial loads may be supplied at sub-transmission levels or at the primary side of the distribution substation. However, commercial and residential loads are supplied at the secondary sides of the distribution transformers and are usually between 120 V (e.g United States) and 230-240 V(e.g United Kingdom).

In the past, all of the generation, transmission, sub-transmission, and distribution subsystems were managed and operated by a single entity, which are able to make investments, sometimes unsound, whose costs are borne by the consumers of electric energy. Nowadays, the operation and management of the electric power systems has been decentralised and re-organised into a more competitive market structure. The operations of power systems are now directed towards the objectives of maximising net economic benefits and minimising the risks of disruption to its services and infrastructures. Consequently, the power system operation is now dictated by market economics under the deregulated structure and the grid is increasingly operated closer to its limits. This is exemplified by the increasing amounts of power being pushed across transmission corridors. Heavily-loaded lines lead to monotonically-decreasing voltages, and with the decreasing voltages, the proximity to voltage collapse or instability (known as the *voltage stability margin*) decreases. The amount of load which may be added to the system to cause voltage collapse is referred to as *loading margin*. Under such circumstance, the failure of protection devices could lead to instability and eventual collapse of the electric power grid, resulting in blackouts.

In the early days of electric power systems operations, generation stations and points of demand were in close proximity. As a result, events could be easily monitored through visual inspection and control decisions passed from one person to another through verbal communications.

---

[1] In the United Kingdom, the transmission voltages are 275kV and 400kV, and subtransmission is 132kV.

As the system became more complex and the distance between generation, demand and control stations increased, the need for a faster and more efficient monitoring and control process was created. The Supervisory Control and Data Acquisition (SCADA) system was introduced to realise the monitoring and control functions. Communications of events and decisions in the early days of the SCADA were achieved over telephone lines.

Further increases in geographical distances between power generation and load points, and the resulting increase in the complexity of the system motivated a drive towards a faster communication and a more efficient monitoring of power system conditions. Next came the minicomputers and microprocessors for events detection and control, and the powerline communication (PLC) for data transmission, which reported information on system components every few seconds. Nonetheless, the increase in power system complexity persists as regional power networks are synchronised and subsequently interconnected to form a national grid. In modern times, the increasing grid complexity is a result of the increase in the integration of renewable energy sources (RES) to the grid, as driven by the quests towards environmental sustainability and cleaner power generation.

1.1.1   Traditional Energy Management Systems

The traditional Energy Management Systems (EMS) are used to manage energy resources for the purpose of ensuring stable power systems operations. They do this by obtaining field data from predetermined monitoring points in the power system, by processing the data, and then by analysing the result for visualisation and control. These functions are usually carried out in the EMS by the SCADA systems, with a typical architecture as shown in Figure 1.1. As can be seen from the figure, SCADA systems rely on monitoring devices, such as Intelligent Electronic Devices (IEDs) and Remote Terminal Units (RTUs) located at substations, for data acquisition. Data is transmitted via an established communication medium to different operator work stations at the control centre for processing, storage, analysis, visualisation, and control. A local work station may be used at the substation to coordinate substation-based processes and to communicate with control centres.

The data from the monitoring devices are usually static measurements of the currents, voltage, energy demand, along with active and reactive power consumptions, and others. These data, obtained in the raw form, are transmitted via a communication medium to the control centre for processing and analyses. At this stage, a computational tool, known as *state estimation* is applied to remove bad data, outliers, and errors, and to estimate the actual states of the measured data. The estimated states may then be stored in a database and/or analysed to gain insights into the power system operation. The analysis carried out by SCADA systems would usually include, but are not limited to, fault checking, topology rearrangement, and consumer load analysis. The SCADA system is also used to estimate the appropriate amount of control to regulate the system. Results of the analysis and state estimation may be displayed for visualisation at the control centre or stored.

SCADA systems are very popular with power systems utilities all over the world. Power system events are monitored at control stations using SCADA systems. The objectives of the monitoring efforts would be to detect events which might lead to undesirable system conditions in the system as well as those of neighbouring systems. However, the static nature of its measurements
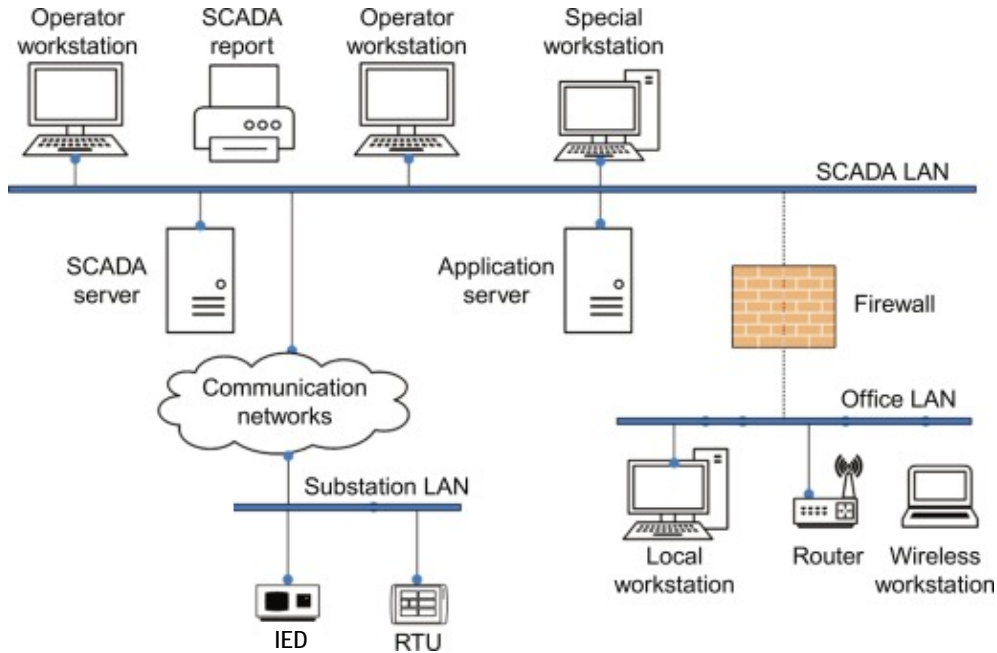
FIGURE 1.1: A typical SCADA architecture (adapted from [1])

of a dynamic power system, its slow reporting rate (once every 2-5 seconds), and the lack of measurement synchronisation [2] are some its limitations. The slow reporting rate of the SCADA system is a limitation of major concern especially with the increasingly complex nature of power systems. In the following section, attempts are made to establish the need for a faster and more efficient measurement and control process than can be obtained from the traditional SCADA.

1.1.2 Motivation for Improved Monitoring and Control

Given the complex nature of the wide area electric power grid, constantly changing demand, and the need to match the demand with generation, it would be unsurprising if undesirable system conditions, such as outages, do not occur more often. The simple explanation is that many steps have been and are taken to maintain stable system operating conditions. These include rigorous planning, long-term assessments, evaluation of what the demand would be minutes, hours, days, months, seasons, or a year into the future, preparing for contingencies and possessing the capability to respond quickly to these contingencies, ensuring that a reserve for generation and transmission is maintained, and having backup capabilities for all critical functions. In the United Kingdom for instance, the Electricity System Operator (ESO) is required, by the Security and Quality of Supply Standards (SQSS) [2], to keep at least 1000MW of generation for emergencies.

However, occurrences of blackouts in major electric grids are often inevitable in spite of all the efforts and preparations that have been put in place to prevent them. In the following section, events leading to two major blackouts are described.

---

[2]Some modern forms of RTUs may possess synchronisation capabilities.

The August 14 2003 United States and Canada blackout

An overgrown tree brushed against a high-voltage line in the northern part of Ohio in the United States one afternoon, causing a fault and the subsequent loss of that line. The end results were the August 14 2003 blackout, service disruption to around 50 million customers for about two days, 11 deaths, and about US$6 billion of economic losses in parts of the United States and Canada. The report, [3] released three months after the incident, identified that the blackout followed from the failure of the alarm system to trip, as expected, upon the loss of line. This was exacerbated by the failure, of the personnel manning the warning systems, to detect that the alarm had failed. Consequently, the neighbouring circuits became overloaded, sagged and brushed into the surrounding trees under the heat of the current. They, too, were eventually lost about 2 hours later. The successive loss of lines triggered a cascading failure that caused a total grid outage in 8 northeastern states of the US and the southeastern parts of Canada.

In summary, it was adjudged that the blackout was caused by a combination of human and operational failure [3], arising from:

1. Inadequate system understanding, in that the personnels at the utility failed to identify a failed component on time and reconcile the events immediately leading to the outage to past events which had reduced the reactive power capabilities in the grid.

2. Inadequate situational awareness, for which it was categorically stated that the utility,

   *"did not have additional or back-up **monitoring tools to understand or visualize the status** of their transmission system to facilitate its operators' understanding of transmission system conditions after the failure of their primary monitoring/alarming systems"* [3]

3. Inadequate tree trimming, leading to overgrown branches brushing against transmission lines.

4. Inadequate diagnostic support from other reliability coordinators (RC), stemming from the utility's failure to alert neighbouring reliability coordinators as the situation degenerated.

The August 9 2019 UK blackout

The much more recent UK blackout of 9 August 2019 [4], [5] was preceded by the loss of a 150 MW embedded generator due to an expected vector shift operation, following a lightning strike on the Eaton Socon–Wymondley Main transmission circuit. This was succeeded by an extremely rare and unexpected event; a loss of 737MW generation at the Hornsea offshore wind farm. This was succeeded by the tripping of steam turbine at the 244MW Little Barford Power Station, leading to the loss of generation at that station. At this point, about 1131MW generation had been lost from the grid. The result was a generation-demand imbalance, a rapid fall in frequency and the triggering of the Rate of Change of Frequency (ROCOF) protection. The activation of the protection device led to a further loss of 350MW embedded generation capacity, making the total loss of 1451MW generation higher than the backup power the Electricity System Operator (ESO) was statutorily obliged to keep under the Security and Quality of Supply Standards (SQSS). Consequently, the frequency deteriorated until it fell to 49.1Hz, outside the allowed ±0.5Hz deviations from the nominal frequency value.

The ESO then deployed all the remaining backup power — a 472MW of battery storage — at its disposal to restore the frequency. This would have served the purpose, but for another tripping of a 210MW gas turbine at Little Barford Power Station, increasing the cumulative generation loss, limiting the frequency restoration to only 48.8Hz and causing 5% of customers to be automatically cut off from the grid following the action of the Low Frequency Demand Disconnection (LFDD) scheme. However, further generation loss of 187MW occurred after the 5% of customers were disconnected. Consequently, an additional number of customers had to be cut off. The final frequency restorative action was to disconnect around 1.1m customers (constituting approximately 1GW of demand) for around 15-45 minutes.

The disconnection of demand took place at the closing hours of a weekend and had disruptive effects on the customer connection in the critical healthcare, aviation and rail transport sectors.

A case for improved monitoring

On account of the interconnected nature of the power system, failure in one part of the grid cascaded into other parts, lending credence to the notion of the power system as one giant machine. The scale of the US blackout and the general consensus —proceeding from the identified sequence of events in [3]—that the outage could have been prevented had the line loss been detected on time motivated the need to view the power grid as one system, rather than a series of independently operating but connected systems. Critical events leading to collapse may happen slowly over a long period of time (minutes or hours), or escalate quickly from a fault of very small durations (in micro-seconds or a few seconds). On account, the potential for these events to go undetected with SCADA system monitoring is high. This led to the adoption and eventual proliferation of a family of devices known as Wide Area Monitoring Systems (WAMS). These devices include Phasor Measurement Units(PMUs), Frequency Disturbance Recorders (FDRs), Waveform Measurement Units (WMU).

The slow speed of the traditional SCADA is mainly a reflection of the rate of data acquisition by its monitoring devices, (i.e.the RTUs and IED)s. In contrast, the PMU, by far the most popular of the WAMS devices, is capable of reporting voltage and current phasors at up to 200-240 samples/s. This enhances the higher-resolution visualisation of events than could have been offered by the slower traditional SCADA systems which report events only once evert 2-5 seconds. To illustrate, consider the Figure 1.2, which shows the traditional SCADA and PMU plots of the Oklahoma Gas & Electric voltage disturbance data at a particular period of the day.

It is easy to see that the nature of system disturbance was captured better with the PMU than was with the SCADA. In general, this improved visualisation is complemented by the fact that PMU phasor data from different parts of the grid are precisely time-stamped to a common clock reference frame provided by a Global Positioning System (GPS) [3]. This is particularly important when measured power system quantities are to be compared across a network.

However, in spite of their many advantages, WAMS have not enjoyed higher proliferation because of the relative high costs of procurement and installation of the measurement devices and their associated communication infrastructure (CI). Utilities may leverage on existing and available CIs, such as power line communication or public cellular network infrastructures, to achieve some cost savings in associated PMU installation costs. If these are not available or sufficient for the particular mission, the focus should be on minimising the costs of laying a CI, with sufficient

---

[3]PMU data are often referred to as *synchrophasors* or *synchronised phasors* for this reason.
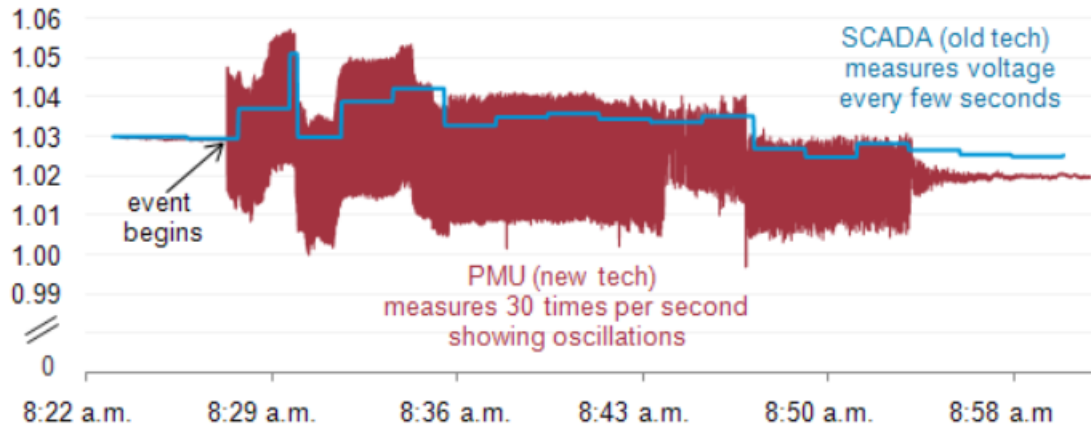
FIGURE 1.2: Traditional SCADA vs PMU plots from a utility's voltage disturbance
data [6]. Note that the *y*-axis is the bus voltage(per unit)

capabilities for a given system operation, along with those of procuring and installing PMUs. For
instance, although power systems utilities have been known to collaborate with cellular network
service providers for smart meter data communication from household to the utility to reduce the
utility's communication overhead [7], [4] there is no evidence that the readily-available public cel-
lular networks have enough capacities to cope with the sheer volume of data that will come from
PMUs with such high reporting rates. Noting that utilities using PMUs often do so to carry out
critical system monitoring and control functions which require very fast response, critical system
operations may be compromised by using a shared cellular network. In this instance, a private cel-
lular with sufficient spectrum or in fibre optic communications will be a viable alternative, albeit at
a much higher cost. In some cases, a hybrid of different communication technologies may be used
to reduce costs. Alternatively, utilities may resort to bespoke solutions, such as a reinforcement of
existing SCADA with monitoring devices of higher reporting rates and synchronisation capabili-
ties or extend synchrophasor functions on dual-use line relays (DULR). It is important to note that
PMUs are meant to complement, rather than replace, SCADA systems. As shown in a simplified
representation of an Energy Management System of Figure 1.3, PMUs may be used together with
traditional monitoring devices in a more modern SCADA arrangement.

A case for a self monitoring and self-healing system

For the UK power outage, control actions to mitigate the effects of undesirable system conditions
were based on established procedures. As can be surmised from the description of the black-
out, rule-based controls and planned procedures may not be adequate for the control of rare and
unexpected events, such as the loss of the Hornsea offshore wind farm generation. In addition,
like the US blackout, events leading to the 9 August 2019 UK blackout had to be identified, by
gathering data and other information, piecemeal, from different sources, in the absence of WAMS-
enabled visualisation and data at a central location. These sources include the Office of the Gas

---

[4]An example [7] is Echelon's Networked Energy Services has been deployed on T-Mobile's Global System for Mobile
Communication (GSM) to enhance smart meter communication with the back-up utility. All communication requirements
are handled by T-Mobile.
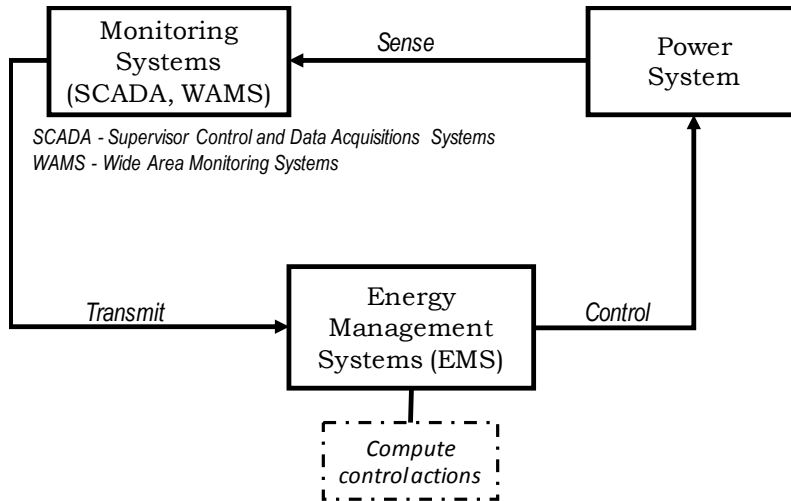
FIGURE 1.3: Traditional SCADA vs PMU plots from a utility's voltage disturbance data [6]. Note that the *y*-axis is the bus voltage(per unit)

and Electricity Market (OfGEM), the Electricity System Operator (ESO), Orsted Power UK Ltd, MeteoGroup, National Grid Electricity Transmission (NGET), Distribution Network Operator (DNO), Govia Thameslink Railway and others.

The *holy grail* for all power systems is a grid which is capable of self-monitoring and self-healing. The PMU is a promising tool to achieve this. Analyses of PMU data can reveal important power system characteristics and a quick inspection of some PMU measurements, such as voltage angles, can help identify an increasing stress in the system as a sign of an impending blackout. In order to find the grail, more and more PMUs need to be deployed in various parts of the grid. Increased PMU deployments will help improve situational awareness and enable the triggering of timely, appropriate, and sufficient control actions to forestall undesirable system operations.

On the back of improved situational awareness comes the need to reduce human interventions in controls to as little as possible, based on the experience from one of the causes of the 14 August 2003 US blackout. With the proliferation of WAMS, the challenge of how to maximise the benefits led to the extension of its application from mainly monitoring to wide area control. This has increased the interest in automated control, where advanced control algorithms [8]–[11] are designed to compute real-time control actions based on the improved visualisations offered by these monitoring systems.

From the foregoing and in the context of this project, it is possible to surmise that the holy grail may be found through the following steps:

1. Establish data sources (place monitoring devices).

2. Obtain and process data from the sources (Data gathering and processing)

3. Design an advanced control algorithm, based on the processed data (Measurement-based control design).

1.1.3   Placement of measurement devices

WAMS are becoming increasing ubiquitous on account of the many benefits they offer. These benefits include, amongst others, increased awareness of real-time events in the grid, fault detection and classification, model validation, and better accuracy of state estimation. On the distribution network, micro-Phasor Measurements Units (μPMUs) [5], a form of WAMS may be used in this regard with the benefit at this voltage discussed in [12]. In general, all forms of PMUs measure time-synchronised and high-resolution voltage and current phasors which are fundamental practical quantities for general grid health monitoring and control. For monitoring purposes, WAMS are placed on specific buses in the grid, for full or partial observability depending on the objective and structure of the electricity market. The concept of full and partial observability in this sense being to be able to obtain a voltage and current phasor measurement of all or selected network buses and branches respectively. In many developed countries, WAMS are majorly installed on the transmission networks, and to a lesser extent, on the distribution networks. This is because distribution network operators (DNOs) are highly reluctant to install expensive WAMS on their networks and would often require a good justification of the benefits they offer to justify the costs of investments. In addition, grid visibility are often enhanced with an observability of the wide area at higher voltage levels. There is little or no investment in WAMS in many with attendant consequences of the loss of the higher measurement resolution and visibility they offer. Many failures in the upstream transmission systems have led to high unreliability in bulk power supply to the distribution grid. In consequence, the distribution companies (DISCOs) have either had to fail to supply power to residential and industrial customers, or resorted to load scheduling among different distribution areas. Furthermore, electricity theft caused by low penetration of metering or monitoring devices, as well as frequent electrical component and line failures are rampant in the lower distribution grid. It then follows from this reasoning that all grid operators would benefit from higher grid visibility in order to improve the reliability of their services. The main goal of the liberated and not-so-liberated market is to make profit. Therefore, any intended investments in any infrastructure must indeed justify its benefits in that market, regardless of its sophistication. The costs associated with PMU placements include the hardware unit purchase price, communication costs, design and engineering costs, costs of labour and materials, costs of ancillary devices such as global positioning systems (GPS) and networking devices, costs of disrupting a substation, associated costs of installing phasor data concentrators (PDCs) [13]. The PDCs serve as data storage and archiving functions for offline analysis and backup in the event of PMU failure. On account of the high costs involved in WAMS installations, the number of monitoring devices installed in a network is upper-bounded by the benefits associated with these installations, such that at a certain number of PMUs, any further installations offers no additional benefits [14].

1.1.4   Model predictive control: An advanced algorithm for voltage control

In order to mitigate the effects of voltage instability and its consequences, three levels of control are generally used; the primary control, which is usually fast, and applied at the generator buses for transient events lasting microseconds to a few seconds. At a higher level, the secondary control handles slower mid- and long-term dynamics, especially those due to slowly-decaying voltage

---

[5]μPMUs are so-called because they are used on the distribution systems which require higher accuracy for its relatively lower voltage level. For instance, where a phase error of $\pm 1^0$ is acceptable for transmission-level phasor measurement, μPMUs can measure a phase at $\pm 0.05^0$

conditions of timescales in the order of several minutes to several hours. The highest level is the tertiary control, where system targets are calculated for updates at the secondary over several hours or days. When designing a secondary voltage controller for practical wide-area power networks, the timeliness of the application of control and the identification of stability limits are critical.

The traditional approach to control is to model the network using linear or non-linear dynamic equations. However, model-based control methods result in time-consuming computations since the representations of the grid under study involves many components. As a result, online and real-time controls may be difficult to achieve, especially for power system that are becoming increasingly complex on account of increasing integration of renewable energy sources. If controls are not applied in time and in the right manner, more frequent blackout may be inevitable in the near future.

Many references and proofs to the online capability of model-based predictive control (MPC) can be found in the literature (see e.g [15], [16]) and therefore its suitability for online modulations of control inputs is well noted. However, its computationally-intensive approach means that control signals may not be computed fast enough to be applied online in a *real*-timely manner. MPC has been applied across many areas of power systems for around two decades. It has been used for emergency voltage control [17], [18], system protection and dynamic security enhancement schemes, [19], [20], voltage control [21]–[28], in the prevention of cascading failures [29]–[31], in frequency and automatic generation control [32], [33] and in the frequency and coordinated supervisory control of multi-terminal HVDC grid [34], [35]. Primary voltage regulations, which require very fast response to controls, are usually handled at the generator terminals by control devices such as automatic voltage regulators(AVRs) and power systems stabilisers (PSSs). The speed of response required for primary voltage regulation, usually in the order of microseconds to a few seconds, may be faster than can be handled by the traditional MPC. Consequently, the popularity of MPC for voltage control in power systems has been mainly focused on mid and long-term instability, where control updates may be required, at the most, seconds, tens of seconds or minutes apart.

1.2 Research Motivation and Objective

For many utilities, the benefits offered by the measurement devices should exceed the costs of investment in the short or long term [36]. As had been mentioned earlier, the cost-effectiveness of device installations has been a major hindrance to a more rapid adoption of the devices in many parts of the world, leading to a high number of publications on the minimisation of placement costs[37]–[53]. However, the costs of deploying WAMS are enormous and often overlooked. The literature on WAMS placement and control is rife with inherent assumptions about the practicalities of the costs of deploying the monitoring devices. A wider evaluation of the number of variables, and their associated costs, involved in the placements, as obtained from reports from utilities in [13] has been largely missing in a majority of the literature.

This project focuses on the cost-effective and optimal placement of WAMS devices as well as on how data from these devices may be used to design model-free controllers for secondary voltage control. This is particularly relevant in many regards. First, it uses a bottom-up approach to a model-free control development to determine the most effective method of deploying the source of data (i.e. the measurement devices) that will be used for the control design. The high-speed

electrical measurements provided by WAMS are a pragmatic but often expensive alternatives for achieving reliable, real-time, on-line indicators for voltage stability [54]–[58]. Currently, WAMS-based control algorithms [9], [11], [59]–[62] are becoming increasing popular. Second, the project explored the utilisation of data from deployed measurement devices for model-free control design using MPC. Model-free control designs will enhance the increased awareness offered by WAMS, and enable networks to respond quicker to events that have been detected. This will enhance the design of more formal and advanced control algorithm in automatic control, signalling a departure from rule-based control which may fail to identify unanticipated but critical events in the grid.

A bottom-up approach to the design of measurement-based controllers should therefore include a comprehensive modelling of the costs of deployments, the process of deployment and then the process of using the data obtained from the deployed devices. It is possible to capture power system dynamics with PMUs and to design computationally-feasible secondary voltage controllers which can be applied online and in real time. To this end, this work is driven by the following motivation:

1. Most methods using predictive voltage control do not provide a clear distinction between primary and secondary levels of controls. Moreover, they rely on exhaustive models of the power system and are not used in conjunction with any stability indicator. This makes them unsuitable for automated real-time applications. To address this, this thesis focuses on the design of a model-free predictive secondary voltage controller in order to control the voltage in the system for small and large disturbances in the short or long term. It also explores how the performance of the controller may be improved through improved situational awareness.

2. In order to use phasor measurements for control, the monitoring devices have to be properly deployed to provide maximum observability for a range of budget and application needs. This part of the work focuses on developing novel practical solutions following concerns raised by industry [13], [49] on the cost factors involved in WAMS deployment. Considerations are made for the presence of multiple PDCs, vendors, and non-homogeneous channel capacities.

In practice, the limitations of using PMU data in control systems are mainly due to measurement noise, challenges in the measurement of reactive power, and signal distortion due to transient and harmonics. Some IEEE standards on WAMS data have been developed to address some of these problems. These standards will be described in Chapter 2.

1.3   Thesis Statement

The research work presented in this thesis seeks to answer the following general question:

Given the increasingly complex nature of electric power systems, with thousands of components spread out over a wide area, it is possible to design an affordable and automated controller which is capable of voltage regulation and stabilisation at secondary level using a model-free predictive control technique

The question is answered by implementing the setup of Figure 1.4. In this respect, the following contributions are made.
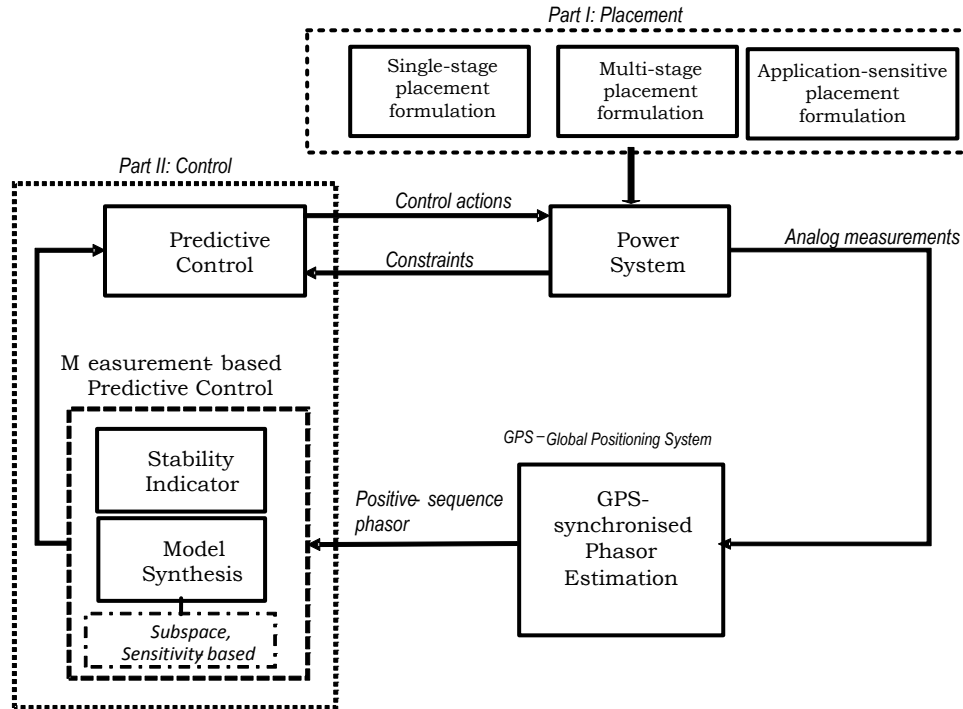
FIGURE 1.4: The measurement-based predictive control set-up

1. **Phasor Measurement Units and Communication Infrastructure co-placement with non-homogeneous channel capacity and multiple vendors:** In order to develop a viable measurement-based control, measurement devices have to be appropriately sited at least cost to suit particular application needs. To this end, novel placement strategies were developed. First, a topology defragmentation method was formulated to provide an alternative and superior solution to the simultaneous placement of PMUs and their communication links. The *channel* capacity of a PMU may be defined as the total number of simultaneous phasor measurements which the device is capable of taking at a single time. The current channel capacity of a PMU is the number of simultaneous current phasor measurement which the device is capable of measuring when placed at a bus. The formulation considered different channel capacities and multiple vendors. In addition to the optimality guarantee without the need for algorithmic parameter tuning, the proposed method provided more detailed than existing meta-heuristic and formal algorithm which had been used to solve the co-placement problem.

2. **Budget-constrained multi-stage placement considering non-homogeneous channel capacities and multiple vendors;** The topology defragmentation method was extended to multi-stage placements and the practical issues around spreading WAMS installation costs over a number of periods. Novel multi-stage placements are developed, discussed, and implemented.

3. **Application-sensitive placements considering non-homogeneous channel capacities and multiple vendors;** Placement formulations for specific application purposes are described. Novel methods of maximising the benefits and minimising the placement costs of measurement devices are introduced, implemented, and discussed.

4. **Numerical sensitivity-based predictive secondary voltage control:** The thesis presents a methodology for the model-free design of a predictive controller using numerical-derivative based sensitivity approach to predict the changes in voltage.

5. **Subspace-based predictive secondary voltage control:** The thesis presents a methodology for the model-free design of a predictive controller, and demonstrated the viability of the method in emergency and normal situations.

1.4   List of Publications

1. D. Okekunle, O. Unigwe, and A. Kiprakis, "On the Cost-Effectiveness of Multistage Deployment of Wide Area Monitoring Systems in Weak Networks under Limited Channel Availability," in 25th International Conference on Electricity Distribution, 2019, no.2122, June, pp. 1–5.

2. D. J. Okekunle, O. Unigwe, and A. E. Kiprakis, "An Optimal Co-placement Method Considering Non-homogeneous PMU Channel Capacities," IET Smart Grids, pp. 1–12, *accepted for publication*

1.5   Thesis Structure

The thesis is organised as follows:

- Chapter 2: Uncontrolled events in the grid may lead to undesirable consequences such as cascading failures, resulting in total blackouts. A proper representation of the power network is necessary for accurate analyses. WAMS data may provide much improved visibility, along with much needed alternatives to rigorous mathematical modelling and control. In this chapter, the causes and types of voltage instability in the system are presented, a background is given into the modelling and control of power systems, introducing the traditional mathematical modelling methods and then the measurement-based alternatives. These give insights into the need for the various methods provided in the later chapters of this work.

- Chapter 3: For deploying Phasor Measurement Units (PMUs) to improve observability of the electric power grid, the focus of recent works on PMU placement have shifted to minimizing more associated practical costs, as opposed to traditional methods that only minimize the unit costs of monitoring devices. These associated costs include those of communication infrastructure (CI) and ancillary equipment whose availability are often critical in practical placement decisions. However, existing methods considering co-placements of CIs with PMUs are often heuristic, optimal only with carefully selected parameters, and often have non-standard co-placement architecture.

  In addition, for many works considering realistic associated costs, the presence of limitations in channel capacity, rather than the more likely availability of non-homogeneous channel capacities, are considered. Here, an ancillary equipment availability and comprehensive associated placement costs models are developed and a multichannel, multi-vendor, PMU-PDC co-placement problem is posed as a NP-hard multi-objective Set Cover Problem (SCP) using an Integer Linear Programming (ILP) method. The proposed approach is illustrated

using multiple IEEE test systems of diverse sizes across different scenarios. Results, among others, show that the feasible placement solution using this approach is optimal and multi-dimensional, but placement decisions depend on the availability of ancillary equipment, as obtainable in practice.

- Chapter 4: Utilities can benefit from Wide Area Monitoring Systems (WAMS) installations to improve grid voltage reliability through increased network observability. Multi-stage placements with long-term full observability seem like a fiscally viable alternative, but are likely to cost more in the end. Here, the focus is on a more viable method of deploying WAMS, especially in terms of fiscal capability, by spreading placement costs over a period of time. Some limited-budget, multichannel, PMU-PDC co-placement problems are introduced, and then the factors affecting continued installations are discussed. In the end, it can be safely concluded that all network utility operators may enjoy the benefits of WAMS installations but must be aware of certain practical factors in multi-stage deployment when budget is of concern.

- Chapter 5: So far we have considered placement from an idealistic full-observability perspective and from a more realistic multi-stage placement. However, in addition to budget limitations, utilities may also wish to install only a number of PMUs as to address a particular application concern. In this chapter, we consider PMU placement with the end goal of using the data for applications like secondary voltage regulation. First, existing literature in this regard is reviewed. Subsequently, an algorithm on PMU placement with specific application intents is proposed. Notable among the novel formulations in this chapter is an adjusted cost function which minimises the costs of placements but maximises the benefits obtained from the measurement devices. Solutions are optimal for all factors considered.

- Chapter 6: For a large and complex electric power system with thousands of buses and components, synthesising a complete state-space model that lends well to traditional predictive control theories is a daunting task. The process becomes even more complicated if the parameters of the components are outdated or unknown. For real-time applications and with intent to take advantage of predictive control algorithm, models must be appropriately sized to enhance computational feasibility. Fortunately, the increasing proliferation of WAMS technology has opened up the possibility of analysing the power system as a grey box with known inputs and measurable outputs. On account, the problem of ageing component parametrisation, model size, and real-time control may be addressed by taking advantage of subspace algorithms which been applied in process engineering using predictive control. This chapter focuses on and describes two model realisations and goes on to implement and describe the performance of one of these methods in the enhancement of an autonomous feedback predictive voltage control system.

- Appendix A: Here, the 6-D matrices used in Chapter 3 are clearly defined in 2-d D space, along with a table for assumptions made on placement costs.

- Appendix B: Additional results from Chapter 5 are included in this appendix.

Chapter 2

Background and Review

Uncontrolled events in the grid may lead to undesirable consequences such as cascading failures, resulting in total blackouts. A proper representation of the power network is necessary for accurate analyses. WAMS data may provide much improved visibility, along with much needed alternatives to rigorous mathematical modelling and control. In this chapter, the causes and types of voltage instability in the system are presented, a background is given into the modelling and control of power systems, introducing the traditional mathematical modelling methods and then the measurement-based alternatives. These give insights into the need for the various methods provided in the later chapters of this work.

2.1 Introduction: voltage instability and the meed for control

The concept of voltage stability follows closely from the ability of electric generation and transmission systems to supply load demand. Changes in system topology due to line faults or loss of critical generator may induce some form of disruption to system operation and limit the amount of deliverable power necessary for continued grid stability. If the undesirable changes to system conditions are not quickly corrected or cleared, this may lead to sustained instability and eventually to voltage values rising above or falling below the desired bands, abnormal system operations, and possible blackouts or voltage collapse, as witnessed in parts of North American system in 2003 [3], [63] and in the Southern Hellenic grid [64] in 2004. This process may take place quickly over a few seconds or slowly over a relatively longer period of time. Nonetheless, given the extent of various dependencies of various sectors of a nation's economy on proper and reliable grid operations, these events often cause huge economic losses. The extent of modelling efforts required to study and control them increase with the increasing proliferation of renewable energy integration. Fortunately, the use of WAMS data presents viable alternatives to rigorous mathematical modelling.

In the following sections, various backgrounds to the thesis' goal of extending the frontiers of WAMS application from mainly to Wide Area Monitoring, Protection and Control (WAMPAC) especially for secondary voltage regulation (SVR) are presented.

2.2 Power System Voltage Stability

An electric power system is voltage-stable if voltage levels are regulated within acceptable levels under normal operating conditions or after a disturbance [65]. The United Kingdom Grid Code [66] defines the acceptable voltage bands as $\pm6\%$ of the nominal for distribution systems above 6.6kV, and ±10 for transmission systems at and above 275kV. The disturbances may be in the form of load

changes or more significantly, loss of a generator. A major cause of instability are the voltage drops, due to inductive reactance, as power flows along transmission lines. It is well known that system voltages are primarily influenced by changes in reactive power, Q. For this reason, the instability of a system may be improved by the injection of Q. Ideally, it is expected that positive changes in Q would be translated to positive changes in the voltage, V. However, in practice, it may happen that V may decrease when $Q-$injection is increased. If this happens for at least one bus, the system would be unstable. This phenomenon is created with an increase in inductive Q, disproportionate to the active power, demand in the grid. With this Q increase, the voltages at the points of demand decrease. If local Q sources like capacitors cannot meet the increased inductive Q demand, the reactive power have to be imported from more distant parts of the grid over transmission lines. This increases the loading on the lines and leads to a further voltage drops on the demand side. The process of increased Q-injection causing voltage decrease may proceed very fast and lead to voltage collapse if not handled properly. In practice, this may happen when a large number of inductive loads like industrial electric motors or air conditioners are switched on. However, this instance is very rare as utilities would have a fairly good idea of the demand in a local area, and would have installed local Q sources to avoid long-distance transmission of reactive power.

The system's response to disturbance varies with the magnitude of disturbance, and may require different forms of analyses. Small-signal instability is the system's ability to maintain an acceptable voltage profile following small changes in system condition, such as incremental changes in bus loads. Steady-state analysis are usually sufficient to analyse small-disturbance voltage stability. These analyses include off-line calculation of system's response following a contingency or evaluating the loading or stability margin. On the other hand, large-signal or large-disturbance stability refer to the system's response to a large perturbation or system events, such as faults of a certain duration, loss of lines, or loss of generators. Since a lot of controls are available in the grid to forestall instability, large-signal voltage stability is concerned with system operating conditions after seconds or tens-of-minutes-long interaction of these controls. Dynamic study of a long duration are often required for a proper analysis of large-disturbance stability.

Voltage stability can also be classified according to the length of time that elapsed before the occurrence of instability, following an event. With respect to this classification, Transient stability is concerned with the response of the system immediately following a disturbance. In contrast, stability in the mid-term is based on the amount of time it takes to synchronise inter-machine oscillations and some occurrences which are slower than can be studied under transient stability. Mostly, mid-term and long-term stabilities are classified together. System events are often anticipated as contingencies and pre-planned control actions may be used to stabilise the system in the event of the occurrence of the anticipated contingency. However, major disturbances may often stretch restorative system resources beyond the limit, and as a result, preplanned actions may be insufficient. This may lead to the system splitting into many parts with pockets of islanded parts still remaining in synchronism. This is usually caused by poor coordination of protection controls. In long term stability, the focus then is on how the islands maintain their individual synchronisation. In addition, long-term or even mid-term studies are concerned with the actions of Over-Excitation Limiters and On-Load Tap Changing (OLTC) transformers, and reactive power limits of generators and reactive-power compensation devices. Long-term stability studies may often require durations of around a few to tens of minutes.

2.2.1 Classification of voltage control

Power losses, among many other undesirable economic consequences, may often accompany attempts to regulate voltage. As a result of seeking to balance economic and technical constraints, the task of maintaining acceptable voltage profile across the grid is considered to be more complex than frequency regulation, and may often be antithetical to economic objectives [67]. Therefore, the voltage control goals often involves prioritising the objective and the regulated bands for voltages, (typically between ±10% of nominal for UK transmission system [66]) are used as soft constraints, rather than the objectives, of voltage control problems.

Traditionally,voltage control is achieved through mechanical switching of reactive power sources such as capacitors, synchronous generators, and synchronous condensers. However, experiences from blackouts in various parts of the world, for example, the August 14 2003 blackout in parts of the United States and Canada[3], as well that in the Southern parts of the Hellenic system in July 2004 [64] have emphasised the need for constant monitoring and more automatic control.

Voltage control strategies may vary from centralised control (with one central controller having full information about respective areas), to a decentralised one,(where each area is controlled independently). For centralised control strategies, the computational resources involved can be enormous, and may be more tractable by breaking them into small parts. In addition, exporting reactive power, necessary for voltage regulation, over long distances across the grid is not desirable as significant losses are incurred along transmission lines. Although decentralised control may not perform optimally without adequate communication infrastructures when certain constraints are present in the network , it was shown that in some cases, the performance is comparable to centralised ones [68]. With adequate communication infrastructure, decentralised control approaches may be more appropriately referred to as distributed controls. However, the challenge is to determine when decentralised, rather than distributed control strategies are needed, and to evaluate accompanying investment in communication infrastructure. The major difference between distributed and decentralised control is that in the former, there are no communications or cooperation between control areas; control decisions are made without taking events in other control area into consideration. This reduces the need CI overhead but may increase the potential for making suboptimal decisions. On the other hand, distributed controls involve a degree of cooperation and communication between different control areas, with events in neighbouring areas taken into account when controls are estimated in each area.

A hierarchical voltage control scheme has been successfully applied in many countries, especially on the European continent [69]–[71], to address the security and operational challenges of voltage control. As shown in Figure 2.1, the scheme consists of three levels of primary, secondary, and tertiary voltage control scheme which are carefully coordinated to address different time constants, control areas, and the automatic control of reactive power resources [72]. The primary voltage regulation scheme handles the every fast transient and works directly on the generator Automatic Voltage Regulators (AVRs). The AVR references are set at the secondary voltage regulation level in addition to the control of reactive power devices. The SVR goal is to track pilot buses set-points and minimise the use of secondary control resources. For strong interactions, the coupling between areas must be considered in the implementation of the SVR. A solution was proposed in [73] to resolve the strong interactions effects. The application of multilevel control structure has been shown to reduce transmission losses by up to 8% on the Italian grid.

The hierarchical control structure mirrors the deregulated market by recognising how different
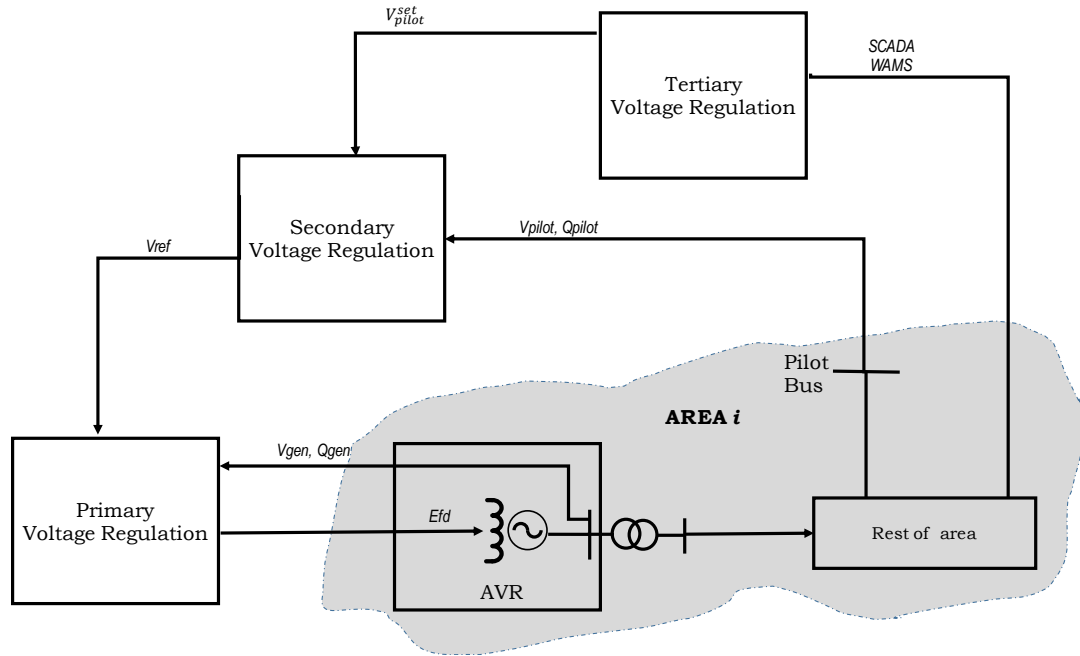
FIGURE 2.1: Voltage - Wide Area Regulation (V-WAR) Scheme

players contribute to voltage support. For the Transmission System Operators (TSOs), the task of automating transmission voltages is particularly simplified by this structure.

2.2.2 Methods of achieving voltage control in normal and emergency operating conditions

Reactive power generated by generators and reactive power compensation devices during system operation increase to meet the increased need for reactive power in the grid. These needs are often influenced by increasing load demands, leading to a decrease in the loading margin and reducing the distance of the operating point to a Hopf bifurcation point.

In order to minimise losses from importing reactive power over long distances, increased demands for reactive powers may be provided locally by Q-compensation devices such as shunt capacitors or SVCs at the point of demand, or by increased reactive power production from nearby generators (which may be induced by transformer tap-changing operations or modulations of AVR references). Note that Q-productions from generators and Q-compensation devices are limited by their capacities. Furthermore, reactive power production in generators is constrained by Overexcitation Limiters (OELs) according to the field currents, and by the quadratic relationship between bus voltage and reactive power for shunt capacitors. When the voltage falls below the required limits, generators are unable to regulate their terminal voltages beyond their Q-capacities. Consequently, PV buses may become PQ buses and no longer participate in grid voltage regulation. When the reactive power of all reactive power sources are exhausted, the system's propensity towards voltage instability may increase. The dynamics of tap-changing operations in trying to restore voltage to reference values and those of voltage-dependent loads may finally push the system into instability in the absence of emergency controls [65].

Path to instability

Generation-load imbalances stress the system, and this may be seen in the form of increased voltage angles and depressed voltage magnitudes especially when load is increased beyond generation at constant power factor. The rates of change of angles are indicative of how fast the system is moving into an emergency condition. For slowly-varying deterioration, such as in the long terms effect of tap-changer operations and the on-and-off changes (where dynamic loads, mostly inductive, tend to connect and disconnect from the grid depending on system voltage), the distance to instability may be detected by the increasing deviations of the operating frequency from the nominal or the descent of voltage-reactive power relationship towards the unacceptable Hopf bifurcation point. Note that bifurcations represent the change in the number of selected operating conditions when a parameter is slowly varied and that Hopf bifurcations occur in power system dynamics that cause the nominal equilibrium to lose their their structural stability as they pass through the bifurcation points. Plots of the variations of voltage with reactive power or V-Q curves, at various buses, are usually useful in the identifications of points at which instability may set in as system's margins decrease in the face of contingencies. This is illustrated from the Figure 2.2, obtained from the report [3] on the 14 August 2003 US blackout.
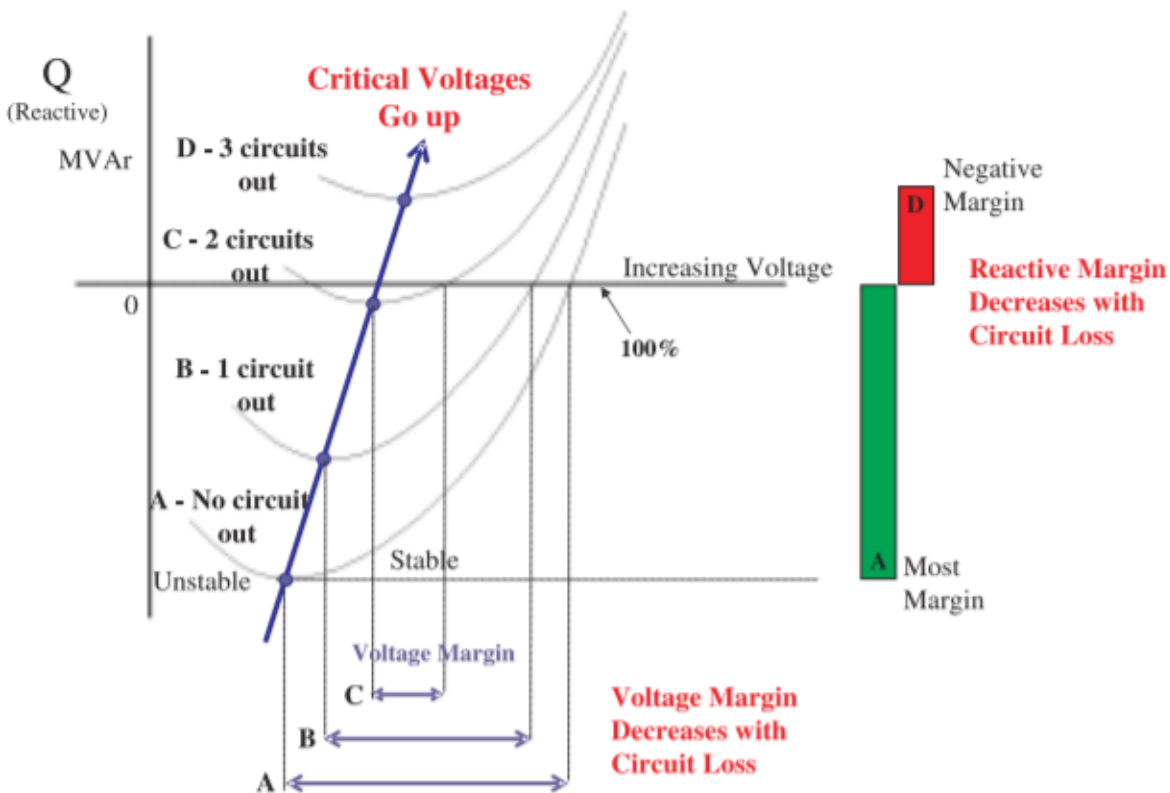
FIGURE 2.2: V-Q (Voltage-Reactive Power) Curves [3]

Curve A is the normal no-contingency V-Q curve while B, C, and D are the V-Q curves with 1, 2, and 3 transmission lines, respectively, lost or tripped. The right and left side of the curves represent the stable and unstable operating points respectively and the noses of the curves are the

Hopf bifurcation point. It is easy to see that the voltage margins[1] and reactive margin [2] decrease as the number of circuits taken out of the system increases. For each curve, starting from the right hand side, it can be observed that the bus voltage decreases as the reactive power decreases, in a quadratic manner, more slowly as the curve approaches the Hopf bifurcation point. Conversely, the region of operation can be moved from the left side to the right side as voltage increase with more reactive power in the system. The shape of the Q-V curve can be explained by the simple relationship (2.1) between the two quantities.

$$Q = BV^2 \tag{2.1}$$

where B is the bus susceptance.

Abrupt changes to system conditions —such as islanding or loss of lines or generators —may be detected through the rate at which frequency changes within a pre-defined period of time. A number of works [74]–[76] have used this as a basis for system restoration.

2.2.3 Pilot buses

The SVR idea can be summarised as the suppression of voltage violations on sensitive buses in a bid to indirectly control other bus voltages. For the SVR scheme described in this chapter, the additional motive is to provide an adaptive form of SVR using PMU data. Boundary buses that exert influences on surrounding buses in a region are critical to the success of the SVR scheme, and the criteria for selecting these buses may be found in a number of power system literature [77]–[80].

Pilot buses are selected through a combination of rule-based and automatic selection method. As a rule of thumb, only load buses at voltage levels of 220kV and above are candidate pilot buses. This is because the buses at lower voltage levels are assumed to be incapable of sufficiently influencing the voltages of the surrounding buses. The remaining high-voltage load buses are then checked for their short-circuit power capacity, coupling threshold, load location, and finally on the availability of the control resources for the pilot nodes.

The pilot nodes

1. must be able to influence the voltages of the other buses in the area.

2. must have low electrical coupling with buses in other areas.

The measure of changes to system's states on the application of a control input or disturbance is the sensitivity of the system's states to the control input. For dynamical systems, the total effect of these changes are often felt over a long period of time. This time is in turn determined by the state of the system.

2.2.4 Control generators

For automated controls, there exists the simultaneous desires for fast response and for the participating controls to have considerable effect on the pilot bus voltage regulation. Fast and reliable controls can be obtained through a reduction in the number of participating generators to those whose reactive power generation change the most in response to changes in pilot bus voltages.

---

[1] The voltage margin is the distance of the bus voltage operating point to instability.
[2] The reactive margin is the distance of bus reactive power operating point to instability.

The control generator chosen to participate in SVR in an area must be able to influence the area's pilot bus voltage. In practice, these generators would be those with the highest reactive power capacities [72]. These could also be generators with the highest participation factors, which contribute the most to voltage or reactive power control. Based on the identification of the capabilities, it is easy to estimate the areas where the regulation of pilot bus voltages may be lost following a depletion in reactive power capacity.

2.3 General description of an electric power system

An electric power system model is usually described by the dynamic equations of its moving components, particularly its generators, exciters, power systems stabilisers (PSS), automatic voltage regulators (AVRs), and dynamic loads, as well as with algebraic equations describing the relationship of voltage and current quantities to the power flow along its connected buses and branches. Thus, a general pair of equation 2.2 describes the static and dynamic behaviours of the power system as a whole.

$$\dot{x} = f(x, h, u) \tag{2.2a}$$

$$0 = g(x, h, u) \tag{2.2b}$$

where the function $f(x, h, u)$ represents the governing equations for the dynamic components, while the algebraic function $g(x, h, u)$ defines the power-flow equations along branches and power injections at buses, as well as the stator equations. x, h are vectors of defined dynamic and algebraic state variables respectively, and u is the vector of control variables. Both functions f and g in 2.2 are non-linear.

2.3.1 Dynamic modelling of power system components

Dynamic models of power system components describe the equation of its generators, exciters, PSSs, SVCs, and its dynamic loads. In the following, the specific forms of the dynamic equations are presented, starting with those of the synchronous machine. However, only brief overviews are given. More detailed explanations of these representations may be found in many literature on the subject such as [65], [81], [82].

2.3.2 Two-Axis Model of the synchronous machine

The two-axis machine representation is a resolution of the synchronous machine's model into two components —d and q —which are separated by an angle of 90°, as shown in Figure 2.3. In power systems, the resolution of the synchronous machine model into d-q frame is a matter convention which helps to simplify the modelling and analysis of the synchronous machine.

The machine's dynamic equation can be described by n equations that describe the extent of machine characterisation, or model order. These details are in turn influenced by the type of power system analyses. For rotor angle stability analyses, the classical machine representations (mainly (2.3b) and (2.3c)) are sufficient. For short-term transient studies, it might be necessary to model the machine's transient and sub-transient characteristics in addition. Equation (2.3) describes a
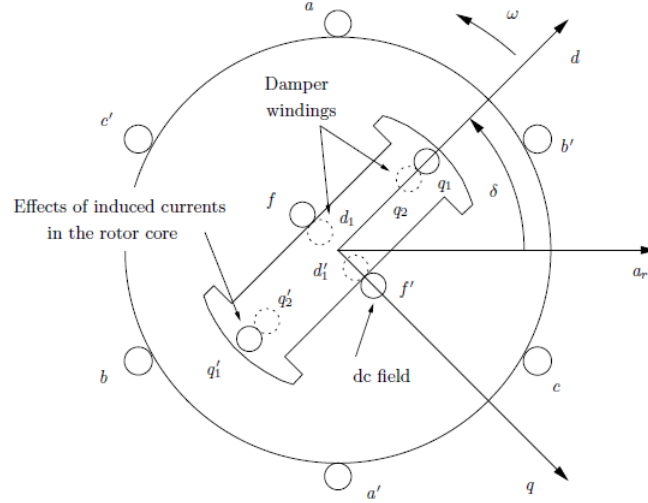
FIGURE 2.3: Synchronous machine two-axis model [65]

$n = 7$-th order machine equation,

$$\dot{\delta}_i = \omega_i - \omega_s \tag{2.3a}$$

$$\dot{\omega}_i = \frac{T_{Mi}}{M_i} - \frac{(E'_{qi} - X'_{di}I_{di})I_{qi}}{M_i} - \frac{(E'_{di} + X'_{qi}I_{qi})I_{di}}{M_i} - \frac{D_i(\omega_i - \omega_s)}{M_i} \tag{2.3b}$$

$$\dot{E}'_{qi} = -\frac{E'_{qi}}{T'_{d0i}} - \frac{(X_{di} - X'_{di})I_{di}}{T'_{d0i}} + \frac{E'_{fdi}}{T'_{d0i}} \tag{2.3c}$$

$$\dot{E}_{di} = -\frac{E'_{di}}{T'_{q0i}} + \frac{I_{qi}}{T'_{q0i}}\left(X_{qi} - X'_{qi}\right) \tag{2.3d}$$

$$\dot{E}_{fdi} = -\frac{K_{Ei} + S_E(E_{fdi})}{T_{Ei}}E_{fdi} + \frac{V_{Ri}}{T_{Ei}} \tag{2.3e}$$

$$\dot{V}_{Ri} = -\frac{V_{Ri}}{T_{Ai}} + \frac{K_{Ai}}{T_{Ai}}R_{fi} - \frac{K_{Ai}K_{Fi}}{T_{Ai}T_{Fi}}E_{fdi} + \frac{K_{Ai}}{T_{Ai}}\left(V_{refi} - V_i\right) \tag{2.3f}$$

$$\dot{R}_{Fi} = -\frac{R_{Fi}}{T_{Fi}} + \frac{K_{Fi}}{(T_{Fi})^2}E_{fdi}, \ \forall i = 1, \ldots, n_g \tag{2.3g}$$

2.3.3   Other dynamical components in the grid

The other dynamical components in the electric power grid are mostly those which combine to provide excitation and stabilisation function to a generator's inputs and/or outputs. These include the exciters, whose function is to provide excitation to a generator's field voltage based on a feedback measurement of the generator's terminal voltage, the PSS, which provide an extra damping signal to the exciters using the generator's speed as feedback measurements. These components are connected to the generator as shown in Figure 2.4. Several forms of these components exist with different governing equation and may be found in [65], [82]. Examples of the transfer functions of these components are shown in Figure 2.4.

TABLE 2.1: Definition of parameters of Equation (2.3)

Parameter	X_{d}, X_{q}	X'_{d}, X'_{q}	T'_{d0}, T'_{q0}	E'_{d}, E'_{q}	E'_{fd}
Description	$d, q-$axis synchronous reactance	$d, q-$axis transient reactance	$d, q-$axis subtransient open-circuit time constant	$d, q-$axis voltage	Field voltage
Parameter	δ	$\omega[\omega_i, \omega_s]$	V_R	R_F	K_A
Description	Rotor angle	Machine speed[at gen, synchronous]	Rotor voltage	Field resistance	Armature constant
Parameter	D	$S_E(E_{fd})$	V	T_E	V_{ref}
Description	Damping factor	Saturation	Voltage	Electrical torque	AVR reference
Parameter	I_d I_q	T_M, M	K_F	T_A	T_F
Description	$d, q-$axis machine current	Mechanical torque	Field constant	Armature time constant	Field time constant
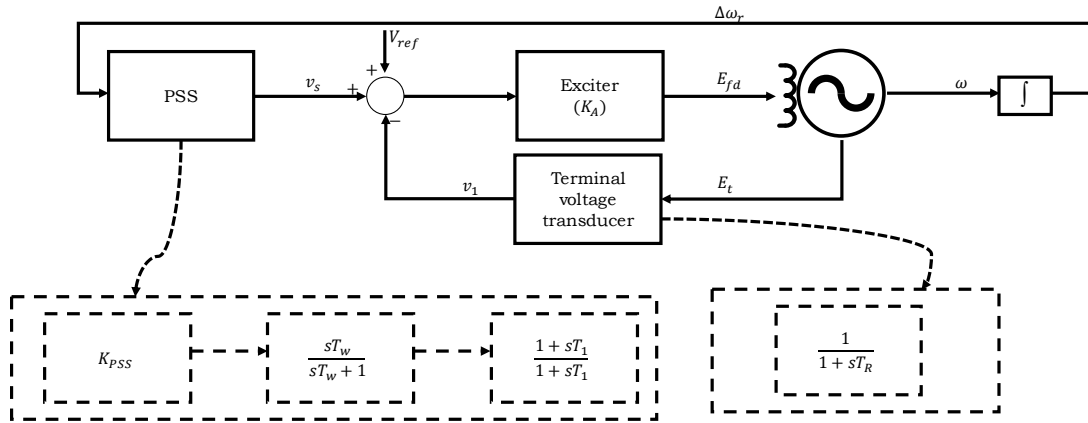
FIGURE 2.4: Excitation systems with AVR and PSS (adapted from [65])

2.3.4 Algebraic equations governing stator and network equations

The function $g(x, h, u)$ in (2.2) defines algebraic equations for generator stator and power systems network governing the non-dynamic parts of the power grid and its equipment, and include generator, network lines and loads. These are modelled in the following.

Stator algebraic equations

The algebraic equations governing the stator of a generator $i \in \Phi_g$ are,

$$0 = V_i e^{j\theta_i} + (R_{si} + jX'_{di})(I_{di} + jI_{qi})e^{j(\delta_i - \frac{\pi}{2})} - [E'_{di} + (X'_{qi} - X'_{di})I_{qi} + jE'_{qi}]e^{j(\delta_i - \frac{\pi}{2})} \tag{2.4a}$$

$$0 = E'_{di} - V_i \sin(\delta_i - \theta_i) - R_{si}I_{di} + X'_{qi}I_{qi} \tag{2.4b}$$

$$0 = E'_{qi} - V_i \cos(\delta_i - \theta_i) - R_{si}I_{qi} + X'_{di}I_{di} \tag{2.4c}$$

Generator buses algebraic equations

The real and reactive power injection equations at the ith generator bus ($i \in \Phi_g$) and along lines connecting the generator bus to other buses in the networks are given by (2.5a) and (2.5b) respectively,

$$P_{Li}(V_i) = \sum_{k=1}^{n} V_i V_k Y_{ik} \cos(\theta_i - \theta_k - \alpha_{ik}) - I_{qi}V_i \cos(\delta_i - \theta_i) - I_{di}V_i \sin(\delta_i - \theta_i) \tag{2.5a}$$

$$Q_{Li}(V_i) = \sum_{k=1}^{n} V_i V_k Y_{ik} \sin(\theta_i - \theta_k - \alpha_{ik}) - I_{di}V_i \cos(\delta_i - \theta_i) + I_{qi}V_i \sin(\delta_i - \theta_i) \tag{2.5b}$$

Load buses algebraic equations

The algebraic equations governing the load flow for a load bus $i, \in \lambda_l$ and connected lines and buses are defined by the equation (2.6).

$$P_{Li}(V_i) = \sum_{k=1}^{n} V_i V_k Y_{ik} \cos(\theta_i - \theta_k - \alpha_{ik}), \tag{2.6a}$$

$$Q_{Li}(V_i) = \sum_{k=1}^{n} V_i V_k Y_{ik} \sin(\theta_i - \theta_k - \alpha_{ik}) \tag{2.6b}$$

2.4   Linearisation of a non-linear electric power system model

The linearisation of the non-linear differential-algebraic equations (DAE) (2.2) about an equilibrium point or along a system's trajectory is sometimes sufficient for power systems analyses.

2.4.1   Model linearisation around an equilibrium point

In order to apply linear system's theories to power system analysis, it is necessary to linearise (2.2). This is usually carried out around a nominal operating point x_0, h_0, u_0, using Taylor's series expansion for each of the variables x, h, u in functions $f(x, h, u)$ and $g(x, h)$.

$$f(x,h,u) = f(x_0,h_0,u_0) + \frac{\partial f(x,h,u)}{\partial x}(x - x_0) + \frac{\partial f(x,h,u)}{\partial h}(h - h_0) + \frac{\partial f(x,h,u)}{\partial u}(u - u_0)$$
$$+ \frac{1}{2!}\frac{\partial^2 f(x,h,u)}{\partial x}(x - x_0) + \frac{1}{2!}\frac{\partial^2 f(x,h,u)}{\partial h}(h - h_0) + \frac{1}{2!}\frac{\partial^2 f(x,h,u)}{\partial u}(u - u_0) \tag{2.7}$$
$$+ \ldots + \text{higher order terms}$$

$$g(x,h,u) = g(x_0,h_0,u_0) + \frac{\partial g(x,h,u)}{\partial x}(x-x_0) + \frac{\partial g(x,h,u)}{\partial h}(h-h_0) + + \frac{1}{2!}\frac{\partial^2 g(x,h,u)}{\partial x}(x-x_0)$$
$$+ \frac{1}{2!}\frac{\partial^2 g(x,h,u)}{\partial h}(h-h_0) + \ldots + \text{higher order terms} \tag{2.8}$$

Neglecting terms with differential order greater than 2 in (2.7) and (2.8) and defining $\Delta x = x - x_0$, $\Delta h = h - h_0$ and $\Delta u = u - u_0$, resulting in

$$\Delta\dot{x} = f(x,h,u) - f(x_0,h_0,u_0) = \frac{\partial f(x,h,u)}{\partial x}\Delta x + \frac{\partial f(x,h,u)}{\partial h}\Delta h + \frac{\partial f(x,h,u)}{\partial u}\Delta u$$
$$0 = g(x,h,u) - g(x_0,h_0,u_0) = \frac{\partial g(x,h,u)}{\partial x}\Delta x + \frac{\partial g(x,h,u)}{\partial h}\Delta h \tag{2.9}$$

Define $A = \frac{\partial f(x,h,u)}{\partial x}$, $B_h = \frac{\partial f(x,h,u)}{\partial h}$, $B_u = \frac{\partial f(x,h,u)}{\partial u}$, $C = \frac{\partial g(x,h,u)}{\partial x}$, and $D = \frac{\partial g(x,h,u)}{\partial h}$ to obtain (2.10)

$$\Delta\dot{x} = A\Delta x + B_h\Delta h + B_u\Delta u \tag{2.10a}$$
$$0 = C\Delta x + D\Delta h \tag{2.10b}$$

If D is invertible, then (2.10b) can be written as $\Delta h = -D^{-1}C\Delta x$ and (2.10) reduces to,

$$\Delta\dot{x} = (A - (B_h D^{-1}C))\Delta x + B_u\Delta u \tag{2.11}$$

Define $A' = (A - (B_h D^{-1}C))$ and write (2.10) as,

$$\Delta\dot{x} = A'\Delta x + B_u\Delta u \tag{2.12}$$

Equation (2.12) defines a general state space model for the electric power systems and lends readily to control designs which are based on state space forms. In the next section, we define the actual form of the general equation (2.2) and seek to derive the main elements of (2.12).

If v is a vector of variables such that,

$$v = \begin{bmatrix} \delta_i & \omega_i & E'_{qi} & E'_{di} & E'_{fdi} & V_{Ri} & R_{Fi} & I_{di} & I_{qi} & \theta_i & V_i & T_{Mi} & V_{\text{ref}i} \end{bmatrix}^T \tag{2.13}$$

and linearising the dynamic model equations (2.3) around small perturbations of the vector v,

$$
\underbrace{\begin{bmatrix} \Delta\dot\delta \\ \Delta\dot\omega \\ \Delta\dot E'_{qi} \\ \Delta\dot E'_{di} \\ \Delta\dot E'_{\mathrm{fd}i} \\ \Delta\dot V_{\mathrm{R}i} \\ \Delta\dot R_{\mathrm{F}i} \end{bmatrix}}_{\Delta\dot{\boldsymbol{x}}_{\boldsymbol{i}}\in\mathbb{R}^{7\times1}}
=
\underbrace{\begin{bmatrix}
\frac{-1}{T'_{\mathrm{do}i}} & 0 & 0 & 0 & \frac{1}{T'_{\mathrm{do}i}} & 0 & 0 \\
0 & -\frac{D_i}{M_i} & -\frac{I_{qi0}}{M_i} & -\frac{I_{di0}}{M_i} & 0 & 0 & 0 \\
0 & 0 & -\frac{1}{T'_{\mathrm{d}0i}} & 0 & \frac{1}{T'_{\mathrm{d}0i}} & 0 & 0 \\
0 & 0 & 0 & -\frac{1}{T'_{\mathrm{q}0i}} & 0 & 0 & 0 \\
0 & 0 & 0 & 0 & -\left(\frac{K_{\mathrm{E}i}}{T_{\mathrm{E}i}}+\frac{\partial S_E(E_{\mathrm{fd}i0})}{\partial E_{\mathrm{fd}i}}+S_E(E_{\mathrm{fd}i0})\right) & \frac{1}{T_{\mathrm{E}i}} & 0 \\
0 & 0 & 0 & 0 & \frac{-K_{\mathrm{A}i}K_{\mathrm{F}i}}{T_{\mathrm{F}i}T_{\mathrm{A}i}} & \frac{-1}{T_{\mathrm{A}i}} & \frac{K_{\mathrm{A}i}}{T_{\mathrm{A}i}} \\
0 & 0 & 0 & 0 & \frac{K_{\mathrm{F}i}}{(T_{\mathrm{F}i})^2} & 0 & -\frac{1}{T_{\mathrm{F}i}}
\end{bmatrix}}_{\boldsymbol{A_i}\in\mathbb{R}^{7\times7}}
\underbrace{\begin{bmatrix} \Delta\delta \\ \Delta\omega \\ \Delta E'_{qi} \\ \Delta E'_{di} \\ \Delta E'_{\mathrm{fd}i} \\ \Delta V_{\mathrm{R}i} \\ \Delta R_{\mathrm{F}i} \end{bmatrix}}_{\Delta\boldsymbol{x_i}\in\mathbb{R}^{7\times1}}
$$

$$
+
\underbrace{\begin{bmatrix}
0 & 0 \\
\frac{1}{M_i}\left((X'_{di}-X'_{qi})I_{qi0}-E'_{di0}\right) & \frac{1}{M_i}\left((X'_{di}-X'_{qi})I_{di0}-E'_{qi0}\right) \\
\frac{(X'_{di}-X_{di})}{T'_{\mathrm{d}0i}} & 0 \\
0 & \frac{(X_{qi}-X'_{qi})}{T'_{\mathrm{d}0i}} \\
0 & 0 \\
0 & 0 \\
0 & 0
\end{bmatrix}}_{B_i^{\mathrm{d\text{-}q}}\in\mathbb{R}^{7\times2}}
\underbrace{\begin{bmatrix} \Delta I_{di} \\ \Delta I_{qi} \end{bmatrix}}_{\Delta\boldsymbol{I_i^{\mathrm{d\text{-}q}}}\in\mathbb{R}^{2\times1}}
+
\underbrace{\begin{bmatrix}
0 & 0 \\
0 & 0 \\
0 & 0 \\
0 & 0 \\
0 & 0 \\
0 & -\frac{K_{\mathrm{A}i}}{T_{\mathrm{A}i}} \\
0 & 0
\end{bmatrix}}_{B_i^{\mathrm{g}}\in\mathbb{R}^{7\times2}}
\underbrace{\begin{bmatrix} \Delta\theta_i \\ \Delta V_i \end{bmatrix}}_{\Delta\boldsymbol{V_i^{\mathrm{g}}}\in\mathbb{R}^{2\times1}}
$$

$$
+
\underbrace{\begin{bmatrix}
0 & 0 \\
\frac{1}{M_i} & 0 \\
0 & 0 \\
0 & 0 \\
0 & 0 \\
0 & \frac{K_{\mathrm{A}i}}{T_{\mathrm{A}i}}
\end{bmatrix}}_{B_i^{u}\in\mathbb{R}^{7\times2}}
\underbrace{\begin{bmatrix} \Delta T_{\mathrm{M}i} \\ \Delta V_{\mathrm{ref}i} \end{bmatrix}}_{\Delta\boldsymbol{u_i}\in\mathbb{R}^{2\times1}}
$$

$$(2.14)$$

Using the definitions in the underbraces of the matrices in (2.14), the state-space model (2.14) can be written in a compact form (2.15),

$$
\Delta\dot x_i = A_i\Delta x_i + B_i^{\mathrm{d\text{-}q}}\Delta I_i^{\mathrm{d\text{-}q}} + B_i^{\mathrm{g}}\Delta V_i^{\mathrm{g}} + B_i^{\mathrm{u}}\Delta u_i \tag{2.15}
$$

For n_g number of generators, the matrices in (2.15) can be written in the block diagonal forms of (2.16).

$$
\underbrace{\begin{bmatrix} \Delta\dot{x}_1 \\ \vdots \\ \Delta\dot{x}_{n_g} \end{bmatrix}}_{\Delta\dot{x}} = \underbrace{\begin{bmatrix} A_1 & \cdots & \mathbf{0}_{7\times7} \\ \vdots & \ddots & \vdots \\ \mathbf{0}_{7\times7} & \cdots & A_{n_g} \end{bmatrix}}_{\boldsymbol{A}\in\mathbb{R}^{7n_g\times7n_g}} \underbrace{\begin{bmatrix} \Delta x_1 \\ \vdots \\ \Delta x_{n_g} \end{bmatrix}}_{\Delta\boldsymbol{x}\in\mathbb{R}^{7n_g\times1}} + \underbrace{\begin{bmatrix} B_1^{\text{d-q}} & \cdots & \mathbf{0}_{7\times2} \\ \vdots & \ddots & \vdots \\ \mathbf{0}_{7\times2} & \cdots & B_{n_g}^{\text{d-q}} \end{bmatrix}}_{B^{\text{d-q}}\in\mathbb{R}^{7n_g\times2n_g}} \underbrace{\begin{bmatrix} \Delta I_1^{\text{d-q}} \\ \vdots \\ \Delta I_{n_g}^{\text{d-q}} \end{bmatrix}}_{\Delta\boldsymbol{I}^{\text{d-q}}\in\mathbb{R}^{2n_g\times1}}
$$

$$
+ \underbrace{\begin{bmatrix} B_1^{\text{g}} & \cdots & \mathbf{0}_{7\times2} \\ \vdots & \ddots & \vdots \\ \mathbf{0}_{7\times2} & \cdots & B_{n_g}^{\text{g}} \end{bmatrix}}_{B^{\text{d-q}}\in\mathbb{R}^{7n_g\times2ng}} \underbrace{\begin{bmatrix} \Delta V_1^{\text{g}} \\ \vdots \\ \Delta V_{n_g}^{\text{g}} \end{bmatrix}}_{\Delta V^g\in\mathbb{R}^{2n_g\times1}} + \underbrace{\begin{bmatrix} B_1^{\text{u}} & \cdots & \mathbf{0}_{7\times2} \\ \vdots & \ddots & \vdots \\ \mathbf{0}_{7\times2} & \cdots & B_{n_g}^{\text{u}} \end{bmatrix}}_{B^u\in\mathbb{R}^{7n_g\times2ng}} \underbrace{\begin{bmatrix} \Delta u_1 \\ \vdots \\ \Delta u_{n_g} \end{bmatrix}}_{\Delta u\in\mathbb{R}^{2n_g\times1}}
\tag{2.16}
$$

$$
\boldsymbol{\Delta\dot{x} = A\Delta x + B^{\text{d-q}}\Delta I^{\text{d-q}} + B^{\text{g}}\Delta V^{\text{g}} + B^{\text{u}}\Delta u}
$$

In addition to generator models, the linearised models of the other dynamical components can be incorporated into a dynamic state space (2.17).

$$
\boldsymbol{\Delta\dot{x}} = \underbrace{\begin{bmatrix} \text{Gen} & & & & & & \\ & \text{Exc} & & & & & \\ & & \text{PSSs} & & & & \\ & & & \text{TG} & & & \\ & & & & \text{SVCs} & & \\ & & & & & P_{load} & \\ & & & & & & Q_{load} \end{bmatrix}}_{\boldsymbol{A}_{all}} \underbrace{\begin{bmatrix} \Delta\text{Gen} \\ \Delta\text{Exc} \\ \Delta\text{PSS} \\ \Delta\text{TG} \\ \Delta\text{SVC} \\ \Delta\text{Pload} \\ \Delta\text{Qload} \end{bmatrix}}_{\boldsymbol{\Delta x}_{all}}
\tag{2.17}
$$

Again, by linearising around the general variable v, the algebraic equations governing the generator stator and buses as well as those of the load buses can be written in a compact form in the manner of (2.10b).

Note that the equations (2.16) and (2.17) are the dynamic equations (2.2a). The inclusion of the algebraic equations of Section (2.3.4) (as (2.2a)) will scale the increase the size of the matrices in (2.16) considerably.

Model linearisation by trajectory sensitivity evaluation

In contrast to traditional method of linearising around an equilibrium point, trajectory sensitivity approaches [83]–[87] linearise the non-linear equation (2.2) around a nominal trajectory. The goal here is to estimate how a state trajectory changes consequent upon a change in the initial condition of a system output or state. The method has been applied in assessing the stability of power system [88] and in the analysis of systems which contain discontinuities [85], [86].

If x, h are the dynamic and algebraic states and x_0, h_0 are the initial conditions of these states, then from (2.2), the sensitivities of the functions $f(x, h, u)$ and $g(x, h, u)$ to the parameter u, following a first-order Taylor's series expansion, can be summarised as,

$$\frac{d}{dt}\left(\frac{\partial x}{\partial u}\right) = \frac{\partial f}{\partial x}\frac{\partial x}{\partial u} + \frac{\partial f}{\partial h}\frac{\partial h}{\partial u} + \frac{\partial f}{\partial u} \tag{2.18a}$$

$$0 = \frac{\partial g}{\partial x}\frac{\partial x}{\partial u} + \frac{\partial g}{\partial h}\frac{\partial h}{\partial u} + \frac{\partial g}{\partial u} \tag{2.18b}$$

It is important to note that $\frac{\partial(.)}{\partial u}$ are time-varying matrices.

Model linearisation by sensitivity evaluation of algebraic power flow equations

The algebraic static power flow equation can be written as,

$$g(x, u) = 0 \tag{2.19}$$

where x represents the state variables and u the control variables. Differentiating the non-linear equation (2.19) partially with respect to variables x and u,

$$\frac{\partial g}{\partial x}\Delta x + \frac{\partial g}{\partial u}\Delta u = 0 \tag{2.20}$$

and the changes in a state variable Δx due to a change in control variable Δu can be estimated mathematically as,

$$\Delta x = -\underbrace{\left(\frac{\partial g}{\partial x}\right)^{-1}\frac{\partial g}{\partial u}}_{S_{xu}}\Delta u \tag{2.21}$$

The degree of change in x is quantified by the product of the sensitivity S_{xu} and the amount of perturbation Δu if no additional disturbance is happening in the grid at the same time, as is the case in steady or quasi-steady states. The value of S_{xu} due to a change in a control variable Δu varies according to the strength of the electrical connection between the two variables for small amounts of perturbations.

If Δx is scalar, the computation of the inverse $\left(\frac{\partial g}{\partial x}\right)^{-1}$ is trivial. However, for large power systems, $\frac{\partial g}{\partial x}$, $\frac{\partial g}{\partial u}$ and consequently S_{xu} in (2.21) are matrices with large dimensions.

2.4.2   Model linearisation by state perturbations

Given a non-linear power system model of the form described by an adaptation of (2.2).

$$\begin{aligned}\dot{x} &= f(x, u)\\0 &= g(x, u)\end{aligned} \tag{2.22}$$

a state-space model (2.23) can be realised by off-line small-signal perturbations of each component of the model (2.22) in turn for known initial states, inputs and outputs.

$$\begin{aligned}\Delta \boldsymbol{x}_{k+1} &= \boldsymbol{A}\Delta \boldsymbol{x}_k + \boldsymbol{B}\Delta \boldsymbol{u}_k\\\Delta \boldsymbol{y}_k &= \boldsymbol{C}\Delta \boldsymbol{x}_k\end{aligned} \tag{2.23}$$

If $y_k \in \mathbb{R}^{N_y}$ is the measured vector of output variables and $z_k \in \mathbb{R}^{N_y}$ is the vector of controlled variables. The states include those of the generators, exciter, PSS, SVC as well as the active and reactive load components, and the outputs include the voltage and powerflows along the lines written as an algebraic sum of the dynamic states. The inputs are those normally used at secondary voltage level; namely the AVR, SVC and turbine governor references, as well as active and reactive power load modulations.

In order to realise the state-space, each column of the state matrix A is formed by perturbing the corresponding dynamic component by $p = \max(\iota, 0.001x_0)$ and then forming

$$A_{i,j} = \frac{d}{p}P \tag{2.24}$$

where $d \in \mathbb{R}^{n_X}$ represents the initial values of each state or input parameters. $P \in \mathbb{R}^{n_x \times n_X}$ is a sparse permutation matrix which selects the states. ι is a small value which lower-bounds the perturbation such that (2.24) is nonzero. X and x are the maximum possible and actual number of states respectively. Input and output variables corresponding to the component are also formed at the same time. More details of the state-space formulation process can be found in [89].

Step response of the perturbed model

The step response measures the system's response to a step change in an input variable. Voltage changes in response to step changes in input disturbances are demonstrated here using the popular Kundur's 2-area 4-generator test system shown in Figure 2.5 and originally described by [65]. The network consists of two areas, Area 1 and Area 2, and has a total of 4 generators and 13 buses. Area 1 exports power to Area 2 via double-circuit tie lines located between Bus 3 and Bus 13 with a midpoint at Bus 101. Each area has a load bus at Bus 4 and Bus 14 respectively.

The plots in Figure 2.6 are the changes in bus voltages of the network in Figure 2.5 in response to changes of 0.01 p.u. (Figure 2.6a) and 0.05 p.u. (Figure 2.6b) in the AVR reference of Generator G_1 respectively. First, we make the trivial observation that step responses ΔV_{bus}^i are nonzero at all buses, meaning that these bus voltages are influenced by modulations in the generator AVR reference. However, ΔV_{bus}^i is unequal across all Bus i.

Most notably, buses closer to the generator G_1 (Buses 1 and 10) have the highest changes in their voltages. In the second observation, it can be seen that the modulation of AVR reference at Generator G_1 is approximately equal to final steady-state values at the buses Bus 1 (especially) and Bus 10. Since these buses are the closest to the generator, they are reflection of the generator's terminal voltage. This implies that bus voltages can be controlled up to a desired level by a corresponding change in the AVR reference.

As a third observation, notice that the amplitude of output response is proportional to the magnitude of input applied at the references. In Figure 2.7a, the maximum amount of the most sensitive bus is ≈ 0.01 while that of the most sensitive bus in Figure 2.7a is ≈ 0.05. This observation is particularly important in the design of a controller, to determine the maximum input that may be applied to the AVR references for a bounded output response.

Similarly, the step response of the bus voltages to perturbation in Area 2 generator 3 are shown in the figures of Figure 2.7. The observations are different from those for Figure 2.6 only in the changes in the buses that have the highest ΔV_{bus}^i. In this case, these are Bus 11 and Bus 110.
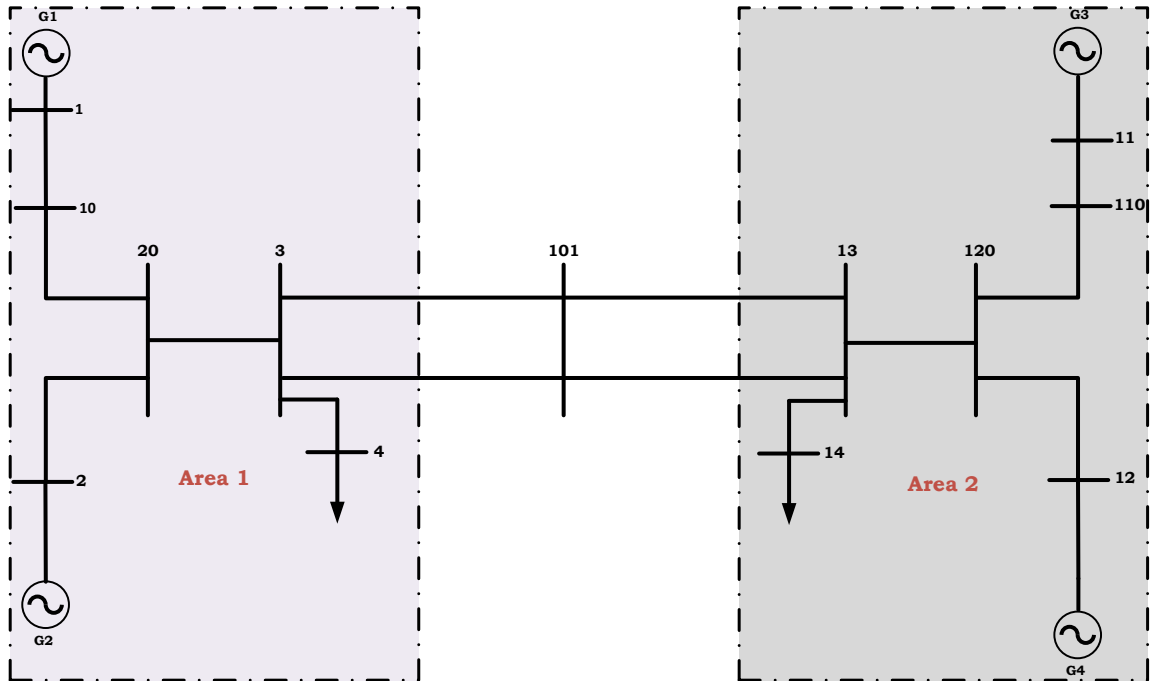
FIGURE 2.5: Kundur's Modified Two-Area Four-Generator Test Network

It can be seen from 2.8 that when the AVR references of Generator G_1 and G_3 are modulated simultaneously with equal changes, there are more significant changes in the final steady values across all buses on the average. Generator terminal buses 1 and 11, followed by (10 and 110) still have the highest ΔV_{bus}^i. In contrast to the other observations, the bus voltages have, approximately, the same steady-state ΔV_{bus}^i when the AVR references of all generators in the network are modulated simultaneously in the same manner in Figure 2.9.

2.4.3   Comment on the linear models

The linearisation methods described in Sections 2.4.1, 2.4.1, and 2.4.2 assume that the states are measurable and that model parameters are available. In reality, measurements devices are needed to observe the states and parameters of the models may be inaccurate, outdated, or simply unavailable. In addition, the model sizes are considerable and impractical for use in a receding horizon sense (which will be described subsequently). For instance, with each generator model is described by 7 equations in (2.3), a network with 500 generators will be described by 3500 equations! This does not include the generators' and their stators' algebraic equations, and those of their exciters, PSSs, SVCs, and loads.

(A) $V_{G_1}^{ref} = 0.01$p.u

(B) $V_{G_1}^{ref} = 0.05$p.u.
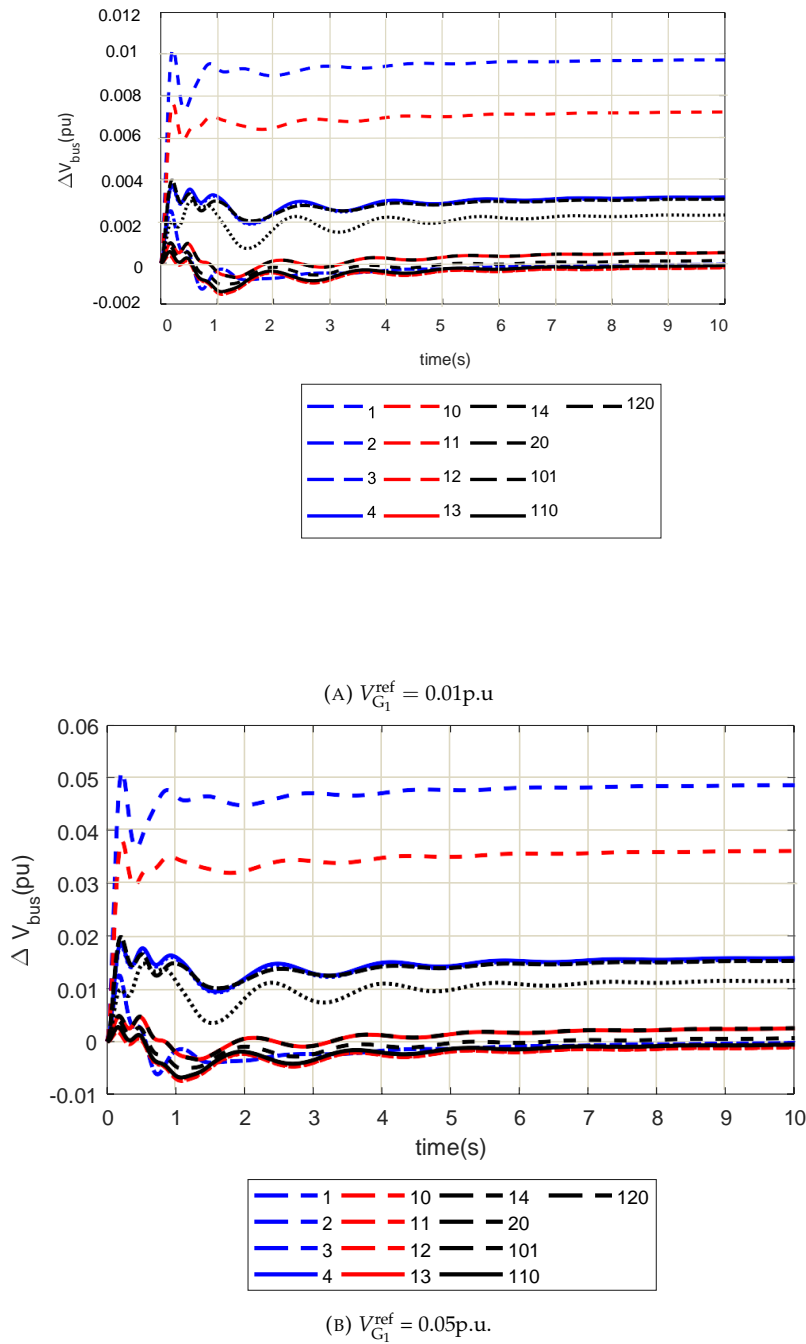
FIGURE 2.6: Step response of bus voltages to changes in voltage reference of Generator 1

(A) $V_{G_3}^{ref} = 0.01$

(B) $V_{G_3}^{ref} = 0.05$
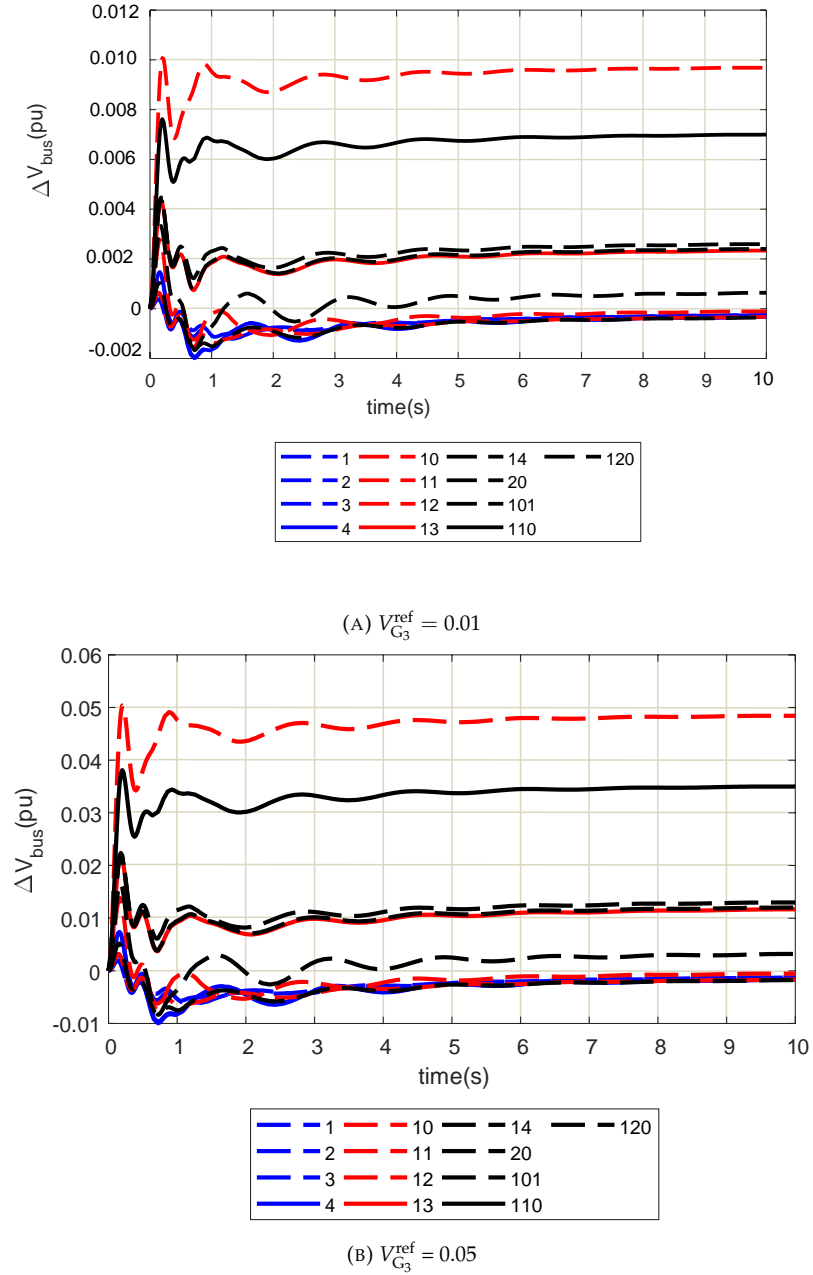
FIGURE 2.7: Step response of bus voltages to respective changes in voltage reference of Generator 3

2.5 Phasors

A time-domain sinusoidal signal $v(t)$ can be represented by the equation

$$v(t) = V_0 \cos(\omega t + \phi) \tag{2.25a}$$

$$\boldsymbol{V} = \frac{V_0}{\sqrt{2}} e^{j\phi} \tag{2.25b}$$
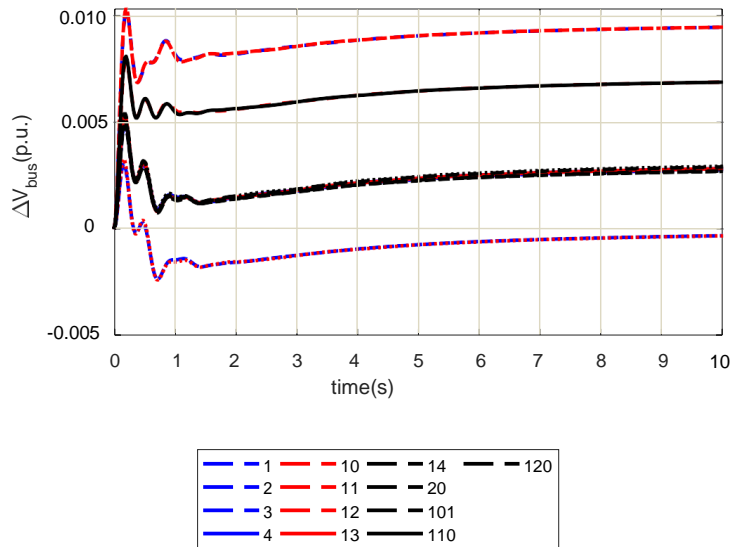
FIGURE 2.8: Step response of bus voltages to 0.01 p.u. changes in voltage reference of Generators 1 and 3
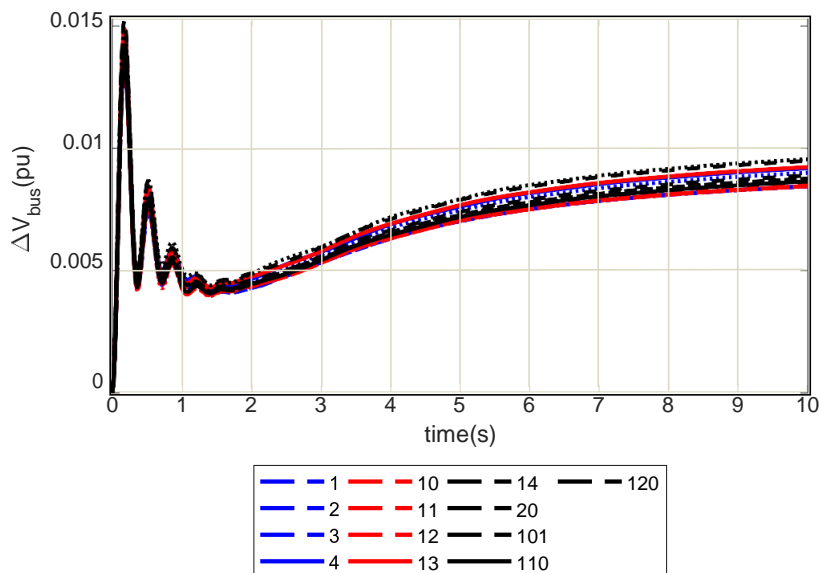
FIGURE 2.9: Step response of bus voltages to 0.01p.u. changes in voltage reference of Generators 1, 2, 3, and 4

where V_0 is the amplitude of the sinusoidal signal, ω is the angular frequency and ϕ is the phase. V is a representation of the signal $v(t)$ in phasor form. The diagram on the left hand-side of Figure 2.10 is the phasor representation of the sinusoid on the right of the figure. In electric power systems, voltage and current signals are measured as sinusoids which can be represented as phasors in magnitude and phase in the form of (2.25b). An observation of these two signals give important measures of the state of the electric power grid. For instance, bus voltage angles are important
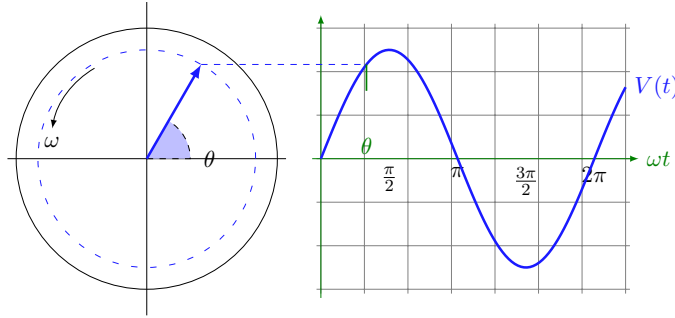
FIGURE 2.10: Phasor representation of a sine wave

indicators of the stress levels of an electric power grid. To illustrate, consider the simple system of Figure 2.11, representing the two boundary buses at two areas 1 and 2 separated by a tie line of reactance jX_{12}. The voltages at each bus are specified in magnitude V_1, V_2 and angles δ_1, δ_2 respectively. The real power transfer P_{12} across the tie line from Bus 1 to Bus 2 is given by (2.26). Clearly, as long the voltage at both ends is non-zero, some amount of P_{12} can be pushed along the tie line if the angle difference $\Delta\delta_{12} = \delta_1 - \delta_2$ is also non-zero. However, this power transfer is maximum when $\Delta\delta_{12} = 90^o$, and the direction of transfer varies with the sign. Up to 90° when P_{12} is maximum, power transfer across the tie line increases, and along with it, the system stress level increases. This implies that the bus voltage angle must be accurately monitored at critical transmission corridors so that the point of maximum power transfer is not exceeded. In order to do this, a fairly accurate idea of the voltage angles at the two buses *at the same time* is needed.

Measurements of phasor quantities must therefore be synchronised for accurate comparison and analysis. The accuracy is especially desired at the distribution end because the angles are generally smaller than those on the transmission network. A method of time-tagging these phasor measurements proceeds from this necessity. This is discussed next in Section 2.5.1.
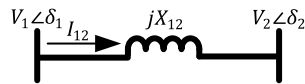
FIGURE 2.11: A simple two-bus system

$$P_{12} = \frac{V_1 V_2}{X_{12}} \sin(\delta_1 - \delta_2) \tag{2.26}$$

Other power system quantities can be estimated from voltage and current signals. For example, the complex power $\hat{S}_{ij}$ transmitted across the tie line can be obtained from current phasor $I_{ij}e^{j\delta_{ij}}$ and voltage phasor $V_i e^{j\delta_i}$ as in (2.27).

With non-sinusoidal signals, the calculation of the reactive power is not quite straightforward.

$$\hat{S}_{ij} = V_i e^{j\delta_i} \{I_{ij}e^{j\delta_{ij}}\}^* = P_{ij} + jQ_{ij} \tag{2.27}$$

Where P_{ij} and P_{ij} are the real and reactive power represented by the real and imaginary parts of the complex power $\hat{S}_{ij}$, respectively. Others like include frequency measurements which can be

obtained from the rate of change of bus voltage angles.

2.5.1   Practical measurements of phasors

Synchronised phasors facilitate accurate measurements and analyses of current situations in various parts of the electric power system. Most importantly, control systems and stability indicators rely on coherent sets of data which may be provided by PMUs to estimate, effectively, control signals and state predictions respectively. In contrast to the conservative approach stemming from a lack of observability, improved grid visibility is key to maximising the benefits of underutilised grid assets. This will aid in the effective balancing of operational and cost constraints in the face of increasing renewable energy integration.

As had been mentioned, power system quantities may be measured in phasor forms by using a phasor measurement unit or PMU. An image of a practical phasor measurement unit device is shown in Figure 2.12 [3].

FIGURE 2.12: A vendor's PMU device

PMUs are connected to the grid through transducers, such as potential and current transformers of sufficient burden, as shown in Figure 2.13. The figure shows three load buses that are connected to a generator through a transformer. A vendor's PMU is used to measure the potential difference on either side of transformers and to measure the branch currents along the three branches. It can be seen observed that the PMU is not connected directly to the lines as the voltage and current it measures have to be stepped down by the transducers to prevent damage to the measurement device. The PMU receives the scaled-down measures [4] of power system quantities in the form of analogue inputs and returns a synchronised phasors through a series of processes shown in the blocks of Figure 2.14.

The analogue signals are filtered within a limited bandwidth prevent anti-aliasing according to specific requirements. The filtered signals are then converted to digital forms through the Analogue-to-Digital converters (ADCs) that are disciplined to a Coordinated Universal Time (UTC)

---

[3]This image is the SEL-487E PMU, as obtained from Schweitzer Engineering Laboratory SEL-487E product brochure.

[4]Note that Instrument transformers introduce some amount of phase errors into the acquired signals. These errors are compensated for using appropriate phase compensation techniques.
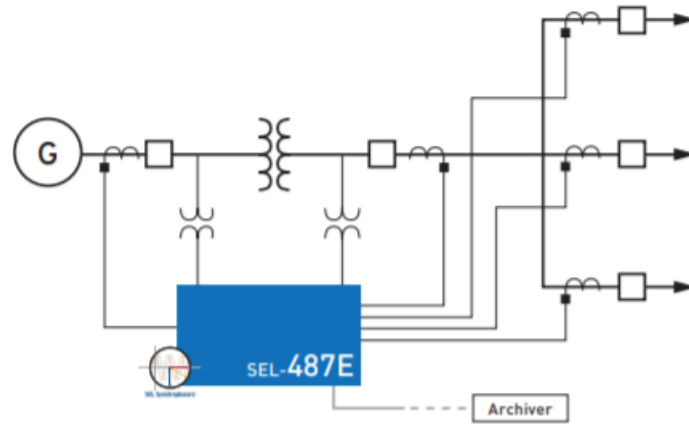
FIGURE 2.13: A typical PMU-grid connection
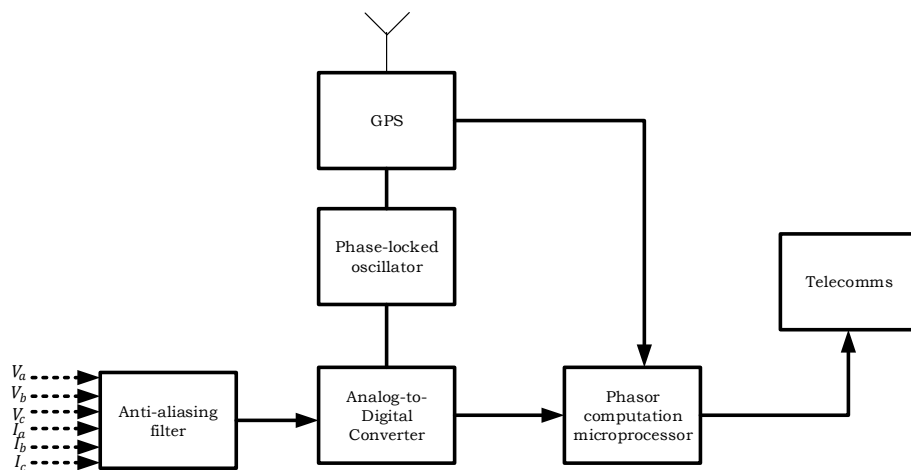
FIGURE 2.14: The phasor estimation process

with signals provided from a GPS. In the phasor computation stage, the digital samples of data are acquired over a period of time, and phasors are calculated using a chosen estimation technique [5]. These include Discrete Fourier Transform (DFT), weighted or adaptive[91] Least Squares (LS) method, or the adaptive mimic phasor estimator (AMPE) [92]. The phasors are transmitted via User Datagram Protocol (UDP) or Transmission Control Protocol (TCP) in the Telecommunications stage to PDC where they are time-aligned, archived, and stored for analysis. UDP and TCP transmission are different in whether or not a confirmation of receipt is obtained before sending the next packet of data. For the UDP, no acknowledgement is necessary; this enables faster transmission of data[6] without guarantee that the data will be received as sent. Lost packets of data are not resent. In the TCP, transmitted packets of data are checked for errors and an acknowledgement of receipt is sent by the recipient, otherwise the packets are sent again.

---

[5]The phasor may be disciplined to the GPS at the phasor computation stage as well. However, disciplining to the ADC eliminates timing error [90]

[6]This may not be the case at all times. In some instances, TCP may be faster than UDP.
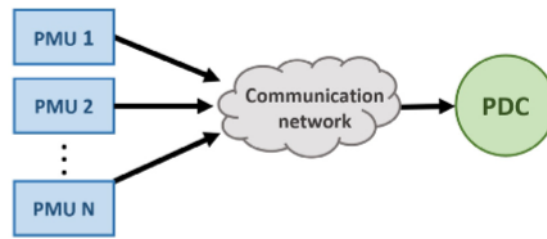
FIGURE 2.15: PMU-PDC Communication [98]

Global Navigation and Satellite System

PMUs require high-precision time synchronisation which are provided by terrestrial or extra-terrestrial clocking signal sources. The most common type of timing signal source is the GPS, which can be used to determine the coordinates of the receiver of the synchronising or timing signals. The accuracy of synchronisation of phasor data is affected by how well time delay corrections has been made within the GPS device and the manner in which the antenna has been set up. It is recommended that GPS antennae have a clear, unobstructed view of the sky. Some vendors provide for the loss of synchronisation signals by allowing the PMU to generate its own internal pulses for a number of seconds, allowing for restoration of synchronisation signals [93]–[95]. Clocking signals may also be provided by other GPS-like devices, such as China's Beidou Navigation Satellite System, and Russia's Global Navigation Satellite System (GLONASS) [96]. All clocking devices are described generically as Global Navigation and Satellite Systems (GNSS). They all produce highly accurate timing and accuracy. However, differences exists between the technologies, in terms of accuracy and strength of coverage. For example, the GLONASS provides accuracy between 5-10m while the GPS provides the accuracy up to between 3.5-7.8m. GLONASS coverage is provided by 31 satellites and GPS's by 24. However, the strength of coverage of GPS is better than that of the GLONASS.

The synchrophasor reference is provided by the UTC from a suitably accurate GNSS. The accuracy of the GNSS is particularly important to reduce error. For example, a time error of 1μs corresponds to a phase error of 0.022 degrees for a 60 Hz system and 0.018 degrees for a 50 Hz system. This is particularly important in view of the fact that 0.57^0 phase error is already equal to the maximum error allowed for all output measurements in the standard [97].

2.5.2 Phasor Data Concentrators

The phasor data concentrator is a platform for managing and processing synchrophasors in real-time. The complete WAMS is a PMU, the communication infrastructure, and the PDC.

Synchrophasor measured by the PMU are sent through a selected communication medium to the PDC where they are time-aligned and timestamped, archived and transmitted as an single output stream of data to other PDCs or to a control centre for analysis.

PMU-PDC communication may be a simple structure, such as shown in Figure 2.15 where multiple PMUs connect to only one PMU or take at a higher level in a hierarchical structure, of the form proposed by the IEEE standard C37.244-2013 [99] and shown in Figure 2.16 where local PMUs connect to a local PDC and all local PDCs within a region are connected to a regional PDC. All regional PDC then connect to a central or super PDC. The scheme facilitates data sharing between
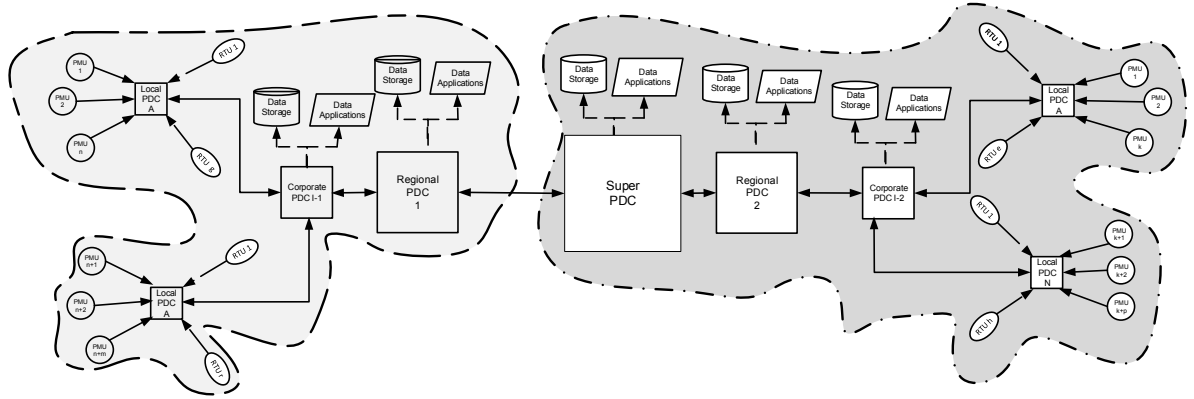
FIGURE 2.16: PDC Hierarchy, (as in [99])

local utilities without compromising a wide area visualisation and centralisation of data storage and analysis.

On account of the sheer volume of data generated by the PMUs, the PDC at all levels must have considerable data storage capacities. It is certain that, a suitable communication medium, cloud-based PDCs could be a viable alternative in the not-so-distant future.

2.5.3   IEEE Standards for Phasor Measurements and Communications

In order to encourage the use of PMUs, the IEEE developed a number of standards [99]–[101]. The IEEE standard 1344 was the precursor of synchrophasor measurement standards. It was introduced in 1995 to harmonise synchrophasor definitions and measurements. The intent of the IEEE 1344 was to specify a synchrophasor platform where measurements can be easily interfaced with other systems. However, the standard provided only loose definitions of phasors and synchrophasors measured at nominal frequency. This led to ambiguity in phasor measurements at off-nominal frequencies. In addition, specifics of data communication was left largely to interpretations by vendors and end-users. The IEEE C37.118-2005 [100] removed the ambiguity in synchrophasor definition by provided a clearer description which avoided references to specific frequencies. Instead, it defined the synchronised phasor in terms of a time shift between positive peaks of waveforms. Furthermore, it combined the errors in estimating phase, magnitude and timing into a single error known as the Total Vector Error (TVE) which is calculated using (2.28).

$$\text{TVE} = \sqrt{\frac{(\text{Re}(\boldsymbol{X}) - \bar{\boldsymbol{X}})^2 + (\text{Im}(\boldsymbol{X}) - \bar{\boldsymbol{X}})^2}{\text{Re}(\boldsymbol{X})^2 + \text{Im}(\boldsymbol{X})^2}} \tag{2.28}$$

for a sinusoidal signal $\boldsymbol{X} = \text{Re}(\boldsymbol{X}) + \text{Im}(\boldsymbol{X})$ with an actual value $\bar{\boldsymbol{X}}$. Figure 2.17 is a visualisation of the TVE. It shows the error in the measured($\bar{V}_1$) and true value ($\bar{V}_1^{\text{true}}$) of a voltage magnitude measurement. The figure also shows the error in phase and time synchronisation between estimation of the error for a voltage angle measurement $\angle V_1$ and that of another voltage phasor $\boldsymbol{V}_2(\angle V_2)$ which is referenced to the same time frame as $\boldsymbol{V}_1$. The TVE is required to be less than 1% across the three quantities of magnitude, phase and timing synchronisation. In addition, two performance levels —Level 0 and Level 1 —were specified for measurements at off-nominal frequency. The Level 0 required the TVE accuracy for measurement at ± 0.5 Hz of nominal, while Level 1 rules
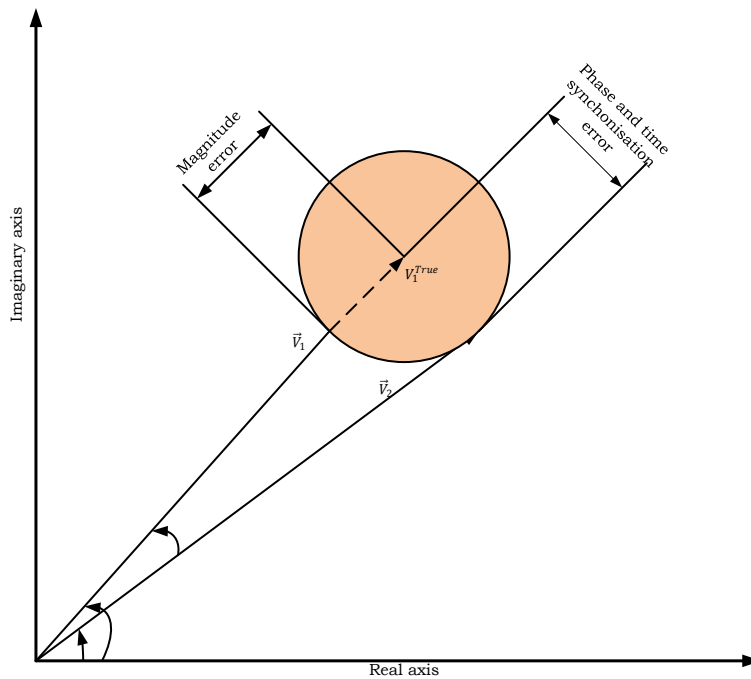
FIGURE 2.17: Total Vector Error (TVE)

that the accuracy specification still holds at ± 5 Hz of nominal. However, instances of applications where the levels are required are not clearly distinguished. Consequently, end-users have been known to request Level-1 PMUs when Level-0 devices would have sufficed [102]. IEEE C37.118-2005 standard was markedly different from the IEEE 1344 not only in the ease of interpretation, but also in synchrophasor definition, error specification, and introduction of performance levels, but also in the specifications of time tagging and communication protocol specifications than were originally available in the previous standard. However, IEEE C37.118-2005 focused on the quality of the output but does not specify the sampling rate, algorithm, synchronisation method, or performances under transient conditions. Furthermore although it requires the provision of frequency and Rate of Change of Frequency (ROCOF) as part of the synchrophasor measurements, it does not specify any method for the calculation of ROCOF. Consequently, PMU measurements, especially under various non-stationary conditions, will vary from one manufacturer to another even when the vendors conform to a either Level 0 or Level 1 performance [103].

The IEEE and International Electrotechnical Commission (IEC) began a collaboration in 2009 to harmonise the communication protocols which were spelt out in the C37.118 standard to conform with the IEC 61850 communication standard. This led to the development of the IEC/TR 61850-90-5:2012(E) which provided specifications for data exchange between PMUs, PDCs and Wide Area Monitoring, Protection and control (WAMPAC), and between control systems. In 2011, separate standards were introduced for data communication and measurements in order to address the growing technology in each area and to harmonise standards with the IEC. The single IEEE C37.118-2005 standard which contained combined specifications of measurement and data communication were replaced with the IEEE C37.118.1-2011[97] and IEEE C37.118.2-2011[101] standards for measurement and communication specifications respectively. Performance levels Level 0

and Level 1 were replaced with performance classes P and M in order to clarify the types of performances required for specific applications. P-class PMUs are to be used for protection applications where less filtering but faster responses are required, and M-class PMUs for measurement systems which require extensive filtering but slower response. It specifies requirement for latency (defined as the time difference between when a signal arrives at the input of the PMU and the time it arrives the output) to be,

$$t_d \leq \frac{1}{4 \times F_s} \tag{2.29}$$

which is to be no more than $\frac{2}{F_s}$ for P-class PMUs and less than $\frac{7}{F_s}$ for the M-class. F_S is the PMU reporting rate.

2.5.4   Estimations of derived quantities under non-sinusoidal signal conditions

Phasor measurements works well for sinusoids. However, the estimation of some derived quantities, such as active and reactive powers, is not straightforward for non-sinusoidal voltage and current signals. The non-sinusoidal signals are composed of signals of different frequencies that are different from the fundamental. A number of works have been developed [104], [105] to address this problem. Many works have attempted to a solution to this problem, with varying degrees of success and shortcomings. In the following, the effort in [104] is described and analysed with insights from [105]. Given a non-sinusoidal voltage signal v and a non-sinusoidal current signal with amplitudes V_m and I_m respectively,

$$P = \sum_h V_m I_m \cos \phi_h \tag{2.30a}$$

$$Q = \sum_h V_m I_m \sin \phi_h \tag{2.30b}$$

$$\tag{2.30c}$$

where h is the harmonic factor and (2.30) is a sum of the product of the voltage and current over all harmonic frequencies for both active and reactive powers.

Equation (2.30) is valid for a periodic but nonsinusoidal signal. However, it was shown [104] that the sum of the square of P and Q in this way is not equal to the apparent power, S

$$S^2 \neq P^2 + Q^2 \tag{2.31}$$

A distortion factor D can be used to make up the difference such that

$$S^2 = P^2 + Q^2 + D^2 \tag{2.32}$$

$$\sum_{k=0}^{H-1} \sum_{h=k+1}^{H} \left[V_k^2 I_h^2 + V_h^2 I_k^2 - 2 V_h V_k I_h I_k \cos (\phi_h - \phi_k) \right]; \tag{2.33}$$

The sum of the reactive power computed according to (2.30) is equal to zero at a power system node. In addition, when no other frequencies apart from the fundamental are present in the signal, $D = 0$. However, there are some issues with this process [105].. First, there is no certainty of

obtaining a unity power factor if the reactive power is zero, as may happen for purely resistive loads. Secondly, measuring the power directly requires a meter which has a unity amplification factor and a 90^0 angle displacement for all frequencies.

The IEEE standard [106] describes the procedures for estimating these quantities under balanced and unbalanced sinusoidal and non-sinusoidal conditions. However, the equations are somewhat involved for three-phase unbalanced non-sinusoidal signals and will not be included. It would suffice to say here the non-straightforwardness of the reactive power estimation under non-sinusoidal conditions is a severe limitation for synchrophasor-based applications.

2.5.5   Phasor measurements at an off-nominal frequency

Power system quantities can be assumed to be constant over a measurement period under a steady-state condition. The phasor angles may be estimated using the convention shown in Figure 2.18.
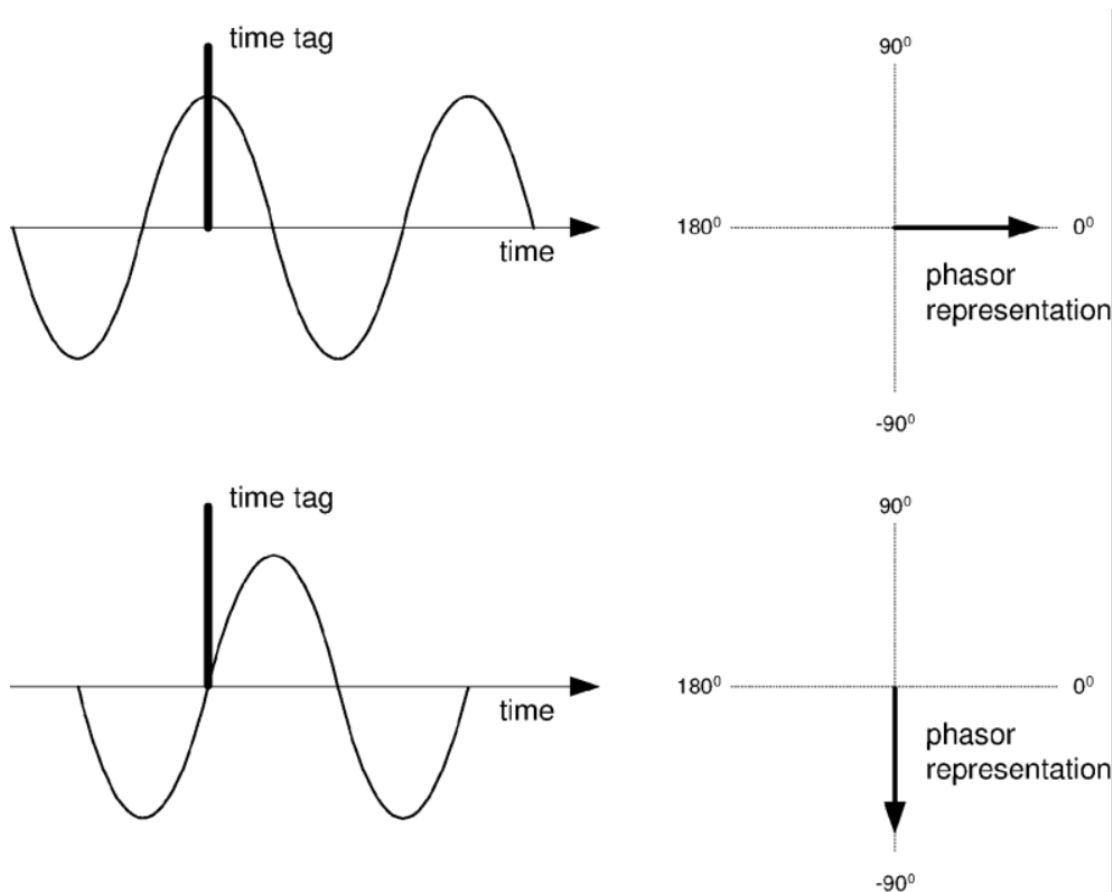
FIGURE 2.18: Angle convention [103]

The possibility of computing phasors from sinusoids rides on the assumption that the sinusoid is pure. If they are not, as is the case when the signal is corrupted with harmonics or transients, a number of different frequencies may be present. Under this condition, phasor computation becomes possible only if all but one of the frequencies are filtered from the signal.

A method of calculating phasors for signals off-nominal but constant amplitude is described in [97]. Given a sinusoidal signal $x(t)$ of the form of (2.34)

$$x(t) = X_m \cos(\omega_0 t + \phi) \tag{2.34}$$

where $\omega_0 = 2\pi f_0$ is the nominal angular frequency and f_0 is the nominal frequency. ϕ is the phase. If f is the offnominal frequency, then the deviation between the nominal and offnominal frequency may be given by

$$\Delta f = f - f_0$$

and if ω_0 in the signal $x(t)$ is replaced with the offnominal angular frequency ω_0, then (2.34) can be written as:

$$x(t) = X_m \cos\left(\int 2\pi f \mathrm{d}t + \phi\right) \tag{2.35}$$

Note all parameters in the equations (2.34) and (2.35) are functions of time. This means that *Deltaf* is also a function of time.

$$x(t) = X_m \cos\left(2\pi \int (f_0 + \Delta f)\mathrm{d}t + \phi\right) \tag{2.36}$$

$$x(t) = X_m \cos\left(2\pi \int f_0 \mathrm{d}t + (2\pi \int \Delta f \mathrm{d}t + \phi)\right) \tag{2.37}$$

$$x(t) = \frac{X_m}{\sqrt{2}} \mathrm{e}^{(2\pi \int \Delta f \mathrm{d}t + \phi)} \tag{2.38}$$

If $X_m(t)$ is constant and Δf is also constant, then the measured phasor will have a uniform rate of change $2\pi\Delta f T_0$ at $f \neq 0$ and $f < 2f_0$. This means that the measured phasor will always wrap around $\pm 180^0$.

2.5.6   Phasor measurements under transient conditions

Electrical events such as faults and switching actions as well as electromechanical actions like the dynamic movements of rotors of motors and generators each cause a degree of transients in the power system. Electromechanical transients can be described using the sinusoidal model (2.39).

$$x(t) = X_m \cos(\omega t + \Theta_0) \tag{2.39}$$

When measuring phasors under this transient condition, the phasors' phase angles and magnitudes change more slowly than the nominal system frequency such that they are almost constant within a short time frame.

On the other hand, electrical transients can be illustrated using Figure 2.19 [103]. The figure is a plot of a signal under a transient conditions. Portions of the signals are selected 3 different data windows; *window 1, window 2,* and *window 3*. Window 1 is the pre-transient data window, window 2 contains a combination of pre-transient, transient, and post-transient window, while window 2 is composed of mainly post-transient data. With window 1 and window 3, the phasor computation is quite straightforward. However, for window 2, there would be sharp changes in phase angles

as events evolve from the pre-transient to transient and then to the post-transient stage. Note that frequency and ROCOF is calculated from the phase angle as in (2.40), (2.41), and (2.42).

$$\omega = \frac{d\theta}{dt} \implies \dot{\theta} = \omega \tag{2.40}$$

Since $\omega = 2\pi f$, this makes the frequency calculable by,

$$f = \frac{1}{2\pi} \frac{d\theta}{dt} \tag{2.41}$$

$$ROCOF = \frac{df}{dt} \tag{2.42}$$

This means that step changes in the phase angles will be amplified in its first and second deriva-
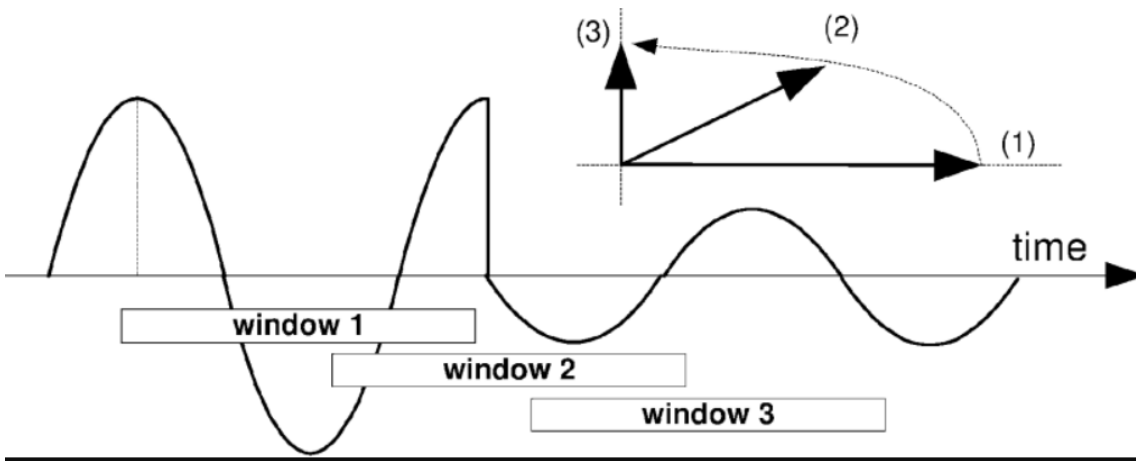
FIGURE 2.19: Phasor transition during electrical transients [103]

tives. [7] These will be seen as sharp spikes in a visualisation of the phasor measurements, but does not reflect the actual change. It is important to take note of the limitations of the PMU in this regard, especially when measurements of the ROCOF and frequency are critical to a synchrophasor application.

In summary, when measuring phasors under transient conditions, actual actual changes may be faster than the PMU measures under electromechanical transients while the measurements may be faster and spurious than actual changes in system conditions when measuring electrical changes.

A degree of measurement fidelity is required from PMUs for reliable performance. A range of tests are specified in the IEEE standard to evaluate measurement accuracies under various conditions. Some of the tests described by the IEEE C37.118.1-2011 [101] will be discussed next.

2.5.7 Static and dynamic performances of phasor measurement units

If the measured power system quantities is not a pure sinusoid —with constant period and frequency—of the form shown in Figure 2.10, it is important to point out that phasor computations will not be straightforward. The incidence of non-sinusoidal signals happen with transients and

---

[7]In this second derivative, i.e. ROCOF, the change will be even higher.

with harmonics.[8]. In this vein, it is possible to analyse the PMU's performance under two operating conditions; at a constant frequency or *steady state* and under a non-constant frequency condition or *dynamic state*. Various IEEE standards, discussed in Section 2.5.3 have been developed to address the accuracy of measurements under the two conditions. The degree of compliance of the PMU to defined standard metrics are measured by the steady-state or dynamic performances.

Measurements of phasors under steady-state conditions

The steady-state of a power system is a condition under which the amplitude, angular frequency and phase are fixed for a period of time. In this context, the time span would correspond to the period of measurement. The steady-state performance of the PMU is measured by the difference between the measured value and the corresponding theoretical values of the real and imaginary parts of the voltage and current phasors, the frequency, and the rate of change of frequency. For the P-class PMU, the IEEE Std C37.118.1-2011 [101] defines a maximum of 1% TVE for frequency measurements that are within ± 2Hz regardless of the reporting rate of the PMU. On the other hand, the range of frequency for which the maximum TVE cannot be allowed to exceed 1% is a function of the reporting rate of a M-class PMU.

$$\pm 2.0, \text{Hz}, \qquad \text{for } F_s < 10$$

$$\pm \frac{F_s}{5}\text{Hz}, \qquad \text{for } 10 \leq F_s < 25$$

$$\pm 5.0\text{Hz}, \qquad \text{for } F_s < 25$$

where F_s is the reporting rate Additional TVE metrics are specified for the P and M-class PMUs at different ranges of frequency, ROCOF, harmonic distortion, and out-of-band interference. This may be found in [101].

Measurements of phasors under dynamic conditions

Three tests are specified for evaluating the dynamic performance of the PMU in the IEEE standard C37.118.1-2011 [97]. These include the measurement bandwidth test, ramp in frequency test, and the step change in amplitude test. These can be evaluated on a system of equations representing sinusoidal signals X_a, X_b, and X_c, as in (2.43). Note that $a, b,$ and c are the phases of the three-phase input sinusoidal signal.

$$X_a = X_m \left[\cos \left(\omega_0 t \right) + \cos \left(\omega t - \pi \right) \right] \tag{2.43a}$$

$$X_b = X_m \left[\cos \left(\omega_0 t - \frac{2\pi}{3} \right) + \cos \left(\omega t - \pi \right) \right] \tag{2.43b}$$

$$X_c = X_m \left[\cos \left(\omega_0 t + \frac{2\pi}{3} \right) + \cos \left(\omega t - \pi \right) \right] \tag{2.43c}$$

1. **Measurement Bandwidth test:** A PMU's dynamic performance may be tested by modulating the sinusoidal amplitude and phase [101]. where X_m is the amplitude of the input signal, ω_0 is the nominal power system frequency, ω is the modulation frequency in radian/s. By

---

[8]Techniques for removing harmonics exist, so this is not quite an issue in phasor computation.

modulating the amplitude and phase of the signals by factors k_x and k_a respectively, (2.43) becomes:

$$X_a = X_m \left[1 + k_x \cos(\omega t)\right]\left[\cos(\omega_0 t) + k_a cos(\omega t - \pi)\right] \tag{2.44a}$$

$$X_b = X_m[1 + k_x \cos(\omega t)] \left[\cos(\omega_0 t - \frac{2\pi}{3}) + k_a cos(\omega t - \pi)\right] \tag{2.44b}$$

$$X_c = X_m[1 + k_x \cos(\omega t)] \left[\cos(\omega_0 t + \frac{2\pi}{3}) + k_a cos(\omega t - \pi)\right] \tag{2.44c}$$

Recall that three-phase electrical signals can be represented in positive, negative, and zero sequences. A positive-sequence representation, X_p of (2.44) is (2.45).

$$X_p = X_m[1 + k_x \cos(\omega t)][\cos(\omega_0 t) + k_a cos(\omega t - \pi)] \tag{2.45}$$

The evaluation of the PMU's dynamic performance is thus focused on how well its positive sequence measurements conforms to the actual values of the signals. If $t = nT$, then the phasor representation of (2.45) should be:

$$X_p = X_{\text{rms}}[1 + k_x \cos(\omega nT)] \angle (k_a cos(\omega t - \pi)) \tag{2.46}$$

where $X_{\text{rms}} = \frac{X_m}{\sqrt{2}}$ is the root mean square value of the signal amplitude. The PMU is deemed to conform to standard if the TVE does not exceed the values given in Table 2.2 over the stated frequency range.

TABLE 2.2: Synchrophasor measurement bandwidth requirements using modulated test signals [101]

Modulation level (radian)	Reference Condition	Minimum range of influence quantity over which PMU shall be within given TVE limit			
		P class		M class	
		Range	Max TVE	Range	Max TVE
$k_x = 0.1$, $k_a = 0.1$	100% rated signal magnitude, f_{nom}	Modulation frequency 0.1 to lesser of $\frac{Fs}{10}$ or 2 Hz	3%	Modulation frequency 0.1 to lesser of $\frac{Fs}{5}$ or 5 Hz	3%
$k_x = 0.1$, $k_a = 0.1$	100% rated signal magnitude, f_{nom}		3%		3%

The requirements on the frequency error (FE) and the rate of change of frequency error (RFE) are as given in Table 2.3.

For further evaluation of the dynamic performance, two other tests are specified by the IEEE C37.118.1-2011. These are the frequency ramp test and the step change in amplitude.

TABLE 2.3: Frequency and ROCOF performance requirements under modulation tests [101]

Modulation level, reference condition, range (use the same modulation levels and ranges under the reference conditions specified in Table 2.2	Error requirements for compliance			
	P class		M class	
	Max FE	Max RFE	Max FE	Max RFE
$F_s > 20$	0.06 Hz	3 Hz/s	0.3 Hz	30 Hz/s
$F_s \leq 20$	0.01 Hz	0.2 Hz/s	0.06 Hz	2 Hz/s

2. **System Frequency Ramp Test:** In this text, the three-phase signal frequency is ramped up linearly according to (2.47)

$$X_a = X_m[\cos(\omega_0 t) + \pi R_f t^2] \tag{2.47a}$$

$$X_b = X_m[\cos(\omega_0 t - \frac{2\pi}{3}) + \pi R_f t^2] \tag{2.47b}$$

$$X_c = X_m[\cos(\omega_0 t + \frac{2\pi}{3}) + \pi R_f t^2] \tag{2.47c}$$

The description of the parameters in (2.48) remain unchanged from those defined in (2.45). R_f is a constant ROCOF or ramp rate. Again, the positive-sequence form X_p of the three-phase signal in (2.47) is as shown in (2.48).

$$X_p = X_m[\cos(\omega_0 t) + \pi R_f t^2] \tag{2.48}$$

With $t = nT$, this can be represented in phasor form as,

$$X(nT) = X_{\text{rms}} \angle \pi R_f (nT)^2] \tag{2.49}$$

The standard required a TVE of 1% for both P and M-class PMUs for a linear ramp rate $R_f = \pm 1.0 \text{Hz/s}$. For P class PMUs, the specification of the TVE is for a frequency which vary ± 2 Hz. The frequency range for the test for M-class PMU is the minimum of ± 5Hz above or below the reporting rate. The errors in frequency and ROCOF are not allowed to exceed 0.01Hz and 0.1Hz/s respectively for P-class PMUs, and 0.005Hz and 0.1Hz/s respectively for M-class PMUs.

3. **Step Changes in Phase and Magnitude Test:** This test is carried out by applying a three-phase step response test of the form shown in (2.50).

$$X_a = X_m[1 + k_x f_1(t)][\cos(\omega_0 t) + k_a f_1(t)] \tag{2.50a}$$

$$X_b = X_m[1 + k_x f_1(t)][\cos(\omega_0 t - \frac{2\pi}{3}) + k_a f_1(t)] \tag{2.50b}$$

$$X_c = X_m[1 + k_x f_1(t)][\cos(\omega_0 t + \frac{2\pi}{3}) + k_a f_1(t)] \tag{2.50c}$$

In a similar vein to the other test descriptions, the positive sequence and phasor representations of (2.50) as shown in (2.51) and (2.52) respectively.

$$X_a = X_m[1 + k_x f_1(t)][\cos(\omega_0 t) + k_a f_1(t)] \tag{2.51}$$

$$X_a = X_{\mathrm{rms}}[1 + k_x f_1(t)][\cos(\omega_0 t) + k_a f_1(t)] \tag{2.52}$$

The step response test would seek to measure the PMU response time, the delay time, and the overshoot percentage within 10 tests. More details on the steps and on the general requirements may be found in [97].

2.5.8 State estimation

Phasor measurements from WAMS sources are subject to the fickleness of telemetry and measurement devices. In the most ideal state, it is desired that WAMS data are obtained the measurement devices for onward transmission to the points of application. However, in practice, a number of events may prevent the direct applications of measured phasors. These include the failure of equipment and/or communication lines (resulting in the loss of data) and the presence of bad data such as outliers. For this reason, phasor data are only used after they have been processed using state estimation techniques [37], [107]. This technique involves the assignment of values to system states, based on the system's measurements. The degree of confidence in a measured data is usually a function of the measurement device accuracy. The state estimation process involves data
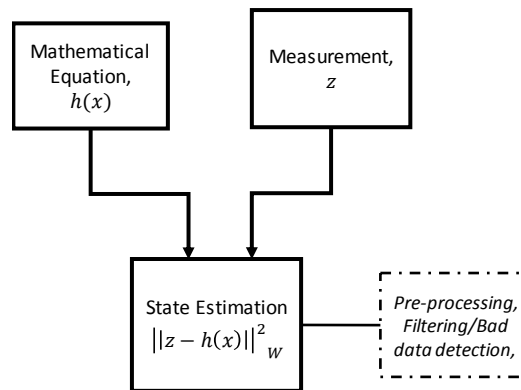
FIGURE 2.20: State Estimation concept

pre-processing to remove the mean, bad data detection, and filtering. In essence, the state estimation process seeks to minimise the deviation of measured values from their true states. Given

m samples of measurements $\boldsymbol{z} \in \mathbb{R}^m$ and an equation $\boldsymbol{h(x)} \in \mathbb{R}^m$ representing the true value of the states, an estimate $\hat{\boldsymbol{x}}$ can be obtained from a weighted least-squares minimisation of the error $\boldsymbol{e} \in \mathbb{R}^m = \boldsymbol{z} - \boldsymbol{h}$,

$$J(x) = \|\boldsymbol{e}\|_{\boldsymbol{W}}^2 \tag{2.53}$$

where $\boldsymbol{x} \in \mathbb{R}^n$ is the vector of system states, and $\boldsymbol{W}$ is a diagonal matrix whose non-zero elements represent the expected accuracy of the measurement devices used in obtaining the corresponding state measurements. The estimated states are given as $\hat{\boldsymbol{x}}$ to differentiate them from unestimated states $\boldsymbol{x}$. In this work, it is assumed that the measurements used have been estimated.

2.6   The receding horizon control (RHC) concept

The receding horizon control (RHC)concepts [108], [109] is a form of feedback control in which a set of inputs are determined over a fixed time horizon by solving an optimisation problem at every time step. The traditional form of the RHC uses an infinite time horizon. However, the computational intractability of the infinite-horizon motivates the adoption of the more tractable finite-horizon RHC [9]. The first of the determined control variables is then applied to a system under study. After the inputs have been applied, measurements are taken, and the control inputs over the same horizon are re-calculated, and the first of them applied again. Estimating solutions over a time horizon means that future quantities are taken into consideration. However, only a set of available measurements are used to determine the inputs over this time period. In contrast to classical feedback controllers, RHC is more complex as it involves solutions of an optimisation problem at every time step. Another name for receding horizon control is model-based predictive control (MPC), implying that the control is based on a model and involves predictions of the model's future states over a time horizon. This model may be a linearised form of a non-linear system —in which case Linear Model Predictive Control principles may be used —or may be in the non-linear form, this requiring more advanced Non-linear Model Predictive Control (NMPC) methods. The model could also be in the continuous-time or discrete-time form.

In this project, the focus will be on the more tractable solution over a finite horizon, using discrete-time linear models of the form described by (2.54). In power systems analyses, (2.54) can be realised by *discretising* the linearised models described in Section 2.4.

$$\begin{aligned} x[k+1] &= Ax[k] + Bu[k] \\ y[k] &= Cx[k] \end{aligned} \tag{2.54}$$

where y is the output, x is the state, A, B, C are state, input and output matrices respectively at time k. If k in (2.54) is the current time step and N is the finite horizon, then the evolution of the model from $k = 0, \dots, N$ can be written as in (2.55). The steps involved in solving a finite-horizon MPC problems given a discrete-time LTI model (2.54) are as follows [15], [108], [109]:

---

[9]The RHC formulations in this thesis will focus on the finite time horizon.

First, the model is reproduced over the time horizon, N.

$$
\begin{aligned}
x[1] &= Ax[0] + Bu[0] \\
x[2] &= Ax[1] + Bu[1] \\
&\vdots \\
x[N] &= Ax[N-1] + Bu[N-1]
\end{aligned}
\tag{2.55}
$$

$x[k]$ can be combined into a single equation in $x[k+1]$. For example,

$$
x[2] = A\left[Ax[0] + Bu[0]\right] + Bu[1]
\tag{2.56}
$$

The process is repeated for all $x[k]$

$$
\begin{aligned}
x[2] &= A^2 x[0] + ABu[0] + Bu[1] \\
x[3] &= \left[A^3 x[0] + A^2 Bu[0] + ABu[1]\right] + Bu[2] \\
&\vdots \\
x[N] &= A^{N_p} x[0] + \sum_{k=0}^{N-1} A^{N-(k+1)} Bu[k]
\end{aligned}
\tag{2.57}
$$

Given that $y[k] = Cx[k]$ (from (2.54)), then by advancing one time step,

$$
y[k+1] = Cx[k+1]
\tag{2.58}
$$

And (2.54) can then written as,

$$
y[N] = Cx[N] = CA^N x[0] + \sum_{k=0}^{N-1} CA^{N-(k+1)} Bu[k]
\tag{2.59}
$$

In summary, the discrete-time model can be combined into a single equation over the time horizon N, as in (2.60) and (2.61).

$$
\underbrace{\begin{bmatrix} y[1] \\ y[2] \\ \vdots \\ y[N] \end{bmatrix}}_{\boldsymbol{y}} = \underbrace{\begin{bmatrix} CA \\ CA^2 \\ \vdots \\ CA^N \end{bmatrix}}_{\boldsymbol{G_x}} \hat{\boldsymbol{x}} + \underbrace{\begin{bmatrix} CB & \mathbf{0} & \mathbf{0} & \cdots & \mathbf{0} \\ CAB & CB & \mathbf{0} & \ddots & \mathbf{0} \\ \vdots & \ddots & \ddots & \ddots & \vdots \\ CA^{N-1}B & CA^{N-2}B & \cdots & CAB & CB \end{bmatrix}}_{\boldsymbol{\Gamma}} \underbrace{\begin{bmatrix} u[0] \\ u[1] \\ \vdots \\ u[N_c-1] \end{bmatrix}}_{\boldsymbol{u}}
\tag{2.60}
$$

$$
\boldsymbol{y} = \boldsymbol{G_x}\hat{\boldsymbol{x}} + \boldsymbol{\Gamma}\boldsymbol{u}
\tag{2.61}
$$

Given that (2.62) is the optimisation problem to be solved at every time step,

$$\underset{\boldsymbol{u}_0,\dots,\boldsymbol{u}_{N-1}}{\text{minimize}}\ \boldsymbol{f}(\hat{\boldsymbol{x}},\boldsymbol{u}) = \sum_{k=1}^{N}\left(\boldsymbol{y}[k+1]-\boldsymbol{r}[k+1]\right)^T\boldsymbol{Q}\left(\boldsymbol{y}[k+1]-\boldsymbol{r}[k+1]\right) + \sum_{k=0}^{N}\boldsymbol{u}[k]^T + \boldsymbol{R}\boldsymbol{u}[k]$$

$$(2.62a)$$

subject to $\boldsymbol{y}[k+1] = \boldsymbol{C}\boldsymbol{A}\boldsymbol{x}[k+1] + \boldsymbol{C}\boldsymbol{B}\boldsymbol{u}[k+1] \qquad k = 0,1,\dots,N$ $\qquad\qquad(2.62b)$

The constraint (2.62b) is the reason for nomenclature model-based control. Over the horizon N, the cost function in (2.62a) may be combined into a single form as in (2.63a) and the model constraint (2.62b) may be written in the form of (2.61).

$$\min_{\boldsymbol{u}}\boldsymbol{f}(\hat{\boldsymbol{x}},\boldsymbol{u}) = (\boldsymbol{y}-\boldsymbol{r})^T\boldsymbol{Q}\left(\boldsymbol{y}-\boldsymbol{r}\right) + \boldsymbol{u}^T\boldsymbol{R}\boldsymbol{u} \qquad\qquad(2.63a)$$

$$\text{subject to } \boldsymbol{y} = \boldsymbol{G_x}\hat{\boldsymbol{x}} + \boldsymbol{\Gamma}\boldsymbol{u} \qquad\qquad(2.63b)$$

Then (2.63) can be transformed into an unconstrained equation (2.64) as,

$$\underset{\boldsymbol{u}}{\text{minimize}}\ \boldsymbol{f}(\hat{\boldsymbol{x}},\boldsymbol{u}) = (\boldsymbol{G_x}\hat{\boldsymbol{x}} + \boldsymbol{\Gamma}\boldsymbol{u} - \boldsymbol{r})^T\boldsymbol{Q}\left(\boldsymbol{G_x}\hat{\boldsymbol{x}} + \boldsymbol{\Gamma}\boldsymbol{u} - \boldsymbol{r}\right) + \boldsymbol{u}^T\boldsymbol{R}\boldsymbol{u} \qquad(2.64)$$

$$\boldsymbol{f}(\hat{\boldsymbol{x}},\boldsymbol{u}) = \hat{\boldsymbol{x}}^T\boldsymbol{G_x^T}\boldsymbol{Q}\boldsymbol{G_x}\hat{\boldsymbol{x}} + 2\left(\hat{\boldsymbol{x}}^T\boldsymbol{G_x^T}\boldsymbol{Q}\boldsymbol{\Gamma} - \boldsymbol{r}^T\boldsymbol{Q}\boldsymbol{\Gamma}\right)\boldsymbol{u} - 2\left(\hat{\boldsymbol{x}}^T\boldsymbol{G_x^T}\boldsymbol{Q} - \boldsymbol{r}^T\boldsymbol{Q}\right)\boldsymbol{r} + \boldsymbol{u}^T\left(\boldsymbol{\Gamma}^T\boldsymbol{Q}\boldsymbol{\Gamma} + \boldsymbol{R}\right)\boldsymbol{u}$$

$$\frac{\partial\boldsymbol{f}}{\partial\boldsymbol{u}} = 2\left(\hat{\boldsymbol{x}}^T\boldsymbol{G_x^T}\boldsymbol{Q}\boldsymbol{\Gamma} - \boldsymbol{\Gamma}^T\boldsymbol{Q}\boldsymbol{\Gamma}\right) + 2\left(\boldsymbol{\Gamma}^T\boldsymbol{Q}\boldsymbol{\Gamma} + \boldsymbol{R}\right)\boldsymbol{u} = \boldsymbol{0} \qquad\qquad(2.65)$$

The optimal control input $\boldsymbol{u}^*$ for the unconstrained minimisation for the regulation is then,

$$\boldsymbol{u}^* = -\left(\boldsymbol{\Gamma}^T\boldsymbol{Q}\boldsymbol{\Gamma} + \boldsymbol{R}\right)^{-1}\left(\hat{\boldsymbol{x}}^T\boldsymbol{G_x^T}\boldsymbol{Q}\boldsymbol{\Gamma} - \boldsymbol{r}^T\boldsymbol{Q}\boldsymbol{\Gamma}\right) \qquad\qquad(2.66)$$

Only the first column of the optimal $\boldsymbol{u}^*$ is used. However, other constraints may exist in the optimisation (2.62), and may require cleverer formulation than had been done in (2.60) and may be found in MPC literature [15], [108], [109]. However, the form of (2.60) remains largely the same. For a wide area power system, the solution of the optimisation (2.62) is therefore not very feasible for real-time control. In the following section, a review of some endeavours in power system literature is undertaken.

2.6.1   Model-based predictive control systems in electric power systems

The quest to automate the control of systems is to reduce human intervention to the barest minimum when there are drastic actions that need to be taken to prevent voltage collapse. This requires monitoring systems events and taking actions based on pre-determined controls, or that which is calculated online based on an advanced control algorithm. The interest in MPC for power systems control has mainly been as a result of its good on-line capabilities, and the ease of adding on many constraints that define power systems physical limits into its formulation. Many references and proofs to the online capability of model-based predictive control (MPC) can be found in literature

Frequency & AGC	Voltage Control	Emergency Voltage Control	HVDC
[32], [33]	[21]–[31]	[17], [18]	[34], [35]

([15], [16], [110]) and therefore its suitability for online modulations of control inputs is well noted. MPC has been applied across many areas of power systems for around two decades, after successful applications of MPC in the process industry. It has been used for emergency voltage control [17], [18], system protection and dynamic security enhancement schemes, [19], [20], voltage control [21]–[28], in the prevention of cascading failures [29]–[31], in frequency and automatic generation control [32], [33] and in the frequency and coordinated supervisory control of multi-terminal HVDC grid [34], [35]. By far, the use of MPC for voltage control [17]–[19], [21]–[27], [29]–[31], [111]–[123] has been more widely researched in power systems circles since it was first introduced in [111] for secondary voltage control. In [111], a decoupled two-level finite-horizon decentralised MPC (assuming weak interactions between neighbouring areas) with reference modulations and linearised dynamic equations was used to drive pilot buses to their set-points.

On the whole, MPC applications in power systems differ in the type of models used for the prediction, the method through which control was achieved, and in the area of power systems research it was applied to. For example, traditionally, many linear MPC (LMPC) approaches rely on the use of state-space models, which may be derived from corresponding non-linear system equations. In power systems applications, these non-linear system equations are a combination of generator, turbine governor, automatic voltage control(AVR), exciter, power systems stabiliser (PSS) and load dynamic equations, in combination with algebraic powerflow equations. The state-space models of the system under study can then be realised by linearising these equations around variables of interests. This is the basis of the modelling in many MPC-based power systems research such as [17], [19] where a heuristic method was combined with predictive control for power systems protection and control, in [23], [33] where load shedding was used to achieve voltage stability, and in trajectory-sensitivity based methods of [18], [20], [22]. Trajectory sensitivity-based methods estimate the deviation of a system's response(to control inputs) from a nominal trajectory, and differ from the linearisation in [111] in that it is linearised around a non-linear and non-smooth trajectory and not around an equilibrium point [124]. The trajectory-sensitivity method of [117] sought to improve the performance of the MPC by evaluating the sensitivity of the voltage stability margin. In [25], [26], [28], the model is an offline powerflow-based sensitivity matrix which is used to scale the control input applied at a previous step. An alternative approach to model realisation and sensitivity-based methods was proposed in [27], using multi-input multi-output impulse response model, updated from an optimal powerflow-based simulations on another platform.

The computationally-intensive approach means that control signals may not be computed fast enough to be applied online in a *real*-timely manner. For instance, the trajectory sensitivity based approaches [22], [117], [125] require a complete knowledge of the system's model, which may be too complex for real-time operations, even in a decentralised sense, for reasonably large power networks. Estimating sensitivities via a linearised powerflow Jacobian may require continuous updates on changes in systems conditions through solutions of AC load flow equations, which are computationally

2.6.2 Research gap

This project seeks to fill the gap in literature in affordable optimal WAMS placement formulations and on the modelling and design of predictive secondary voltage control. The significance then lies in the description of a bottom-up approach to affordable model-free control design; considering placement of WAMS and controllers designed based on this system of measurement.

Each chapter in this thesis begins with a review of the literature, addressing the specific gaps that will be filled. However, the central idea in the placement and control methods that will be proposed are summarised in the following paragraphs.

The co-placements of critical communication links and the attendant practical costs of deploying WAMS have not been adequately modelled in literature. The focus of many WAMS placement literature have been on minimising the costs of WAMS. However, insights from industry [13], [49] show that the procurement cost only accounted for 5% of the total cost of WAMS installation. In addition, the availability of installation equipment such as instrument transformers have been reported to help reduce an originally-estimated total costs by 50%. Consequently, there is a need to adequately model these costs, account for the presence of important installation equipment, and include all factors which affect the costs of placement. These factors include the presence of multiple vendors and devices which are capable of functioning as PMUs. If indeed PMU functionalities can be activated in relatively cheaper devices, it makes sense to include their presence in formulations which seek to minimise the costs of placement. A formulation which returns an optimal solution depending on the range of parameters considered gives sufficiently clear ideas of the costs involved in deploying WAMS devices and promotes good planning for present and future deployments. In Chapter 3, the presence of multiple vendors and multiple data storage locations (PDCs) are considered along with the costs of laying communication infrastructure and labour in a proposed optimal placement formulation. In order to encourage the use of WAMS, different methods of spreading out the practical costs that have been considered must also be described. For all utilities, the benefits must be more than the costs. Multi-stage and application-sensitive placements methods will be described in Chapters 4 and 5 to address these.

In the second part of the work, the focus will be on the challenge of exhaustive mathematical modelling. In model predictive control literature that have been addressed in the previous sections, the main challenge has been on obtaining an adequate internal model on which the predictive controllers will be based. Most of the works depended on a knowledge of the system parameters and states which cannot be easily obtained or measured. This work addresses the modelling issues and proposes a number of model-free approaches in the later chapter. The proposed controllers are simulated in a real-time set-up. The project also provided opportunities for further investigations of the proposed works by setting up a laboratory platform for a Real-Time Hardware-in-the-Loop examination of the practical limitations of the work.

2.7 Summary

The general background to modelling, measurement and control have been presented in this chapter. The efforts required to completely model the power system in a linear form that would be suitable for power systems analysis was presented and shown to be impractical for a control algorithm which is intended for a real-time application. The use of WAMS is an alternative approach to comprehensive modelling, and model-free methods are more promising to real-time control. A

background to the standards and processes involved in the use of measurements, such as state estimation, and various standards required for the measurement devices are also presented. In the next chapter, novel optimal measurement placement methods are introduced, and then measurement-based predictive control designs are presented.

Chapter 3

A placement method for power systems monitoring

For the purpose of deploying PMUs to improve observability of the electric power grid, the focus of recent works on PMU placement have shifted to minimizing more associated practical costs, as opposed to traditional methods that only minimize the unit costs of monitoring devices. These associated costs include those of communication infrastructure (CI) and ancillary equipment whose availability are often critical in practical placement decisions. However, existing methods considering co-placements of CIs with PMUs are often heuristic, optimal only with carefully selected parameters, and often have non-standard co-placement architecture. In addition, for many works considering realistic associated costs, the presence of channel limitations, rather than the more likely availability of non-homogeneous channel capacities, are considered. Here, an ancillary equipment availability and comprehensive associated placement costs models are developed and a multichannel, multivendor, PMU-PDC co-placement problem is posed as a NP-hard multi-objective Set Cover Problem (SCP) using an Integer Linear Programming (ILP) method. The proposed approach is illustrated using multiple IEEE test systems of diverse sizes across different scenarios. Results, among others, show that the feasible placement solution using this approach is optimal and multidimensional, but placement decisions depend on the availability of ancillary equipment, as obtainable in practice.

3.1 Introduction to the use of PMU for monitoring

Consider an instance of a network, which has a bus with a connected generator, buses with connected loads, and a bus with neither generators nor loads connected, as in Figure 3.1. Notice that the generator bus Bus 1 is connected to the load buses Bus 3, Bus 4, and Bus 5 through Bus 2, which is a zero-injection (ZI) bus, by definition, because it has neither load nor generator connected. The network of Figure 3.1 may be seen to describe a segment of a transmission network with aggregated loads L_3, L_4, and L_5, whose transmission lines ij with resistance $\bar{r}_{ij}$ and inductive reactance $\bar{x}_{ij}$ have been assumed, for simplicity, to have $\bar{r}_{ij} << \bar{x}_{ij}$ such that $\bar{r}_{ij} \approx 0$. $V_i \angle \theta_i$ and $I_{ij} \angle \theta_{ij}$ are the per unit phasor magnitude values, with angles in degrees, of the bus voltage i and line current of branch ij respectively. Applying Kirchoff's current law at Bus 2,

$$I_{12} = I_{23} + I_{24} + I_{25} \tag{3.1}$$

where $\bar{I}_{ij} := I_{ij} \angle \delta_{ij}$ is the phasor current with magnitude I_{ij} and angle δ_{ij}. The algebraic Kirchoff equation (3.1) is applicable at ZI buses and states that if all but one of the current quantities at a
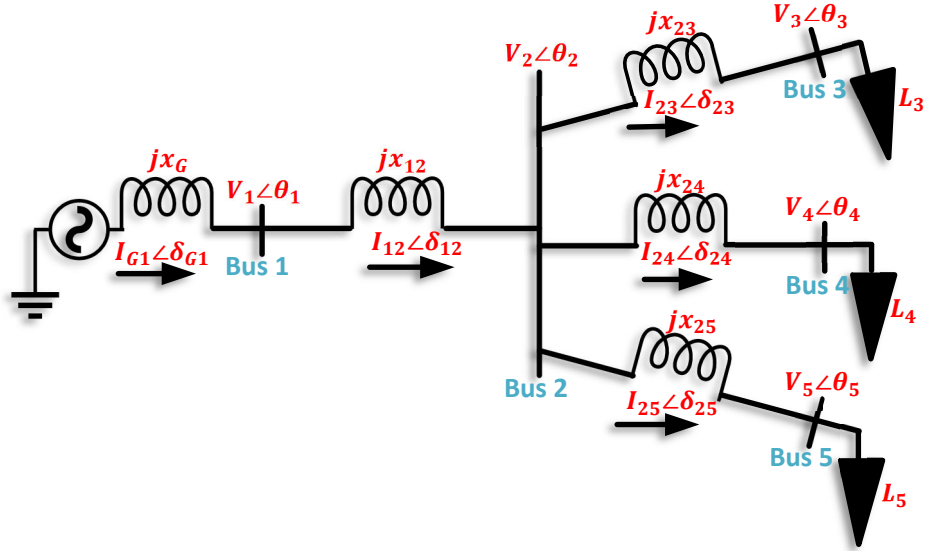
FIGURE 3.1: An example network showing a generator connected to a three loads
via a zero-injection bus

ZI bus is known, then the one can be calculated. For the $k-th$ ZI bus in a $n-$ bus transmission network, (3.1) can be written as,

$$\sum_{j \in ZI_k^{\text{br}}} \boldsymbol{I}_{kj} = 0 \tag{3.2}$$

where ZI_k^{br} is the set of all buses connected to the $k-$th ZI bus. In general, the current across each transmission line ij is related to the voltage difference at its end by the simple ohmic relationship (3.3),

$$\boldsymbol{I}_{ij} = \frac{V_i \angle \theta_i - V_j \angle \theta_j}{j \bar{x}_{ij}} \tag{3.3}$$

Since x_{ij} is a line parameter, it is easy to see from (3.3) that any one of $\bar{V}_i$, $\bar{V}_j$, and $\bar{I}_{ij}$ can be evaluated if the other two are known. Most notably and for example, if the voltage at V_i and I_{ij} can be measured, then the adjacent bus voltage V_i can be calculated using (3.3). Note that (3.3) can also be extended for impedances $\boldsymbol{Z}_{ij} = \bar{r}_{ij} + j\bar{x}_{ij}$, when $\bar{r}_{ij} \neq 0$.

Following from the intuition garnered from (3.1) and (3.3), it is easy to see, from Figure 3.1 that in order to observe the voltage at Bus 1, we may either obtain a direct measurement by placing a monitoring device at Bus 1 or obtain a *pseudo*-measurement, using (3.3), through the placement of a similar device on Bus 2, if the current measurement $\boldsymbol{I}_{12}$ is also available. For this simple network, one may proceed to manually place measurement devices strategically until all the desired phasor quantities are either directly or indirectly obtained using equations one or both (3.2) and (3.3). Note that (3.2) is often neglected if the effect of ZI buses are not considered.

Over the years, a number of literature have been developed on how to deploy measurement devices which may be used for monitoring power systems quantities such as voltage, current, real and reactive power, and frequency over a wide area of the electric power grid. This family of devices are known as Wide Area Monitoring Systems (WAMS). Examples of WAMS include

Frequency Disturbance Recorders (FDRs), Waveform Measurement Units (WMUs), and Phasor Measurement Units (PMUs). The data obtained from PMUs are known as *synchrophasor* data because they are time-stamped and time-aligned using a common Global Positioning System (GPS) reference frame. synchrophasor are useful and can be applied in a number of ways for example in online applications such as state estimation, oscillation monitoring and analysis, voltage stability, remedial action schemes, islanding detection and monitoring, and in wide area visualization and alarming. synchrophasor can also be applied for offline uses such as generator and system model validations, disturbance monitoring and event analyses, as well as frequency response analysis.

3.1.1 Communication infrastructures for synchrophasor transmission

The complete WAMS is a combination of the PMU, the PDC and the communication medium. Power system quantities are measured by PMUs through transducers and reported as synchronised phasors at 10-240 samples/second. The synchrophasors are then transmitted over a communication medium to the PDC, which acts as a historian by aligning the data according to their timestamps, as well as archiving and storing them for possible replay. Note that the data communication may be implemented over different levels of PDC hierarchy, as shown in Figure 3.2.

This section focuses on the evaluation of a complementary communication medium to transmit the high volume of synchrophasors. Most importantly, the medium must be capable of facilitating the transmission of data to realise a stable operation of the power system. Note that to achieve the stable real-time grid operation, synchrophasors must be transmitted at high fidelity and low latency. Moreover, the communication medium itself must have a low failure rate. Synchrophasors can be transmitted using wireless or wired communication technologies. Satellite and cellular network communication are wireless while communications through PLC and fibre optic are wired. These technologies are described briefly below, along with their advantages and disadvantages.

Wireless Communication Technologies

1. **Satellite Communications:** Advancements in space technology over several years have made satellite communication a viable means of synchrophasor transfer. This wireless communication involves a number of earth stations that are connected to PMUs sending synchrophasor to space-stationed satellites equipped with Tracking Telemetry and Control (TT&C) [126]. Consequently, synchrophasor transfer can be effected over a wide geographical area. The reliability of satellite communications is unaffected by weather. On the other hand, the propagation delay is very high and the technology may not be readily available to utilities.

2. **Cellular Network Communications:** Given the high proliferation of mobile network communications in modern times, synchrophasor can be readily transferred over existing cellular network infrastructure. This eliminates the costs of and time spent on of building or setting up communication infrastructure when deploying monitoring equipment and also enhance the range over which data may be communication since all communication requirement will be handled by the owner of the cellular network. Other benefits of using mobile networks are anonymity and low maintenance costs [7], [126]. The major drawback cellular network communication is that the infrastructure is shared by the public. For the transmission of high-resolution synchrophasors, utilities may require a dedicated communication line. However, shared networks degrade the speed of communication. Furthermore, cellular networks
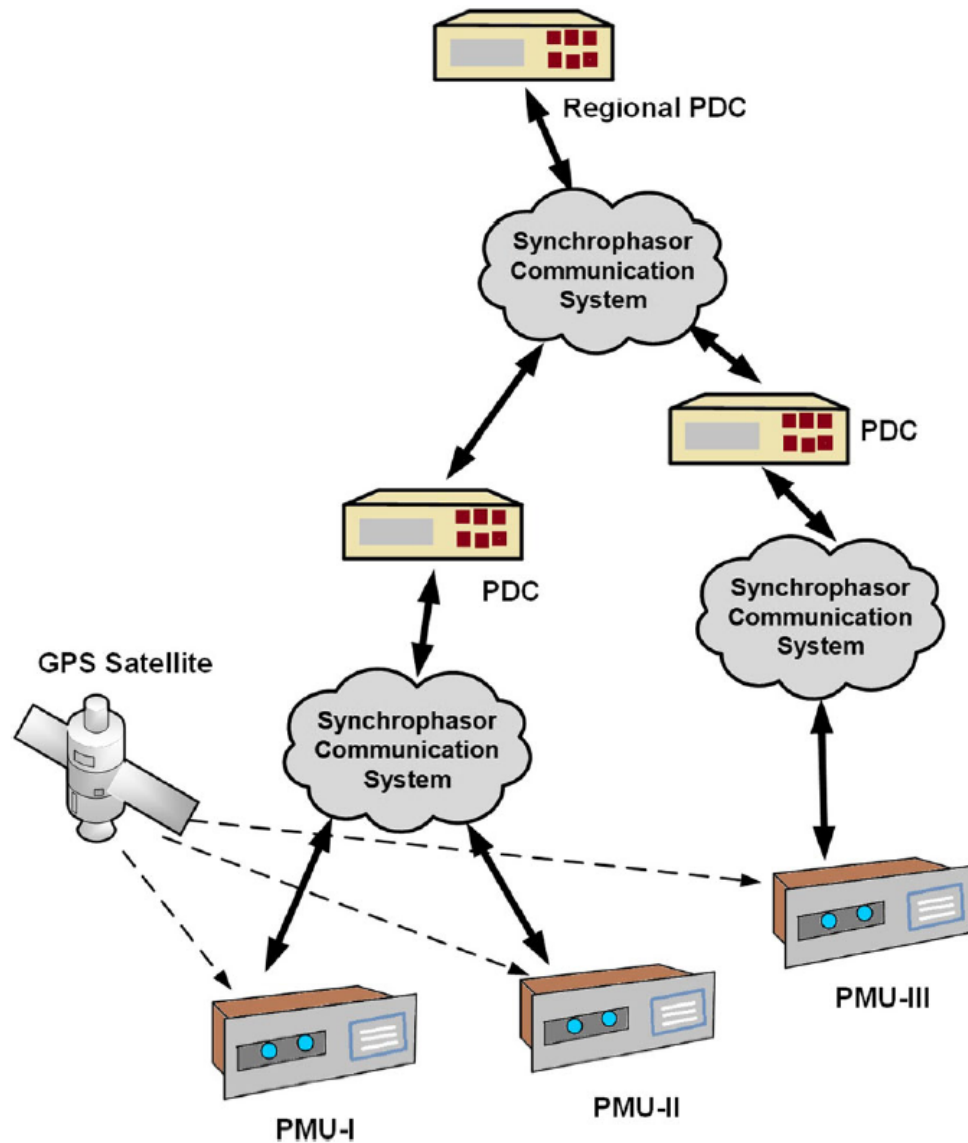
FIGURE 3.2: A hierarchical communication structure [126]

may also be sensitive to severe weather conditions when it is necessary to keep the lights on. One solution is to invest in a relatively more technologically-advanced private network with broader spectrum.

Wireless Communication Technologies

1. **Power Line Communications:** The PLC provides perhaps the fastest means of deploying communication infrastructure as it uses existing power lines. As had been mentioned for cellular networks, a broad spectrum is required for data transmission in order to avoid a degraded performance. Consequently, of the two types of technology which can be used for PLC, the Broad Band PLC is preferred over the Narrow Band PLC since narrow bands may affect critical synchrophasor operation. The drawback with PLCs is that they have a low signal to noise ratio (SNR). This may induce instability in a controlled system from noise

amplification by a high-gain controller. This noise issue may be mitigated by implementing a hybrid communication medium; for example, by combining PLC with cellular network communication.

2. **Fibre Optics Communications:** Communications over fibre optics involve the conversion of synchrophasors into optical signals by an optical transmitter, and then transmitted through optical fibres and repeaters to the PDC. Repeater The benefits of using optical fibres include high data rates, low signal attenuation, and high reliability. This is probably responsible for their popularity in synchrophasor applications.

   Fibre optic communications are however expensive and suffer from slow rate of deployment. Their installation is particularly challenging in mountainous terrains.

Communication delays

The choice of communication medium is critical to the achievement of a smooth data transmission, especially for one required for control. The amount of delays in the medium may affect a controller's speed of response to grid situations. This may lead to grid instabilities or oscillations [127]. Communication delays in synchrophasor transfer can be calculated as a sum of its causative factors. These factors include delays from voltage and current transformers measurements, number of samples used in Discrete Fourier Transform (DFT) for phasor computation, delays in conversion from current and voltage transformer readings to phasors, due due to PMU data size, delays due to multiplexing, delays due to the PDC, and lastly the delay due to the communication medium itself [127]. This may be expressed in (3.4) (as obtained from [127] with a slight change in some notations).

$$\tau = \tau_f + \tau_p + \frac{\phi_L}{\phi_R}\phi_a + \nu \tag{3.4}$$

τ is the total link delay, τ_p is the inherent propagation delay of the medium, τ_f is the lump sum of the delays due to transducers, DFT processing, multiplexing, and data concentration, ϕ_L is the amount of transmitted data, ϕ_R, data transmission rate, and ν is the random delay jitter.

Typical delays in communication media are shown in Table 3.1 as estimated from (3.4). Further details on the calculation may be found in [127].

TABLE 3.1: Estimated delays in some communication media [127]

Communication link	Associated one-way delay (milliseconds)
Fibre-optic cables	$\approx$ 100-150
Power line	$\approx$ 150-350
Telephone lines	$\approx$ 200-300
Satellite links	$\approx$ 500-700

3.2   Co-placement of phasor measurement units and communication infrastructures

The minimisation of PMU costs has been the objective of many traditional PMU placement problems (PPP) [128], [129]. However, insights from the power systems industry, such as those reported from surveys carried out among various practitioners in [13] and [49] as well as the work in [45] show that some other practical costs far outweigh the unit cost of the PMU. These include costs associated with setting up the communication infrastructure(CI) and cyber-security, labour costs, costs attendant with the loss of loads and generations at installation time, and with commissioning the newly installed equipment at a substation or bus. Furthermore, the costs of ancillary equipment, necessary for PMU installations, such as potential and current transformers are reported to be about six times the unit PMU cost [130]. Indeed, the report in [13] shows that the unit PMU cost only accounts for about 5-30% of the total cost of a single PMU installation at a substation. The availability or otherwise of the ancillary equipment or infrastructures may have considerable effect on the total PMU installation. Therefore, an optimisation setup which merely minimises the total unit PMU costs may give misleading results.

The selection of a communication medium must be carried out with careful consideration of their benefits and disadvantages, as had been described earlier in the chapter. As a quick overview, recall that Table 3.1 shows that the fibre optic communication medium has the least amount of delay and satellite links the most. Moreover, PLCs have been described as having a low SNR, meaning that along with their relatively higher delays, they may not be the best choice for communication medium where feedback control, as is the focus of this project. Cellular networks have been shown to require a broad spectrum which may not be available on already-existing public infrastructure. It is however recognised that cellular networks may represent a viable communication medium, on account of their ready availability and accompanying reduction in the total PMU installation costs. For the average utility around the world, access to satellite communication may be difficult. Lastly, fibre optic communications is encumbered only by labour-intensive effort required for, and a high cost of, installation. In order to enjoy its advantages, the total costs of procurement and labour must be minimised.

This project will focus on the deployment of wired communication media for synchrophasor transfer. It may happen that if there may be no need to install a communication medium along a preferred circuit if one (perhaps the PLC) already exists along that path. This will be taken into account in the model to provide an ooportunity for a hybrid, albeit wired, communication media. An assumption made here is that utilities already have the *right-of-way* along the routes that the communication path will be laid and that these will follow the same path as existing transmission or distribution lines. It is recognised that this may not be the case in practice. However, this complication, along with those associated with interference issues with power lines, will not be addressed here.

It is important to note that in the wider body of literature on PMU placement, voltage, rather than current, observability of network buses is usually implied when any reference is made to observability. However, current measurements along some branches are usually needed to achieve a specified level of voltage observability. In the following sections and for the rest of this thesis,*voltage* observability of any specified level will be referred to, simply, as observability, at the specified level.
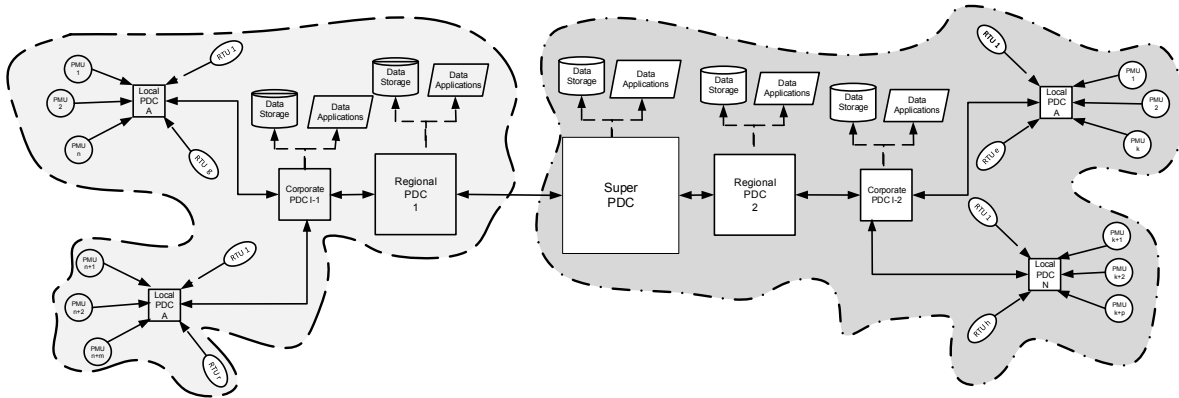
FIGURE 3.3: PDC Hierarchy, (as in [99])

3.2.1 A brief review of related work on co-placements

In order to develop a viable and practically applicable PMU placement solution, it is necessary to identify the key variables which are likely to affect the installation costs and seek to minimise them using realistic costs, [130]. Chief among these costs is the cost of laying CIs, which require considerable investments especially for stand-alone PMU units. [131]–[136] proposed PMU installation cost reduction strategies through simultaneous placements of the measurement devices and their communication links. In particular, [132] considered the costs of switches and routers as well as the length of the transmission media in their formulations. More recently, [135] described, in addition, the use of repeaters in order to minimise propagation delay and a cyber-security network using a more practical network. Most of these works use mainly heuristic methods —such as Genetic Algorithms (GA) [132], [135], or the modified form of GAs [131] —to obtain the placement solutions. Although GAs are able to obtain a global solution over a wide range of functions, they depend on the choice of parameters to do so, and therefore global optimality is not always guaranteed. Since the probability of line outage increases with the length of the transmission lines, it is prudent to reduce PMU-PDC distance to a minimum.

For co-placements of CIs and PMUs, some methods such as [136] have discussed the placement of a Phasor Data Concentrator (PDC) at every PMU location. In the main, this would imply that every connection to the regional or central PDCs would require each a CI. A more cost-conservative approach would be to connect PMUs to the nearest local PDCs, which may be owned by a local utility. In turn, each local PDCs can be connected to a regional PDCs or to a set of cooperative PDCs. Each regional PDCs in the network is then connected to a central PDC [99]. Figure 3.3 shows an example of this hierarchical structure.

The possibility of driving down the installation costs by using, exclusively, flow devices with extensible PMU capabilities has been explored in [130]. These devices are known as Dual-Use Line Relays (DULRs) and are capable of measuring voltage phasors at either ends of the buses to which they are connected, as well as the current phasors along the branches connecting the buses, at PMU rFate (30 samples/s). Yu, *et al* [137] also developed a multi-objective minimisation of the costs of DULRs as well as those of the CIs, stand-alone PMUs, PDCs, and substation shut-down. Although both of these works(i.e. [130] and [137]) used ILP which guarantee optimality under respective situations, only an exclusive use of DULRs was considered in [130]. Since phasor measurement is

only an added functionality on the DULR, careful calibration is often needed before they can be used. Although the effects of PMU channel limitations have been examined in some works(see, e.g [138]–[141]), the majority did not consider the presence of multiple channel capacities in their setups. Such non-homogeneous mix was examined in [138], but only two different capacities were considered at a time in the results. The consideration of the presence of many different channel mixes drives down costs, minimises channel wastage, and is more reflective of real-life scenarios.

In [13], it was reported that utilities installed PMUs from at least 7 different vendors between them. Compatibility issues in connecting PMUs from multiple PMU manufacturers to the same PDC often present a challenge to utilities. This is because the various IEEE PMU standards did not stipulate any particular method for phasor measurement calculations, resulting in a lack of confidence in comparing phasor estimations obtained from the different approaches. The compatibility challenge can be modelled in PPP by accounting for the presence of multiple vendors. This hopes to eventually avoid co-placement solutions which involve the connection of incompatible PMUs to a common PDC. In addition, since the unit cost of a PMU is often a function of device reliability and the number of add-on functions provided by the vendor, utilities may wish to take advantage of the diverse pricing of the measurement devices, but may not wish to compromise network reliability in the process. Here we show that for a pre-defined system reliability threshold, significant costs savings can be achieved whilst satisfying the reliability criterion. However, this chapter does not consider the cost incurred in submitting and evaluating bids from multiple vendors.

3.2.2   Contributions of the chapter

In this chapter, we develop realistic models for the cost factors affecting PMU installations, along with the modelling of the availabilities of ancillary and general PMU installation equipment in a general Integer Linear Programming (ILP) optimisation framework. In the light of the foregoing, and building on the work in [138], the chapter's contributions are as follows:

1. Obtain a global solution to the PPP through a minimisation of, as many as possible, costs associated with practical variables influencing the total installation costs. This would be different from methods in [131]–[135] in the sense that an ILP is used, and different from [137] in the SCP approach. In addition, [131]–[135], [137] did not consider non-homogeneous channel capacities and attendant variability in channel costs.

2. Determine a global minimum cost with a number of competing vendors. To the best of our knowledge, this has not been considered in literature.

3. Determine the exact number of PMU channels to be installed at a candidate bus, along with a PDC hierarchy of the type suggested in [99] for the standard IEEE C37.244-2013. In which, compared to [138], considered CIs and obtained fewer number of PMUs under a non-homogeneous channel consideration.

4. Show, by considering various practical scenarios, that although a global solution to a PMU placement problem can be obtained, PPP solutions in general are actually equipment-availability and/or network-situation specific.

3.3 Placement formulation

In this section, brief backgrounds are presented to the traditional Integer Linear Programming (ILP) placement problem, beginning with an introduction to graph theory. Thereafter, the proposed placement formulation is described, along with further definitions related to graph theory.

3.3.1 A brief background on integer linear programming-based traditional placement formulations

The electric power network can be represented as a graph, such as that shown in Figure 3.4. This graph would be made up of buses or nodes and branches or edges, where electric power flows across the branches from one bus to another.
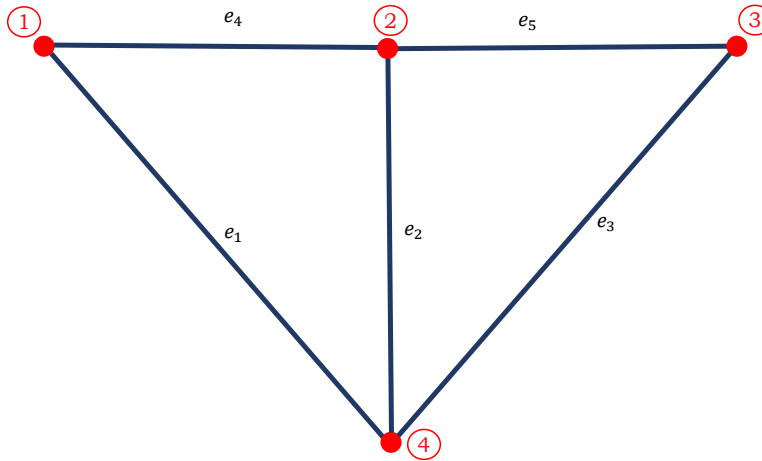
FIGURE 3.4: A simple graph showing nodes branches

Figure 3.4 has four nodes 1, 2, 3, and 4, as indicated by the red numbered circles, and five edges. The edges would usually be described by the two nodes they connect along with an associated weight. For example, an edge connecting nodes 1 and 2 with an associated weighted w would be described as Edge $w(1,2)$. In electric network, this weight could be the length of or the associated cost of laying transmission or distribution lines connecting buses. Note that in Figure 3.4, the edges are simply described as $e_1, \ldots, e_5$. If I is the set of nodes and e the set of branches, then the typical formulation of the traditional ILP-based PMU placement problem can be described as follows: A connectivity matrix, a_{ij} of size $|I| \times |I|$ can be formed to describe whether a node i is connected to another node j in the graph. Here, it is assumed that every node is connected to itself.

$$a_{ij} = \begin{cases} 1 & \text{if node } i \text{ is connected to node } j, \\ 1 & \text{if } i = j, \\ 0, & \text{Otherwise} \end{cases} \tag{3.5}$$

This summarily converts the graph into a matrix. As an example, the matrix (3.6) is the connectivity matrix for the graph of Figure 3.4.

$$
a_{ij} = \begin{bmatrix} 1 & 1 & 0 & 1 \\ 1 & 1 & 1 & 1 \\ 0 & 1 & 1 & 1 \\ 1 & 1 & 1 & 1 \end{bmatrix} \tag{3.6}
$$

Note that the nodes represent the points of connection of generators and/or loads, and the branches would usually include all lines[1] and transformers[2] connecting network buses. The formulation of the connectivity matrix a_{ij} is the basis of many traditional ILP-based PMU placement methods [107], [142], [143].

$$
\operatorname*{minimize}_{\boldsymbol{x}} \; \boldsymbol{C}^T \boldsymbol{x} \tag{3.7a}
$$

$$
\text{subject to } \boldsymbol{A}\boldsymbol{x} \geq \mathbf{1} \tag{3.7b}
$$

$$
\boldsymbol{x} \in \{\mathbf{0}, \mathbf{1}\} \tag{3.7c}
$$

where $\boldsymbol{C} \in \mathbb{R}^{|I|\times 1}$ is the vector of PMU costs, $\boldsymbol{A} \in \mathbb{R}^{|I|\times|I|}$ is an expression of a_{ij} in matrix form. $x \in \mathbb{R}^{|I|\times 1}$ is the vector of binary decision variables. In most formulations, $\boldsymbol{C}$ is a vector of ones, meaning that neither real or relative PMU costs are used in the formulation. Constraint (3.7b) is the observability constraint which specifies that each bus must be *voltage*-observable at least once. The formulation (3.7) does not consider co-placements of CIs. However, this approach may not suffice for the co-placement problem when communication infrastructure are intended for co-placement with PMUs, especially when devices of different capacities are available for placement. For this reason, an alternative formulation is developed in the following sections.

3.3.2   A description of the proposed placement formulation

The *channel* capacity of a PMU may be defined as the total number of simultaneous phasor measurements which the device is capable of taking at a single time. The current channel capacity of a PMU is the number of simultaneous current phasor measurement which the device is capable of measuring when placed at a bus. By extension, a PMU's total channel capacity is the sum of its current channels and a single channel dedicated to voltage measurement at its bus. For example, if there are l current channels, then the total capacity of the PMU is $L = l + 1$. The placement of PMUs with the same number of channels in electric grids has been well discussed in [138]. In this section, the background is laid for the formulation of a more practical PMU placement, which considers the presence of different kinds of PMU channel capacities. This involves the definitions and descriptions of some important terms, using the Western System Coordinated Council (WSCC) 9-bus test system for illustrations.

---

[1]Double-circuit lines are usually neglected.

[2]Some formulations such as [130] treated nodes connected through transformers as *supernodes*
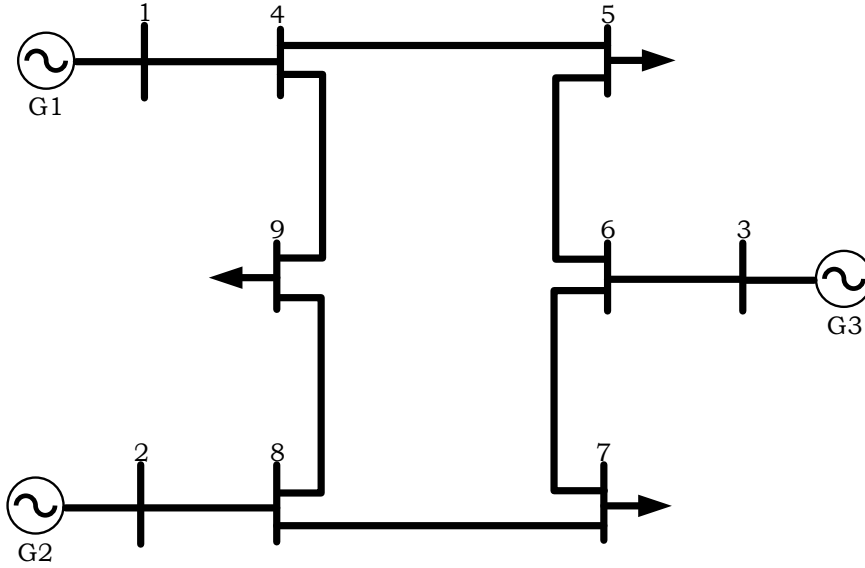
FIGURE 3.5: Placement under limited channel consideration

Set of all buses, (I)

Let I be the set of all buses in a network such that the cardinality of the set, $n := |I|$ is the total number of buses in the network. In this case, the buses may include all substation, generator, load, and zero-injection buses. Using the 9-bus test system of Fig 3.5 as an illustration,

$$I = \{1, 2, 3, 4, 5, 6, 7, 8, 9\} \text{ and } n = 9$$

Sets of all bus connections (Branches), (S_j)

In addition, let S_j be the set of all buses connected to a bus j including j itself. In our example, $S_1 = \{1, 4\}, S_2 = \{2, 8\}, \ldots, S_6 = \{6, 3, 5, 7\}, \ldots, S_9 = \{9, 4, 8\}$.

Centre of the sets, (j) :

j is the dominating element in the set S_j and may be referred to as the *centre* of the set S_j. The centre in this instance may be directly defined as the bus i with an identity $i = j$ for which the set S_j is being formed. For the set S_1 and S_2 respectively, 1 and 2 are the centres of the sets.

Sets of the number of bus branches, (E)

Clearly, the number of branches e_j connected to any bus j in the set S_j is one less than the cardinality of the set such that $e_j = |S_j| - 1$. It follows that the set of all number bus branch connections, $E = \{e_1, e_2, \ldots, e_n\}$. For Fig 3.5, $E = \{1, 1, 1, 3, 2, 3, 2, 3, 2\}$

Maximum and Minimum Branch Connections, $(\Delta(E), \delta(E))$

Let $\Delta(e), \delta(E)$ represent the maximum and minimum numbers, respectively, of all branch connections over all buses in the network such that,

$$\Delta(e) = \max_j e \text{ and } \delta(e) = \min_j e$$

Clearly, in our example, $\Delta(e) = 3$ and $\delta(e) = 1$.

Total $(l+1)$**, Device Current** (l)**, Maximum Current** (L)**, Channel Capacities**

Suppose $l = 1, 2, \ldots, L$ is the range of current measurement channels present in the PMU devices available for placement, and an extra channel is available for voltage phasor measurement in each device, then the total capacity of each PMU is $(l+1), \forall l = 1, 2, 3, \ldots, L$. We assume that there is no limit on the number of each $l+1-$channel devices available for procurement. From the preceding, two cases are possible:

1. *The non-homogeneous limited channel case,* $L < \Delta(e)$ This is the case where the sets of PMU devices with the maximum number of channels across different ranges of channels have the number of current channels L less than the maximum number of branches. Clearly, it is not possible to find any PMU, among the non-homogeneous mixes, which can measure all branches connected to bus j with $e_j > L$. For example, if $L = 2(\implies l = 1, 2)$, it is not possible for find any PMU which is able to measure all current phasors along branches of each of buses $4, 6,$ and 8.

2. *The non-homogeneous multichannel case,* $L = \Delta(e)$: Here, the maximum current channel capacity in the mix is equal to the maximum number of branches. Compared to the previous case, a fewer number of devices can be deployed.

Given that the unit cost of a PMU devices is likely to increase with each additional channel capacity[136], it is not reasonable, in the economic sense, to consider a third scenario where $L > \Delta(e)$ unless spare channels are intended for future branch current measurements. Indeed, if $L > \Delta(e)$, and the $(L+1)-$channel PMU is deployed on a bus j with e_j branches, then at least $L - e_j$ channels of the PMU are unused.

Sets of similar current channel capacities (S_{jl})

Define S_{jl} to be a subset of the set S_j such that S_{jl} has a cardinality $|S_{jl}| = l + 1$ and contains the centre j of the set S_j. Clearly, j is also the centre of the subset S_{jl} and $|S_{jl}| > 1$.

Number of Subsets (r_{jl}) **in** S_{jl}

It follows that the number of possible subsets S_{jl} from S_j is determined by the combinatorial problem of the number of ways l can be obtained from e_j. Specifically, if r_{jl} is the number of subsets of the set S_{jl}, then

$$r_{jl} = \begin{cases} \binom{e_j}{l} & \text{if } l \leq e_j \\ 0, & \text{if } l > e_j \end{cases} \tag{3.8}$$

where

$$\binom{e_j}{l} = \frac{e_j!}{(e_j - l)!l!}$$

From (3.8), the total number of possible subsets S_{jl} of a set S_j at each bus is,

$$r_j = \sum_{l=1}^{L} r_{jl}, \qquad \forall j \in I \tag{3.9}$$

Total number of subsets (r^T) of all r_j and Maximum number of Subsets (r^s) in S_{jl}

Let $r^T = \sum_{j=1}^{n} r_j$ be the total number of subsets across the network. In addition, let $r^s (:= \max_j r_j)$ be the maximum number of subsets across all S_j.

The subsets S_{jlr} of the subset S_{jl}

Since $r_j \geq 1$, let S_{jlr} represents the $r-$th S_{jl} subsets of the set S_j. Whilst r_{jl} contains the number of possible combinations of the subset S_{jl}, S_{jlr} contains the actual buses composing the sets. We give an example of our definitions and descriptions so far in Table 3.2.

Table 3.2 shows the sets and subsets of selected buses $1, 6, 9$ of Figure 3.5 for $L = 2(\implies l = 1, 2)$. Notice that for $r > r_{jl}$, the set S_{jlr} is empty and that since $L < e_6$, this is the case of the non-homogeneous limited channel mixes. S_{jlr} may be interpreted as sorting the available branches according to the number of channels available for placement.

TABLE 3.2: Example: Sets and Subsets of some buses in the 9-Bus Network

		S_{jlr} ($L = 2$, $l = 1, 2$)								
		$l = 1$				$l = 2$				
j	S_j	$r = 1$	$r = 2$	$r = 3$	r_{j1}	$r = 1$	$r = 2$	$r = 3$	r_{j2}	r_j
1	$\{1,4\}$	$\{1,4\}$	$\{\}$	$\{\}$	1	$\{\}$	$\{\}$	$\{\}$	0	1
6	$\{6,3,5,7\}$	$\{6,3\}$	$\{6,5\}$	$\{6,7\}$	3	$\{6,3,5\}$	$\{6,3,7\}$	$\{6,5,7\}$	3	6
9	$\{9,4,8\}$	$\{9,4\}$	$\{9,8\}$	$\{\}$	2	$\{9,4,8\}$	$\{\}$	$\{\}$	1	3

3.3.3 A compact set

Following from the definitions above, it is possible to form a compact subset S_{jlr}^{dv} which represents the option of purchasing a PMU of channel $l + 1$ from a vendor v, installing on a bus j and then connecting said PMU to a local PDC d. The subsets S_{jlr}^{dv} may be seen as binary variables whose values depend on whether or not they meet *all* conditions for which they have been defined. For example, if we desire PMU connections to only the local PDCs in their region, we could set the subsets representing bus PMU connections to a local PDC in another location to zero.

3.4 Modelling of phasor measurement units and ancillary equipment costs

The costs associated with PMU installations, as identified in [49] and [130], include the cost of a unit PMU installation which is dependent on either the bus or its associated transmission paths or both, and on the availabilities of necessary ancillary equipment. These costs are interwoven and on account, their modelling may require some assumptions. However, in the following, these costs

and their dependencies are identified, as we have mentioned in a previous section, and their effects are modelled as best as possible.

3.4.1   Costs of unavailable instrument transformers

A single set of instrument transformers - through which PMUs connect to lines and buses- comprising one three-phase PT and one three-phase CT, costs about 6 times the value of a unit PMU [130]. Some utilities reported [13] that they were able to save 50% of their original total estimated PMU installation costs from having instrument transformers (that can be used for PMU installation) already available at their substation. With respect to the scenarios outlined in [130] regarding 1) the availability of the instrument transformer but not for PMU use out of security concerns 2) the availability but not for PMU use due to performance concerns, and 3) the availability but not for PMU use in order to keep existing circuits separate, we define an *effective availability* as the scenario where the instrument transformers are available for PMU use without aforementioned concerns. A separate scenario is also possible, where the instrument transformers are effectively available in the light of the preceding but where the available PMUs have a burden greater than the capacity of the existing instrument transformer circuit. This scenario is modelled separately in Section (3.6.4). Let the cost of installing necessary instrument transformers be defined as,

$$C_{jlr}^{\text{IT}} = \rho^{\text{Pt}} C^{\text{Pt}} + \sum_{p \in S_{jlr}} \rho_p^{\text{Ct}} C^{\text{Ct}} \tag{3.10}$$

$$\rho^{\text{Pt}}(\text{or } \rho_p^{\text{Pt}}) = \begin{cases} 1, & \text{PT(or CT) is NOT } \textit{effectively} \text{ available} \\ 0, & \text{Otherwise} \end{cases}$$

where $C^{\text{Pt}}, C^{\text{Ct}}$ are the costs of procurement of a three-phase potential and current transformer respectively and (3.10) defines a total cost for the installation of the PT and CTs. $\rho_p^{\text{Pt}}, \rho_p^{\text{Ct}}$ respectively model the availability of three-phase potential transformers at the substation bus and those of three-phase current transformers for each connected bus branches respectively.

3.4.2   Costs of unavailable communication infrastructure

Communication infrastructures, which should be interpreted as a combination of the communication medium and other communication equipment, may be classified as passive or active devices [132]. Examples for the former include communication lines and repeater, while the latter include switches, routers, and Global Positioning Systems (GPS). We model their costs and availabilities as follows.

Passive communication devices

These refer to the costs of laying PMU-PDC communication lines. The costs $C_{jlr}^{\text{pcom},d}$ associated with laying a single line from a bus j to a local PDC d is given by,

$$C_{jlr}^{\text{pcom},d} =$$

$$\eta \left(C_{\text{perkm}}^{\text{pcom},d} (m_j^d - \eta_j^d) \right) + C_{\text{perrep}}^{\text{pcom},d} \left(\text{round} \left(\frac{m_j^d}{100} \right) - \lambda_{\text{rep}} \right) \tag{3.11}$$

where m_j^d is the shortest distance of the bus j to the local PDC d. $C_{\text{perkm}}^{\text{pcom},d}$ is the cost per kilometre of laying a communication line to the local PDC d and is dependent on the substation's communication requirements for synchrophasor connection, especially in terms of the available bandwidth.

η^d_{jlr} is the length of line already available for use at the substation. The second term on the RHS is the cost of installing a repeater at every 100km along the communication line. When transmitting over a long distance, it is necessary to install repeaters at every 100km in order to avoid signal degradation [135]. $C^{\text{pcom}}_{\text{perrep}}$ is the cost of a unit repeater device. λ_{rep} is the number of repeaters that are already available for use.

$$\eta = \begin{cases} 1, & \text{Viable comm. line to PDC } d \text{ NOT available} \\ 0, & \text{Otherwise} \end{cases}$$

The need for a CI is determined by whether or not the PMU is required to have a dedicated CI or to transmit the synchrophasor using exiting communication circuits for remote terminal units (RTUs) or Intelligent Electronic Devices (IEDs). For existing DULRs and stand-alone PMUs, the communication line to neighbouring equipment are most likely pre-existing, therefore CI costs may be minimal, at the worst, if an upgrade is required. In contrast, the costs of communication lines for non-existing but planned PMU installations is quite substantial.

Active communication devices

Switches and routers are also needed for PMU data aggregations and are installed at the PDCs.

$$C^{\text{acom},d}_{jlr} = \gamma C^{\text{acom}}_{\text{swi}} + \kappa C^{\text{acom}}_{\text{rou}} \tag{3.12}$$

where $\gamma, \kappa \in \{0,1\}$ model the unavailability or otherwise of switches and routers which are needed at the PDC d. $C^{\text{acom}}_{\text{swi}}$ and $C^{\text{acom}}_{\text{rou}}$ are the unit costs of a switch and a router respectively.

The total communication cost is the sum of (3.11) and (3.12).

3.4.3 Labour costs

This includes all general expenses incurred by labour while commuting around installation sites as well as those actually incurred on the sites [13]. In the main, labour costs are a function of the distance of the PMU site to the PDC. In general, the labour cost, $C^{lab,d}_{jlr}$ can be expressed as,

$$\begin{aligned} C^{lab,d}_{jlr} = {} & \eta^{\text{wages}} C^{\text{wage}} + \eta^{\text{labcomm}} C^{\text{labcommperkm},d} m^d_j \\ & + C^{\text{fld},d}_{jlr} + C^{\text{trav},d}_{jlr,\text{perkm}} m^d_j + \eta^{\text{train}} C^{\text{train},d}_{jlr} \end{aligned} \tag{3.13}$$

where $\eta^{\text{wages}}, \eta^{\text{labcomm}}, \eta^{\text{train}} \in \{0,1\}$ specify the labour wages specifically for when external workforces are used, where a communication line is needed to connect to a local PDC d and where labour need to be trained to carry out installations respectively. C^{wage} is the actual labour cost associated with installation at a bus j and may assume to increase from a base cost by a specified amount for every extra channel to be installed. $C^{\text{labcommperkm},d}$ is the labour wages per km for laying a communication line from a bus j to a local PDC d. $C^{\text{trav},d}_{jlr,\text{perkm}}$ is the charge per km of travel from bus to the local PDC, while $C^{\text{fld},d}_{jlr}$ is the field expenses incurred from installing the PMU at a bus j and from laying the communication lines to the local PDC d. $C^{\text{train},d}_{jlr}$ is the cost of training specialised or local crews for the purpose of PMU installations. In practice, the higher the cost $C^{\text{trav},d}_{jlr,\text{perkm}} m^d_j$ of specialised crew travelling from one installation location to another, the lower the cost $C^{\text{train},d}_{jlr}$ of training the crew[13], and vice-versa.

3.4.4 Commissioning and cybersecurity costs

Some steps have to be taken before the PMU is fully ready for use. These include but are not limited to the calibration of measurement devices, software upgrade of existing DULRs to activate their PMU functions, testing the PMU devices in readiness for installations. Although some utilities do not consider PMUs as critical cyber-security assets yet, PMU data must be protected from dangerous cyber attacks. A flat cost may be assumed for setting up security for a PMU to be installed at a bus j as follows. Both of these costs are modelled together as,

$$C_{jlr}^{\text{CMS}} = C_{jlr}^{\text{calibr}} + C_{jlr}^{\text{test}} + C_{jlr}^{\text{security}} \tag{3.14}$$

The costs of commissioning may be a one-off costs that is generally incurred when installing the equipment. However, this cost may also be recurrent if it expands to include the costs of maintenance or sales support which may non-complementary after an agreed period of time.

Being a communications-dependent scheme, the general cyber-security of PMUs or its data will, most likely, be an ongoing concern, especially when susceptible data communication and/or storage media are deployed. Recurring costs will include the costs of setting up, implementing, and maintaining security measures, such as the procurement and renewal of anti-spy and/or anti-hacking software licences.

It is important to note that the model (3.14) only accounts for the initial costs at installation.

3.4.5 Procurement

The unit costs of a PMU has been the main focus of many PPP literature. However, depending on the availability of the ancillary equipment and sensors needed for the PMU installation, this is merely about 5-30% of the total installation costs [13]. In addition, these units can be obtained from a number of vendors at different prices, range of off-the-shelf applications, methods of phasor computation, compatibilities, and reliabilities. In essence, earlier works on PPP can be seen as the minimisation of costs from a single vendor.

Procurement from a number of competing vendors

Let the unit procurement cost of a $(l+1)-$channel PMU from one vendor v out of V numbers of vendor for the purpose of installing it on a bus j and connecting the installed PMU to a PDC d be,

$$C_{jlr}^{\text{mproc},dv} \tag{3.15}$$

3.5 The optimisation formulation

Following from the preceding, a realistic cost-based ILP combining the non-homogeneous and limited channel cases of Section II with the cost models of Section III are incorporated into an optimisation setup whose objective is to minimise these costs. In traditional placements, it is common to define a connectivity matrix,

$$a_{ij} = \begin{cases} 1, & \text{if } i = j \\ 1, & \text{if } i \text{ is connected to } j \\ 0, & \text{otherwise} \end{cases}$$

The proposed formulation for the OPP whose multidimensional vector output gives decisions on the bus j on which the PMU is to be installed, the number of PMUs to be placed on the bus, the sets

of branches which the PMU on bus, the number of PMU channels to be used at the bus, the local PDC to connect to, and the vendor to buy from, at the cheapest costs is described as,

$$\underset{x_{jlr}^{dv}}{\text{minimize}} \sum_{v=1}^{V} \left[\sum_{d=1}^{D} \left[\sum_{j=1}^{n} \sum_{l=1}^{L} \sum_{r=1}^{r^s} C_{jlr}^{\text{tot},dv} x_{jlr}^{dv} \right] \right] \tag{3.16a}$$

$$\text{subject to} \sum_{v=1}^{V} \left[\sum_{d=1}^{D} \left[\sum_{j=1}^{n} \sum_{l=1}^{L} \sum_{r=1}^{r^s} b_{ijlr}^{dv} x_{jlr}^{dv} \right] \right] \geq R_i + 1, \forall i \in I \tag{3.16b}$$

$$x_{jlr}^{dv} \in \{0,1\} \tag{3.16c}$$

where

$$b_{ijlr}^{dv} = \begin{cases} 1, & \text{if } (i=j) \cap (i,j \in S_{jlr}^{dv}) \\ 1, & \text{if} (i \in S_{jlr}^{dv}) \cap (j \in S_{jlr}^{dv}) \\ 0, & \text{otherwise} \end{cases}$$

x_{jlr}^{dv} in (3.16c) is the binary decision variable indicating whether or not an $(l+1)-$channel procured from a vendor v with the purpose of connecting it via communication lines to a local PDC d is to be placed on a bus j to measure the current phasors along the $r-$th set of branches. $C_{jlr}^{\text{tot},dv}$ is the cost associated with this variable.

$$\begin{aligned} C_{jlr}^{\text{tot},dv} = {} & C_{jlr}^{\text{IT},dv} + C_{jlr}^{\text{com},dv} + C_{jlr}^{\text{CMS},dv} \\ & + C_{jlr}^{\text{lab},dv} + C_{jlr}^{\text{shutdown},dv} + C_{jlr}^{\text{mproc},dv} \end{aligned} \tag{3.17}$$

R_i, in constraint (3.16b), is the number of measurement redundancy desired in the optimisation setup. If $R_i = 0, \forall i$ the RHS of (3.16b) merely defines the conditions that all buses must be observable. If $R_i > 0$ at some, but not all of the buses, this is a selective enforcement of redundancy at those buses for which $R_i > 0$. The equation (3.16) is a form of the Set Covering Problem (SCP) which have been shown to be NP-hard. Moreover, (3.16) may be seen as a resource allocation problem.

Equation (3.16) is a general formulation in the sense that solutions which are not of interest may be eliminated from the setup. For instance, if there is a pre-existing exclusive contact with a single vendor, the variable v may be eliminated from the formulation, and (3.16a) may be written as $\sum_{d=1}^{D} \left[\sum_{j=1}^{n} \sum_{l=1}^{L} \sum_{r=1}^{r^s} C_{jlr}^{\text{tot},d} x_{jlr}^{d} \right]$ with corresponding modifications in constraints (3.16b) and (3.16c) as well as in cost equation (3.17).

3.6 Practical considerations

The optimisation setup described so far is the base case of the respective situations. It is good practice to anticipate factors, other than costs, which might otherwise affect the solutions obtained with the formulation. In the following, we consider and model the factors in turn.

3.6.1 Contingency

Contingencies refer to the loss of transmission or distribution lines leading to changes in system topology, or to the loss of measurement devices due to operating failure.

Loss of line(s)

It is possible to model the changes in the system topology due the loss of line as in [142].

$$
a_{ij}^k = \begin{cases} 0, & \text{if line } k \text{ is between buses } i \text{ and } j \\ 1, & \text{if } i = j \text{ or } i \text{ is still connected to } j \\ 0, & \text{otherwise} \end{cases}
$$

and to replace the containment parameters b_{ijlr}^{dv} with $b_{ijlr}^{dv,k}$ in (3.16). Note that more than one line k can be considered for a_{ij}^k.

Loss of phasor measurement unit device

The observability of buses or certain buses in the grid as *a going concern* may be ensured by setting $R_i > 0$ in constraint (3.16b) leading to the measurement observation from more than one PMU source.

Measurement device reliabilities

Alternatively, it is also possible to specify that only highly reliable measurement devices, which have very low probability of failure, be placed. We can define a system-wide observability threshold, $R_{\min}$ such that the product of the probability that each component is in good working condition is greater than or equal to this threshold. In the presence of multiple vendors, the reliabilities of the instruments may be defined in relative terms for each vendors as the amount by which a vendor exceeds the TVE specifications set by the IEEE standard.

Using the general formulation (3.16), it is possible to write this reliability constraint as,

$$
\sum_{v=1}^{V} \left[\sum_{d=1}^{D} \left[\sum_{j=1}^{n} \sum_{l=1}^{L} \sum_{r=1}^{r^s} x_{jlr}^{dv} \log\left(\bar{R}_{jlr}^{dv} \right) \right] \right] \geq \log(\bar{R}_{\min}) \tag{3.18}
$$

The formulation (3.18) models - in a linearised suitable for a Mixed Integer Linear Program(MILP) - the product of the measurement reliabilities of installed PMUs only. As a constraint, it ensures that only the combination of PMUs which meet the system reliability threshold $\bar{R}_{\min}$ are placed.

3.6.2 Limits on the number of phasor measurement units to be installed on a Bus

It is possible to specify that only a certain number of PMUs can be installed at any bus or substation j.

$$
\sum_{v=1}^{V} \left[\sum_{d=1}^{D} \left[\sum_{j=1}^{n} \sum_{l=1}^{L} \sum_{r=1}^{r^s} e_{ijlr}^{dv} x_{jlr}^{dv} \right] \right] \leq E_{\max}^i, \quad \forall i \in I \tag{3.19}
$$

$$
e_{ijlr}^{dv} = \begin{cases} 1, & \text{if } i = j \\ 0, & \text{otherwise} \end{cases}
$$

Equation (3.19) states that the total number of PMUs installed at a substation or bus j must be at most $E_{\max}^i$.

3.6.3 Pre-existing conventional/phasor measurement devices

Flow measurement devices are almost always pre-existing in electric power networks, especially to measure flows along the branches connecting to generator buses. If these existing flow measurement devices have extensible PMU capabilities, we can assume that a PMU already exists for that

branch. Note that these flow measurement devices can measure the current along their branches as well as the voltage phasor at one end of the bus. Their existence can be modelled as,

$$\sum_{v=1}^{V} \left[\sum_{d=1}^{D} \left[\sum_{j=1}^{n} \sum_{l=1}^{L} \sum_{r=1}^{r^s} f_{ijlr}^{dv} x_{jlr}^{dv} \right] \right] = 1, \forall i \in S_{jlr}^{\text{flow},dv} \tag{3.20}$$

$$f_{ijlr}^{dv} = \begin{cases} 1, & \text{if } (i = j) \cap (i \in S_{jlr}^{\text{flow},dv}) \\ 0, & \text{otherwise} \end{cases}$$

If a total number of pre-existing measurement α^i are present at the same bus i with distinct measurement subsets S_{jlr}, it is necessary to specify the different subsets. In other words, $f_{ijlr}^{dv} x_{jlr}^{dv}$ can only be 1 once for each i in the formulation (3.20). Therefore, (3.20) is valid for the presence of either or both conventional flow measurement devices and existing PMUs, and can be extended to all cases in Section 3.5.

3.6.4 Voltage-limited measurement units and measurement device burden on effectively available ancillary devices

The electric power grid consists of distribution and transmission voltage networks. However, some PMUs can only be used at distribution voltage levels. In this case, we can prohibit the placement of these particular devices on transmission voltage-level buses. In addition, if instrument transformers are already available at a substation, then, given the exorbitant costs of these devices, as outlined in Section 3.4.1. It is reasonable to require that procured measurement devices which are to be installed at that substation must have burdens which are not higher than the circuit capacities of the effectively available instrument transformers. In the general case, the formulation (3.21) can be applied to prohibited buses, PDCs, or substations for which the devices may not be installed at, supplied from, or connected to respectively.

$$\sum_{v=1}^{V} \left[\sum_{d=1}^{D} \left[\sum_{j=1}^{n} \sum_{l=1}^{L} \sum_{r=1}^{r^s} g_{ijlr}^{dv} x_{jlr}^{dv} \right] \right] = 0, \quad \forall i \in I^{\text{gprohib}} \tag{3.21}$$

$$g_{ijlr}^{dv} = \begin{cases} 1, & \text{if } (i = j) \cap (i \in I^{\text{gprohib}}) \cap (d, v \in G^{\text{dvprohib}}) \\ & \cap (d \in G^{\text{dprohib}}) \\ 0, & \text{otherwise} \end{cases}$$

I^{vprohib} are the set of buses on which the devices cannot be placed, and G^{dvprohib} represents the instances where a device cannot be supplied from a vendor, or placed at a particular PDC, or both for a given bus i.

3.6.5 Handling unknown transformer tap ratio

The assumption that transformer tap ratios are known may lead to the unrealistic reasoning that the current measurement along the transformer from a PMU placed at an adjacent bus may give an estimated voltage phasor at a bus of interest. Here, we simply assume that all buses connected via transformer are unconnected, i.e $a_{ij} = 0$ for buses connected as shown in Figure 3.6 below. If the observability is still desired under this condition, estimated measurements from transformer connections are avoided, and measurements can be obtained via other bus connections.
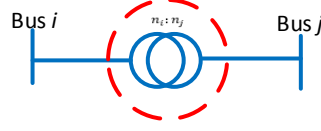
FIGURE 3.6: Substation: two buses separated by a transformer

3.7   The complete setup in compact form

It is possible to write the OPP (3.16) with additional constraints (3.18),(3.19), (3.20), and (3.21) in a compact form.

$$\underset{X}{\text{minimize}}\ C^T X \tag{3.22a}$$

$$\text{subject to}\ BX \geq R_{\text{b}} + 1\ \ [\text{from (3.16b)}] \tag{3.22b}$$

$$R^T X \geq R_{\min} \qquad [\text{from (3.18)}] \tag{3.22c}$$

$$HX \leq h \qquad [\text{from (3.19)}] \tag{3.22d}$$

$$FX = f \qquad [\text{from (3.20)}] \tag{3.22e}$$

$$GX = g \qquad [\text{from (3.21)}] \tag{3.22f}$$

$$X \in \{0, 1\} \tag{3.22g}$$

where $X, R, M^F, M^G, M^H \in \mathbb{R}^{(V \times D \times n \times L \times r^s) \times 1}$ and $B, E, F, G, H \in \mathbb{R}^{n \times (V \times D \times n \times L \times r^s)}$

More compactly, (3.22) can be written as,

$$\underset{X}{\text{minimize}}\ C^T X \tag{3.23a}$$

$$\text{subject to}\ \Omega X \geq Y \tag{3.23b}$$

$$\Psi X = M \tag{3.23c}$$

$$X \in \{0, 1\} \tag{3.23d}$$

where $\Omega = \begin{bmatrix} B \\ R^T \\ -E \end{bmatrix}$, $\Psi = \begin{bmatrix} F \\ G \end{bmatrix}$, $Y = \begin{bmatrix} R_{\text{b}} + 1 \\ \bar{R}_{\min} \\ -E_{\max} \end{bmatrix}$, and $M = \begin{bmatrix} f \\ g \end{bmatrix}$

Note that the elements of the vectors and matrices in (3.22) and (3.23) have values as defined in Sections 3.5 and 3.6. The actual forms of the matrices in (3.23) can be found in Appendix B.

3.8   Results and discussions

In order to demonstrate results from the discussion so far, relatively realistic PMU and associated PMU placement cost values, expressed in monetary units and as may be found in literature, are used. In summary, Figure 3.7 describes how the various software were used in the implementation of the proposed algorithm.
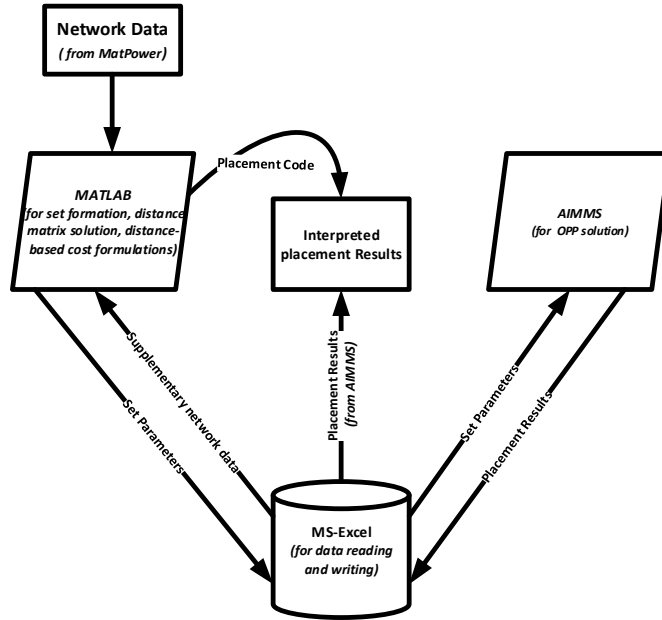
FIGURE 3.7: Structure and software for implementation of the proposed algorithm

3.8.1 Base case

The proposed OPP (3.16) gives some interesting results, which will be discussed here and in subsequent section. First, as base case, we examine a more traditional formulation by removing the variables d and v from the OPP (3.16). This is synonymous to neglecting multiple-vendor procurement and co-placement of CIs. In addition, only the network connectivity information and channel-influenced unit costs of the PMU are used as parameters for $R_i = 0$. Any current channel capacity, l has an associated cost c_l which is $0.1(l-1) \times c_1$, with $c_1= 1$p.u, as suggested in [136]. Table 3.3 shows the base case results of OPP (3.16) for the IEEE 9-Bus test system. This table shows the buses to be placed, the observed branches, as well as the number of channels to be deployed at each solution PMU buses. Since $\Delta E = 3$, we simulated only for $L = 1, 2, 3$ contingent upon the reason stated previously in Section 3.3.2. Note that $L = 1$ and $L = 2$ represent the limited channel cases and $L = \Delta E = 3$ is the multichannel case. At $L = 1$, 6 double-channel PMUs was the minimum number to be deployed at buses 1, 2, 3, 4, 5, and 6. Note that $L = 1$ is synonymous to the deployment of mainly DULRs into the system, which was examined in [130]. When the option of increased channel capacities was presented at $L = 2$, the OPP solution was 4 double-channel PMUs at buses 1, 2, 3, and 7 and only a single 3-channel PMU at Bus 4. At $L = 3$, the installed buses were bus 1, 6, and 8. Each bus is observed only once. This prevents *accidental* redundant placements and gives tighter control over the selection of buses where redundancy is desired. Only one PMU is placed at each bus for $E_{\max}^i = 1, \forall i$ in (3.19). The bar charts and embedded plots in Figures 3.8a and 3.8b Figures 3.8 show how the solutions converge for different IEEE test cases at different values of L. Notice that a certain number L which may be less than ΔE, the solution of the OPP giving the number of PMUs to be installed cannot be less than a certain number. In essence, we state that following from this observation, it must be verified that any claim of channel limitation in OPP must be verified to be less than the absolute minimum at which the solution at $L + 1$ converges

TABLE 3.3: Base Case: Non-homogeneous [Limited and Multichannel] Placement for the IEEE 9-Bus Network, $R_i = 0, \forall i$.

Bus	L = 1 l_1	L = 2 l_1	L = 2 l_2	L = 3 l_1	L = 3 l_2	L = 3 l_3
1	1–4	1–4		1–4		
2	2–8	2–8				
3	3–6	3–6				
4	4–9		4–5–9			
5	5–4					
6	6–7				6–3–5	
7		7–6				
8						8–2–7–9
9						
Total	6	4	1	1	1	1
	6	**5**		**3**		

to the same value as that obtained for *L*. Note that the solution of the OPP are in general optimal but non-unique. This implies that placements at some other buses may give the same minimum placement costs as those obtained from stated values. Alternative solutions may often be seen as in Figure 3.8, where different channel mixes are seen when OPP is simulated for values beyond when solutions have already converged. The number ζ at which there is a sufficient maximum channel capacity available in the mix such that a global solution equal to the number of traditional placements is a function of the network topology and/or the maximum number of branches, ΔE in the network.

Conformity with expectations from graph theory

The results of Table 3.3 shows that the total number of current measurement is a constant independent of the value of *L*. At each value of *L*, the total number of current branches is always 6. This conforms with expectations from graph theory, as expressed is equal to the number of current paths [3].

3.8.2   Procurements from multiple vendors

Here, we neglect only the variable *d* in the formulation (3.16). Suppose there are three vendors and that Vendor 1 has the same quote for its PMUs as specified in Section 3.8.1, Vendor 2 PMUs are 10% more expensive than Vendor 1's, and Vendor 3 PMUs is 50% less expensive than Vendor 1's.

It is easy to see that the solution would be similar to that in Section 3.8.1, with all devices supplied by Vendor 3, who has the cheapest products. However, suppose that the constraint (3.18) is enforced, and that the vendors supply products which have uniform reliabilities of 0.985, 0.998, and 0.978 across all their respective devices, the OPP (3.16) would modulate procurements amongst vendors to satisfy the system reliability requirement $R_{\min}$ as shown in Figure 3.9, which depicts the number of PMU procurements from each vendor at different specifications of $R_{\min}$. Note that, in general for the plots shown in Figure 3.9, all PMUs are procured from Vendor v_3 without any minimum reliability specification (i.e. at $R_{\min} = 0$) while all are procured from Vendor v_2 when the highest level of minimum system reliability is required ($R_{\min} = 0.935$). However, at other specifications of $R_{\min}$, at least one PMU is procured from each of the three vendors. This aims to achieve

---
[3]Many thanks to Dr. Micheal Merlin for this observation
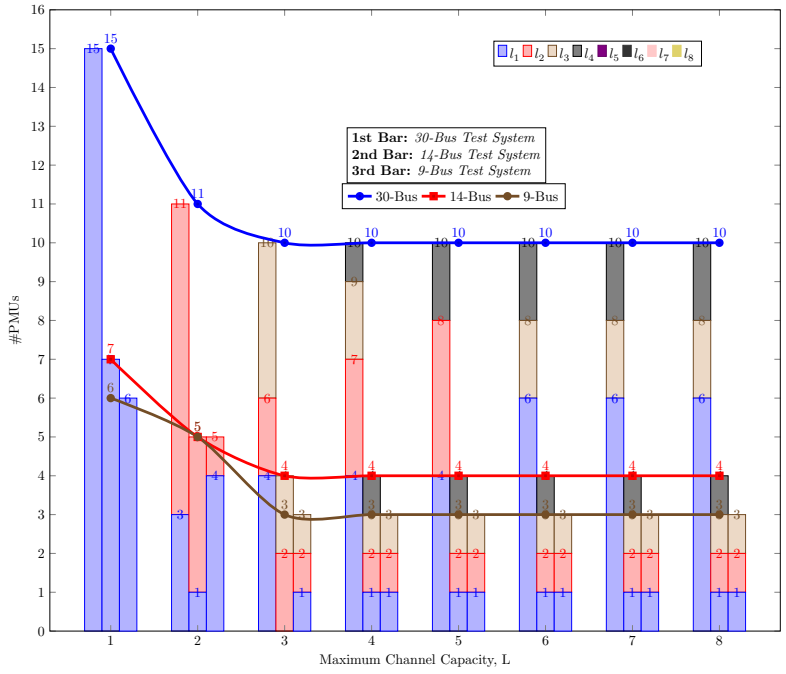
(A) Placements 30-Bus, 14-Bus, and 9-Bus Networks
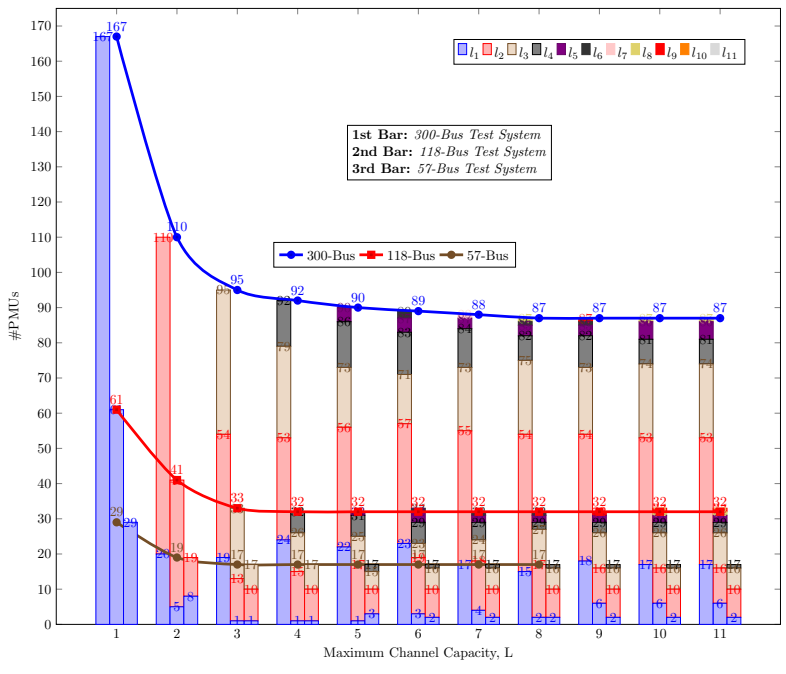
(B) Placements for 300-Bus, 118-Bus, and 57-Bus Networks

FIGURE 3.8: Base Case: Stacked charts and superimposed plots showing placement comparisons using 6 IEEE Test Cases as case studies at $R_i = 0, \forall i$. The stacks show the channel capacities deployed for each network at different values of L.

the specified minimum system reliability at the minimum installation cost. The system reliability
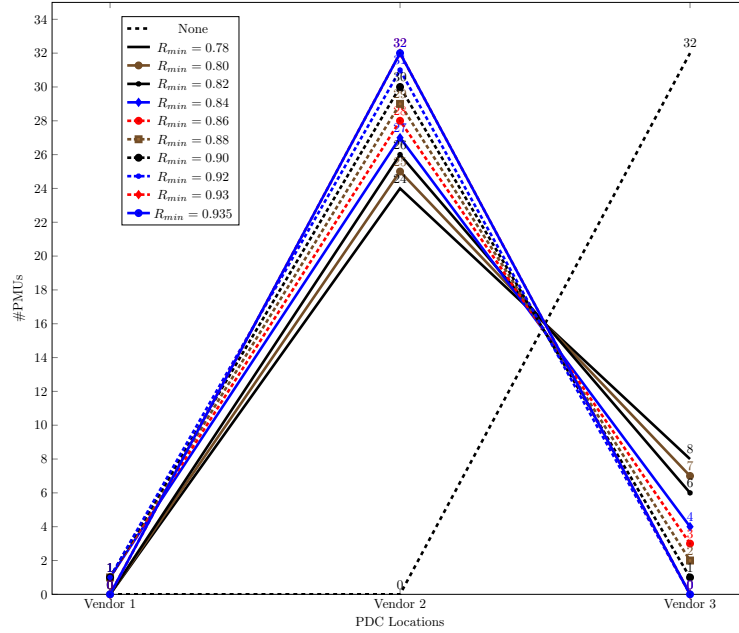
FIGURE 3.9: Procurements from Multiple Vendors: Plots showing placement distributions among the vendors by numbers at different values of $R_{\min}$, using the IEEE 118-Bus Test System for the $L = 9$ *(Non-homogeneous Multichannel Case)*

of 0.938 is the highest that can be achieved for the particular network with the given vendor PMU reliabilities. This is only achievable if no other PMUs except for those from Vendor 3 are used, as is the case at $R_{\min} = 0.935$. The constraint (3.18) ensures that only the most reliable devices are used if the reliability expectations are high. If $R_{\min} > 0.9379$, the OPP becomes infeasible for the network at PMU reliability values used in this scenario.

It is important to add that the maximum system measurement reliability $R_{\min}$ value which can be specified for the network depends on the number of PMUs needed to achieve its observability goals, since the constraint (3.18) is a product of reliabilities. For full network observability, for instance, the number of PMUs would depend on the size of the network. Since the reliability of the PMUs, $R < 1$, the probability of all devices working perfectly at all times would decrease as the size of the network increases. For a non-homogeneous limited channel case, it is expected that the number of PMUs needed for full observability would be greater than that of a corresponding non-homogeneous multichannel placement. It would then become necessary to reduce the expectation $R_{\min}$ for the same network. In other words, a higher system reliability index can be achieved at the multichannel case than at the limited channel case using the formulation (3.18).

TABLE 3.4: Base Case: PMU Placements and Vendor Selection by Channel Mixes at Selected R_{min}, $L = 9$ *Non-homogeneous Multichannel* Case

Vendors	R_{min}				
	None	0.78	0.90	0.92	0.935
1	{}	{}	100(7)	49(8)	{}
T1 @ R_{min}	0	0	1	1	0
2	{}	1(1),5(2),9(2), 15(2),21(2),25(2), 28(2),34(2),41(1), 45(2),52(1),62(3), 64(2),68(2),70(2), 71(2),78(2),86(1), 91(1),92(2),105(2), 110(3),114(2), 118(2)	2(1),5(2),9(2),11(2), 12(3),17(5),21(2),25(3), 29(2),34(3),37(3),40(2), 45(2),53(1),56(3),62(3), 63(2),68(3),70(3),71(2), 76(2),78(1),85(4),87(1), 90(1),92(2),96(4),105(2), 110(3),114(2)	1(2),5(4),9(1),12(3), 15(4),17(2),20(1),23(4), 29(2),30(2),34(1),35(2), 40(2),45(2),52(1),56(3), 62(3),63(2),68(3),71(3), 75(2),77(3),80(5),85(4), 87(1),91(2),94(2),101(2), 105(5),110(3),115(2)	1(1),5(3),9(1),12(5), 15(2),17(4),20(2),23(4), 28(1),30(2),36(2),40(3), 44(1),45(1),49(7),53(1), 56(4),62(3),64(1),68(3), 71(3),75(2),77(4),80(3), 85(3),86(1),90(2),94(4), 101(2),105(4),110(4), 115(2),
T2 @ R_{min}	0	24	30	31	32
3	2(1),5(3),9(2),12(4), 15(3),17(3),21(2),23(2), 25(2),29(2),34(3),37(2), 40(3),45(2),49(4),52(2), 56(4),62(4),63(2),68(3), 71(2),75(3),77(3),80(5), 85(4),87(1),91(2),94(2), 101(2),105(4),110(4),115(1)	12(5),17(5),37(4), 49(8),56(4),85(4), 96(4),100(7)	49(8)	{}	{}
T3@ R_{min}	32	8	1	0	0
Total@ R_{min}	32	32	32	32	32
R_{sys}@ R_{min}	n/a	0.79771	0.90718	0.92573	0.93795

Number in parentheses are the current channel capacities of the PMU's placed at PMU buses, (outside parentheses). Note that the actual branches are part of the solutions but are not shown in the table

3.8.3 Co-placements of phasor measurement units and phasor data concentrators

If only the multi-vendor variable v is neglected in OPP (3.16), it is possible to analyse the OPP's performance in simultaneous CI-PMU placement. Using the IEEE 118 test network as case study, the distance between the buses is obtained from [144]. As shown in Figure 3.10, the network is divided into 3 regions, and all buses separated by a transformer are assumed to form a substation location with PDCs. These are at 8-5, 26-25, 30-17, 38-37, 63-59, 64-61, 65-66, 68-69, and 81-80, are labelled alphabetically as PDCs A-I respectively. The shortest distances between buses and PDCs was estimated using MATLAB's Bioinformatics toolbox.
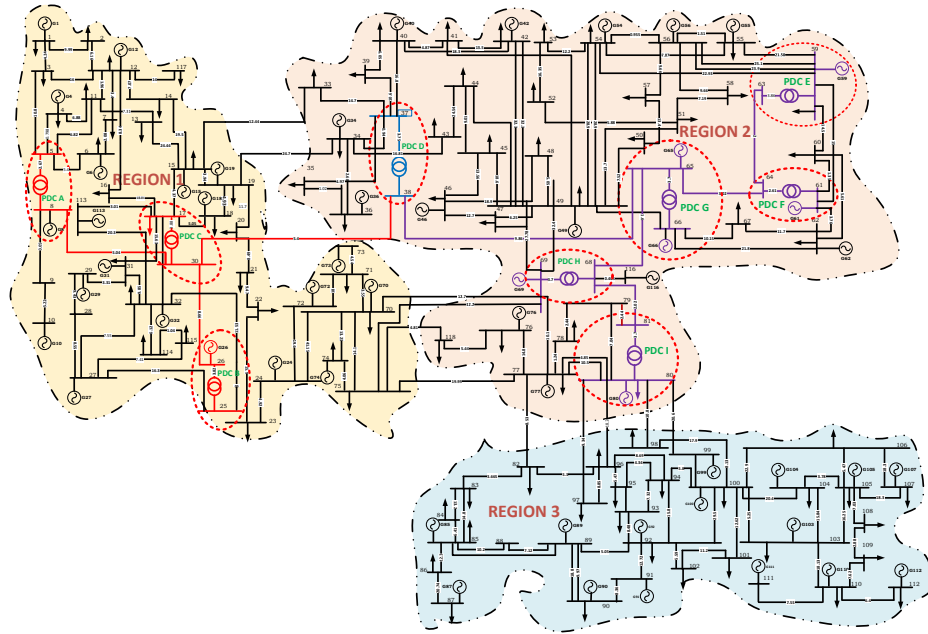
FIGURE 3.10: 3-Region IEEE 118-Bus Test System with local PDC locations indicated in red broken ellipses

0.667 unit was assumed to be the cost per kilometre length of the communication line, in addition to the parameters of PMU channel costs used in Section 3.8.1. The distribution of PMU and channel capacities are shown in Figure 3.11. In comparison with multi-objective approaches seeking to simultaneously place PMUs and CI, this approach is more detailed in the base case, in terms of the number of output decisions and in the consideration of channel limitations and non-homogeneous mixes.

3.8.4 Co-placements of phasor measurement units and phasor data concentrators with procurement from multiple vendors

The complete OPP formulation (3.16) combines all previous results of Sections 3.8.1, 3.8.2, and 3.8.3. So far, only the costs of communication line and PMU costs have been used. Here, we report, in addition, the capabilities of the OPP when all the cost models of Section 3.4 are used, with and without existing measurements, in conjunction with the availabilities or otherwise of instrument transformers at all generator buses of the IEEE 118-bus test network, for $E^i_{max} = 1, R_i = 1, \forall i$, and $R_{\min} = 0.84$. With respect to conventional flow constraint (3.20), for the proposed formulation, it
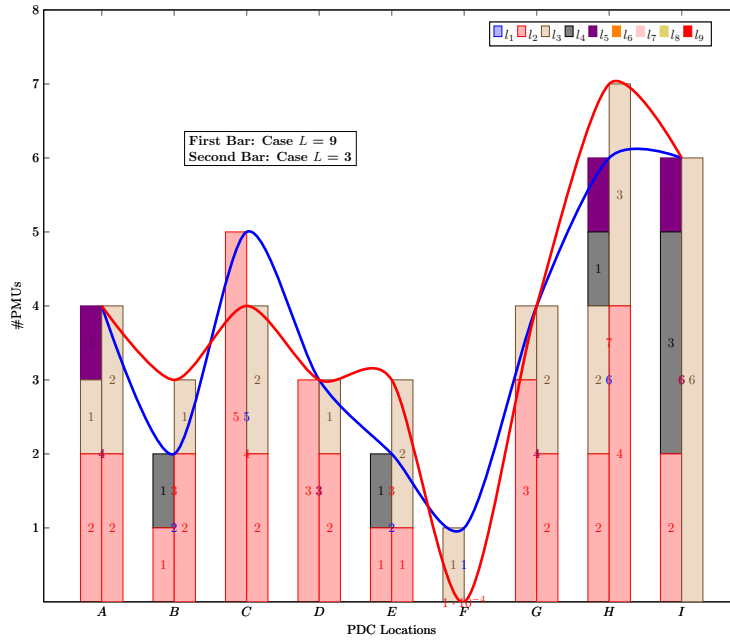
FIGURE 3.11: PMU-PDC Co-Placement: PMU Placements by Channel Mixes and
PDC Locations using the IEEE 118-Bus Test System, $L = 9$ *(Non-homogeneous Multi-channel Case* and $L = 3$ *(Non-homogeneous Limited Channel Case)*

is not enough to state that measurement devices already exists at a bus or branch, but to specify
the details as shown in Table 3.5. The costs parameters used here may be found in Table A.1
of Appendix A. Tables 3.6 and 3.7 show the complete OPP (3.16) solution considering existing
measurements as assumed in Table 3.5 without and with available generator buses instrument
transformers respectively. Without counting the existing measurement devices, the total numbers
of new deployments are 29 and 30 at respective instances. The number of PMUs in Table 3.7 being
higher as a result of the OPP favouring more generator buses than in Table 3.6, on account of readily
available ancillary equipment. The total costs of installation is reduced from 964.172 units in 3.6 to
720.798 units in 3.7. Since the existing measurement may not be at the optimal location, the total
installed PMUs is higher than the number converged to for the same network in Figure 3.8.

Without existing measurements, the OPP is more amply disposed to making more optimal
decisions. As can be seen in Figure 3.12, the total installation costs without existing measurements
is less than those incurred with. The complete base case OPP (3.16), even with the consideration of
communication line, does not give a realistic expectation of installation costs. Clearly, the proposed
OPP (3.16) returns the minimum costs when necessary ancillary equipment are present or absent,
as desired in practice.

3.8.5   Discussion

The following points may be noted in view of the results and formulation.

1. The sensitivity of the solution parameters can be made by adjusting the relative values of the
   cost of the equipment used for the optimisation. It is expected that if these cost parameters
   are modulated within the relative costs obtainable in practice, the results described in the
   various scenario will remain roughly the same.

TABLE 3.5: Assumed Scenario for pre-existing measurements at Buses 10,12,49, and 73

Existing Scenario					
Bus	Device	Capacity	Branch	Vendor	PDC
10	DULR	2	10-9	3	A
12	PMU	4	12-7,12-14, 12-117	1	B
49	PMU	8	49-42,49-45, 49-48, 49-50, 49-54, 49-66,	2	G
73	DULR	2	73-71	3	C
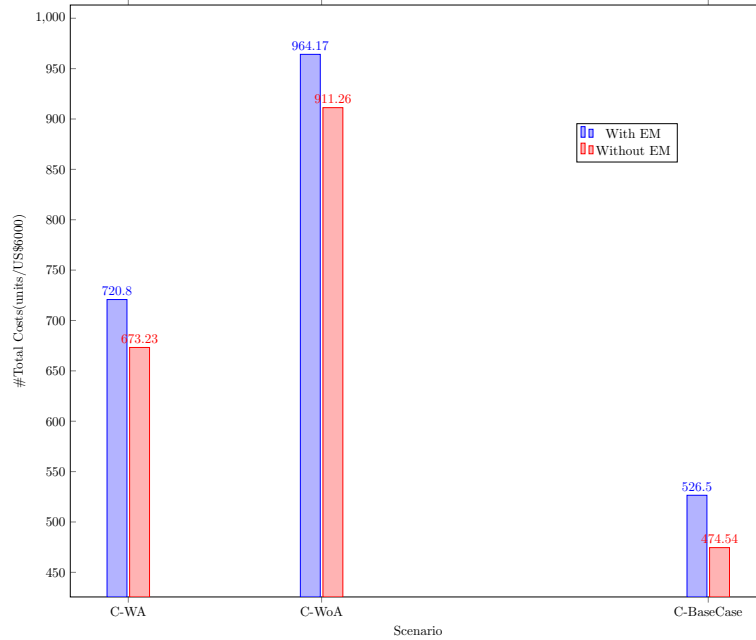
FIGURE 3.12: Complete Case: Total installation costs for different scenarios. Grouped Bars 1-2: complete (3.16) with respect to Section 3.4 WA(WoA) = with(out) available instrument transformers at all generator buses. Grouped Bars 3: complete (3.16) Base Case = with only the communication line costs. EM = Existing measurements (as in Table 3.5),$[E_{max}^i = 1, R_i = 1, \forall i, R_{min} = 0.84]$

2. It is important to note that this chapter does not consider the ongoing costs that are associated with PMU placements; such as those of PMU maintenance and repair, obtaining and renewing software for cybersecurity, testing, and sales support from vendors. However, a form of these ongoing costs is discussed next in the multistage placement of Chapter 4.

3. Furthermore, the intent on the setup here is to avoid accidental over-provisioning. Intentional over-provisioning was briefly mentioned as a third scenario, in Section 3.3.2., where $L > \Delta(e)$,. Should there be an intent to over-provision, this would be only a matter adding an extra dummy bus to the formulation of the subsets S_{jlr}, or adding an extra channel to each candidate bus solution provided by the formulation.

TABLE 3.6: Detailed Case: PDC-Multiple Vendor Placement Consideration of Pre-existing measurements at Buses 10,12,49, and 73

	Vendors						
PDC	1	T1	2	T2	3	T3	*TPDC
A			1(1)	1	5(5), **10(1)**	2	3
B	**12(3)**	1	24(3),25(2) 114(2)	3			4
C			15(8),17(5), 21(2),29(1)	4	**73(1)**	1	5
D			34(1),37(4), 40(1), 43(1)	4			4
E			56(4), 63(1)	2			2
F			62(3)	1			1
G			47(1),**49(7)**, 52(2)	3			3
H			68(2),75(1), 77(3),85(4),86(1)	5			5
I			91(2),94(2), 101(2),105(4), 110(4)	5	80(6)	1	6
*TV	1		28		4		33
**TC			964.172 units				

Pre-existing measurements placements are in bold. Number in parentheses are the respective current channel capacities of the PMUs. Note that the actual branches are part of the solutions but are not shown in the table.
*TV, TPDC = Total Number of PMUs at Vendor v, PDC d
**TC = Total Installation Costs
$L = 9$ Multichannel Case, All equipment unavailable,
$E_{max}^i = 1, R_i = 1, \forall i, R_{min} = 0.84,$

3.9 Summary

This work describes an optimal multivariable solution to a multiobjective, multi-vendor, multi-channel PMU-PDC co-placement problem by solving an NP-hard combinatorial problem through an ILP approach.

Solutions under various scenarios were obtained for a range of IEEE test networks considering different availability cases. Overall, the strength of the proposed algorithm lies in its ability to eliminate channel wastage by optimally and dynamically allocating device channel resources from a range of non-homogeneous mixes of channel capacities, determining between the options of deploying cheaper DULRs or more expensive stand-alone PMU units, and the flexibility to take on many practical factors and determine the optimal solution with any given feasible condition. In addition, the setup implemented the minimisation of placement costs using an IEEE-recommended PMU-PDC co-placement architecture, incorporated the costs and reliabilities of devices from multiple vendors, with consequent effects on a pre-defined system reliability threshold.

The sensitivities of placement solutions to network situations such as pre-existing equipment availability and measurement devices were also examined. It was shown that (from results of Tables 3.6 and 3.7, and the bar chart of Figure 3.16 that placement costs and solutions would vary in accordance to the specific scenario being considered. In practice, this allows utilities to focus on

TABLE 3.7: Detailed Case: PDC-Multiple Vendor Placement Consideration of Pre-existing measurements at Buses 10,12,49, and 73

| PDC | Vendors | | | | | | *TPDC |
	1	T1	2	T2	3	T3	
A			1(2),5(4)	2	**10(1)**	1	3
B	**12(3)**	1	24(2),26(1), 27(3),32(3)	4			5
C			15(3),17(2), 21(2),31(1)	4	**73(1)**	1	5
D			36(2),40(3), 43(1)	3			3
E			56(3),59(3)	2			2
F							
G			47(1),49(7), 52(2),65(2), 66(2)	5			5
H			75(2),77(3), 85(4),86(1), 116(1)	5			5
I			91(2),94(2), 101(2), 110(3)	4	80(6), 105(5)	2	6
*TV	1		29		4		34
**TC	720.798 units						

$L = 9$ Multichannel Case, Instrument Transformers Available at all generator buses, $E_{max}^{i} = 1, R_i = 1, \forall i, R_{\min} = 0.84$
'**See comments under 3.6

the cost-savings that may be achieved from a consideration of available installation equipment and measurement devices.

This setup will proceed to analyse, in the next chapter, the multistage placements of measurement devices when detailed costs models, multiple vendors, and the presence of non-homogeneous channels are considered.

Chapter 4

Multistage Placements of PMUs for Electric Power System Monitoring

4.1 Introduction

Utilities can benefit from Wide Area Monitoring Systems (WAMS) installations to improve grid voltage reliability through increased network observability. Multi-stage placements with long-term full observability seem like a fiscally viable alternative, but are likely to cost more in the end. Here, the focus is on a more viable method of deploying WAMS, especially in terms of fiscal capability, by spreading placement costs over a period of time. Some limited-budget, multichannel, PMU-PDC co-placement problems are introduced, and then the factors affecting continued installations are discussed. In the end, it can be safely concluded that all network utility operators may enjoy the benefits of WAMS installations but must be aware of certain practical factors in multi-stage deployment when budget is of concern.

4.2 A preview of multi-stage placements

In varying degrees, PMU Placement Problems (PP) algorithms aim to minimise total placement costs with the condition that all buses must be observable. Observability in this sense does not imply that WAMS are installed on all buses. Indeed, all buses connected to a bus i, with a PMU m_i installed are deemed observable because their measurements can be indirectly estimated from the voltage drop obtained from their known line impedances, as shown in Section 3.1 of Chapter 3. Most of literature are primarily focused on minimising the total cost of placement, without a realistic consideration of what the final cost might be, in terms of affordability and necessity. The goal being to monitor all buses in a one-time placement,(see e.g [12]) or over time spreading out the number of placement per time using incremental placement over a period of time, as obtained in multi-stage scheduling methods of [145]–[147] with a long-term focus on full observability. However, financial realities compel probing of the full observability realities. For this reason, some papers have addressed the placing of the PMUs only on certain buses based on the criticality or relative importance of these buses with respect to an intended application.

The multi-stage algorithms [145]–[147] have examined the placement problem in different ways. In [145], [146] the focus has been on quantifying the reliability of electrical line and communication, and this has been used as a factor for determining candidate PMU buses. Some of the earliest work on multi-stage placement was done in [147], where the number of components placed at each stage is pre-determined such that the total number of placements is equal to the total determined from a system-wide optimization with full-observability objective. To the best of our knowledge, many multi-stage algorithms have not examined the possibility of the decreasing unreliability of already-installed equipment, the consequences of a limited budget and the loss of inflationary rates

on budgets, nor have they examined the possibility of adopting WAMS in financially-constrained networks.

4.3   Contribution of the chapter

The contribution of this chapter are,

1. To formulate a budget-constrained channel-constrained multi-stage placement method using a multivariable integer linear programming.

2. To address various practical problems in multi-stage placements. These problems include limited channel capacity and multi-vendor compatibility issues

3. To examine the possibilities of the adoption of WAMS in budget-constrained market and to examine the factors influencing incremental placement of PMUs such as equipment degradation and time lapse between placements.

4.4   Background to Multistage Placements

The placement problem with budgetary constraints is focused on determining the number of PMUs which may be realistically placed considering unavoidable financial constraints. For phased placements due to budget considerations, it is easy to see that the full observability condition enforced by the constraint (3.16b) in the OPP formulation (3.16) of Chapter 3 together with budget consideration may result in an infeasible optimisation problem, depending on the size and consideration of the budget. Traditionally, financial constraints are neglected with the assumption that funds are available to cover the full costs of placements, or that the quest for full observability should be delayed until such a time as the costs for full observability may be fully covered.

In the following, a phased placement method is described for the set-up introduced in Chapter 3, considering all the multivariate factors therein.

4.5   Multistage Placement with Limited Budget and Limited Channels Considerations

In this chapter, a two-step method to the solution of the multi-stage, inspired by [142], [147] but different in its multivariate, multichannel approach, and in its consideration of attendant practical factors affecting placement, is followed. The first step involves a solution of the formulated OPP (3.16), where a flexible multichannel, multi-vendor, and PMU-PDC co-placement set-up was described. The OPP (3.16) is written here again for convenience.

Step 1: Solution of the Full Observability OPP (3.16)

$$x^* = \underset{x_{jlr}^{dv}}{\text{minimize}} \sum_{v=1}^{V} \left[\sum_{d=1}^{D} \left[\sum_{j=1}^{n} \sum_{l=1}^{L} \sum_{r=1}^{r^s} C_{jlr}^{\text{tot},dv} x_{jlr}^{dv} \right] \right] \tag{4.1a}$$

$$\text{subject to} \sum_{v=1}^{V} \left[\sum_{d=1}^{D} \left[\sum_{j=1}^{n} \sum_{l=1}^{L} \sum_{r=1}^{r^s} b_{ijlr}^{dv} x_{jlr}^{dv} \right] \right] \geq R_i + 1, \forall i \in I \tag{4.1b}$$

$$x_{jlr}^{dv} \in \{0,1\} \tag{4.1c}$$
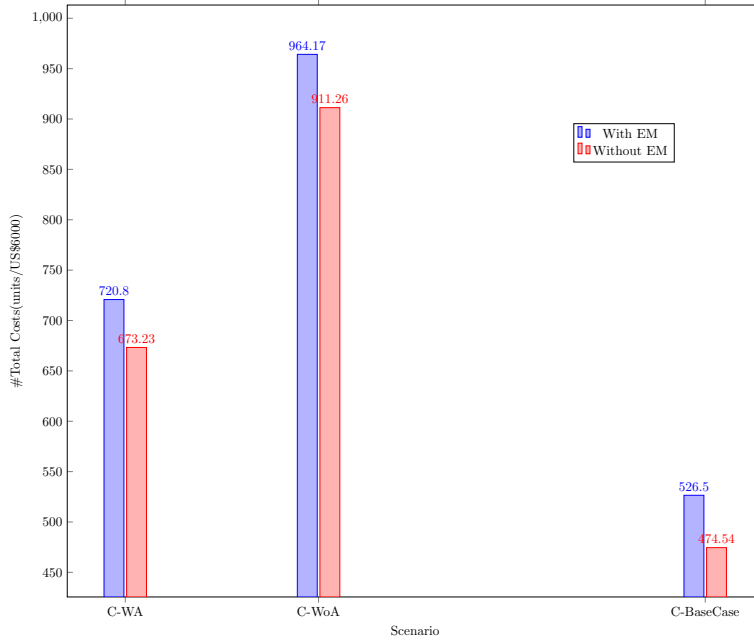
FIGURE 4.1: Complete Case: Total installation costs for different scenarios. Grouped Bars 1-2: complete (3.16) with respect to Section 3.4 WA(WoA) = with(out) available instrument transformers at all generator buses. Grouped Bars 3: complete (3.16) Base Case = with only the communication line costs. EM = Existing measurements (as in Table 3.5),$[E_{max}^i = 1, R_i = 1, \forall i, R_{min} = 0.84]$

where $\boldsymbol{x}^* \in \mathbb{R}^{(n \times L \times r^s \times D \times V) \times 1}$ is the optimal solution to the OPP. Let $\boldsymbol{x}_{\text{sol}}^*$ be the solution vector for when $\boldsymbol{x}^* = 1$ where a PMU is placed at a bus j which is the dominant bus in the set S_{jlr}^{dv}. The total number of placements can then be evaluated by the summation,

$$N_{\text{pmu}}^{\text{fo}} = \sum \boldsymbol{x}_{\text{sol}}^* \tag{4.2}$$

and the total cost of placement in this first step is,

$$C_{\text{pmu}}^{\text{fo}} = C_{\text{sol}}^T \boldsymbol{x}_{\text{sol}}^* \tag{4.3}$$

where $C \in \mathbb{R}^{(n \times L \times r^s \times D \times V) \times 1}$ is the vectorised form of the cost $C_{jlr}^{\text{tot},dv}$ in (3.16).

Step 1 can be seen as the planning stage where all the decisions of the quantity, quality, specifications of vendors and channel capacities are made such that a blue print is drawn for the improvement of the wide area monitoring over the next period of time.

Step 2: Solution of the Full Observability PPP

The solution of Step 1 is the expected total number of installations which would give full observability of the network. In Step 2, the objective is to maximise the observability of bus and branches given that the PMU connected to a bus i given a finite amount of budget, and follows from the solution of Step 1. As was discussed in section 3.8.4 of Chapter 3, pre-planned placements reduces the cost needed to realise the same specification of observability, as opposed to arbitrary PMU deployments. This was illustrated in Figure 3.12, shown again here for convenience.

$$\underset{u_i}{\text{maximize}} \sum_{i=1}^{n} u_i \tag{4.4a}$$

$$\text{subject to} \sum_{v=1}^{V} \left[\sum_{d=1}^{D} \left[\sum_{j=1}^{n} \sum_{l=1}^{L} \sum_{r=1}^{r^s} b_{ijlr}^{dv} \hat{M}_{ijlr}^{dv,k} x_{jlr}^{dv,k} \right] \right] \geq u_i, \forall i \in I \tag{4.4b}$$

$$\sum_{v=1}^{V} \left[\sum_{d=1}^{D} \left[\sum_{j=1}^{n} \sum_{l=1}^{L} \sum_{r=1}^{r^s} \left(M_{ijlr}^{dv,k} + \tilde{M}_{ijlr}^{dv,k} \right) x_{jlr}^{dv,k} \right] \right] = 0, \quad \forall i \notin \boldsymbol{x}* \tag{4.4c}$$

$$\sum_{i=1}^{n} \left[\sum_{v=1}^{V} \left[\sum_{d=1}^{D} \left[\sum_{j=1}^{n} \sum_{l=1}^{L} \sum_{r=1}^{r^s} \hat{M}_{ijlr}^{dv,k} C_{jlr}^{\text{tot},dv,k} x_{jlr}^{dv,k} \right] \right] \right] \leq B_{\text{phase}}^{k} \tag{4.4d}$$

$$x_{jlr}^{dv,k}, u_{jlr}^{dv,k} \in \{0,1\} \tag{4.4e}$$

where u_i is the binary observability index which indicates that a bus is observable, directly or indirectly, from a PMU procured from a vendor v and connected to a PDC d at stage k. B_{phase}^{k} is the budget assigned for placement at a stage k. The selection parameters $\tilde{M}_{ijlr}^{dv,k}$, $\hat{M}_{ijlr}^{dv,k}$, and $M_{ijlr}^{dv,k}$ are described below in Section 4.5.1. The other variables and parameters are as defined in Chapter 3.

4.5.1 Modulation of the selection parameters

The selection parameters are,

1. The full candidate solution selection parameter which captures all the planned solutions of Step 1 and is defined as,

$$M_{ijlr}^{dv,k,\text{full}} = \begin{cases} 1, & \text{if } (i = j) \cap (x_{jlr}^{dv} \in \boldsymbol{x}*) \\ 0, & \text{otherwise} \end{cases}$$

   and does not change over the multi-stage deployment period.

2. The selection parameter for the candidate and already deployed solutions. Note that at $k = 1$, $\tilde{M}_{ijlr}^{dv,k} = 0, \quad \forall i$. However, at $k \geq 2$,

$$\tilde{M}_{ijlr}^{dv,k} = \begin{cases} 1, & \text{if } (i = j) \cap \left(x_{jlr}^{dv} \in \boldsymbol{x}* \right) \cap \left(x_{jlr}^{dv,\zeta(|\zeta < k)} = 1 \right) \\ 0, & \text{otherwise} \end{cases}$$

   The formulation (4.4) recognises the PMU buses in this category as already existing measurement devices in constraint (4.7e). However, the constraints (4.4b) and (4.4d) ensure that they do not influence the observability and budgets, respectively, at the stage k. ζ represents all previous stages of placements.

3. The selection parameter for the candidate but not yet deployed solution. $\hat{M}_{ijlr}^{dv,k}$ is the selection matrix for the decision variables which are part of the candidate solutions in Step 1 but have not yet been placed at Stage k of Step 2.

$$\hat{M}_{ijlr}^{dv,k} = \begin{cases} 1, & \text{if } (i = j) \cap \left(x_{jlr}^{dv} \in \boldsymbol{x}* \right) \cap \left(x_{jlr}^{dv,\zeta(|\zeta < k)} = 0 \right) \\ 0, & \text{otherwise} \end{cases}$$

   Alternatively, obtain $\hat{M}_{ijlr}^{dv,k}$ from,

$$\hat{M}_{ijlr}^{dv,k} = M_{ijlr}^{dv,k,\text{full}} - \tilde{M}_{ijlr}^{dv,k}, \quad \forall k$$

4. The selection parameter for the solutions which must not be deployed because they were not candidate solutions in Step 1. This seeks to capture the set of buses excluded from placements.

$$
M_{ijlr}^{dv,k} = \begin{cases} 1, & \text{if } (i = j) \cap (x_{jlr}^{dv} \notin \boldsymbol{x}*) \\ 0, & \text{otherwise} \end{cases}
$$

4.5.2   Number of deployed PMUs at each stage

If $N_{\text{pmu}}^{\text{fo}}$ is the number of PMU to be deployed for the realisation of full observability blueprint at Step 1 and $N_{\text{pmu}}^{\text{STG},k}$ is the number of PMUs deployed at each stage k, then

$$
N_{\text{pmu}}^{\text{fo}} = \sum_{k=1}^{T} N_{\text{pmu}}^{\text{STG},k} \tag{4.5}
$$

where T is the total number of stages it would take to implement Step 1 in Step 2. (4.5) means that the total number of deployments across all stages in Step 2 must be the same as that originally planned in Step 1. Moreover,

$$
S^{\text{fo}} = \{S^{\text{STG},1}\} \cup \{S^{\text{STG},2}\} \cup \{S^{\text{STG},3}\} \cup \ldots \cup \{S^{\text{STG},T}\} \tag{4.6}
$$

implying that the exact specifications of bus, lines, branches, PDCs, and possibly vendors may be adhered to in order to realise the expected cost and observability planned in Step 1.

4.5.3   Measurement reliability in multi-stage placements

In Chapter 3, a threshold $\bar{R}_{\text{min}}$ was defined for the system measurement reliability. For phased deployments, $bar R_{\text{min}}$ may be defined in three ways. The first would be to define a stage reliability threshold R_{min}^{k} at each stage k. The second approach would be to seek to maximise the reliability and observability in the second step of the multi-stage placement, specifically by modifying the objective (4.4a). Lastly, a reliability constraint in the form of (3.18) maybe added to the formulation in Step 1 with expected R_{min} defined. In the last instance, if (4.6) is strictly adhered to, the system reliability should converge to the specified R_{min} at the $T-$th stage.

4.5.4   Network topology changes

During the course of the multi-stage deployment, the network may be upgraded through the addition of transmission lines or buses. Such upgrades lead to changes in topology of the network, and potentially to a lack of observability of the newly-added lines and/or buses. Suppose the modification to the network were to take place at a stage k of Step 2 and some of the candidate PMUs have been added from the stage $k = 1$ up to the $k - 1-$th stage, then the deployment plan must be

reformulated by repeating Step 1 with the addition of constraint (4.7e) .

$$x^* = \underset{x_{jlr}^{dv}}{\text{minimize}} \sum_{v=1}^{V} \left[\sum_{d=1}^{D} \left[\sum_{j=1}^{n} \sum_{l=1}^{L} \sum_{r=1}^{r^s} C_{jlr}^{\text{tot},dv} x_{jlr}^{dv} \right] \right] \tag{4.7a}$$

$$\tag{4.7b}$$

$$\text{subject to} \sum_{v=1}^{V} \left[\sum_{d=1}^{D} \left[\sum_{j=1}^{n} \sum_{l=1}^{L} \sum_{r=1}^{r^s} b_{ijlr}^{dv} x_{jlr}^{dv} \right] \right] \geq R_i + 1, \forall i \in I \tag{4.7c}$$

$$\tag{4.7d}$$

$$\sum_{v=1}^{V} \left[\sum_{d=1}^{D} \left[\sum_{j=1}^{n} \sum_{l=1}^{L} \sum_{r=1}^{r^s} \tilde{M}_{ijlr}^{dv,k} x_{jlr}^{dv,k} \right] \right] = 1, \quad \forall i \in x^a * \tag{4.7e}$$

$$x_{jlr}^{dv} \in \{0,1\} \tag{4.7f}$$

where $x^a *$ is the set of buses which are part of the candidate solutions in the original plan and have been placed at the Stage k.

4.5.5   Full or selective observability

If full observability is not desired, some elements of the vector $R_b + 1$ may be set to 0 at the desired buses in the OPP. For the maximisation of observability with long term full observability objective, at each stage of Step 2 in (4.4), the optimisation seeks to maximise the observability across the network. When the intention is to maximise observability across a particular region of the network, it might be necessary to replace (4.4) with (4.8).

$$\underset{u_i}{\text{maximize}} \sum_{i=1}^{n} \bar{W}_i u_i \tag{4.8a}$$

$$\text{subject to} \sum_{v=1}^{V} \left[\sum_{d=1}^{D} \left[\sum_{j=1}^{n} \sum_{l=1}^{L} \sum_{r=1}^{r^s} b_{ijlr}^{dv} \hat{M}_{ijlr}^{dv,k} x_{jlr}^{dv,k} \right] \right] \geq u_i, \forall i \in I \tag{4.8b}$$

$$\sum_{v=1}^{V} \left[\sum_{d=1}^{D} \left[\sum_{j=1}^{n} \sum_{l=1}^{L} \sum_{r=1}^{r^s} \left(M_{ijlr}^{dv,k} + \tilde{M}_{ijlr}^{dv,k} \right) x_{jlr}^{dv,k} \right] \right] = 0, \quad \forall i \notin x* \tag{4.8c}$$

$$\sum_{i=1}^{n} \left[\sum_{v=1}^{V} \left[\sum_{d=1}^{D} \left[\sum_{j=1}^{n} \sum_{l=1}^{L} \sum_{r=1}^{r^s} \hat{M}_{ijlr}^{dv,k} C_{jlr}^{\text{tot},dv,k} x_{jlr}^{dv,k} \right] \right] \right] \leq B_{\text{phase}}^{k} \tag{4.8d}$$

$$x_{jlr}^{dv,k}, u_{jlr}^{dv,k} \in \{0,1\} \tag{4.8e}$$

$\bar{W}_i$ is a positive integer denoting the relative importance of the observability of a bus i compared to other buses in the network. In other words, if $W_i > W_{i+1}$ then the observability of bus i is prioritised over that of the bus $i + 1$. The constraint (4.8b) and objective (4.8a) ensure that the observability of the selected buses are prioritised, while the constraint (4.8c) ensures that no buses, different from those originally planned in Step 1 are selected on account of the prioritisation. The last constraint (4.8d) then stipulates that the observability of the priority buses is achieved through the placement of some or all of the candidate solutions which have not been placed without exceeding the available stage budget.

4.6 Factors affecting assigned budgets at each placement stage

4.6.1 Carried-over balances

A viable installation planning is influenced by a practical knowledge of the total cost of procuring, installing, and commissioning a unit PMU, with all expectations of further increases in costs due to the peculiarities of particular networks taken into consideration. The total amount of investment in WAMS in a given time period can be expected to be limited by the maximum allowable amount which utilities may be willing to invest in a given time period such that the cost of investment does not exceed the benefits offered by increased grid visibility in the long term [14]. The budget per phase is more highly influenced by short term planning and may be assumed to be evenly spread throughout a future time period T years. Suppose, in the first stage, that $N_{\text{pmu}}^{\text{fo}}$ PMUs are required for full observability, and a realistic cost $C_{\text{pmu}}^{\text{fo}}$ (monetary units) is estimated for a unit component working installation, then the budget at each stage,

$$B_{\text{phase}}^k = \frac{C_{\text{pmu}}^{\text{fo}} = \boldsymbol{C}_{\text{sol}}^T \boldsymbol{x}_{\text{sol}}^*}{T} \tag{4.9}$$

From the optimisation setups above, it is clear that the number of installed PMUs in the multi-stage placements are determined by the budget B_{phase}^k allocated to that phase, with a pre-determined (i.e. from Step 1) number of installations. If the placement is planned over the next known T period, (4.9) may be applied to evaluate B_{phase}^k. In this instance, it may be safely assumed that utilities are willing and able to execute the plan in Step 1 consistently. On the other hand, if T is not pre-determined, this may translate to utilities carrying out the deployment when they are willing and able to. If follows then that the number of installations over all k stages cumulatively determine the time T required for the realisation of full grid observability.

If at any $k-$th stage for non-uniform placements, the assigned budget is less than the least cost of installing a unit PMU, then no installation is done at that time. Consequently, the budget can be carried over and the new budget for the following stage $k + 1$ period becomes,

$$B_{\text{phase}}^{k+1,\text{new}} = B_{\text{phase}}^{k+1} + B_{\text{phase}}^{k,\text{carry}} \tag{4.10}$$

and

$$B_{\text{phase}}^{k,\text{carry}} = B_{\text{phase}}^k - C_{\text{phase}}^{k,\text{inst}} \tag{4.11}$$

where $C_{\text{phase}}^{k,\text{inst}}$ is the actual cost of installing $N_{\text{pmu}}^{\text{STG},k}$ PMUs at a stage k. with a proper applications of (4.10) and (4.11) and in the absence of other extenuating factors, the sum of the stage cost $C_{\text{pmu}}^{\text{STG},k}$ across all stages should be the same as the optimal cost $C_{\text{pmu}}^{\text{fo}}$ of Step 1.

$$C_{\text{pmu}}^{\text{fo}} = \sum_{k=1}^{T} C_{\text{pmu}}^{\text{STG},k} \tag{4.12}$$

In the next sections, it will be shown that It will be shown that $C_{\text{pmu}}^{\text{fo}}$ may change over the years due to a number of factors.

4.6.2 Deteriorating performances of already installed components

A good incremental or multi-stage PMU placement algorithm models for limited budget consideration must account for time lapse between successive placements. Therefore, the probability that a PMU installed at a bus i will continue to work for a number of years until the PMU determined by an incremental placement is installed at another location j is not fully guaranteed. Although

the reliability of measurement devices is typically high, budgetary allocations determine if the unreliability of already installed PMUs would not have deteriorated to such a level as to warrant significant maintenance costs. To allow for this, a certain percentage of the total budget for the current stage is allocated to maintaining existing components. This may include the cost for routine maintenance, re-calibration, or activation. At the $k+1-$th stage, the maintenance cost for PMUs installed at Stage k may be assumed as 0.1% of the total cost of installations already made. Hence, the cost for routine maintenance may be calculated as,

$$MC^k = 0.001 \sum_{f=1}^{k} C_{\text{phase}}^{f,\text{inst}} \tag{4.13}$$

where MC^k is the maintenance cost for the already-installed devices which must be taken into consideration when evaluating the new budget at a later stage $k+1$.

Moreover, the reliability threshold specified in the previous section may be interpreted to mean that there is a $((1 - R_{\text{sys}}^k) \times 100)$% chance that some of the measurement devices which have already been installed are in need of preventive maintenance or repair. Suppose that a total number $\sum_{f=1}^{k} N_{\text{pmu}}^{\text{STG},f}$ PMUs have been installed at the $k-$th stage, it can be calculated that $100(1 - R_{\text{sys}}^k)$% of the total installations at stage k are in need of repair. Furthermore, the repair cost may be assumed as 3% of the total cost of the components in need of repair. Since the devices themselves are not known, the cost of one damaged PMU is evaluated as an average cost of the total number of installations at that stage. In essence, the repair cost at stage k then becomes,

$$RC^k = 0.03 \times (1 - R_{\text{sys}}^k) \sum_{f=1}^{k} C_{\text{phase}}^{f,\text{inst}} \tag{4.14}$$

In sum, the cost of maintaining and repairing already-components may be estimated as,

$$RMC^k = MC^k + RC^k \tag{4.15}$$

With the consideration of maintenance and repair costs, the new stage budget for all stages $k+1$ with $k > 1$, may be modified from (4.10) to obtain (4.16).

$$B_{\text{phase}}^{k+1,\text{new}} = B_{\text{phase}}^{k+1} + B_{\text{phase}}^{k,\text{carry}} - RMC^k \tag{4.16}$$

4.6.3   Inflation Rate and Improvement in Technology

Year on year inflation may affect the projected cost of the PMU at any future $k+1-$th stage. This financial reality has been overlooked in current literature on multi-stage placements. Inflation generally reduces the purchasing power of a currency, affects general costs of installations, and results in a decrease in anticipated installations. One may account for its effect by adjusting for it early on in the planning stage by varying the cost over each incremental phase using a knowledge of past inflation rates, or by varying the cost by the inflation rate over each incremental phase. In order to account for the effect of inflation, the cost of components, labour, and equipment as outlined in Section 3.4 are adjusted in the constraint (4.4d) for candidate PMUs which have not been installed. Consequently, the budget assigned for the stage reduces in purchasing power, and the installation cost at stage $k+1$,

$$C_{jlr}^{dv,k+1} = (1+h)C_{jlr}^{dv,k} \tag{4.17}$$

where h is the inflation rate at the stage $k+1$.

On the other hand, an improvement in PMU manufacturing technology may result in the reduction of unit procurement costs for future procurements, or results in advanced communication and measurement protocols with attendant interoperability issues with already installed devices. However, in the case studies, the effect of improvement in technology will not be included in the model.

4.7 Budget-Constrained Multistage Placement Algorithm (BCM-PP)

The flowchart below describes an algorithm for the budget constrained multi-stage placement problem (BCM-PP), following from the previous sections. For a given network topology, costs and mixes of PMU channel capacities, number of vendors, and location of PDCs, the BCM-PP is a dual-step process.The first step involves the planning of the optimal locations for the deployment from the OPP (3.16) and the cost for the required level of observability is evaluated from the solution of the OPP. In the second step, the available budget is used to deploy a number of PMUs for the observability at that stage. If no critical buses are present at any Stage k of Step 2, OPP (4.4) is used for normal deployment. However, if the observability of some buses are desired at the Stage k, OPP (4.8) is used. At each stage, the installation costs are constrained to be below or equal to the available budget. After the installations, the actual costs are calculated and the balance is carried over to the next stage. The maintenance and repair costs at the previous stage is calculated and subtracted from the available budget for Stage k. If there is a change in the network topology at any stage, planning at Step 1 is repeated by considering the presence of the already-deployed measurement devices, and the optimal locations are revised. The process is repeated until all planned PMUs have been deployed.

4.8 Case studies

In the following, the formulation is illustrated with two IEEE test cases; the IEEE 14-bus and the 118-bus test systems. For the 14-bus network, only the multichannel deployments without and with the consideration of the factors listed in Section 4.6 are considered. This allows comparison of the solutions of the proposed formulation with those obtained in other works such as [147]. A complete deployment is also considered for the co-placement multi-vendor case without and with the factors of Section 4.6 using the larger 118-bus network as described in Chapter 3.

4.8.1 Case A: Base multi-stage deployment

The base cases uses the IEEE 14-bus and 118-bus networks first without considering CI co-placements and multiple vendors and then with the considerations.

14-bus Network: Exclusive deployment of DULRs

An exclusive deployment of DULRs is first examined for the IEEE 14-bus network using a more simplistic version of OPPs (3.16) and (4.4), i.e. without the consideration of multiple vendors and co-placements. This is the deployment of uniform-cost PMUs of current channel capacities $l = 1$. If the cost of a DULR is 1 unit and a budget of 3 units is assigned to each stage of Step 2, then the simplified forms of OPP (3.16) and (4.4) give candidate solutions as in the Table 4.1 below. In Step 1, a total of 7 DULRs was determined as the minimum number that would be required to
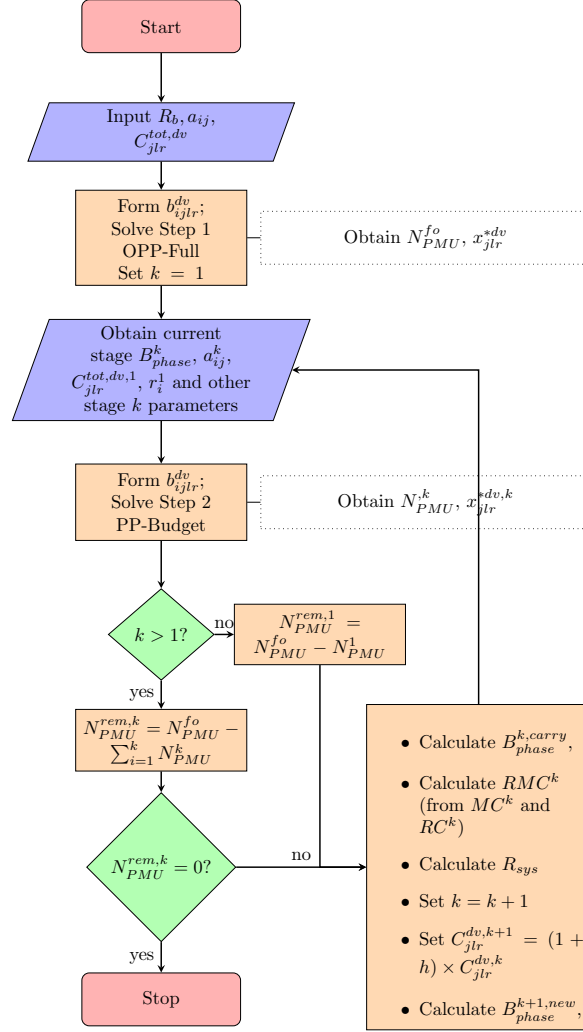
FIGURE 4.2: Flowchart for the Budget Constrained Multistage Placement Algorithm

yield full network observability without any redundancy. Since the stage budget is known and no maintenance and repair costs are considered in this case, the period of deployment can be easily estimated from (4.9) as $T = 3$. As shown in Table 4.1, each bus is observable only once, emphasising the efficacy of the formulation in minimising the cost of deployment by reducing unspecified redundancies. On account of the specified limited budget, only 3 DULRs were deployed in each of the first 2 stages of Step 2, and the remaining DULR was deployed in Stage 3. For the present illustration there was no carry over of balances and so the application of (4.11) and (4.10) was not necessary.

In the preceding, it has been assumed that the observability of some buses are not prioritised over others. In order to set priorities for placements, the optimal solution is determined in Step 1 using OPP (3.16). However, a formulation of the form of OPP (4.8), rather than (4.4), is applied in Step 2. Suppose that the priorities of the buses are set as given in Table 4.2, following the description in Section 4.5.5. In the table, buses 1, 6, 7, and 13 are assigned weights between 2 and 3 while the other buses have unity priorities. With weights $W_7, W_{13} = 3$, the buses 6 and 13 are considered to
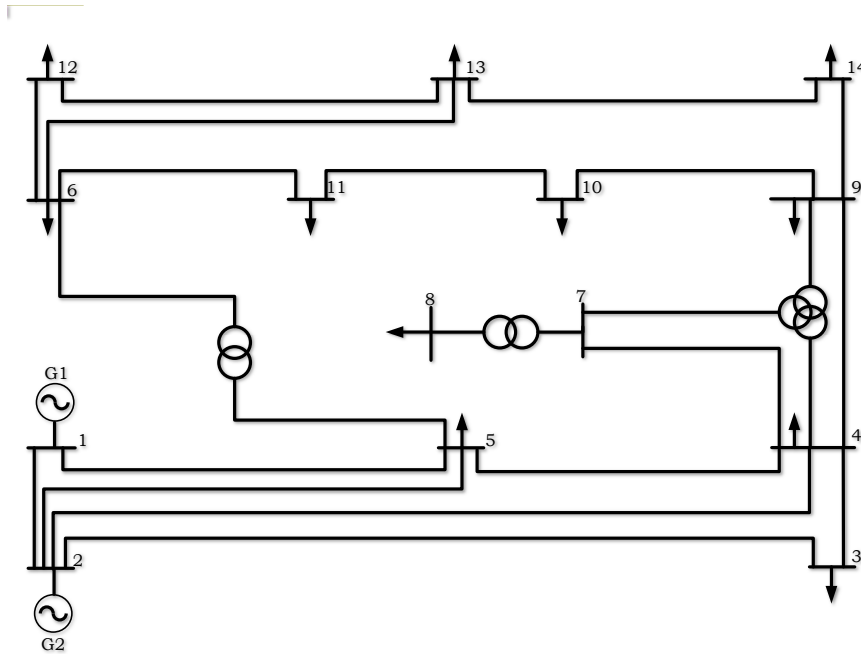
FIGURE 4.3: The IEEE 14-Bus Test System

TABLE 4.1: Case A: Multistage placement result for the IEEE 14-bus network with
no prioritisation of bus observability

Step 1		Step 2		
Bus	Branches	Stage 1	Stage 2	Stage 3
3	3-2	√		
4	4-9	√		
5	5-1	√		
8	8-7		√	
11	11-10		√	
12	12-6		√	
13	13-14			√
#placed	7	3	3	1

have higher priorities than the other priority buses 1 and 8. Note that of all the buses, only Bus 13 is part of the original candidate PMU buses as determined in Step 1. The stage budget used in the previous analysis with no set priority buses remains unchanged.

The result of applying (4.8) in Step 2 is shown in Table 4.3. At Stage 1, the higher priority Buses 6 and 13 are observed through the placements of DULRs at candidate PMU buses 12 and 13 respectively. Due to budget limitations, of the other priority buses 1 and 7, only Bus 1 is observed though a DULR placement at Bus 5 in this stage. At the second stage, bus 7 is observed through the placement of a DULR at bus 8. Since the last priority bus 8 has now been observed, two non-critical (with criticality as arbitrarily defined in Table 4.2) deployments can now be carried out at buses 3 and 4. With the budget exhausted for stage 2, and with 6 out of 7 originally planned placements already done, the last DULR at bus 11 is deployed at Stage 3.

TABLE 4.2: Case A: Assumed priority values for buses in the 14-bus Network

Bus, i	1	2	3	4	5	6	7	8	9	10	11	12	13	14
Weight, $\bar{W}_i$	2	1	1	1	1	3	2	1	1	1	1	1	3	1

TABLE 4.3: Case A: Multistage DULR placement result for the IEEE 14-bus network with prioritisation of bus observability

Step 1		Step 2		
Bus	Branches	Stage 1	Stage 2	Stage 3
3	3-2		$\checkmark$	
4	4-9		$\checkmark$	
5	5-1	$\checkmark$		
8	8-7		$\checkmark$	
11	11-10			$\checkmark$
12	12-6	$\checkmark$		
13	13-14	$\checkmark$		
#placed	7	3	3	1

Case Study A: 14-bus network - multi-stage deployment of dual-use line relays and stand-alone phasor measurement units

Next, the presence of non-homogeneous mixes of PMU channel capacities can be considered. As illustration, a maximum current channel capacity $L = \Delta E = 5$ is used. The same simplified OPP models, which do not consider multiple vendors and CI co-placements, similar to those in the previous section, are used in this analysis at steps 1 and 2. In essence, the focus here is to demonstrate the efficacy of the proposed OPP set-up when standalone units and DULRs are available for deployment in the grid. As shown in Table 4.4, only 4 PMUs are deployed in this case; one each of DULR, 3-channel, 4-channel and 5-channel PMUs. Using the weights in Table 4.2, all prioritised buses 1, 6, 7, and 13 can be observed by through the deployments of a 3-channel and 4-channel PMU at buses 2 and 6 respectively. The installation cost for both deployments at this stage was 2.7 units. For a stage budget of 3 units, a balance of 0.3 unit is carried over to the next stage where a DULR and a 3-channel PMU are deployed at buses 8 and 9 to monitor the yet to be observed buses. The deployments at Stage 2 cost 2.2 units.

Compared to the exclusive DULR placement, the non-homogeneous deployment of PMUS considered in this section required the installations of fewer PMUs at fewer number of stages and at a lesser cost. Although this result might seem to encourage non-homogeneous placements, the outcome may be different in practice depending on the cost differentials between diverse channel capacities, the existence of DULRs, and the availabilities of PMU installation equipment, as discussed in Chapter 3. In the next section, the multi-stage placement method is discussed using the complete forms of the OPP models in the context of the factors outlined in Section 4.6.

Case Study A: 118-bus network - multi-stage deployments with homogeneous channel, multi-vendor and communication infrastructure co-placement consideration

In the multi-vendor multi-objective consideration, no adjustment is made to the complete set-up in (3.16) and (4.4). This represents the planning and deployment stages, and with an additional

TABLE 4.4: Case A: Multistage Nonhomogeneous capacity PMU placement result
for the IEEE 14-bus network with prioritisation of bus observability

Bus	Step 1 Branches	Step 2 Stage 1	Stage 2
2	2-1-3-4	✓	
6	6-5-11-12-13	✓	
8	8-7		✓
9	9-7-14		✓
#placed	4	2	2
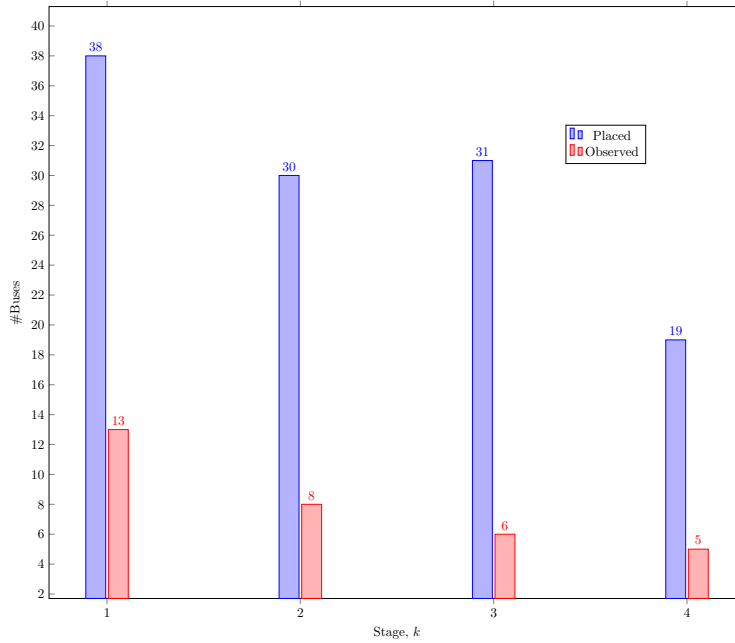
FIGURE 4.4: Case A: (118-bus test network) Number of observed and placed buses
at each stage k

reliability requirement, as in (3.18). The complete cost model of Section 3.4 is used. At the beginning, it may be assumed that no measurement device has been deployed and that there are no available instrument transformers in place. However, $R_{min} = 0.84$ and $L = 9$. In the light of the preceding, it may be assumed that all other parameters of Section 3.8 of Chapter 3 are re-used here. Note that the algorithm is implemented as described in Figure 3.7. At Step 1, $N_{pmu}^{fo} = 32$ and x^* as shown in Table 4.5. This essentially expresses the result of Section 3.8.4 for the case with no existing measurement and availability of instrument transformers. The optimal objective of the OPP (3.16), corresponding to the total cost that would be needed for deployment is obtained as 911.26 units. Here, the vendors, PDCs, channel capacities, buses, and branches that must be installed to realise full observability at $R_i = 0$ are fully specified. At the second step, the stage budget was estimated from (4.9) for a chosen number of deployment stages $T = 4$ as $B_{phase}^k = 227.82$ units. This resulted in the deployment of 13 PMUs at Stage 1 of Step 2 with 38 observed buses from these placements. At Stages 2, 3, and 4 of Step 2, increases of 30, 31, and 19 additional observed buses were obtained for the deployments of 8, 6, and 5 PMUs at the respective stages. This is shown in the bar chart of Figure 4.4. The 2nd, 3rd and 4th rows of Table 4.6 shows that the budget of 227.82 units at the stage

TABLE 4.5: Case A: Multistage placement result for the IEEE 118-Bus Network

	Step 1				Step 2			
Bus	Branches	Number of Channels	PDC	Vendor	Stage 1	Stage 2	Stage 3	Stage 4
3	3-1	2	A	v_2	√			
5	5- 4- 6 9	3	A	v_2	√			
9	8 10	2	C	v_2	√			
12	12-2-7-11 -14-16 -117	7	C	v_2			√	
15	15-13	2	C	v_2	√			
17	17-18-113	3	C	v_2	√			
20	20-19-21	3	C	v_2		√		
23	23-22-24-32	4	B	v_2		√		
26	26-25-30	3	B	v_2	√			
29	29-28-31	3	C	v_2		√		
34	34-36-43	3	D	v_2	√			
37	37-33-35-38-39	5	D	v_2	√			
40	40-42	2	D	v_2	√			
45	45-44-46	3	G	v_2			√	
49	49-42-47-48-50 -51-54-66	8	G	v_3			√	
52	52-53	2	G	v_2		√		
56	56-55-57-58-59	5	E	v_2			√	
62	62-60-61-67	4	F	v_3	√			
63	63-64	2	E	v_2	√			
68	68-65-116	3	H	v_3	√			
71	71-70-72-73	4	H	v_3		√		
75	75-74-118	3	H	v_3	√			
77	77-76-78-82	4	H	v_3		√		
80	80-79-81-96-97 -98-99	7	I	v_2		√		
85	85-83-84-88-89	5	H	v_2				√
86	86-87	2	H	v_2				√
91	91-90	2	I	v_2				√
94	94-92-93-95-100	5	I	v_1			√	
101	101-102	2	I	v_2			√	
105	105-103-104-106 -107-108	6	I	v_3				√
110	110-109-111-112	4	I	v_3				√
115	115-27-114	3	B	v_2		√		
#placed	32				13	8	6	5

$R_i = 1, L = 9, T = 4$

1 was not fully used, resulting in the carry-over of a balance of 5.920 units to Stage 2 using (4.11). At Stage 2, the new stage budget thus became 233.74 units with the application of (4.10). At Step 2, a balance of 15.772 units was added to the budget at Stage 3, giving a new budget of 243.08 units at that stage. At the last stage, no carried over balances were incurred, and the total cost across all stages was equal to the optimal cost of Step 1 according to (4.12). In summary, it can be seen that although a uniform stage budget of 227.82 units has been assigned to each of the 4 stages of Step 2, carrying over the balances at the end of each stage ensured that all PMUs are deployed at the pre-determined number of stages and at the optimal cost.

TABLE 4.6: Case A: (118-bus test network) stage budgets and reliabilities

Stage	1	2	3	4
Base	227.82	227.82	227.82	227.82
Actual	221.9	218.4	222.97	248.01
Carry	5.92	15.34	20.19	0
Reliability	0.97	0.94	0.87	0.85

The last row of Table 4.6 shows how the system reliability converges to the specified threshold $R_{\min} = 0.84$ as stages in Step 2 progress, for a redundancy of $R_i = 0$. At Stage 1, the system measurement reliability was 0.974 for 13 deployed PMUs. This decreased to 0.938 for 21 deployed PMUs when 8 more were added in Stage 2, and then to 0.875 for 27 total installations at Stage 3. At Step 4, the threshold realised conformed to that originally planned in Step 1. The system measurement reliability indices at each stage merely indicated the probability of losing grid observability, and rises when the number of measurement components in the grid increases. This means that at Stage 1 of Step 2, the chances of loosing grid observability for a small portion of the grid was 2.57 % and this probability is lesser than 15.32% when the whole grid had to be monitored with a wider array of measurement devices at Stage 4.

4.8.2 Case B: Multistage deployment with the consideration extenuating factors affecting stage budget

Compared to the previous case, the maintenance and repair costs incurred on already-placed devices are subtracted from the available budget at the next stage, and the installation cost is assumed to rise by an inflation rate h% compared to the cost at the previous stage. Depending on whether separate provisions have been made to cover the extraneous expenses, the originally planned period of deployment, T may increase. Table 4.7 shows the placement result when no separate allowances have been made for maintenance, repair, and inflation, with $h = 1$. The installation took place over 5 stages, rather than the original 4. Table shows the costs incurred on the factors considered as the stages progress.

With the reliability decreasing with increasing number of installations as shown in Table 4.8, the tendency for the devices to fail increases with every new installation. At the first two stages, the repair costs are negligible and the number of PMUs deployed at each stage is the same as those of the same stage in the previous section.

However, at Stages 3 and 4, the extra costs incurred affected the planned placements, and only 5 PMUs (compared to 6 and 5 at the same stages in the previous sections) are installed, as shown in

TABLE 4.7: Case B: Multistage placement result for the IEEE 118-Bus Network with the consideration extenuating factors affecting stage budget

	Step 1				Step 2				
Bus	Branches	Number of Channels	PDC	Vendor	Stage 1	Stage 2	Stage 3	Stage 4	Stage 5
3	3-1	2	A	v_2	✓				
5	5- 4- 6 9	3	A	v_2	✓				
9	8 10	2	C	v_2	✓				
12	12-2-7-11 -14-16 -117	7	C	v_3			✓		
15	15-13	2	C	v_2	✓				
17	17-18-113	3	C	v_2	✓				
20	20-19-21	3	C	v_2		✓			
23	23-22-24-32	4	B	v_2		✓			
26	26-25-30	3	B	v_2	✓				
29	29-28-31	3	C	v_2		✓			
34	34-36-43	3	D	v_2	✓				
37	37-33-35-38-39	5	D	v_2	✓				
40	40-42	2	D	v_2	✓				
45	45-44-46	3	G	v_2			✓		
49	49-42-47-48-50 -51-54-66	8	G	v_3			✓		
52	52-53	2	G	v_3		✓			
56	56-55-57-58-59	5	E	v_2			✓		
62	62-60-61-67	4	F	v_3	✓				
63	63-64	2	E	v_1	✓				
68	68-65-116	3	H	v_3	✓				
71	71-70-72-73	4	H	v_3		✓			
75	75-74-118	3	H	v_3	✓				
77	77-76-78-82	4	H	v_3		✓			
80	80-79-81-96-97 -98-99	7	I	v_2		✓			
85	85-83-84-88-89	5	H	v_2				✓	
86	86-87	2	H	v_2				✓	
91	91-90	2	I	v_2				✓	
94	94-92-93-95-100	5	I	v_1			✓		
101	101-102	2	I	v_2				✓	
105	105-103-104-106 -107-108	6	I	v_3					✓
110	110-109-111-112	4	I	v_3					✓
115	115-27-114	3	B	v_2		✓			
#placed	32				13	8	5	4	2

TABLE 4.8: Case B: (118-bus test network) stage budgets with the complete application of the BCM-PP algorithm (along with stage reliability and inflation rates)

| Description | Stage | | | | |
	1	2	3	4	5
Budgeted(m.u)	227.82	227.82	227.82	227.82	0
Actual(m.u)	221.9	220.65	187.52	183.26	113.64*
Carry(m.u)	5.92	9.12	36.53	50.79	0
MC(m.u)	0	-2.24	-4.49	-5.93	-8.35
RC(m.u)	0	-3.97	-12.89	-27.64	-41.07
System Reliability	0.97	0.94	0.88	0.87	0.85
Inflation Rate(%)	1	1.01	1.02	1.03	1.04

Figure 4.5. At the end of stage 4, only 30 of the original 32 PMUs have been installed. Unplanned budgets have to be spent on installing the two remaining PMUs.

4.9 Summary

In this chapter, a novel multi-stage placement algorithm has been described using a two-step multi-objective PMU ILP optimisation formulation. The first step involves the planning of the optimal PMU locations and the second is concerned with the implementation of the plan over a period of time depending on the financial capability of the utility. In addition to the description of the multi-stage budget-constrained algorithm, the chapter also included a discussion of the effect of inflation costs on planned installations, the effect of maintenance and repair costs on already-installed components, changes in network topology, and the prioritisation of the observability of some buses during the multi-stage placements.

The algorithm returns an optimal solution which compares favourably with existing work in literature. The performance is demonstrated on the IEEE 14-bus and the IEE 118-bus test networks across a number of scenarios using a simplified versions and subsequently, a complete model, considering, essentially, the presence of multiple vendors, multiple PMU capacities, and co-placement with PDCs.
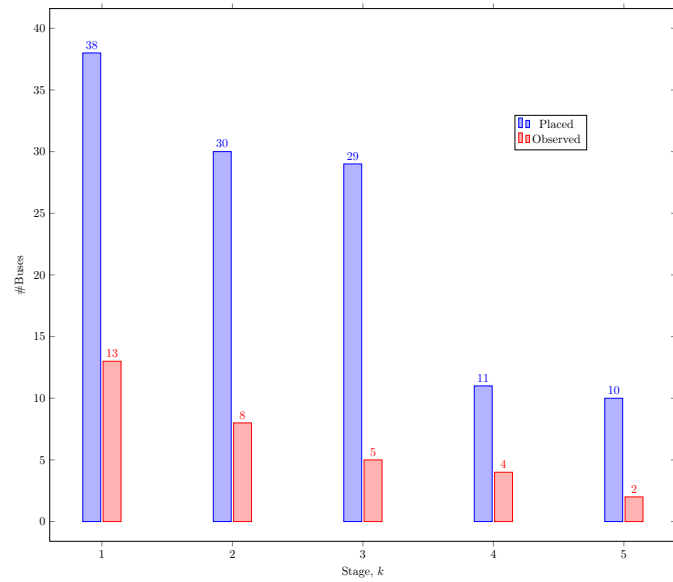
FIGURE 4.5: Case B: (118-bus test network) Number of observed and placed buses at each stage *k* with the complete application of the BCM-PP algorithm

Chapter 5

Placements with Focus on Specific Applications

5.1 Introduction

So far we have considered placement from an idealistic full-observability perspective and from a more realistic multi-stage placement. However, in addition to budget limitations, utilities may also wish to install only a number of PMUs as to address a particular application concern. In this chapter, PMU placement methods, with the end goal of using the data for applications like secondary voltage regulation, are described. For this type of placements, the focus is on how the PMUs deployed would help to enhance a particular application or a fixed set of applications. In most cases, a select number of buses are targeted as critical for that application. Therefore, full observability may not be a priority. The chapter is organised as follows. First, existing literature in this regard is reviewed. Subsequently, an algorithm on PMU placement with specific application intents is proposed. Notable among the novel formulations in this chapter is an adjusted cost function which minimises the costs of placements but maximises the benefits obtained from the measurement devices. Solutions are optimal for all factors considered.

5.2 The multi-objective application-focused PMU placement

This chapter focuses on how the placement algorithm of OPP (3.16) may be extended to placements that are focused on particular applications, such as voltage control, oscillation damping, and islanding detection, and model validation. Since voltage control is the central theme of this thesis, the approach will to focus on voltage application-focused PMU placement strategies, using the 39-bus New England network [148] and the previously-used 118-bus system, which was described in Section 3.8.3, as test-beds. The 39-bus test system has 10 generators, 19 loads, 36 transmission lines and 12 transformers and represents a vastly reduced form of the representative network. It has been widely used for dynamic and static voltage analyses by researchers. Its modified data may be found in [149] and may be considered sufficient for the present purpose.

5.2.1 A brief review of similar application-focused placements

It has been mentioned in Section 4.6 that utilities may invest in monitoring devices only so far as the benefit of improved visibility offered by these devices are higher than the investment in the short or longer term. In close relation with the more practical multistage placement of Chapter 4, utilities may aspire towards application-focused WAMS deployment for economic reasons. For utilities seeking to apply phasor data for voltage monitoring, analysis and control, a set of critical buses and lines may be pre-identified either through experience, extensive dynamic simulations, or multiple runs of static load flow studies. For secondary voltage control in particular, the objective is

to find the buses which have the largest short-circuit sensitivity, or in other words, have the smallest voltage response to reactive power injections. The central idea being to regulate the voltages of the more intransigent nodes and indirectly bring those of the more sensitive buses to within desired bands. These influential nodes are known as *pilot* buses and their selections should be determined by the secondary voltage control objective which may be to keep voltage within statutory limits, reduce active power losses, or minimise reactive power injection [80]. Since secondary voltage control uses the voltage involves an estimation of the level of control needed over the generators and voltage compensation devices in order to keep the pilot buses a steady state, the voltages at these select buses need to be monitored, most ideally through a Wide Area Monitoring System (WAMS) such as a PMU.

The first known PMU placement for secondary voltage control was carried out by [150]. Without considering a full observability of the system, a simulated annealing approach was used to provide some form of observability to the pilot buses, which were identified through a number of pre-described approaches. More recently, the work in [40] also addressed placements, with a constraint of full observability of all network buses and the use of a non-linear objective function. PMU placement at pilot nodes was ensured via a heavy penalty on the respective buses in the objective function, using pilot buses described in the works of [79], [151]. In [40], [150], the pilot buses were identified as the buses with the smallest voltage sensitivities to reactive power injections, $\frac{\partial V_i}{\partial Q_j}$ within a clustered group of electrically close buses. The methods used to determine the $\frac{\partial V_i}{\partial Q_j}$ sensitivities are static in nature, and could not therefore guarantee the characteristics of the system other than that under which it had been evaluated. In order to account for a wider range of grid behaviour, [152] applied a fast-decoupled probabilistic load flow (PLF) to the $2q + 1$ point estimate method (PEM) of [153]. The $2q + 1$ PEM is a reliability engineering concept which aims to estimate the moments of a random quantity which, in turn, depends on a number of random variables. Note that in this instance, q is the number of random variables affecting the quantity.

5.3   Contribution of the chapter

None of the existing methods of PMU placements for voltage control applications considered channel limitations, co-placement with CI, nor aspired to address compatibility issues arising from deployments of PMUs with different methods of phasor computations. In addition, some of th approach to formulation, such as a non-linear objective used in [40] may be impractical, the methods heuristic, and not guaranteed to yield an optimal solution even in the light of the limited factors considered in the setups (e.g the use of the simulated annealing method in [150].

In the following, we describe how the algorithm we have introduced previously in Chapter 3 may be extended for application in secondary voltage control. Consequently, the objective of this chapter would be to,

1. Describe how the previously formulated multi-variable and multi-objective PMU placement method may be used for secondary voltage control and state estimation.

2. Describe how observability may be maximised compared to existing methods in voltage-control-sensitive PPP.

3. Address channel, CI co-placement and vendor-compatibility issues in voltage-control-sensitive PPP.

5.3.1 Selective observability of pilot buses

Phasor data from any bus may be obtained directly by placing measurement devices on the bus, or indirectly through a device at the adjacent node using Ohm's law, as previously described in 3.1. However, direct monitoring of pilot buses do not necessarily maximise the observability which may be obtained with a similar number of devices using a more strategic placement. To illustrate, consider the Figure 5.1, which has figures describing different placement strategies for a clustered region A. Note that clusters are groups of buses which have strong interconnection through close electrical distances and that a cluster may have one or two pilot buses which should be able to influence the voltages of the other buses in the group. For this example, the node at 3 may be assumed to be the pilot bus of the cluster A in both figures of 5.1. Green lines indicates that the current phasors may be successfully measured along that line. Voltage phasors may also be monitored at green nodes. In both instances, it can also be assumed that the PMU has sufficient channel capacities to measure the voltage at its bus and the currents at all branches connected to that bus. A deployment of a PMU at pilot node 3 in Figure 5.1a shows that only one node voltage (at Node 2) may be measured in addition to the node voltage at 3. In Figure 5.1b, the same number of deployment resulted in the observability of two additional node voltages and an equal increase in the number of monitored line currents.

(A) Placement at pilot bus in clustered region

(B) Placement to maximise observability in clustered region
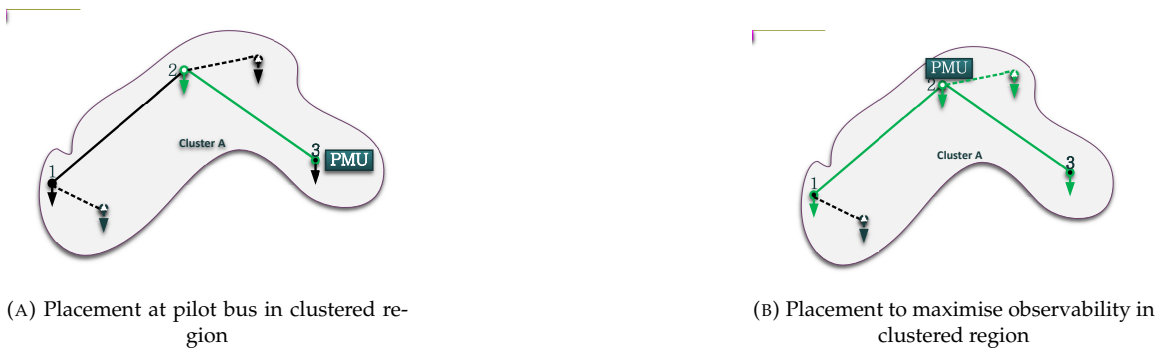
FIGURE 5.1: Placement strategies for voltage stability application

From [151] and [78], the test system can be partitioned into four areas with one or more pilot buses in each area. The pilot buses and generators for the 39-bus network are taken from [151] and shown in Table 5.1. In a similar manner, the pilot buses for the 118-bus network are obtained

TABLE 5.1: Generators and pilot buses selection for the 39-bus New England network

Area	1	2	3	4
Pilot Bus	1	28	7, 11	3,16
Generators	39	38	31, 32	30,33,34, 35,36,37
Bus	1,9	28,29	4,5,6,7,8,11,12, 13,14,15	2,3,16,17,18,19,20,21, 22,23,24,25,26,27

from [79] and are shown in Table 5.2 according to the regions in Figure 3.10, which is shown in this chapter for convenience.
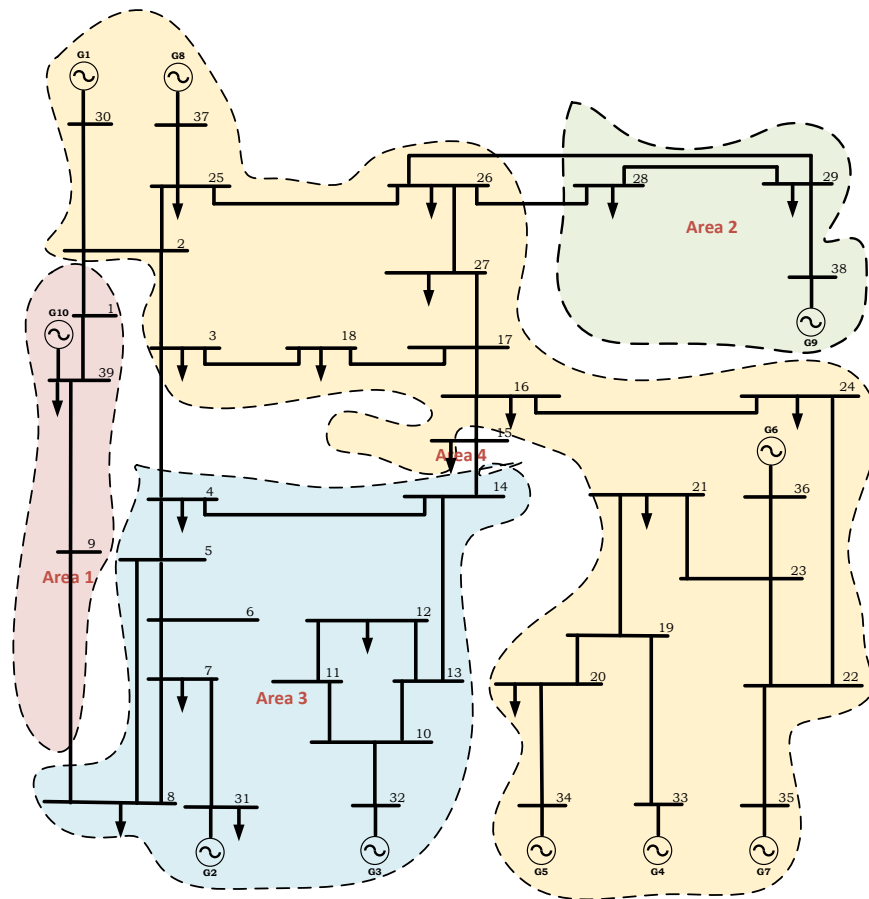
FIGURE 5.2: 4-Region IEEE 39-Bus Test System

TABLE 5.2: Pilot buses for the 118-bus IEEE network

Region	1	2	3
Pilot Bus	2 ,19	39,56,68 70,80	88,103, 114

5.4 Achieving observability with and without placement on pilot buses: full and selective observability

For secondary voltage control applications, the observability of pilot buses are considered critical. In this section, PMU placement for this application is described by considering the following deployment strategies.

1. Placements which enforce observability of pilot buses through direct deployment of PMUs on the pilot buses

2. Placements which seek PMU installations at any bus as long as the observability of pilot buses are ensured.

3. Placements which provide for the full observability of all buses, without enforcement of direct placement on pilot buses.

FIGURE 5.3: 3-Region IEEE 118-Bus Test System with local PDC locations indicated
in red broken ellipses

4. Placements in which all buses are observable but require direct PMU deployments on pilot
   buses.

.

The OPP (3.16), introduced in Chapter 3, is the foundation for the proposed formulation in this
section. The OPP may be simplified by eliminating d and v variables from the equation, equivalent
to not considering multiple vendors and CI co-placements in the setup. Both full and simplified
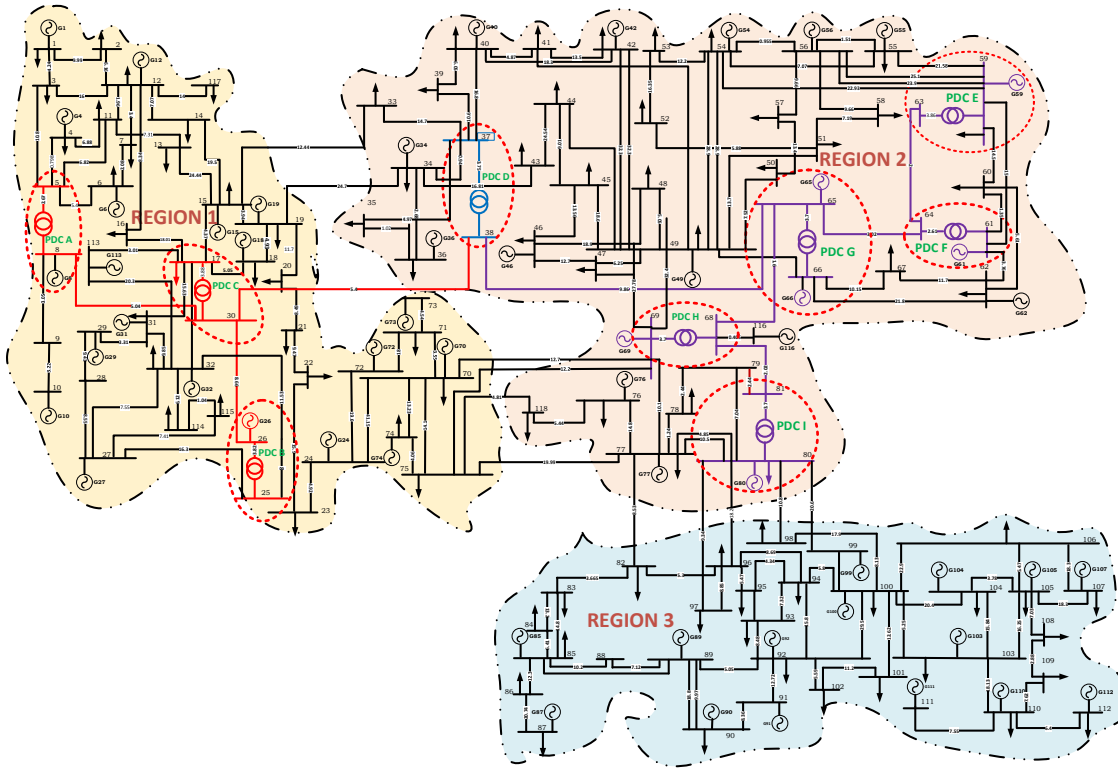models may be used alternately on the 39-bus and 118-bus networks to illustrate the efficiency of
OPP setups which will be described in this section.

The chart in Figure 5.4 shows how the strategies listed above may be used with the simplified
and complete OPP models.

The placement strategies listed above can be achieved in two ways. The first method is to
minimise the costs of placement with the specifications of either full or selective observability. Se-
lective observability in this case refers to monitoring of only a pre-determined number of buses, as
opposed to full observability where all network buses are monitored, directly or indirectly. The sec-
ond approach is a two-step process, similar to the method used in the multistage method described
in chapter 4. The first step in this second method of placement being to first determine the optimal
number of PMUs that would be needed for the full observability of the network, given the net-
work topology, and the second step would be to maximise the observability across the prioritised
buses(in this case, pilot buses) subject to the available budget.
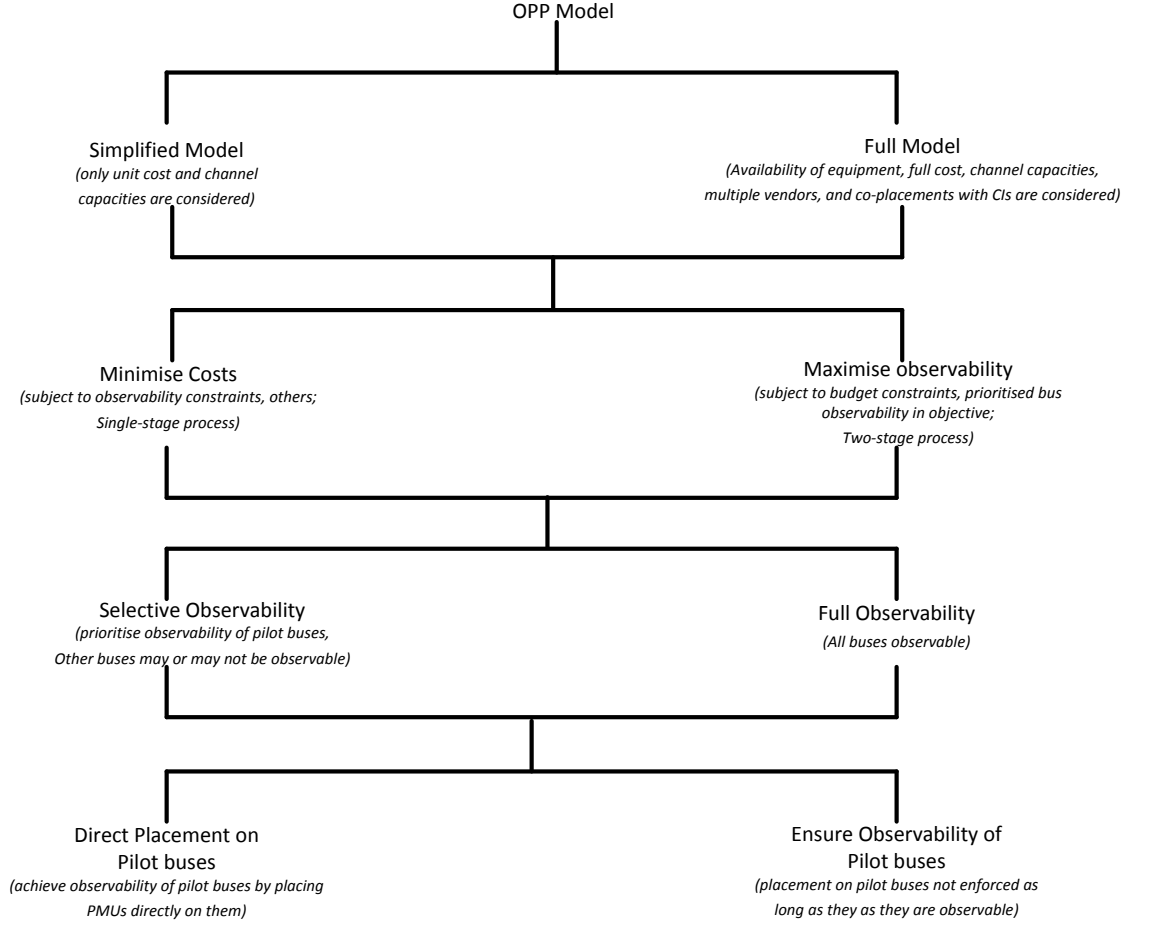
FIGURE 5.4: An overview of proposed placement strategies for secondary voltage
control applications, models used, and their implementations.

5.4.1   Minimising costs

The PMU placement formulation for voltage control application is first presented as (5.1), a modified form of the OPP (3.16) of Section 3.5, i.e. without the consideration of co-placement with CIs and multiple vendors. The formulation 5.1 ensures that pre-identified pilot buses are observable at the best minimum cost.

$$\underset{x_{jlr}}{\text{minimize}} \sum_{j=1}^{n} \sum_{l=1}^{L} \sum_{r=1}^{r^s} C_{jlr} x_{jlr} \tag{5.1a}$$

$$\text{subject to} \sum_{j=1}^{n} \sum_{l=1}^{L} \sum_{r=1}^{r^s} b_{ijlr} x_{jlr} \geq \kappa, \forall i \in I \tag{5.1b}$$

$$x_{jlr} \in \{0,1\} \tag{5.1c}$$

Note that,

$$
b_{ijlr} = \begin{cases} 1, & \text{if } (i = j) \cap (i, j \in S_{jlr}) \\ 1, & \text{if}(i \in S_{jlr}) \cap (j \in S_{jlr}) \\ 0, & \text{otherwise} \end{cases}
$$

All the notations in (5.1) retain their previous definitions from Chapter 3. In addition, for selective observability of pilot buses,

$$
\kappa = \begin{cases} R_i + 1, & \text{if bus } i \text{ is a pilot bus} \\ 0, & \text{otherwise} \end{cases}
$$

In addition, the linearity of OPP (5.1) is not compromised since the RHS of constraint (5.1b) is a product of two linear parameters. C_{jlr} is the channel-influenced unit device costs as used in Section 3.8.1, where a two-channel PMU device was assumed to cost 1 unit and each additional channel was assumed to cost an extra 0.1 unit. Note that the availability and cost models of Section 3.4 are not used in the initial setup (5.1). Therefore, for selective observability of pilot buses, the formulation seeks to minimise, through a reduction in the channel usage, the costs of observing, but not necessarily directly monitoring, the pilot buses to be used for secondary voltage control purposes. For non-pilot buses where the RHS of (5.1b) ≥ 0, the constraint (5.1b) simply specifies that observability requirements for these buses are not binding. An inherent but necessary assumption is that the pilot buses and control areas do not change with system dynamics, as PMUs may not be redeployed after they have been installed.

In essence, the OPP (5.1), encourages the deployment of more readily available and affordable DULRs while accounting for channel limitations, depending on the choice of the maximum number of channel capacity, L in the non-homogeneous mix of deployable PMUs. This already poses an advantage over the methods in [40], [150], [152] which do not account for channel limitations and the use of DULRs in their voltage control-sensitive PMU placements.

Tables 5.3 and 5.4 show the result of implementing the OPP (5.1) on the IEEE 118-bus test system for maximum current channel capacity $L = 2$ and $L = 3$. At $L = 2$, the solution to OPP (5.1) is the deployment of 8 DULRs and 1 3-channel PMUs at $R_i = 0$. The main difference in the results for $L = 2$ and $L = 3$ is mainly at the redundancy level $R = 2$, leading to a difference in deployed number of channels at this level. However, the total number of PMUs placed are the same in both cases. At increased redundancy levels of 1 and 2, the number of DULRs deployed for double observability of the pilot buses increased by 100% and over 200% respectively. Results from Tables 5.3 and 5.3 show that DULRs are largely deployed for selective observability, even for a relatively large network. Specifically, at redundancies $R_i = 0, 1, 2$, DULRs constitute 88.9%, 88.9%, and 92.5% of the total number of installations respectively at $L = 2$, and 88.9% at each redundancy level at $L = 3$.

5.4.2 Maximising observability

The second approach is to seek to maximise the observability of the pilot buses in a network. In order to do this, a two-step process is proposed, similar to the approach in Chapter 4. In the first step, the candidate solutions for full network observability are obtained using OPP (3.16) of Chapter 3, or a simplified form of the OPP model in this case. In the second step, the objective

TABLE 5.3: 118-bus network: Selective observability with no enforcement of placement on pilot buses at $R_i = 0, 1, 2$ (at pilot buses) and $L = 2$

Bus	$R_i = 0$		$R_i = 1$		$R_i = 2$	
	l_1	l_2	l_1	l_2	l_1	l_2
1	1-2		1-2		1-2	
2			2-1		2-1 2-12	
15	15-19		15-19			
18			18-19		18-19	
19					19-34	
20					20-19	
32	32-114		32-114			
37	37-39		37-39			
39			39-37		39-37 39-40	
40					40-39	
54	54-56		54-56			
55			55-56		55-56	
57					57-56	
58					58-56	
69		69-68-70		69-68-70		69-68-70
70			70-71			
71					71-70	
74					74-70	
77	77-80					
79			79-80			
80					80-79 80-81	
81				81-68-80	81-68	81-68-80
85	85-88		85-88		85-88	
88			88-85		88-85 88-89	
100	100-103		100-103			
103			103-110		103-110 103-105	
104					104-103	
114			114-32		114-32 114-115	
115					115-114	
Total by channels	*8*	*1*	*16*	*2*	*25*	*2*
Total	**9**		**18**		**27**	

*The pilot buses are 2, 19, 39, 56, 58, 70, 80, 88, 103, and 114.

TABLE 5.4: 118-bus network: Selective observability with no enforcement of placement on pilot buses at $R_i = 0, 1, 2$ (at pilot buses) and $L = 3$

	$R_i = 0$		$R_i = 1$		$R_i = 2$		
Bus	l_1	l_2	l_1	l_2	l_1	l_2	l_3
1	1-2		1-2		1-2		
2			2-1		2-1		
					2-12		
15	15-19		15-19		15-19		
19			19-34		19-34		
					19-20		
32	32-114		32-114		32-114		
37	37-39		37-39		37-39		
39					39-37		
40			40-39		40-39		
54	54-56		54-56		54-56		
55					55-56		
59			59-56		59-56		
69		69-68-70		69-68-70		69-68-70	69-68-70-77
75			75-70		75-70		
77	77-80						
80			80-79		80-79		
					80-81		
81				81-68-80		81-68-60	
85	85-83		85-88		85-88		
88					88-89		
89			89-88		89-88		
100	100-103		100-103		100-103		
103					103-110		
105			105-103		105-103		
114			114-32		114-32		
					114-115		
Total by channels	8	1	16	2	24	2	1
Total	**9**		**18**		**27**		

*The pilot buses are 2, 19, 39, 56, 58, 70, 80, 88, 103, and 114.

would be to maximise the observability of the network through a solution of the OPP (5.2).

$$\underset{u_i}{\text{maximize}} \sum_{p=1}^{n_{\text{pil}}} \bar{W}_p u_p + \sum_{k=n_{\text{pil}}}^{n} \bar{W}_k u_k \tag{5.2a}$$

$$\text{subject to} \sum_{j=1}^{n} \sum_{l=1}^{L} \sum_{r=1}^{r^s} b_{ijlr} \hat{M}_{ijlr} x_{jlr} \geq u_i \qquad \forall i \in I \tag{5.2b}$$

$$x_{jlr}, u_i \in \{0, 1\} \tag{5.2c}$$

In (5.2), the weights $\bar{W}_p$ and $\bar{W}_k$ are positive integers used for the prioritisation of observability of pilot and non-pilot buses respectively. For selective observation of pilot buses, the weight $\bar{W}_p > \bar{W}_k, \forall p, k$. Note that $\hat{M}_{ijlr}$ is the parameter of candidate solutions obtained from Step 1. If the placement is to be carried out with budget requirements, an extra constraint in the form of (5.3) may be added to OPP (5.2).

$$\sum_{j=1}^{n} \sum_{l=1}^{L} \sum_{r=1}^{r^s} \hat{M}_{ijlr} C_{jlr}^{\text{tot}} x_{jlr} \leq B \tag{5.3}$$

where B is the amount of available budget, and $\hat{M}_{ijlr}, C_{jlr}$ retain their previous definitions from Chapter 4.

5.4.3   Full observability with and without direct placements on pilot buses

In order to enforce the placement of PMUs on pilot buses, [40] formulated a setup with a nonlinear objective,

$$\sum_{i=1}^{m} C_i (x_i - 1)^2 + \sum_{m+1}^{n} w_i x_i \tag{5.4}$$

without any loss in notation, n is the total number of buses in a network containing m pilot buses. x_i are the binary variables as defined previously. However C_i and w_i are the weights assigned to nonlinear and linear terms in the objectives for the pilot and non-pilot buses respectively such that with $C_i >> w_i$, the formulation is biased towards placing PMUs on pilot buses.

The formulation (5.4) is deficient in a number of ways. First, the definition of weights precludes the inclusion of the real costs of PMU in the objective. Second, the non-linear term in the objective may increase the solution time since the resulting integer program is no longer linear. Although the placement strategy (5.4) may not result in a higher number of placements with bias towards placement on pilot buses specified as in (5.4) in [40], the specification of the cost and PMU channel capacities required to achieve the stated number of PMUs are not described. It is possible to reason with the intent of [40], i.e. to allow for instances where utilities may wish to install PMUs directly on the pilot buses with additional specification for observability of all network buses. However, this must be done with a good idea of the cost involved. Consequently, a more efficient and realistic solution, which accounts for real costs, channel limitations, and a linear ILP formulation is

TABLE 5.5: 39-bus network: Full grid observability with no enforcement of placement on pilot buses at $\kappa = 1, 2$

R_i	PMU Bus and Connected Branches																				Total
	2	5	6	9	10	11	13	14	16	17	19	20	22	23	25	29	33	34	35	39	
0	2 1 3 30		6 5 7 31	9 39	10 11 32		13 12	14 4		17 18 27	19 16 33		22 21 35	23 24 36	25 26 37	29 28 38		34 20			**13**
2	2 3 30 2 1 3 30	5 4 8 5 7 31	6 7 31 6	9 8 39	10 32 10 11 13 32	11 12	13 12 14	14 4 15	16 15 21 24	17 18 27 17 16 18 27	19 33	20 34	22 21 35	23 36 23 24 36	25 37 25 26 37	29 28 38 29 26 28 38	33 19	34 20	35 22	39 1 9	**27**

proposed here in the form of OPP (5.5).

$$\underset{x_{jlr}}{\text{minimize}} \sum_{j=1}^{n} \sum_{l=1}^{L} \sum_{r=1}^{r^s} C_{jlr} x_{jlr} \tag{5.5a}$$

$$\text{subject to} \sum_{j=1}^{n} \sum_{l=1}^{L} \sum_{r=1}^{r^s} b_{ijlr} x_{jlr} \geq R_i + 1, \forall i \in I \tag{5.5b}$$

$$\sum_{j=1}^{n} \sum_{l=1}^{L} \sum_{r=1}^{r^s} p_{ijlr} x_{jlr} \geq 1, \forall i \in \Xi_{\text{pilot}} \tag{5.5c}$$

$$x_{jlr} \in \{0, 1\} \tag{5.5d}$$

$$p_{ijlr} = \begin{cases} 1, & \text{if } i = j \cap (i, j \in \Xi_{\text{pilot}}) \\ 0, & \text{otherwise} \end{cases}$$

where Ξ_{pilot} is the set of all pilot buses. The constraint (5.5c) ensures that at least one PMU is placed at each pilot bus. Note that zero-injection buses and co-placement with CIs are not considered in this instance. The solution of OPP (5.5) are shown in Tables 5.5 and 5.6 for solutions without and with the use of constraint (5.5c), representing the lack of enforcement or otherwise of placement on pilot buses respectively.

For redundancy, $R_i = 0, \forall i$, 13 PMUs are installed in respective totals when there is no requirement for direct placements on pilot buses, compared to 18 PMUs when there is an enforcement of constraint (5.5c), representing an increase of anout 38.4% in the total number of deployments of the latter case over the former. Specifically, from Table 5.5, , 4 DULRs, as well as 6 and 2 3-channel and 4-channel PMUs, respectively, are required for placement without any redundancies when the costs are accounted for. In comparison with the result shown in Table 5.6 for solutions with an enforcement of placement on pilot buses, 16 DULRs and 2 3-channel PMUs are required for placements, at the same level of revel of redundancy. It can be easily seen from Tables 5.5 and 5.6 that there is a slightly less pronounced increase of 11% in the number of deployments at $R_i = 1, \forall i$.

For placements involving the consideration of non-homogeneous channel capacities, the number of deployments may not often be the best metric to compare the optimality of a placement algorithm. Compared with [40], the results in Tables 5.5 and 5.6 are more realistic and practical,

TABLE 5.6: 39-bus network: Full grid observability with enforcement of placement on pilot buses at $\kappa = 1, 2$

	Redundancy, R_i					
	$R_i = 0$		$R_i = 1$			
Bus	l_1	l_2	l_1	l_2	l_3	l_4
1	1-39		1-39			
2	2-30		2-30			
3	3-2		3-4			
6		6-5-31	6-31			6-5-7-11-31
7	7-8		7-8			
8				8-5 9		
9	9-8		9-39			
10		10-13-32	10-32			
11	11-12		11-12			
13				13-12 14		
14					14-4-13-15	
15	15-14					
16	16-21				16-15-21-24	
17					17-16-18-27	
19			19-33			
20	20-34		20-34			
22	22-35		22-35	22-21 -35		
23				23-24 -36		
25				25-26 -37		
27	27-17		27-17			
28	28-26		28-26			
29				29-28 38		
32			32-10			
33	33-19		33-19			
34			34-20			
36	36-23		36-23			
37	37-25		37-25			
38	38-29		38-29			
Total by channels	16	2	20	6	3	1
Total	**18**		**30**			

Placement enforced on pilot buses 1,3,7,11,16, and 28

because they are obtained from formulations which consider costs and channel capacities. For placements involving the use of DULRs for example, the installation efforts required for deployments are less compared to those involved with deployment for higher-capacity PMUs. Therefore, a qualitative comparison of placement results should be based on the number of factors that have been considered in the formulation of OPP, and the extent of information which are available in the solution.

5.5 Placement to maximise the range of applications

The IEEE C37.118.1-2011 specifies that PMUs must be capable of measuring voltage and current phasor as well as the rate of change of frequency (ROCOF). In addition to these standard requirements, many vendors have also developed a number of off-the-shelf applications which are available without additional costs to utilities. These extraneous applications include, but are not limited to,

1. Oscillation detection,

2. Prony analysis,

3. Islanding detection,

4. State estimation,

5. Voltage control,

6. Stability indication.

In practice, it may happen that although the DULRs with added PMU functionalities may be much cheaper than stand-alone PMUs, they may not have the same expanse of applications that can be obtained from the stand-alone units. Utilities may wish maximise the range of applications they may obtain with good juxtaposition of the added application values and economy. Following from this, the new, more practical objective would be to maximise the benefits offered by these devices in the form of added off-the-shelf functionalities and to minimise the costs of procuring these devices. If an adjusted cost,

$$C_{jlr}^{\text{totadj},dv} = C_{jlr}^{\text{tot},dv} - \bar{B}_{jlr}^{\text{tot},dv} \tag{5.6}$$

and

$$\bar{B}_{jlr}^{\text{tot},dv} = \sum_{\varrho=1}^{n_{app}^l} \mu_{\varrho,v}^l \bar{B}_\varrho \tag{5.7}$$

From Section 3.5, $C_{jlr}^{\text{tot},dv}$ is the total cost of the availability and cost models of Section 3.4. $\bar{B}_\varrho$ is the benefit, relative to cost, of purchasing a PMU which has an add-on application capability ϱ from a specific vendor. n_{app} is the total number of applications under consideration. The benefit $\bar{B}_\varrho$ may be evaluated in practical terms as the cost that would have been incurred if the application ϱ were to be built in-house, or purchased separately. B_ϱ may also be evaluated in terms of the relative importance to the application needs at the time of placement. For instance, if improved observability for voltage control is the PMU deployment goal, add-on capabilities such as voltage instability prediction and state estimation may be assigned higher benefits, relative to those of other applications offered by the vendor. $\mu_{\varrho,v}^l$ is a binary parameter indicating whether or not a

particular application is offered as an add-on by a vendor v for the PMU of channel capacity $l + 1$, and $\bar{B}_\varrho$ is the benefit, in monetary unit, of the add-on as evaluated by the utility. In essence, $\bar{B}^{\text{tot},dv}_{jlr}$ is the total benefit, in monetary unit, of all the applications offered by the vendor for a PMU of capacity $l + 1$.

The OPP (3.16) may then be modified to incorporate (5.6), resulting in (5.8).

$$\underset{x^{dv}_{jlr}}{\text{minimize}} \sum_{v=1}^{V} \left[\sum_{d=1}^{D} \left[\sum_{j=1}^{n} \sum_{l=1}^{L} \sum_{r=1}^{r^s} C^{\text{totadj},dv}_{jlr} x^{dv}_{jlr} \right] \right] \tag{5.8a}$$

$$\text{subject to} \sum_{v=1}^{V} \left[\sum_{d=1}^{D} \left[\sum_{j=1}^{n} \sum_{l=1}^{L} \sum_{r=1}^{r^s} b^{dv}_{ijlr} x^{dv}_{jlr} \right] \right] \geq R_i + 1, \forall i \in I \tag{5.8b}$$

$$x^{dv}_{jlr} \in \{0, 1\} \tag{5.8c}$$

From a vendor's perspective, the added capabilities would usually be a function of PMU capacities. For instance, with DULRs, the additional functionality is its primary capability, namely, to serve as relays. stand-alone units may have facilities for more additional functionalities, proportional to the units' sizes. Therefore, for DULRs, one may choose $n_{app} = 1$ while $n_{app} \geq 2$ for stand-alone units. Note that the choice of n_{app} may differ in general for all types of PMUs in practice.

5.5.1   Case study: Scenario

In the following, the sensitivity of the placement results to the parameters introduced in Section 5.5 are examined using the IEEE 118-bus test system as case study, along with the vendor reliability parameters of Chapter 3. In section 3.8.2 of Chapter 3, the relative costs of PMUs from 3 vendors was assumed as seen in the second column of Table 5.7b, with v^c_1 being the unit price of the respective PMUs of different capacities offered by a vendor v_1, and those of vendors v_2 and v_3 being 10% more and 50% less respectively. The subsequent columns of the table also contains some hypothetical vendor application availability binary variables μ_{av}, defined across all applications as the union of all available add-ons offered by a vendor v, over all of the channel capacities. For any vendor v and application, ϱ,

$$\mu_{\varrho,v} = \cup_{l=1}^{L} \mu^l_{\varrho,v} \tag{5.9}$$

$\mu_{\varrho,v}$ in the equation (5.9) is simply the acknowledgement of the availability of a particular application in a vendor's range of offered products. In contrast, $\mu^l_{\varrho,v}$ signifies whether or not the application is actually available on a particular product specification which has a channel capacity, l. It follows that $\mu^l_{\varrho,v}$ cannot be greater than $\mu_{\varrho,v}$

Application	1	2	3	4
Benefit B_ϱ (units)	1	3	3	6

(A) Assumed benefits of add-ons

Vendor	Relative Costs	Application Offered ($\mu_{\varrho,v}$)			
		1	2	3	4
v_1	v^c_1	1	0	1	0
v_2	$1.1 \times v^c_1$	1	1	0	1
v_3	$0.5 \times v^c_1$	1	0	0	0

(B) Assumed Availability of add-ons from 3 vendors

TABLE 5.7: Assumed benefits and availabilities of add-on applications

TABLE 5.8: Assumed availability $\mu_{\varrho,v}^l$

App	$l=1$			$l=2$			$l=3$			$l \geq 4$		
	v_1	v_2	v_3	v_1	v_2	v_3	v_1	v_2	v_3	v_1	v_2	v_3
1	√	√	√	√	√	√	√	√	√	√	√	√
2	×	×	×	×	√	×	×	√	×	×	√	×
3	×	×	×	√	×	×	√	×	×	√	×	×
4	×	×	×	×	×	×	×	×	×	×	√	×
n_{app}^l	1	1	1	1	2	1	2	2	1	2	3	1

In Table 5.8, all vendors offer the same number of add-on applications for a 2-channel PMU (or DULR). Since all vendors offer the same number of incentive for $l = 1$, the adjusted cost $C_{j1r}^{\text{totadj},dv} = C_{j1r}^{\text{tot},dv}$. Vendor v_3 does not offer any additional add-on on higher-channel devices, but vendor v_1, with a maximum of 2 add-ons across all of its products, offered the full range of its add-ons beginning from $l = 2$. On the other hand, although vendor v_2 has the same number of offerings as vendor v_3 at $l = 2$, it does not deploy the full range of its incentive until $l \geq 4$. In Table 5.7a, the application 4 offered by vendor v_2 at $l \geq 4$ was deemed by the utility to be very important to its deployment solution with a benefit of 6 units. In essence, although vendor v_2 has the most expensive line of products, the consideration of the benefits of its add-on may put its actual cost into proper perspective.

It is then possible to form the partitioned matrix which expresses equation (5.7) using the data in Tables 5.7 and 5.8, as in (5.10),

$$
\underbrace{\begin{bmatrix}
1 & 0 & 0 & 0 \\
1 & 0 & 1 & 0 \\
1 & 0 & 1 & 0 \\
1 & 0 & 1 & 0 \\
\cdots & \cdots & \cdots & \cdots \\
1 & 0 & 0 & 0 \\
1 & 1 & 0 & 0 \\
1 & 1 & 0 & 0 \\
1 & 1 & 0 & 1 \\
\cdots & \cdots & \cdots & \cdots \\
1 & 0 & 0 & 0 \\
1 & 0 & 0 & 0 \\
1 & 0 & 0 & 0 \\
1 & 0 & 0 & 0
\end{bmatrix}}_{\mu_{\varrho,v}}
\underbrace{\begin{bmatrix} 1 \\ 3 \\ 3 \\ 6 \end{bmatrix}}_{B_\varrho}
\tag{5.10}
$$

The matrix $\mu_{\varrho,v}$ has been partitioned by vendors.

5.5.2 Case study: Results

The scenario in Section 5.5.1 can be summarised as follows,

1. Vendor v_1 offers products which are less expensive than those offered by Vendor v_2 but are more expensive than Vendor v_3's. (Cost: $v_2 > v_1 > v_3$)

2. Vendor v_1 has more range of add-ons than Vendor v_3 but has less than Vendor v_2's the most reliable line of products. (Range: $v_2 > v_1 > v_3$)

3. Vendor v_1 has the most reliable line of products (Reliability: $v_2 > v_1 > v_3$)

When the benefits of add-on application are considered, it is possible to examine the sensitivities of placement solution to the additional consideration of vendor reliability, level of observability, and degree of redundancy. The results are discussed for full and selective observability in the following sections.

Full observability

For full and selective observability, the number of placements increases as the level of redundancies increases but may only marginally decrease when the maximum allowable number of placements **h** on buses increases. For the simulation, it has been assumed that redundancy level **R** and maximum allowable placement **h** have been specified, respectively, equally for all buses. In both scenarios, the adjusted costs makes the most expensive vendor the most viable option for procurement even without the consideration of vendor reliabilities.

    The placement results with the adjusted costs are summarised in the bar charts of Figure 5.5. The first bar chart show results with the consideration of the vendors' product reliabilities. In spite of the high costs of products from Vendor v_2, all of the total number of PMUs procured are from this vendor with no redundancy $\boldsymbol{R} = 1$. Notably, no PMUs were procured from Vendors v_1 and v_3. This can be at once attributed to the high reliability specifications which can only be met by procuring from Vendor v_2 and its wider range of add-ons. the state of affairs barely changed when the required level of redundancy was raised from $\boldsymbol{R} = 1$ to $\boldsymbol{R} = 2$, with vendor v_3 supplying only 4 of the PMUs Without the consideration of reliabilities, it can be seen from the second bar chart of Figure 5.5 that more PMUs are procured from the other vendors. However, the wider range of add-ons obtained from purchasing from Vendor v_2 presents an attractive option still. Consequently, the majority of the PMUs are still procured from this vendor.

    The complete placement results (although without the specifications of the actual branches to be placed) with and without reliability considerations may be found in Tables B.1 and B.2, respectively, of Appendix B.

Selective observability

The selective placement on pilot buses considering application benefits is summarised in the bar charts of Figure 5.6. For this selective placement, vendor reliability is not considered. The focus was however on the change in placement results with changes in the parameters **R** and **h**.

5.6   Summary

In this chapter, a number of PMU placement algorithms has been described for application-focused PMU placements by extending the OPP 3.16 of Chapter 3. For secondary voltage control application where the observability of certain *pilot* or boundary buses are critical, proposed solutions for full and selective observability was shown to be superior to other voltage control deployment algorithms, even with a simplified form of the algorithm. In addition, for SVR applications, it was shown that a better strategy for utilities would be to maximise the number of observed buses without the enforcement of direct PMU placement, as found in some practice, on pre-identified pilot
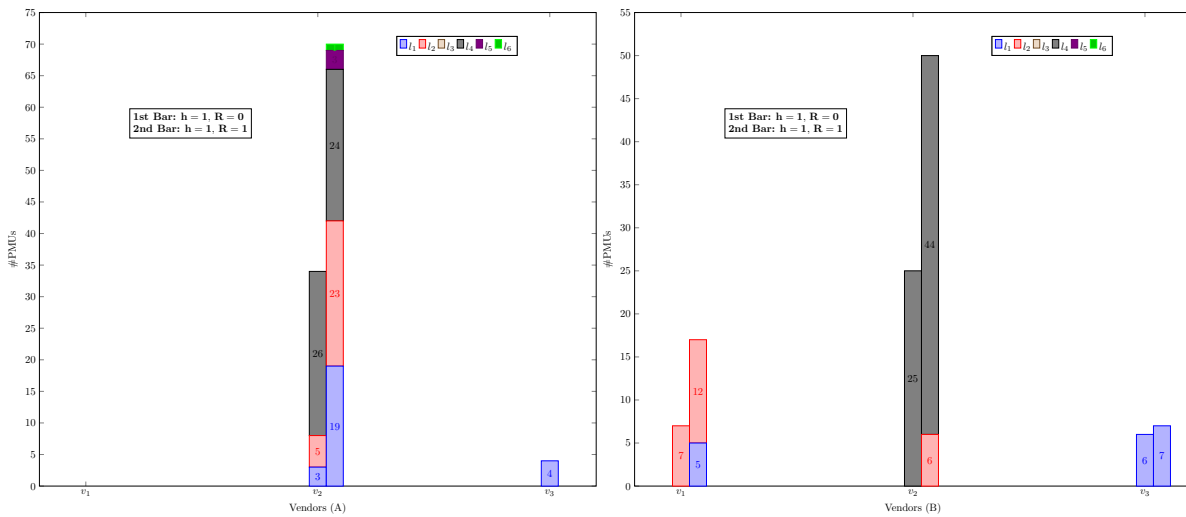
FIGURE 5.5: Full observability: Placement results when application benefits was considered (A) with vendor measurement reliability (B) without vendor measurement reliability
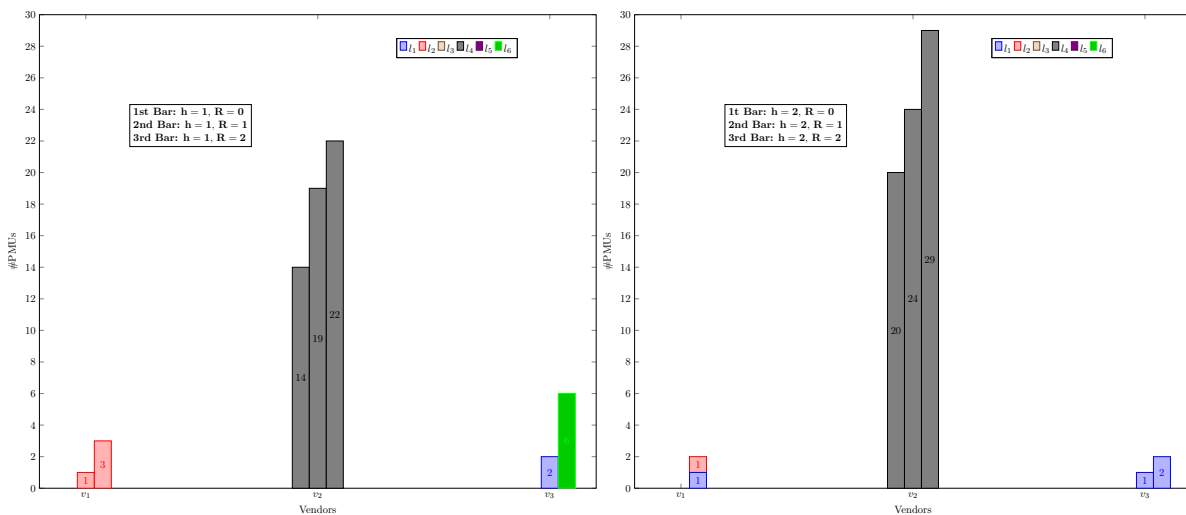

FIGURE 5.6: Selective observability: Placement results when application benefits was considered without reliability at different redundancy and maximum number of bus placements

buses. This would translate to increased observability of more buses, a better use of resources and does not compromise the observability of pilot buses.

To extend to applications such as oscillation detection, state estimation, voltage control, islanding detection, and voltage instability prediction which may be offered as add-on incentives by vendors, the multi-objective multi-vendor OPP 3.16 was reformulated to account for the range of add-on applications. The new formulation not only sought to minimise the cost of deployment, as done in the old, but also to maximise the range of applications by using an adjusted cost which accounted for the benefits offered by each additional application. A number of hypothetical scenarios was used to illustrate the validity of the proposed algorithms.

Chapter 6

Synchrophasor-Based Modelling and Control

In Chapter 2, we reviewed the various MPC methods available in electric power systems literature, with respect to their applications, control structures, modelling, and implementation approaches. It is expected that this, together with previous chapters, has provided sufficient background for this chapter. Here, a novel sensitivity-based predictive control algorithm based purely on synchrophasor measurements, primarily focusing on transmission-level secondary voltage regulation applications is introduced.

6.1   Introduction: from placements to control

In Chapter 1, it was stated that the quest towards a self-monitoring, self-healing power grid could follow the trajectory:

1. Establish data sources (place monitoring devices).

2. Obtain and process data from the sources (Data gathering and processing)

3. Design an advanced control algorithm, based on the processed data (Measurement-based control design).

   PMU placements algorithms have been developed in Chapters 3, 4, and 5 for either selective or full observability of the power systems at various levels of redundancies and channel capacities. Here, the focus is on how data from the strategically located measurement devices may be used with predictive control algorithm for power systems secondary voltage regulation (SVR) using selected control variables. A placement method for voltage control application in particular was described in Chapter 5 by building on the formulations in Chapter 3. The criticality of pilot bus was described and various placement scenarios were discussed. This chapter focuses on the the use of synchrophasors for secondary voltage control. It is assumed that the practical business of selecting and placing monitoring devices for use in an EMS has been taken care of. It then takes one step further towards the realisation of a self-healing grid.

6.2   Introduction: choosing a model for control

For many control applications, the choice of an appropriate model is a fundamental problem in the design of dynamic controllers. For example, traditionally, many linear MPC (LMPC) approaches rely on the use of state-space models, which may be derived from corresponding nonlinear system equations. In power systems applications, these nonlinear system equations are a combination of generator, turbine governor, automatic voltage control(AVR), exciter, power systems stabiliser

(PSS) and load dynamic equations, in combination with algebraic power-flow equations. The state-space models of the system under study can then be realised by linearising these equations around variables of interests. This is the basis of the modelling in many MPC-based power systems research such as [17], [19] where a heuristic method was combined with predictive control for power systems protection and control, in [23], [33] where load shedding was used to achieve voltage stability, and in trajectory-sensitivity based methods of [18], [20], [22]. In [25], [26], [28], the model is an offline power flow-based sensitivity matrix which is used to scale the control input applied at a previous step. An alternative approach to model realisation and sensitivity-based methods was proposed in [27], using multi-input multi-output impulse response model, updated from an optimal power flow-based simulations on another platform.

The methods using exhaustive mathematical modelling of dynamic and algebraic of power systems components as well as those employing static sensitivity or trajectory sensitivity-based methods will fail if the modelled network spans over more than a small area. In others not using the intensive modelling approach, where recourse has been made to the use of static power flows and model-based sensitivity matrices, the offline sensitivity matrix is static and does not account for many system dynamics. In essence, with the increasing complexity of the power system resulting from increasing renewable energy sources (RES) penetration as well as the changes in system parameters due to ageing of modelled devices, offline static power flows and model-based sensitivity matrices formed thereof are not altogether reliable. The degree of changes in voltage and reactive power flow to control inputs such as active and reactive power control from distributed generations (DGs), and On-Load Tap Changers(OLTCs), were obtained from solutions of mathematical power-flow equations in [26], [121]. It is desired [26], [154] that the sensitivities of voltages be updated frequently especially when there are significant changes in system operating conditions. However, for traditional methods relying on static or quasi-static load flows for computing sensitivities, accurate voltage increments can only be obtained from time-consuming AC load flows. This is compounded by the fact that load flow sensitivities rarely capture the dynamics of the generators. As a result, the sensitivities are rarely updated.

Two methods of obtaining models from measured data are introduced in this chapter. The first involves updating the sensitivity matrices from PMU data and the second takes a drastically different approach by using systems identification techniques. The first method proceeds from the intuition that for PMUs which supply high-resolution data at about 30-60 samples per second, numerical derivative calculation of the sensitivity matrices provide small enough changes in the estimation of sensitivities to approximate non-linear characteristics over a narrow linear range. The derivatives are evaluated online and in real-time from directly measured and derived quantities with respect to their changes to known control inputs. However, it will be shown that changes due to applied controls can be easily evaluated using a finite-difference ratio when the data is observable through a PMU. The time step is governed by the reporting rate of the PMUs. In this way, system dynamics at different operating states can be captured in the sensitivity calculation. Sensitivities to selected control variables evaluated in this way can be used in feedback controls without the need for power-flow solutions, with the additional advantage of fast online and real-time updates. Furthermore, the method can also be used to estimate sensitivities of one power system quantity to a non-control quantity (such as the variation of voltage to line active and reactive line power flows) can be used as early warning signals [56]. A coordinated secondary voltage regulation (CSVR) scheme using numerical sensitivities in a model-free predictive control set-up with

early-warning signals is described in this chapter. The numerical sensitivity evaluation provides a basis for the design of an automated secondary voltage controller for the electric power transmission network, which is capable of intelligent sensing and online, real-time automated predictive voltage control action. For intended applications in feedback controls such as may be implemented in a receding-horizon control such as in [25], [26], the proposed synchrophasor-based sensitivity matrix may be included as the model constraint in the set-up, thus providing a way of resolving the challenges described by the authors. In addition, the proposed numerical sensitivity-based method provides a more viable alternative to rigorous model-based trajectory sensitivity calculation used in [22], [23], [111].

Model-based Predictive Control, in its traditional form, relies, mostly, on the use of a state-space model. Predictive controllers based on state-space models of small test systems can be obtained using available parameters of such systems. For example, in [21], a sixth-order model of the 10-bus,3-generator test system was the basis for the design of a MPC to stabilize voltage through load shedding. However, in practical power systems with thousands of devices and equipment, state-space models defining the networks are difficult, if not impossible, to realize. Even if such a realization were possible, the order of the model would make it computationally complex and hence practically infeasible for online applications. Consequently, for works involving larger test systems, the internal model of the MPC would usually be based on offline power-flow solutions and sensitivity matrices calculated thereby (see for instances, [25], [26]), or the use of trajectory sensitivities as in [22]. From a practical point of view, the complications that may arise from these approaches would often stem from the fact that the static power-flow solutions rely on model parameters, for example generator inductances, which may have changed due to the ageing of the equipment. On account, under such circumstances, these solutions may not reflect the current state of the power system.

The second method seeks to provide the state-space model for use in the traditional control sense by using Subspace State-space Identification (4SID) algorithms. The approach is to use readily-available measurement data to synthesize a linear state space model which captures, as much as possible, selected voltage dynamics using systems identification techniques. This is implemented by exciting the system with known inputs and then taking the measurement of interests at the boundary or *pilot* buses. The known inputs are chosen to be of a small magnitude in order not to drive the system into a non-linear region. However, they are significant enough to excite some useful dynamics which can be captured by a linear model. Our goal is to design, using an internal state-space model, a secondary voltage controller which can respond reasonably well to faults and $N-1$ contingencies through the modulation of the voltage references of automatic voltage regulators (AVRs), and voltage compensation devices such as Static VAR Compensators (SVCs), and, for emergency situations, load shedding. The relevance of this measurement-based control algorithm lies in its potential to be applied in online secondary voltage control of an already-existing power system without an explicit knowledge of the mathematical model of the system. Model synthesis and subspace-based predictive control is described and simulated in a RT-HIL-ready environment. The challenge of designing a linear controller for the voltage regulation of a highly-non-linear power system is handled by successive feedbacks inherent to the predictive control, and through bumpless transfers of the regulation tasks between different controllers with internal models designed for different operating conditions. The transfers are triggered by early-warning

signals from PMU-based indicators, such as ROCOF and reactive power reserve margins. The approach is primed for the incorporation of a hardware-in-the-loop measurement in which the effect of communication on the feedback-control system can be evaluated.

In the following sections, the focus would be first on evaluating the sensitivities of bus voltages to the secondary voltage control inputs and then on a complete description, model synthesis, controller design and implementation of the subspace method. The inputs that will be considered in both cases include modulations of generators' automatic voltage regulators (AVRs) set-points at generator buses, those of Static VAR Compensator (SVCs) at selected *pilot* buses, and load shedding. In essence, it is demonstrated for controls that are implemented through indirect control of generators' and SVCs' reactive powers within the limits of their capacity and, for generators, those allowed by the over-excitation limits from the measure of their field currents. As shown in Chapter 2, a modulation of AVR references may increase generators' terminal voltages by an equal amount, and with it a corresponding increase in the reactive power support from the generators in order to hold the generators' voltages constant at the new set-point.

6.3   Contribution of the chapter

The contributions of this chapter are as follows:

1. Proposal of a method for the estimation of sensitivities to control inputs using measurement-based numerical derivatives.

2. Derivation of sensitivities expressions, and the method of incorporating them in a receding-horizon set-up.

   Second part

3. The design, as an alternative approach to model-based control, of a subspace-based predictive controller for secondary voltage regulation.

4. A description of how linear power systems models may be synthesised from phasor measurements of a system's voltage response to known, deliberate perturbations using subspace state-space identification (4SID).

5. An implementation of the feedback subspace-based control on a real-time platform and examine the effect of model orders and other controller parameters on the performance.

6. An examination of the controller's performances in the regulation of non-viable voltage profiles as well as for voltage stabilisation in emergency conditions.

7. A description of how the subspace-based controller's performances may be improved using real-time voltage stability indicators.

6.4   Part I: Modelling sensitivities to inputs using numerical derivatives

Traditionally, sensitivities are obtained by partial differentiation of power flow equations with the aim of evaluating the changes in system parameters due to the perturbation of other system parameters. For instance, this would include the change in bus voltages due to the reactive power

flows across lines in the network, or the changes in bus voltage angles due to the changes in real line power flows. The evaluation of sensitivities using the conventional method has been used to determine the contribution of generator buses to voltage support or collapse, or to evaluate the distance of the systems to instability using a voltage stability index.

$$
\begin{bmatrix} \Delta P \\ \Delta Q \end{bmatrix} = \begin{bmatrix} \frac{\partial P}{\partial \delta} & \frac{\partial P}{\partial V} \\ \frac{\partial Q}{\partial \delta} & \frac{\partial Q}{\partial V} \end{bmatrix} \begin{bmatrix} \Delta \delta \\ \Delta V \end{bmatrix} \tag{6.1}
$$

In [56], a measurement-based approach which made use of differences between synchrophasor measurements at successive time instances was proposed.

$$
S_{\delta v} = \begin{bmatrix} \frac{\Delta \theta_i}{\Delta P_{ik}} & \frac{\Delta V_i}{\Delta P_{ik}} \\ \frac{\Delta \theta_i}{\Delta Q_{ik}} & \frac{\Delta V_i}{\Delta Q_{ik}} \end{bmatrix} \tag{6.2}
$$

where

$$
\frac{\Delta \theta_i}{\Delta P_{ik}} = \frac{\theta_i(t) - \theta_i(t-1)}{P_{ik}(t) - P_{ik}(t-1)}
$$

$$
\frac{\Delta V_i}{\Delta P_{ik}} = \frac{V_i(t) - V_i(t-1)}{P_{ik}(t) - P_{ik}(t-1)}
$$

$$
\frac{\Delta \theta_i}{\Delta Q_{ik}} = \frac{\theta_i(t) - \theta_i(t-1)}{Q_{ik}(t) - Q_{ik}(t-1)}
$$

$$
\frac{\Delta V_i}{\Delta Q_{ik}} = \frac{V_i(t) - V_i(t-1)}{Q_{ik}(t) - Q_{ik}(t-1)}
$$

Although this method might require investments in filtering and preprocessing of measured data, it is, on account of its simplicity, more computationally-efficient for real-time sensitivity calculation than analytical approaches. In addition, it takes into account more of the current dynamic changes in the system parameter under observation than sensitivities which have been calculated.

6.4.1 Bus voltage sensitivities

The sensitivity of a dependent variable Δy to a controllable variable Δu may be defined as the magnitude of the change in the variable x to small, often deliberate changes in the variable y. In electric power systems, this may be the sensitivity of the voltage at a bus i to the reactive power injection Q_k at another bus k, or the sensitivities of the bus voltage magnitudes and angles to changes in the active power flows along the lines.

In this chapter, it is assumed that at the secondary voltage control is achieved only through a modulation of the following,

- Voltage references of generators. V_g^{ref}

- Voltage references of SVCs. $V_{\text{svc}}^{\text{ref}}$

- Load shedding. λ

The modulations of the first two control variables are common in secondary voltage regulations. The third, namely load shedding, is considered drastic and should serve as a last resort for voltage regulation. It is assumed that the sensitivities of the bus voltages can only be estimated through the observations of PMU-measurable quantities.

6.4.2 Bus voltage sensitivities to generator voltage references

At the PV operating mode, it is well known that the terminal voltage of generators change by an amount which is approximately equal to the modulation at the AVR references. For effective control actions, the generator bus voltage, and consequently, bus voltages of non-generator buses, should respond to a change in the voltage references of generators in the grid. However, the change is influenced by the reactive power limits of generators. The extent of the influence S_{vg}^{ir} of the r generators g with set-points $V_r^{ref_g}$ on the bus voltage of another bus V_i is

$$\Delta V_{\text{g}}^i = \sum_{r \in \Omega} S_{\text{vg}}^{ir} \Delta V_r^{\text{ref,g}} \tag{6.3}$$

where ΔV_{g}^i is the algebraic sum of products of the respective changes in generator voltage due to changes in the reference value of generators in the network, S_{vg}^{ir} is the sensitivity of bus i voltage to the voltage reference modulation of the generator AVR at bus r, $\Delta V_r^{\text{ref,g}}$ is the magnitude of changes in the reference set-point of generator bus r, and Ω is the set of all generator buses.

6.4.3 Bus voltage sensitivities to SVC voltage references

SVCs may inject or absorb reactive power and influence local bus voltages. Define the degree of influence of the modulation of the voltage set-points of a SVC at a bus c on the voltage magnitude of a bus i as S_{vs}^{ic}.

$$\Delta V_{\text{s}}^i = \sum_{c \in \Psi} S_{\text{vs}}^{ic} \Delta V_c^{\text{ref,s}} \tag{6.4}$$

where ΔV_{s}^i is the algebraic sum of products of the respective changes in generator voltage due to changes in the reference value of generators in the network, S_{vc}^{ic} is the sensitivity of bus i voltage to set-point changes of a bus c SVC, and $\Delta V_c^{\text{ref,s}}$ is the magnitude of changes in the SVC reference set-point of bus c.

6.4.4 Bus voltage sensitivity to load variations at load buses

Load shedding is considered drastic, but can be used when other measures fail to restore voltage to pre-contingency levels. Bus voltages are affected by load changes, $\Delta \lambda_l$ which take places in buses in the network to different degrees, which are measured by their sensitivities, $S_{\text{v}\lambda}^{il}$.

$$\Delta V_{\lambda}^i = \sum_{l \in \Lambda} S_{\text{v}\lambda}^{il} \Delta \lambda_l \tag{6.5}$$

where $S_{\text{v}\lambda}^i$ is the sensitivity of bus i to load changes at load buses. The voltage at bus i is expected to respond to the load changes, $\Delta \lambda$ at load buses Λ by a magnitude ΔV_{λ}^i.

6.4.5 Total voltage sensitivities

The total voltage changes at bus i are expected to be the scaled sum of deliberate perturbations at control buses. If the set of controls is defined as $U = \begin{bmatrix} \Delta V^{\text{ref}_g^T} & \Delta V^{\text{ref}_s^T} & \Delta \lambda^T \end{bmatrix}^T$, then the total effect of the perturbations on the bus i voltage is,

$$\Delta V^i = \sum_{u \in \Delta U} \Delta V_i^{\text{u}} \tag{6.6}$$

Note that $\Delta V^{\text{ref},g} \in \mathbb{R}^{n_r}, \Delta V^{\text{ref},c} \in \mathbb{R}^{n_c}$, $\Delta \lambda \in \mathbb{R}^{n_l}$, and $U \in \mathbb{R}^m$, where n_r, n_c and n_l are the number of generator, SVC, and load buses respectively. ΔV_i^{u} is the vector of changes in the bus voltage magnitudes due to the controls and $m = n_r + n_c + n_l$ is the number of controls.

The equations can be combined in the matrix,

$$\Delta V^i = \begin{bmatrix} S^i_{\text{vg}} & S^i_{\text{vs}} & S^i_{\text{v}\lambda} \end{bmatrix} \begin{bmatrix} \Delta V^{\text{ref},g} \\ \Delta V^{\text{ref},s} \\ \Delta \lambda \end{bmatrix}$$

$$\Delta V = \underbrace{\begin{bmatrix} S^i_{\text{vg}} & S^i_{\text{vs}} & S^i_{\text{v}\lambda} \\ S^{i+1}_{\text{vg}} & S^{i+1}_{\text{vs}} & S^{i+1}_{\text{v}\lambda} \\ \vdots & \ddots & \vdots \\ S^n_{\text{vg}} & S^n_{\text{vs}} & S^n_{\text{v}\lambda} \end{bmatrix}}_{\text{Sensivity block matrix, } S_{\text{vu}}} \underbrace{\begin{bmatrix} \Delta V^{\text{ref},g} \\ \Delta V^{\text{ref},s} \\ \Delta \lambda \end{bmatrix}} \tag{6.7}$$

$$\implies \Delta V = S_{\text{vu}} \Delta U \tag{6.8}$$

Where,

$$S^i_{\text{vg}} = \begin{bmatrix} S^{i1}_{\text{vg}} & S^{i2}_{\text{vg}} & . & . & . & S^{i,n_r}_{vg} \end{bmatrix}$$

$$S^i_{\text{vs}} = \begin{bmatrix} S^{i1}_{\text{vs}} & S^{i2}_{\text{vs}} & . & . & . & S^{i,n_l}_{\text{vs}} \end{bmatrix}$$

$$S^i_{\text{v}\lambda} = \begin{bmatrix} S^{i1}_{\text{v}\lambda} & S^{i2}_{\text{v}\lambda} & . & . & . & S^{i,n_\lambda}_{\text{v}\lambda} \end{bmatrix}$$

S_{vu} is a dense, linearly independent $n \times m$ matrix. The size may be reduced and sparsity may be improved by the use of fewer generators and buses. The selected generators are those which have the greatest influence on the control of the selected buses. The selected buses are those which are able to impose control on the surrounding buses in a local areas.

6.4.6 Generator bus Q-sensitivities

Generators participate in voltage regulation by supplying reactive power, within their respective capabilities, to keep their terminal voltages at reference levels. When the reactive power is exhausted, the generators can no longer participate in voltage control, and this may lead to long-term voltage instability problems. It becomes imperative, on account, to evaluate how the generators' reactive power change with respect to the controls, ΔU. In a similar vein to (6.3)-(6.5), we anticipate that the respective generators buses Q-changes are a sum of the product of their respective sensitivities to perturbations.

$$\Delta Q^i_{\text{g}} = \sum_{r \in \Omega} S^{ir}_{Qg} \Delta V^{\text{ref},g}_r \tag{6.9}$$

$$\Delta Q^i_{\text{s}} = \sum_{c \in \Psi} S^{ic}_{Qs} \Delta V^{\text{ref},s}_c \tag{6.10}$$

$$\Delta Q^i_\lambda = \sum_{l \in \Lambda} S^{il}_{Q\lambda} \Delta \lambda_l \tag{6.11}$$

Following from (6.7), write,

$$\Delta Q = S_{\text{Qu}} \Delta U \tag{6.12}$$

with S_{Qu} in (6.12) formed in the same way as S_{vu} in (6.7).

6.4.7   Sensitivities to a sum of inputs

The change in bus i voltage ΔV^i can be expressed as a scaled sum of the inputs which influence the change ((6.7)). Mathematically, this can be written as the Jacobian

$$\Delta V_p = \frac{\partial V_p}{\partial u_1} \Delta u_1 + \frac{\partial V_p}{\partial u_2} \Delta u_2 + \ldots + \frac{\partial V_p}{\partial u_m} \Delta u_m \tag{6.13}$$

So far, our analysis have relied on the major assumption that individual contributions of each sensitivity can be separated. However, when measurements, rather than traditional partial differentiations, are used for the sensitivity analysis, the individual contribution of the respective input variables becomes difficult to quantify. Consequently, it makes more sense to evaluate the bus voltage change ΔV_i as the result of a single sensitivity, S_{vu}^{si} to a sum of input perturbations.

$$\Delta V^i = S_{\mathrm{vu}}^{si} \left(\sum_{r \in \Omega} \Delta V_r^{\mathrm{ref},g} + \sum_{c \in \Psi} \Delta V_c^{\mathrm{ref},s} + \sum_{l \in \Lambda} \Delta \lambda_l \right) \tag{6.14}$$

Define $\mathbb{1}_{n \times m}$ as a matrix of ones with n rows and m columns, then (6.14) can be written succinctly across all buses as

$$\Delta \boldsymbol{V} = \underbrace{\left(\boldsymbol{S}_{\mathrm{vu}}^{\mathrm{s}} \cdot \mathbb{1}_{n \times m} \right)}_{\boldsymbol{S}_{\mathrm{vu}}^{\mathrm{t}}} \Delta \boldsymbol{U}$$

$$\implies \Delta \boldsymbol{V} = \boldsymbol{S}_{\mathrm{vu}}^{\mathrm{t}} \Delta \boldsymbol{U} \tag{6.15}$$

$\boldsymbol{S}_{\mathrm{vu}}^{\mathrm{t}}$ and $\boldsymbol{S}_{\mathrm{vu}}^{\mathrm{s}} = \begin{bmatrix} S_{\mathrm{vu}}^{s1} & S_{\mathrm{vu}}^{s2} & \ldots & S_{\mathrm{vu}}^{sn} \end{bmatrix}^T$ are the matrix and vector bus voltage sensitivities of all buses respectively, due to the sum of different input perturbations and the input vector $\Delta \boldsymbol{U}$ is as defined in a previous section.

In the same manner, we define the changes in reactive power injections due to the sum of different input perturbations as,

$$\Delta \boldsymbol{Q} = \boldsymbol{S}_{\mathrm{Qu}}^{\mathrm{t}} \Delta \boldsymbol{U} \tag{6.16}$$

where $\boldsymbol{S}_{\mathrm{Qu}}^{\mathrm{t}} = \left(\boldsymbol{S}_{\mathrm{Qu}}^{\mathrm{s}} \cdot \mathbb{1}_{n \times m} \right)$ is the Q-sensitivity matrix due to a sum of different input perturbations and $\boldsymbol{S}_{\mathrm{Qu}}^{\mathrm{s}}$ is a vector of individual buses Q-sensitivities.

The equations (6.14) and (6.16) can be combined as,

$$\Delta \boldsymbol{X} = \boldsymbol{S}_{\mathrm{vQu}} \Delta \boldsymbol{U} \tag{6.17}$$

6.4.8   Sensitivity estimation using numerical derivatives

The sensitivity of a response to a perturbation is estimated by the change of a response to an input perturbation. For dynamic processes, the total change in the value of the response due to the input may not be instantaneous but may take place slowly over a period of time, such that, in the absence of any further perturbations or other disturbances, a time Δt elapses before the difference in the value of the output —from the time the input is applied —is calculated. However, the total changes can be measured by a summation of the changes taking place over small steps using the differences in the reported output quantities at successive time instants. For a PMU with a reporting rate f_R, the change in an output y at instant k is the finite-difference equation (6.18),

$$\Delta y[k] = \frac{G_y \left(y[k] - y[k-1] \right)}{t_R} \tag{6.18}$$

where $t_R = \frac{1}{f_R}$, is the time interval between each report and G_y is the amount of scaling or gain which is used magnify the degree of change over the interval k to $k-1$. With regards to the IEEE std. C37.118.1-2011, the reporting rate f_R (hence t_R) is fixed. Therefore, the equation (6.18) can be written as,

$$\Delta y[k] = G_y y[k] - y[k-1] \tag{6.19}$$

for a known t_R.

From a purely input-output perspective, if a perturbation of magnitude Δu_1 causes a change Δy_1 in a response of interest, y, then another perturbation(preferably from the same source) of magnitude Δu_2 will cause a change Δy_2 in the response. Furthermore, in the absence of any other disturbance in the system, the change in the output Δy_2 is in fact a scaled value of the input perturbation, Δu_2, with a scale equal to the sensitivity of the system at the time the input Δu_1 was applied.

$$\Delta y_2 = \frac{\Delta y_1}{\Delta u_1} \Delta u_2 \tag{6.20}$$

The SVR under study is concerned with the modulations of AVR and SVC set-points. The applied input perturbations have indirect effects on bus voltages, with the primary control acting more directly in response to the new set-points to regulate the bus voltage to the desired band. In order to allow time for the primary control to act, the actual change in bus voltage of concern is measured as an algebraic sum of the changes between successive time instances, for a number of time instants Δk_a .
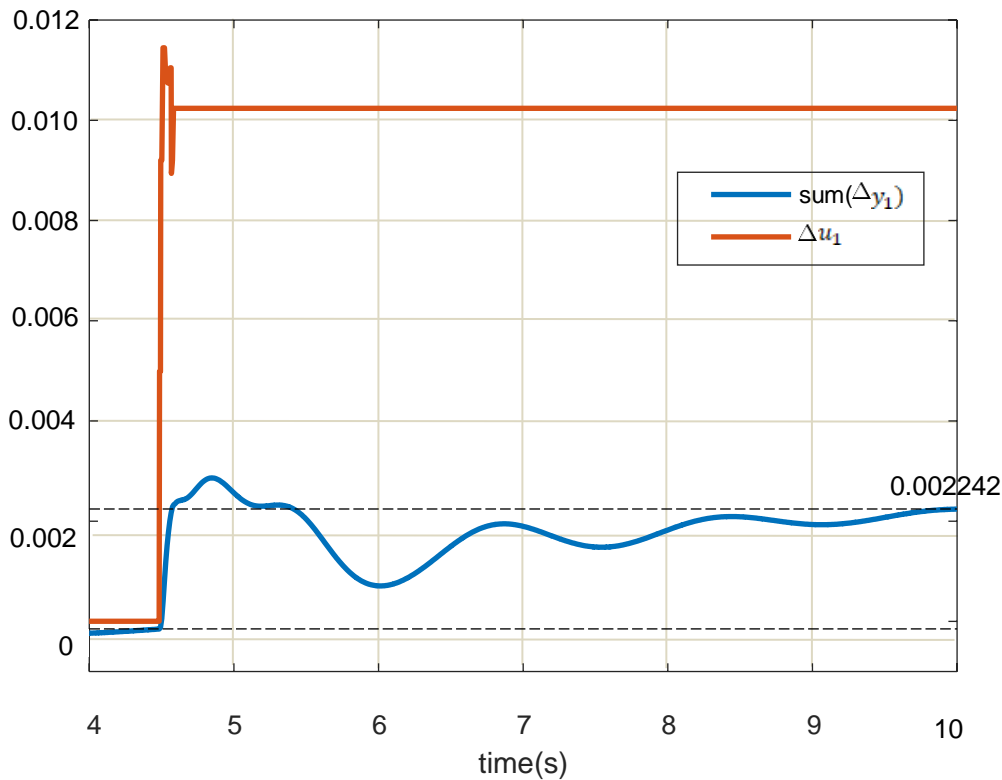
FIGURE 6.1: Change in voltage (p.u.) of a non-generator bus due to a step change in AVR reference of a generator bus
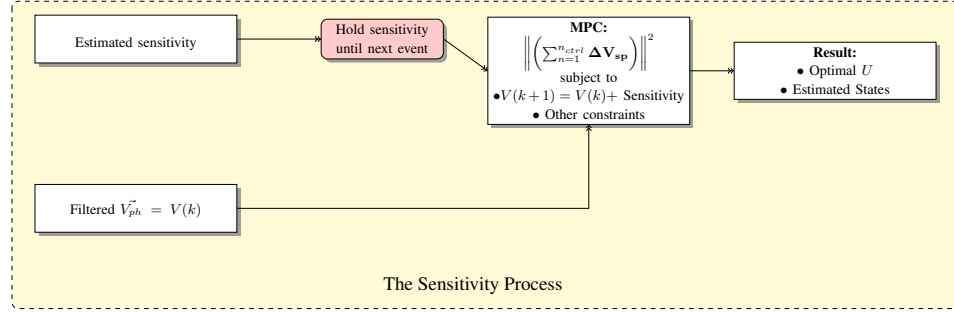
FIGURE 6.2: The Sensitivity Process

$$\Delta V_i = \sum_{f=k}^{k+\Delta k_a} \Delta V_i(f) \tag{6.21}$$

At time instant *k*, the change in bus voltage $\Delta V_i(f = k) = V(k) - V(k-1)$

6.4.9   Updating the sensitivity estimation

However, given that the sensitivities are calculated based on successive differences in measurements, sensitivity values are often instantaneous. On account, it might be necessary to define a threshold for the current sensitivity calculation as:

$$S_{vu} = \begin{cases} S_{\text{vu}}^{\text{new}}, & \text{if } u_k - u_{k-1} > 0 \\ S_{\text{vu}}^{\text{old}}, & \text{if } u_k - u_{k-1} = 0 \end{cases} \tag{6.22}$$

where $S_{\text{vu}}^{\text{new}}$ and $S_{\text{vu}}^{\text{old}}$ are new and old values of the sensitivities measured at current and previous time instants respectively.

6.4.10   The complete sensitivity-based predictive voltage control setup

$\Delta \boldsymbol{V}$ in (6.7) is an expression of in ΔV_i in (6.6) in vector form. Since the SVR acts on long-term stability post-contingency, it is safe to assume that the (6.7) assumes that the changes in bus voltages are caused only by the applied controls. Therefore, over a control interval, the expected voltage magnitudes in the next time instant are a sum of the present voltage magnitude and the expected change in the voltage magnitude at the present time instant.

$$\boldsymbol{V}(k+1) = \boldsymbol{V}(k) + \boldsymbol{S}_{\text{vu}}^{(k)} \Delta \boldsymbol{U}(k) \tag{6.23}$$

If tertiary voltage control is active, the reference voltage may change over time. For simplicity, the tertiary voltage control may remain fixed over the prediction horizon such that $V^{\text{ref}}(k + N) = ... = V^{\text{ref}}(k + 1) = V^{\text{ref}}(k) = V^{\text{ref}}$ such that the 2-norm of the voltage deviations at every bus and at every time step, *k* follow from (6.23)

$$J_1 = \left\| \boldsymbol{V}^{\text{ref}} - \boldsymbol{V}(k+1) \right\|_Q^2$$
$$\implies \left\| \boldsymbol{V}^{\text{ref}} - \boldsymbol{V}(k) - \boldsymbol{S}_{\text{vu}}^{(k)} \Delta \boldsymbol{U}(k) \right\|_Q^2 \tag{6.24}$$

Note that $\boldsymbol{V}(k), \Delta\boldsymbol{U}(k)$, and $\boldsymbol{S}_{\text{vu}}^{(k)}$ of (6.23) and (6.24) imply that the quantities $\boldsymbol{V}, \Delta\boldsymbol{U}$ and $\boldsymbol{S}_{\text{vu}}$ respectively change at every time step, k.

From a practical point of view, it is necessary to compel that the rates of modulations of generator and SVC voltage set-points as well as the amount of load shedding be limited to a specific range of values. From a production point of view, it is also necessary to minimize the number of times the controls are used.

$$J_2 = \sum_{k=0}^{N_c-1} \left\| \bar{\boldsymbol{U}} - \boldsymbol{U}(k) \right\|_{\boldsymbol{R}}^2 \tag{6.25}$$

$$J_3 = \|\Delta\boldsymbol{U}(k)\|_R^2 \tag{6.26}$$

Moreover, the minimisation is expected to take place over a control interval, N_c.

$$\underset{\Delta u, Y}{\text{minimise}}\ J = \sum_{k=1}^{N_p} \left\| \boldsymbol{V}^{\text{ref}} - \boldsymbol{V}(k+1) \right\|_Q^2 + \sum_{k=1}^{N_p} \|\mathbf{Y}(k)\|_{\boldsymbol{Q}_{\mathbf{Y}}^2} + \sum_{k=0}^{N_c-1} \left\| \bar{\boldsymbol{U}} - \boldsymbol{U}(k) \right\|_{\boldsymbol{R}}^2 + \sum_{k=0}^{N_c-1} \|\Delta\boldsymbol{U}(k)\|_{\boldsymbol{R}_r}^2 \tag{6.27a}$$

$$\text{subject to } \boldsymbol{X}(k+1) = \boldsymbol{X}(k) + \boldsymbol{S}_{\text{vQu}}^{(k-1)} \Delta\boldsymbol{U}(k), \qquad \forall k = 1, ..., N_p \tag{6.27b}$$

$$\underline{\boldsymbol{X}}(k) - \mathbf{1}\underline{\mathbf{Y}}\ \leq \boldsymbol{X}(k) \leq\ \overline{\boldsymbol{X}}(k) + \mathbf{1}\overline{\mathbf{Y}}, \qquad \forall k = 1, ..., N_p \tag{6.27c}$$

$$\underline{\Delta\boldsymbol{U}}\ \leq\ \Delta\boldsymbol{U}(k)\ \leq\ \overline{\Delta\boldsymbol{U}}, \qquad \forall k = 0, ..., N_c - 1 \tag{6.27d}$$

$$\underline{\boldsymbol{U}}\ \leq\ \boldsymbol{U}(k)\ \leq\ \overline{\boldsymbol{U}}, \qquad \forall k = 0, ..., N_c - 1 \tag{6.27e}$$

Where $\underline{\boldsymbol{X}} = \begin{bmatrix} \underline{\boldsymbol{V}}^T & \underline{\boldsymbol{Q}}^T \end{bmatrix}^T$ and $\overline{\boldsymbol{X}} = \begin{bmatrix} \overline{\boldsymbol{V}}^T & \overline{\boldsymbol{Q}}^T \end{bmatrix}^T$ are the lower and upper limits respectively on the voltage and reactive power states. The vectors, $\underline{\mathbf{Y}} = \begin{bmatrix} \underline{\boldsymbol{\xi}}^T & \mathbf{0}^T \end{bmatrix}^T$ and $\overline{\mathbf{Y}} = \begin{bmatrix} \overline{\boldsymbol{\xi}}^T & \mathbf{0}^T \end{bmatrix}^T$ are added to soften the constraints $\underline{\boldsymbol{V}}(k), \overline{\boldsymbol{V}}(k)$ on the voltage states in order to improve the feasibility of the problem. $\mathbf{Y} = \begin{bmatrix} \mathbf{Y}_1^T & \mathbf{Y}_2^T \end{bmatrix}^T$ is added to the objective function in order to minimize the degree of violations (quantified by slack variables $\underline{\boldsymbol{\xi}}$ and $\overline{\boldsymbol{\xi}}$ in $\underline{\mathbf{Y}}$ and $\overline{\mathbf{Y}}$ respectively) of the constraints on the voltage outputs, $\boldsymbol{V}$. Since the generators cannot produce more than their respective reactive power capabilities, we assume that the constraints $\underline{\boldsymbol{Q}_G}(k), \overline{\boldsymbol{Q}_G}(k)$ on the generators' reactive power generation, $\boldsymbol{Q}_G(k)$ are hard. The use of slack variables is necessary to prevent the infeasibility of the optimisation problem (6.27) over the prediction horizon N_p when the voltage enters a non-viable region. With this allowance, the controller is able apply a control input to drive the voltage value to desired operating bands, with minimum violations of the bands. In contrast, a continuous tightening of the voltage constraints was adopted in [26] over the prediction horizon. The softness of the limits was progressively decreased until a hard constraint were enforced at the end of the prediction horizon.

6.5 Part II: Predictive control based on a subspace-based model realization

If the electric power system is assumed to be of the linear time-invariant form which can be described by a model (6.28) with input and output measurement noises which are Gaussian distributed, then the input and output relationship can be captured in a state-space model which lends very easily to predictive control designs.

$$\Delta \boldsymbol{x}(k+1) = \boldsymbol{A}\Delta \boldsymbol{x}(k) + \boldsymbol{B}\Delta \boldsymbol{u}(k) + \boldsymbol{w}(k) \tag{6.28a}$$

$$\Delta \boldsymbol{y}(k) = \boldsymbol{C}\Delta \boldsymbol{x}(k) + \boldsymbol{D}\Delta \boldsymbol{u}(k) + \boldsymbol{v}(k) \tag{6.28b}$$

If n is the number of states, m the number of inputs, and p the number of outputs, then the state matrix, $\boldsymbol{A} \in \mathbb{R}^{n \times n}$, input matrix, $\boldsymbol{B} \in \mathbb{R}^{n \times m}$, the output matrix, $\boldsymbol{C} \in \mathbb{R}^{p \times n}$, and the state transition matrix, $\boldsymbol{D} \in \mathbb{R}^{p \times m}$. The state, input, and output vectors are $x \in \mathbb{R}^n$, $\boldsymbol{u} \in \mathbb{R}^m$, and $\boldsymbol{y} \in \mathbb{R}^p$, respectively. $w(k)$ and $\boldsymbol{v}$ are usually unmeasurable disturbance and noise quantities. The order of the system is equivalent to the number of states, n, and k is the current time step.

In the absence of stochastic variables $\boldsymbol{w}, \boldsymbol{v}$, the model (6.28) is deterministic, and the state space describes the effect of the input variable $\boldsymbol{u}$ on the output $\boldsymbol{y}$. For secondary voltage control, outputs of interest are those which reflect the voltage conditions as well as reactive power needs and generations at pilot and generator buses. The inputs are those which are applicable at the voltage control level and may include AVR references at generator buses and loads at load buses. For observable power systems quantities such as can be obtained from PMU measurements, the influence of small known modulations of AVR references on the pilot bus voltages can be used to synthesize a state-space model of the form of (6.28). However, it may be difficult to quantify the magnitude of the perturbation which may be needed to excite a system to synthesise a power system model without driving the system itself into a non-linear region. Nevertheless, for sufficiently small inputs, a linear time-invariant model may be obtained using subspace methods.

For the control of complex dynamic processes, it has always been desired, especially in the process industry, to identify models from finite sets of noisy input and output data for control applications. The traditional method of doing this has been through the use of polynomial prediction error methods (PEM) [155] and the Instrumental Variable Method (IVM) [156]. These methods perform well in practice but suffer from parametrisation issues (as they depend on *á priori* knowledge of the model order and other parameters) and may be numerically unstable, especially for multiple-inputs multiple-output (MIMO) systems.

Subspace state-space method are based on the pioneering work in [157], where a method for identifying a linear model from input and output data were first described. These include the Canonical Variate Analysis (CVA) [158], the Numerical Algorithm for Subspace State Space Identification (N4SID) [159]–[162], the state-space auto-regressive with exogenous inputs(SSARX), the Multivariable Output-Error State Space (MOESP) [163], [164]. A detailed review of the similarities and differences between subspace methods can be found in [165] and a preliminary inroduction in Chapter 2. Here, it should suffice to mention that the various subspace approaches differ mostly in their methods of reducing noise and on whether they are iterative or non-iterative. These identification methods offer significant advantages over traditional methods in that they are data-driven, non-iterative, more computationally feasible, and do not depend on previous knowledge of model parameters. Since input-output data are more readily available in process control industries, the use of subspace methods are much more popular than can be found in power systems research or applications.

Nevertheless, in power systems control applications, a number of identification methods involving PMU and time-series data have been used mostly for modal analysis and PSS tuning. These include the use of Eigensystem Realisation Algorithm [166] for modal analysis [167], least-squares prediction error method for PSS tuning [168], and MIMO-feasible state-space methods for

modal analysis [169] and centralised generator speed control [170] and generator parameter estimation [171]. The use of PMU data for power systems wide area monitoring are more common than may be found for wide-area protection and control. The application of subspace methods for voltage and/or model predictive control are rarer to find in power systems research, although subspace-based predictive control may be found in some process engineering works [172]. However, measurement-based analysis and control designs have been particularly encouraged in power systems studies by the proliferation of PMU data availability, especially for modal analysis and PSS tuning. A detailed description of various methods may be found in the IEEE task force report [173].

6.5.1 Model Realization

Ambient, Probing, and *Ringdown* data are the most common types of measured responses in power systems. Ambient responses of the system are due to random variations in loads across the network. Ringdown signals, on the other hand, are a result of transients which may in turn be caused by faults or loss of lines or generators. Probing data are caused by the deliberate injection of a known perturbation and magnitude into the network. An example is the insertion of a 1400 MW Chief Joseph brake resistor (as done in [174]) into the Pacific DC inter-tie. For the purpose of synthesising a model for voltage control, a probing signal is used to excite the system and the output of interests are measured.

An important point in designing a viable controller based on the synthesised model when using measurement data is to determine an appropriate data window which contains enough dynamics as to not capture any non-linearities. Subspace identification theories are then applied to construct a state-space model from the chosen data window. In this chapter, the focus is to synthesise state-space models of different orders using the non-iterative subspace state-space algorithms [158], [161]–[163], [175] with the end-goal of designing a predictive voltage controller that is based on these models. Although other state-space estimation methods exist, we focus on these two non-iterative methods. The flow chart below summarises the steps used to realize the model. Although other state-space estimation methods exist, the focus here will be on these non-iterative approaches. The flow chart of Figure 6.4 below summarises the steps used to realize the model. The accuracy of the realised models depend on the chosen order, realisation algorithm, and the prediction horizon used in the identification process. Relatively higher model orders may capture the underlying dynamics of the system, yield higher fitness percentages (Equation (6.31)), and lesser errors (Equation (6.32)). However, they may be too large to be feasible for real-time/online model predictive control application. In contrast, smaller model orders may give less desirable metrics (fitness and errors) but may be more computationally-feasible for real-time applications. The higher the number of outputs which are simultaneously captured in the model response, the higher the model orders that will be needed to give satisfactory fitness percentages across all output signals.

The Subspace State Space Identification (4SID) process

The electric power grid may be visualised as a system of connected components where the output of one subsystem is an input to another. It is then easy to conceptualised that measured responses, for instance those obtained from phasor measurements, are a result of the applications of excitation signals from components like generators, or Static Var Compensators (SVCs). For m inputs from these sources, there then exists a vector $u_k \in \mathbb{R}^m$ that have been applied in the past to influence current evolutions of system responses. Similarly, over a time projection into the future, there

should exist inputs that will be applied to the system. For these past and future inputs, a first-order block Hankel matrix of past inputs $U \in \mathbb{R}^{i \times j}$ and can be written as,

$$
\begin{pmatrix} U_p \\ - \\ U_f \end{pmatrix} =
\begin{bmatrix}
u_0 & u_1 & \cdots & u_{j-1} \\
u_1 & u_2 & \cdots & u_j \\
\cdots & \cdots & \ddots & \cdots \\
u_{i-1} & u_i & \ddots & u_{i+j-2} \\
-- & -- & -- & -- \\
u_i & u_{i+1} & \cdots & u_{i+j-1} \\
u_{i+1} & u_{i+2} & \cdots & u_{i+j} \\
\cdots & \cdots & \ddots & \cdots \\
u_{i+h-1} & u_{i+h} & \cdots & u_{i+h+j-2}
\end{bmatrix},
\begin{pmatrix} Y_p \\ - \\ Y_f \end{pmatrix} =
\begin{bmatrix}
y_0 & y_1 & \cdots & y_{j-1} \\
y_1 & y_2 & \cdots & y_j \\
\cdots & \cdots & \ddots & \cdots \\
y_{i-1} & y_i & \ddots & y_{i+j-2} \\
-- & -- & -- & -- \\
y_i & y_{i+1} & \cdots & y_{i+j-1} \\
y_{i+1} & y_{i+2} & \cdots & y_{i+j} \\
\cdots & \cdots & \ddots & \cdots \\
y_{i+h-1} & y_{i+h} & \cdots & y_{i+h+j-2}
\end{bmatrix}
\tag{6.29}
$$

In a similar vein, a second-order Hankel matrix may be formulated by applying a future input in the present and to obtain a set of response y is,

$$
\begin{pmatrix} U_{p+} \\ - \\ U_{f-} \end{pmatrix} =
\begin{bmatrix}
u_0 & u_1 & \cdots & u_{j-1} \\
u_1 & u_2 & \cdots & u_j \\
\cdots & \cdots & \ddots & \cdots \\
u_{i-1} & u_i & \ddots & u_{i+j-2} \\
u_i & u_{i+1} & \cdots & u_{i+j-1} \\
-- & -- & -- & -- \\
u_{i+1} & u_{i+2} & \cdots & u_{i+j} \\
\cdots & \cdots & \ddots & \cdots \\
u_{i+h-1} & u_{i+h} & \cdots & u_{i+h+j-2}
\end{bmatrix},
\begin{pmatrix} Y_p \\ - \\ Y_f \end{pmatrix} =
\begin{bmatrix}
y_0 & y_1 & \cdots & y_{j-1} \\
y_1 & y_2 & \cdots & y_j \\
\cdots & \cdots & \ddots & \cdots \\
y_{i-1} & y_i & \ddots & y_{i+j-2} \\
y_i & y_{i+1} & \cdots & y_{i+j-1} \\
-- & -- & -- & -- \\
y_{i+1} & y_{i+2} & \cdots & y_{i+j} \\
\cdots & \cdots & \ddots & \cdots \\
y_{i+h-1} & y_{i+h} & \cdots & y_{i+h+j-2}
\end{bmatrix}
\tag{6.30}
$$

The parameter i, h are usually larger than the chosen system order n.

The description of the subspace state-space algorithms are somewhat involved. However, it suffices here to state that the 4SID methods CVA [158], MOESP[163], [164], and N4SID [161], [162], [175] differ in the weighting methods used in the realisation of the state-space models and applicability to stochastic or deterministic systems, but are similar in that they are built from the Singular Value Decomposition (SVD) of Hankel matrices that are formulated from input and output data.

6.5.2   Accuracy of the synthesized model

The accuracy of the synthesized model is measured by how its response would fit to the original signal. For the $i-$th pilot bus with PMU-measured voltage magnitude $\bar{V}_i^{\mathrm{p,pmu}}$, the fitness level of the synthesized model (of the form (6.28)) obtained by systems identification methods would be,

$$
\mathrm{FTP}_i = \left(1 - \frac{\left\| \bar{V}_i^{\mathrm{p,pmu}} - \bar{V}_i^{\mathrm{p,mod}} \right\|_1}{\left\| \bar{V}_i^{\mathrm{p,pmu}} - \frac{1}{N} \sum_1^N \bar{V}_i^{\mathrm{p,pmu}} \right\|_1} \right) \times 100
\tag{6.31}
$$

where $V_i^{\mathrm{p,mod}}$ is the synthesised model output response and $V_i^{\mathrm{p,pmu}}$ is the PMU-measured voltage magnitude. Equation (6.31) is a normalised 1-norm deviation from a PMU-measured signal, of the synthesised model response corresponding to a bus i. It is easy to define a vector $\mathbf{FTP}_i$ whose i-th element is FTP_i

The accuracy may also be evaluated using the mean of the squares of errors between the measured signal and the original signal generated from input perturbations. The MSE in (6.32) is an average of the 2-norm deviation of across all bus i responses.

$$\text{MSE} = \frac{1}{N} \underbrace{\left(\bar{\boldsymbol{V}}^{\text{p,pmu}} - \bar{\boldsymbol{V}}^{\text{p,mod}} \right)^T \left(\bar{\boldsymbol{V}}^{\text{p,pmu}} - \bar{\boldsymbol{V}}^{\text{p,mod}} \right)}_{\text{square of error, } \boldsymbol{e}^T \boldsymbol{e}} \tag{6.32}$$

In the next section, the fitness of the synthesised models is considered sufficient to determine the accuracy of the synthesis. However, all models are synthesised with MSE ≈ 0. A MSE that is approximately zero indicates that there is almost no error in the deviations of the modelled response from the measured data.

Model Realisation based on voltage output measurements

For the purpose of synthesising models from measurements as an alternative to rigorous mathematical modelling the electric power grid, the topology of the network —especially the locations of generator and load buses —are assumed to be known. Consequently, the grid, for which certain quantities of interest, such as voltage, is to be controlled may be seen as a grey box, rather than a completely black box. The goal of the 4SID process is to then synthesise a n-th order model that captures the dynamics of the quantities of interest.
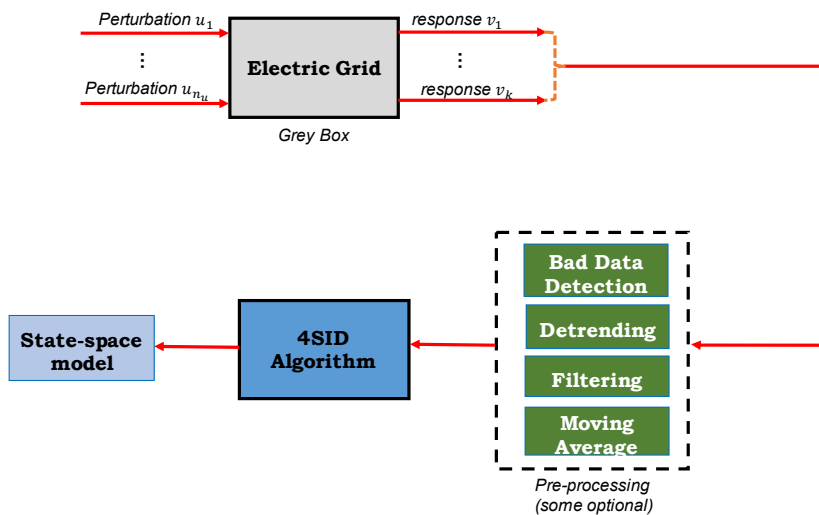
FIGURE 6.3: The 4SID Process

Figure 6.3 and the flow chart in Figure 6.4 summarise the steps which can be used to realise models from input-output data relationship using the subspace state-space algorithms. Probing signals are used to excite the system and the responses are captured and saved for offline processing to be later incorporated in a model-based control setup as time-invariant models or for online synthesis as time-varying models. For online applications, a moving window of data of finite length is used to capture current system dynamics.

In offline and online applications, the captured signals should be pre-processed to remove trends, filter undesirable frequency ranges, detect and remove bad data and outliers. For online processes, it may be necessary to compute the moving average of finite data samples in addition.

A significant and necessary step in the pre-processing stage is to remove the DC offset, and especially for stochastic signal, to filter noise and improve the quality of measurements. For online state-space identifications, down-sampling may be necessary to improve the computational feasibility of online model estimations. High-frequency contents may be filtered from signals and a moving average of the filtered signals may be used for the estimation. Offline modelling particularly gives the chance of synthesising models of different orders until a model with suitable compromise between model order and fitness is selected. This description is illustrated with the flow chart of Figure 6.4.
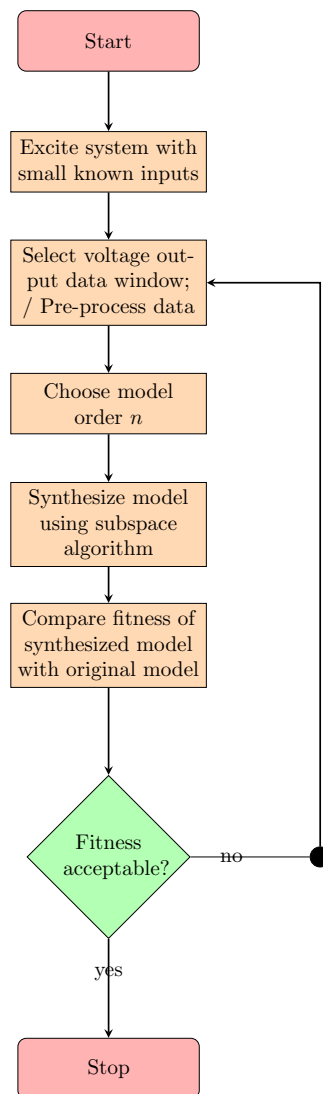
FIGURE 6.4: Flow chart summarising steps taken for model realization

Model Identification: Case Study A

The process in the flow chart of Figure 6.4 is illustrated using the two-area, four-generator test system of Figure 6.5 . The input changes are to the AVR references of the generators G_1, G_2 in Area 1 and those of generators G_3, G_4 in Area 2 and are denoted as $\Delta u_1, \Delta u_2, \Delta u_3,$ and Δu_4 in that
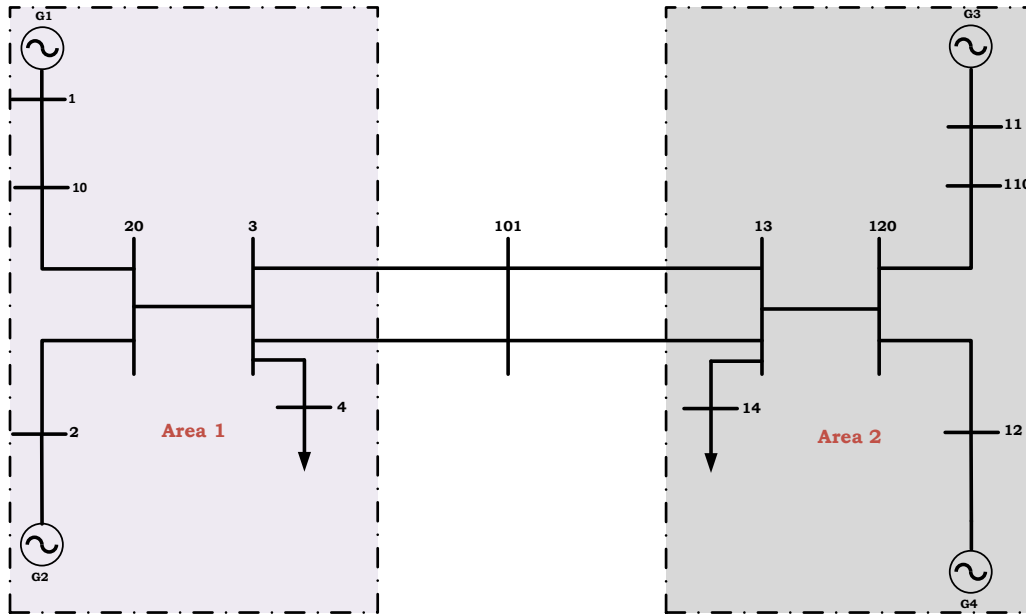
FIGURE 6.5: Kundur's Modified Two-Area Four-Generator Test Network

order. The outputs are $\Delta y_1, \Delta y_2$, for the voltage magnitudes of the two load buses respectively. Each $\Delta y_i = y_i - y_i^{\text{nom}}$ is the deviation of the voltage output of a bus i from a nominal value y_i^{nom} determined by a power-flow steady-state solution. The excitations are caused by small changes Δu_j (to nominal AVR references u_j^{nom}) that are applied as step inputs of magnitude 0.01p.u. starting from $t = 40s$, lasting for 20s and spaced 20s apart.

The two-area four-generator test network model was simulated in Simscape Power Systems in discrete-time mode with a fixed sampling time, $T_s = 50\mu s$. Three-phase measurements are fed from the load buses to phasor estimators at $F_s = \frac{1}{T_s}$, and estimated phasors are reported at $f_R = \frac{1}{333 T_s} \approx 60$ samples/s. For each input, a positive step signal applied for 20s was succeeded by a negative step input, in the form of a falling signal of the same magnitude.

Significantly-improved fitnesses are obtained for 12-th order model whose response comparisons with the original signal is shown in Figures 6.6 and 6.7. As can be seen from the figure, the individual responses of the higher-order models match the original signals much more closely than those of the 4th-order. A slightly lower model order $n = 10$ may compare less favourably (in fitness) than an order $n = 15$ but may give an acceptable performance for closed-loop control purpose. Increasing the model order from 15 may give better fitness estimates, but result in computationally-intensive models that are not ideal for real-time closed-loop control. Clearly, a lower model model order than 4 would compare more poorly to the original signal than was obtained for the 4th-order model of Figures 6.6 and 6.7.

Note that the bumps in the waveforms of Figure 6.6 and 6.7 are caused by the transient response to successive triggering of the AVR inputs.

Model Identification: Case Study B

Next, a state-space model is identifies for the modified 39-bus New England test network with a slightly different zoning arrangement than was used for Figure 5.2 in the placement method of
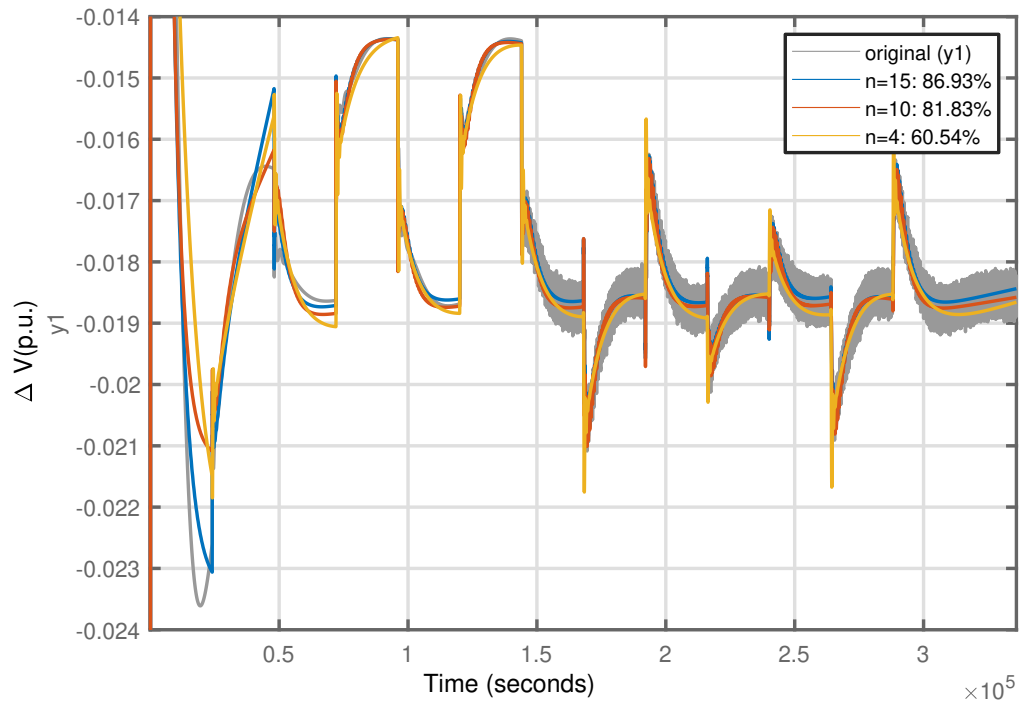
FIGURE 6.6: Comparison of the fitness for models of different orders (response for Bus 3)
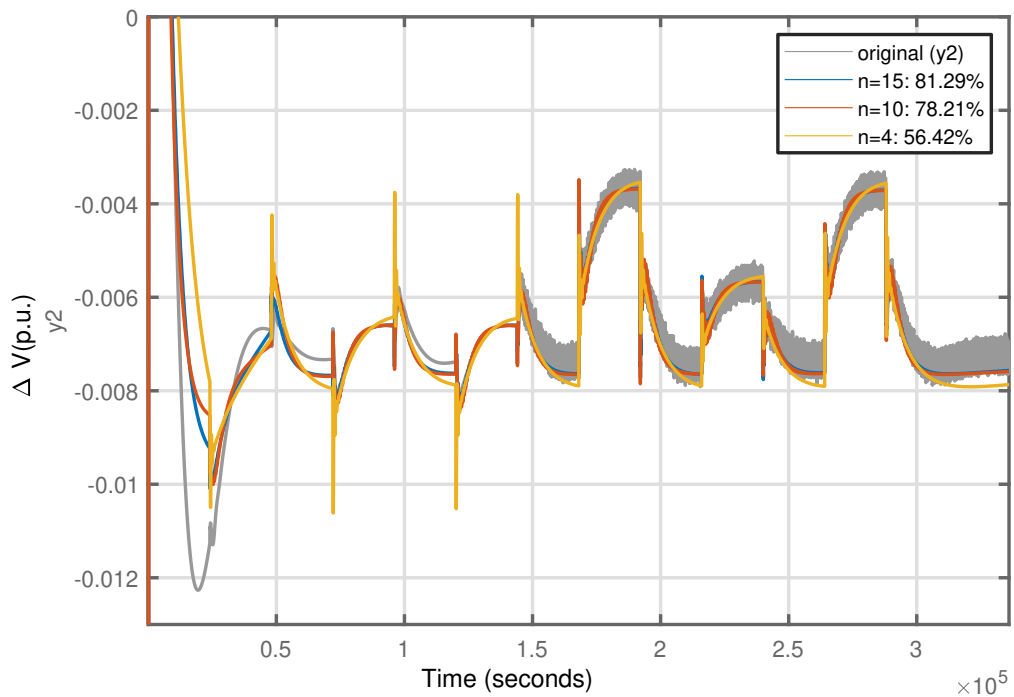
FIGURE 6.7: Comparison of the fitness for models of different orders (response for Bus 13)

Chapter 5. The test system is divided into West, East, and North zones with two subzones in each cardinal zone. In other words, there are 6 regions, West 1, West 2, East 1, East 2, North 1, and North 2, as shown in Figure 6.8. The system is simulated as a discrete-time dynamic model with

a sampling time $T_s = 25\mu s$. Detailed models of 10 synchronous generators with static exciters and governors, and 19 constant-PQ loads are used for the simulation. However, only generator G_1 is equipped with a PSS.
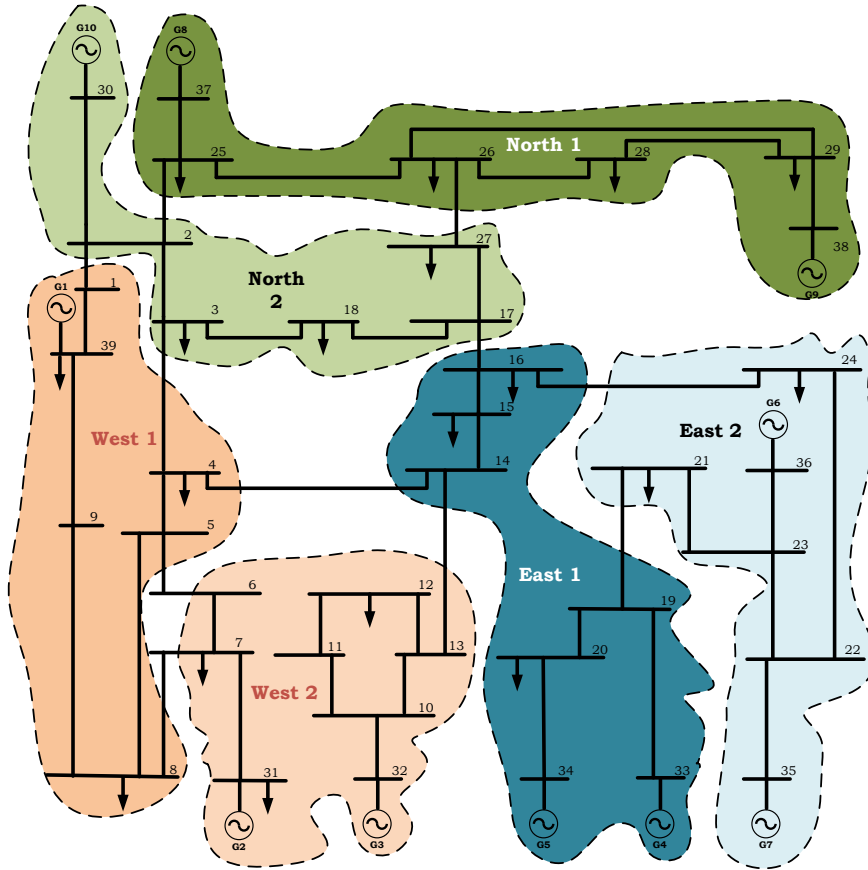
FIGURE 6.8: A Modified 6-region 39-Bus New England Test Network

For the relatively larger test system, the responses selected for the identification process are 18 of the 19 load bus voltages, excluding the load at Bus 32. The modulated inputs are the generators' A-VR set-points. In a similar manner to Case Study A, a step change of 0.01 p.u. was applied for 20s to each of 9 generator AVR references (excluding G_{10}) in turn, spaced 10s apart, as shown in Figure 6.9.

The models are synthesised for orders $n = 4, 10, 18$, and the responses for each model order are compared with the measured response obtained from the excitation, as shown in Figures 6.10, 6.11, and 6.12 for some selected load buses in the North, West, and East zones respectively.

Table 6.1 shows the fitness of the synthesised model to the original signal for all load buses. As expected and seen from Figures 6.10, 6.11, and F=6.12 and from Table 6.1, model fitnesses to the original signal decrease as the chosen model order decreases, and vice-versa.

Stability of synthesised models

The state-space models realised from measured data and which are intended for use in a predictive control sense must fulfil the requirements for traditional predictive control conditions: that the model be controllable and observable, or at least stabilizable and detectable [15]. A discrete-time
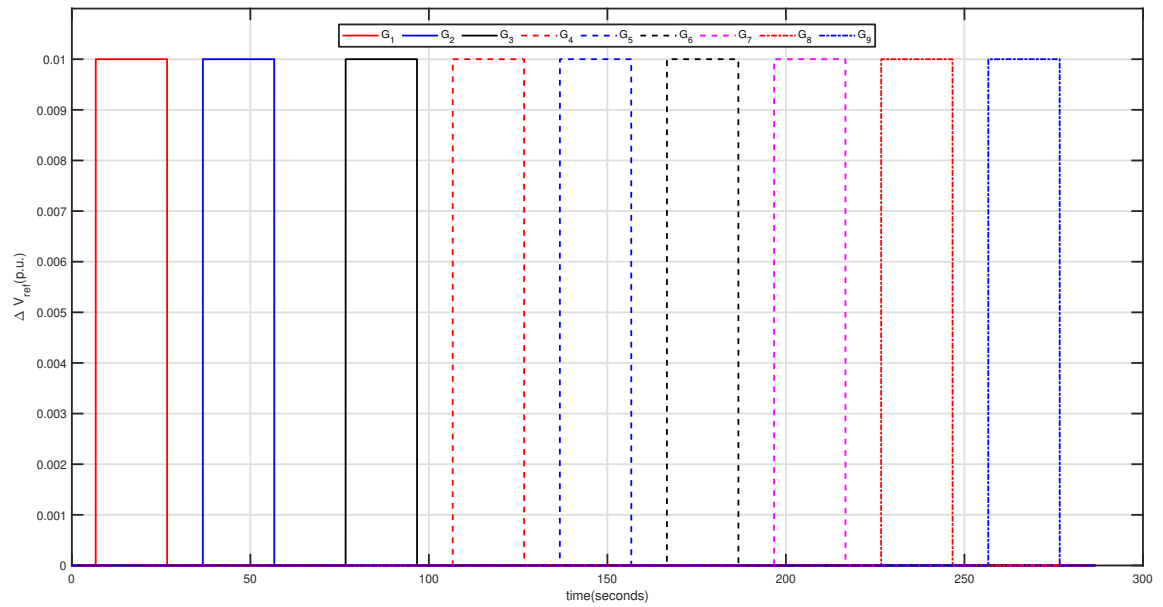
FIGURE 6.9: AVR reference modulation signals used for the 39-bus test network
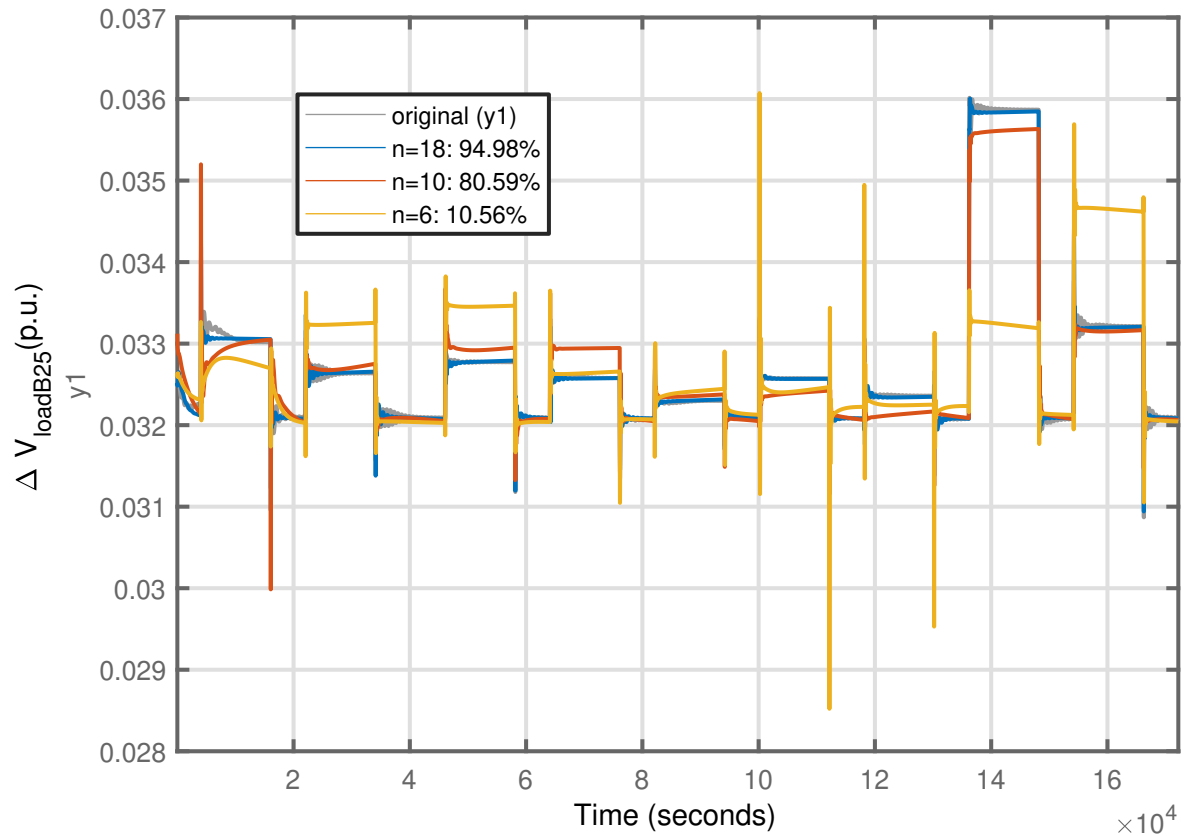
FIGURE 6.10: Comparison of responses of different model orders used (North zone
of the 39-bus test network)

state-space model is stable if all eigenvalues obtained from the state matrix have a magnitude less
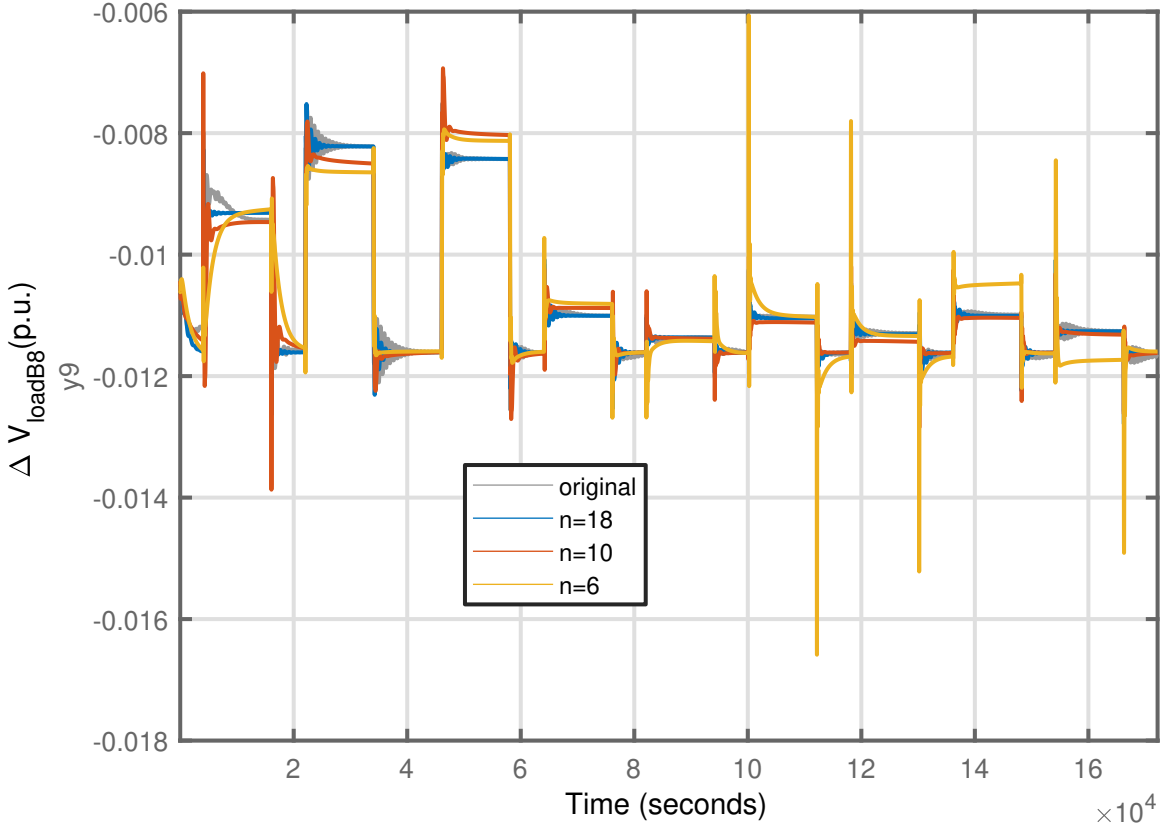
FIGURE 6.11: Comparison of responses of different model orders used (West zone of the 39-bus test network)

than 1, and are marginally stable if any of the eigenvalues is 1.

$$|\rho(A)| \leq 1 \tag{6.33}$$

The stability of the model is illustrated using the 6th, 10th, and 18th-order models realised for the 39-bus test network of Case Study B by estimating their respective eigenvalues. The compass plots of Figures 6.13, 6.14, and 6.15 show that the eigenvalues of all n-th order models lie in the unit disk in the discrete-time domain. Consequently, the internal model is stable for all orders.

Since the models are realised from measured (therefore observable) responses and known inputs, the predictive control conditions are met using the 4SID algorithms. However, the observability and controllability of the models can be established in more formal terms. Consider the observability matrix

$$\Theta = \begin{bmatrix} C & CA & CA^2 & \dots & CA^{n-1} \end{bmatrix}^T \tag{6.34}$$

and the controllability matrix

$$\Pi = \begin{bmatrix} B & AB & A^2B & \dots & A^{n-1}B \end{bmatrix} \tag{6.35}$$

If the rank$(\Theta) \in \mathbb{R}^{m \times nm} = n$ of (6.34), the system is observable. Similarly, if $(\Theta) \in \mathbb{R}^{pn \times p} = n$ of (6.35) is full-rank, the system is controllable. It then becomes straightforward to prove that the models realised from the systems identification process are both observable and controllable for the models used as case studies in this section.
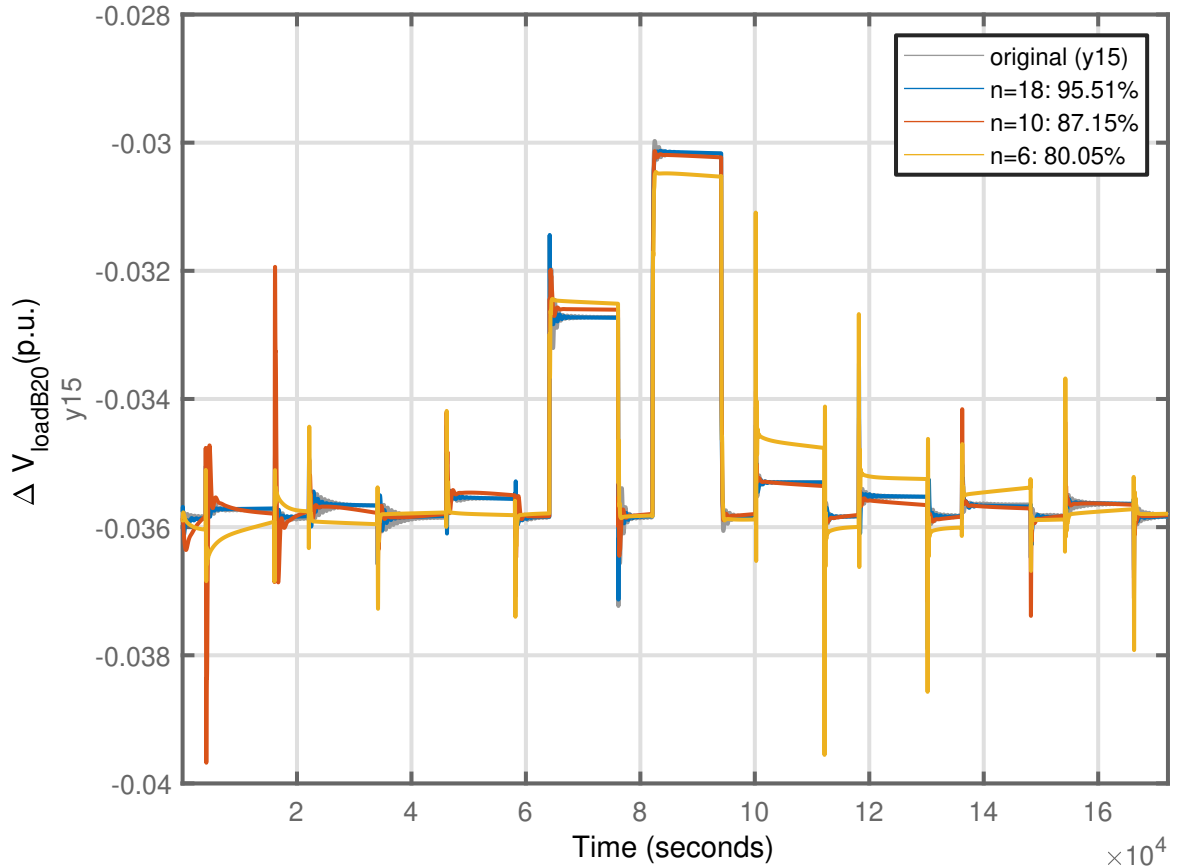
FIGURE 6.12: Comparison of responses of different model orders (East zone of the 39-bus test network)

However, although the internal model is controllable and observable, it must be noted that it is an approximation of a far larger and more non-linear system with more outputs and inputs. On account, the controller should be designed to handle small changes in the nonlinear system over which the linear internal model is valid.

6.6   Subspace-based Predictive Voltage Control (SBPVC)

The predictive control set-up based on subspace model realisation is posed as an objective function which minimises the voltage deviation from pilot bus voltage set-points, minimises the use of a defined set of controls and the rate at which the chosen sets of inputs are allowed to change. The constraints are the identified subspace model, the range of physically-imposed limits on the controls and their rates of change, as well as the range of (possibly) softened limits on the voltages of pilot buses.
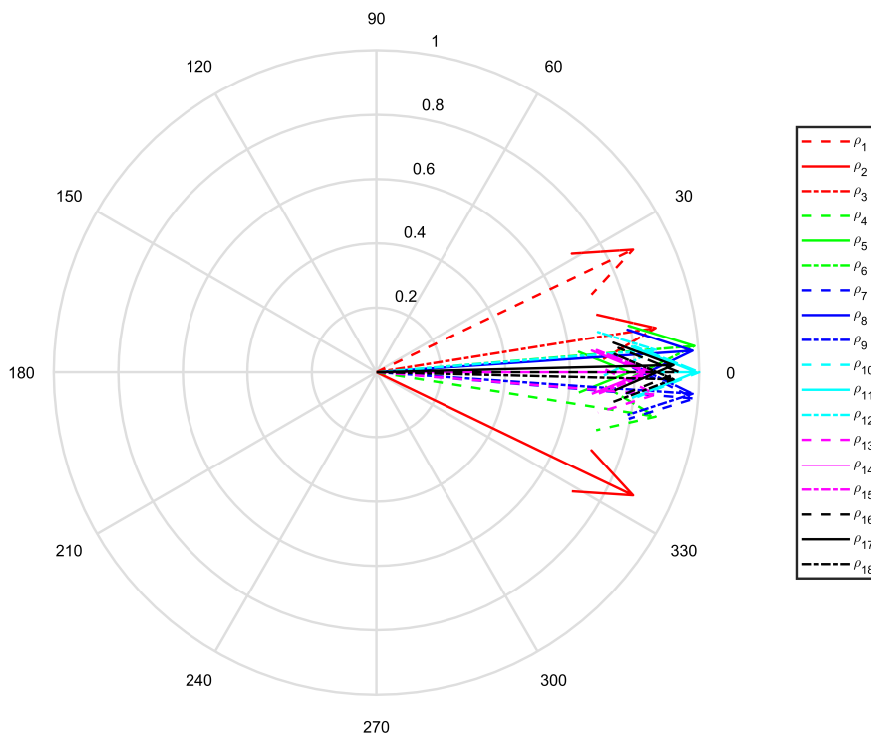
FIGURE 6.13: $n = 18$
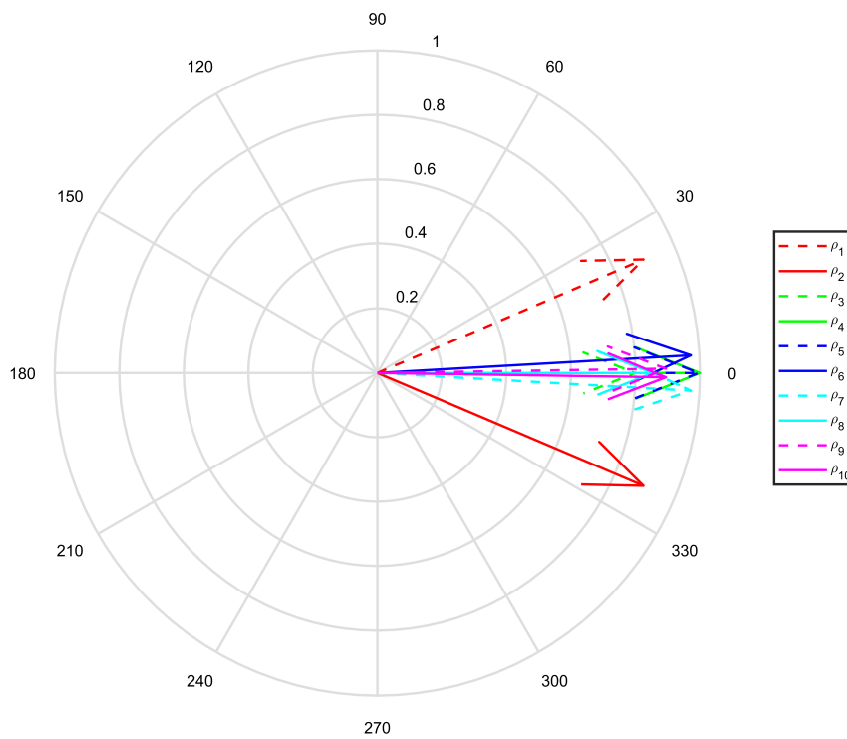
FIGURE 6.14: $n = 10$

TABLE 6.1: Fitness of the synthesised model to original signal across the IEEE 39-bus
load buses

Zone	Bus	Fitness (%) of synthesized model of order n relative to the original signal		
		n=18	*n=10*	*n=6*
North 1	25	94.98	80.59	10.56
	26	96.05	90.18	72.21
	28	96.31	93.11	83.29
	29	96.28	93.28	79.56
North 2	3	91.33	76.88	51.16
	18	94.25	78.90	61.81
	27	95.15	87.69	69.75
West 1	4	93.23	83.69	72.70
	8	92.06	77.54	65.23
	39	88.72	76.36	59.47
West 2	7	92.50	77.31	66.41
	12	95.03	70.17	58.90
East 1	15	93.97	76.81	68.43
	16	95.04	74.91	68.41
	20	95.51	87.15	80.05
East 2	21	94.30	79.99	63.06
	23	96.19	75.81	59.89
	24	94.80	81.82	72.92

$$\underset{\boldsymbol{u}_0,\dots,\boldsymbol{u}_{N_c-1}}{\text{minimize}} \sum_{k=0}^{N_p} \left[\|\boldsymbol{Q}\left(\Delta\boldsymbol{y}_{k+1}\right)\|_2^2 + \|\varepsilon_{k+1}\|_2^2 \right] + \sum_{k=0}^{N_c-1} \left[\|\boldsymbol{R}\left(\boldsymbol{u}_k\right)\|_2^2 + \|\boldsymbol{R}_\Delta\Delta\boldsymbol{u}_k\|_2^2 \right] \tag{6.36a}$$

$$\text{subject to } \Delta\underline{\boldsymbol{y}} - \underline{\varepsilon}_{k+1} \le \Delta\boldsymbol{y}_{k+1} \le \overline{\boldsymbol{y}} + \overline{\varepsilon}_{k+1} \qquad k = 0, 1, \dots, N_p - 1 \tag{6.36b}$$

$$\Delta\boldsymbol{y}(k+1) = \boldsymbol{C}\boldsymbol{A}\Delta\boldsymbol{x}(k) + \boldsymbol{C}\boldsymbol{B}\Delta\boldsymbol{u}(k) \qquad k = 0, 1, \dots, N_p - 1 \tag{6.36c}$$

$$\Delta\underline{\boldsymbol{u}_r} \le \Delta\boldsymbol{u}_r = \Delta\boldsymbol{u}_k - \Delta\boldsymbol{u}_{k-1} \le \Delta\overline{\boldsymbol{u}_r} \qquad k = 0, 1, \dots, N_c - 1 \tag{6.36d}$$

$$\underline{\Delta\boldsymbol{u}} \le \Delta\boldsymbol{u}_k \le \overline{\Delta\boldsymbol{u}} \qquad k = 0, 1, \dots, N_c - 1 \tag{6.36e}$$

$\boldsymbol{Q}, \boldsymbol{R}$, and $\boldsymbol{R}_\Delta$ are positive semi-definite diagonal matrices which exact penalties on all or some of the deviations from the reference vector or on all or some of the control variables and their rates of change. $\Delta\boldsymbol{y}_{k+1}$ is the deviation of the pilot bus voltages from a pre-defined reference r calculated at the tertiary voltage regulation level. The reference r may be assumed to be fairly constant over long intervals of k in the absence of the consideration of tertiary voltage control.

N_p and N_c are dimensionless quantities representing the prediction and control horizons respectively. The essence of the prediction is to enable the control to anticipate future changes in system states, and to seek to minimise the effect of these changes by accounting for them in the present.

It is possible to implement the subspace-based MPC process in two ways. The first is to identify a state-space model offline and then implement the internal model of the control as a linear time-invariant model which is not updated during the process. A series of feedback process is then expected to compensate for the modelling error due the use of a linear and invariant model which is not updated. The advantage of this method is that the closed-loop is relatively faster and more
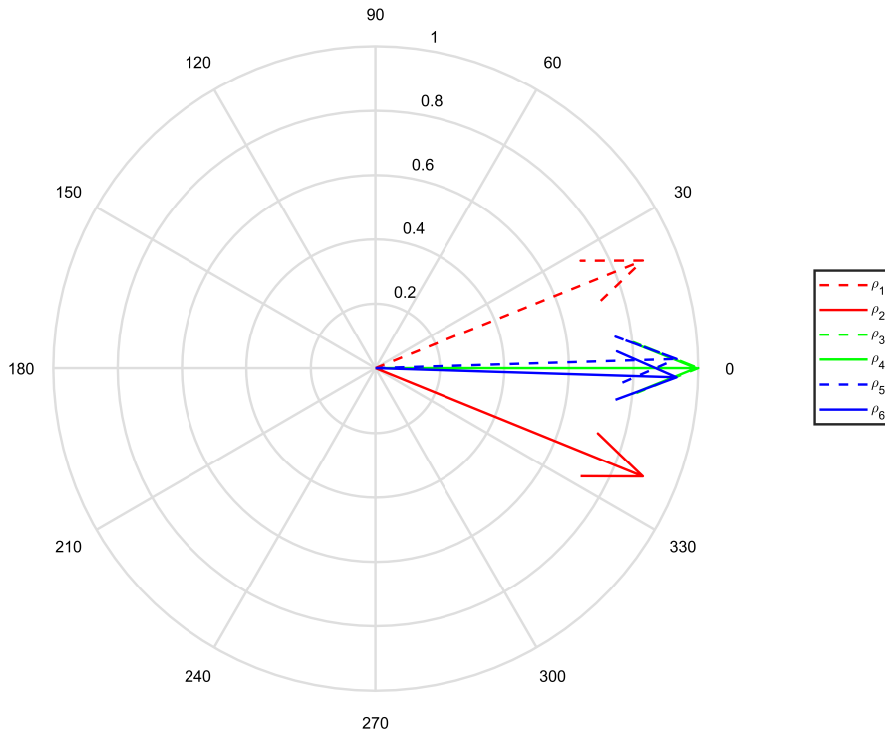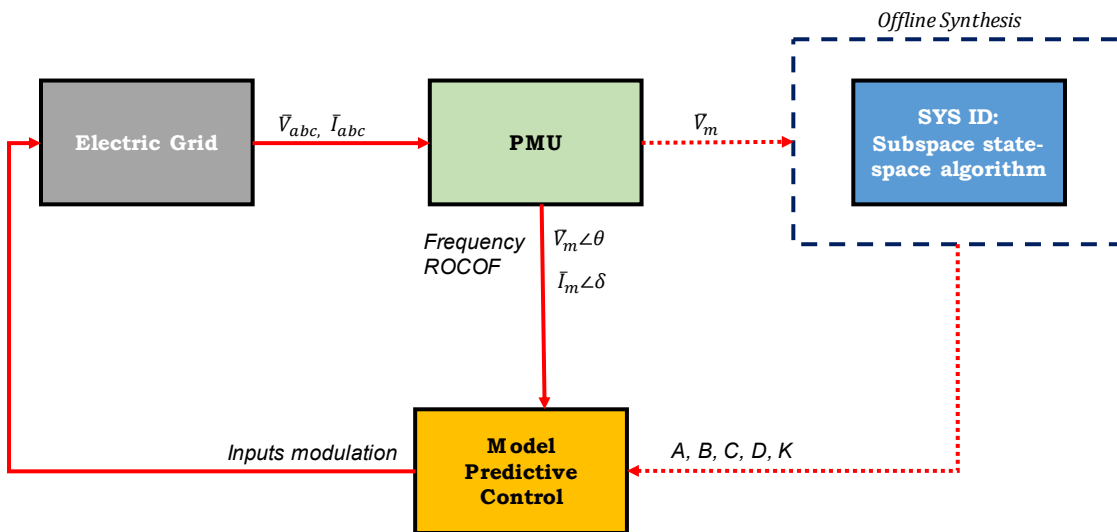
FIGURE 6.15: $n = 6$

FIGURE 6.16: The Subspace-based Predictive Control Setup

applicable for real-time operations. The closed-loop subspace-based predictive control is as shown in Figure 6.16. Following from the system identification process described in the previous sections, the identified models are incorporated into the controller to determine the feedback control signal for closed loop.

The second approach is to update the models online using a moving time window of finite length. This would appear to capture more current dynamics in the system, but may require much

more computational resources, which may slow down the voltage control process and reduces its feasibility in a real-time application. In a predictive control application, this would be implemented as a time-varying adaptive predictive controller whose internal state-space model is updated at pre-determined time intervals to capture more current system dynamics.

6.7 Implementation

The performance of the Subspace-based Predictive VoltageControl (SBPVC) is demonstrated on the Simscape PowerSystems platform using the 2-Area 4-generator test network [65]. Each generator is equipped with a PSS and static exciter, which accounts for the presence of primary controls, and oscillation damping capability. Since these components are available in practice, the occurrence of non-viable voltages with their presence in the system should emphasise the need for a higher-level controller. In order to instigate a voltage instability scenario in this test model, constant-PQ parallel RLC loads at load buses 4 and 7 are replaced with constant-PQ parallel RL loads. To achieve control through the reference modulations of Static VAR Compensators (SVC), the 200 MVAR and 300 MVAR capacitors at load buses 4 and 7 respectively are replaced with SVCs which are capable of providing both capacitive and inductive MVAR supports equal to those previously supplied by the capacitors. In the nominal case, around 400 MW of power is pushed from Area 1 across the double-circuit tie lines connecting the areas to Area 2. Without any fault, loss of line, loads, or generators, all buses voltages are within acceptable bands and the generators operate at the nominal voltage set-points.

6.7.1 Case Study A: Scenario

The description of the performance of the SBPVC is preceded by a description of the system's behaviour without the use of controls. For this case, a 3-phase line-to-ground fault is first applied to the one of the tie lines at $t = 10s$. The fault is cleared one-twelfth of a cycle later by opening the faulted tie line. This increased the effective impedance and loading on the second tie line and caused the voltages at the monitored load buses 4 and 7 to decrease to about 0.93 p.u, respectively, which are below the minimum allowable band. The primary controls settled the system into a stable post-fault state in about 40s. However, in the steady state, the voltages are below the minimum required level of 0.95 p.u. At $t = 120s$, a drastically-sudden (albeit unrealistic) load increase of about 100% is witnessed at Load Bus 4 in Area 1. The substantial load increase caused a reverse power flow across the remaining tie line. This further degrades the voltage profiles at the load bus 4 to 0.9 p.u even when the system had recovered to a steadier state. In the absence of OLTCs, there are no tap operations which may seek to regulate the bus voltages back to within acceptable bands. Furthermore, voltage-dependent dynamic loads which may cause system instability in the presence of non-viable voltage profiles are not used in this case. Consequently, in the absence of the dynamics of OLTCs and voltage-dependent loads, the system is expected to be long-term stable. However, load bus voltages are not within acceptable bands, and therefore secondary voltage control is needed to correct the anomaly.
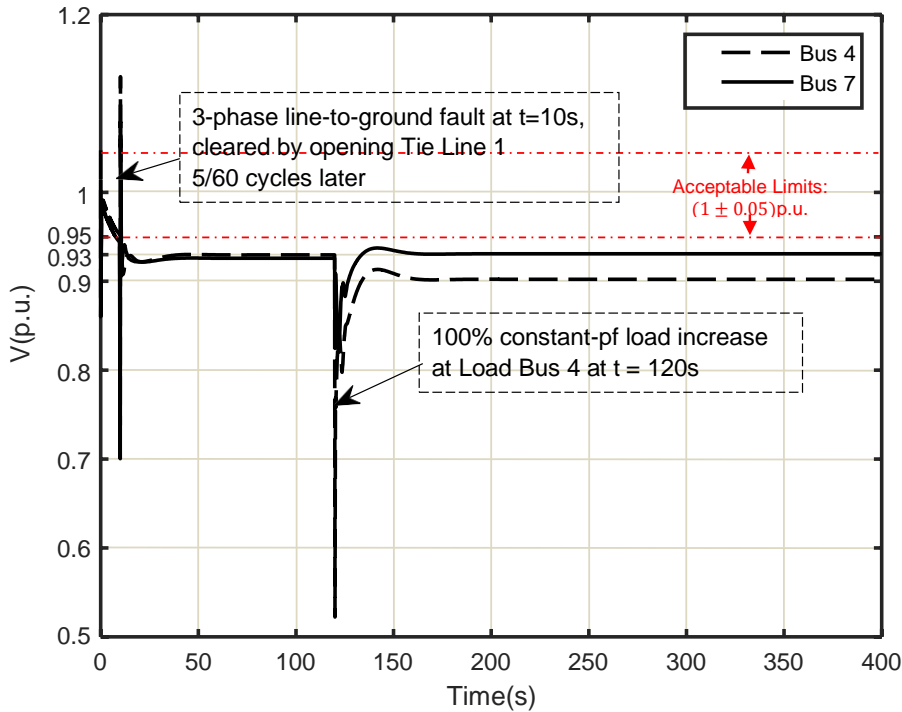
FIGURE 6.17: Case Study A: Voltage profile without SBPVC

6.7.2 Case Study A: Performance of the SBPVC in non-viable voltage regulation

The SBPVC uses the PMU signal measurements at the load or pilot buses in the feedback control of the bus voltage. In this implementation of the SBPVC, the central idea is to influence primary controls to stimulate the modulations of generators' terminal voltages (hence the generators' reactive power production), and SVCs' reactive power production through direct modulations of the set-points of the generators' AVRs and those of the SVCs at the pilot (or load) buses.

For proper time-differentiations between primary and secondary controls, some intervals must be allowed for previous set-points changes at reactive power sources to be implemented before new set-points are sent to the primary controls. Therefore, the internal model of the controller is synthesised with a sampling time of $T_s = 20s$ and the controller's prediction horizon is set to $T_{pred} = 200s$. This implies that new set-points are estimated every 20s based on the SBPVC's prediction of the system's behaviour 200s into the future. The control horizon T_{ctrl} is chosen to be the same as the prediction horizon, T_{pred}. The control inputs are constrained to a rate of ± 0.01p.u. in order to prevent the introduction of undesirable transients into the system when controls are applied, and to allow for the utilisation of all controls with a proportion adjusted by the relative *cheapness* (or otherwise) of the control variables. For the present purpose, modulations of SVC set-points are assumed to be cheaper than changing generators' AVR references. In the objective of (6.36a), each of the diagonal entries of the output-deviation weights Q is set to zero. It is considered sufficient for the output constraints to be obeyed, without setting output-regulation objective in a [possibly] new operating state should there be a change in the system's condition, such as may be caused by faults and/or changes to system's loading conditions. It is expected that this should at once allow the system to operate closer to constraints (at the end of the horizons) since the

controller is now biased towards the minimisation of control modulations and the rate at which new set-points are modulated.
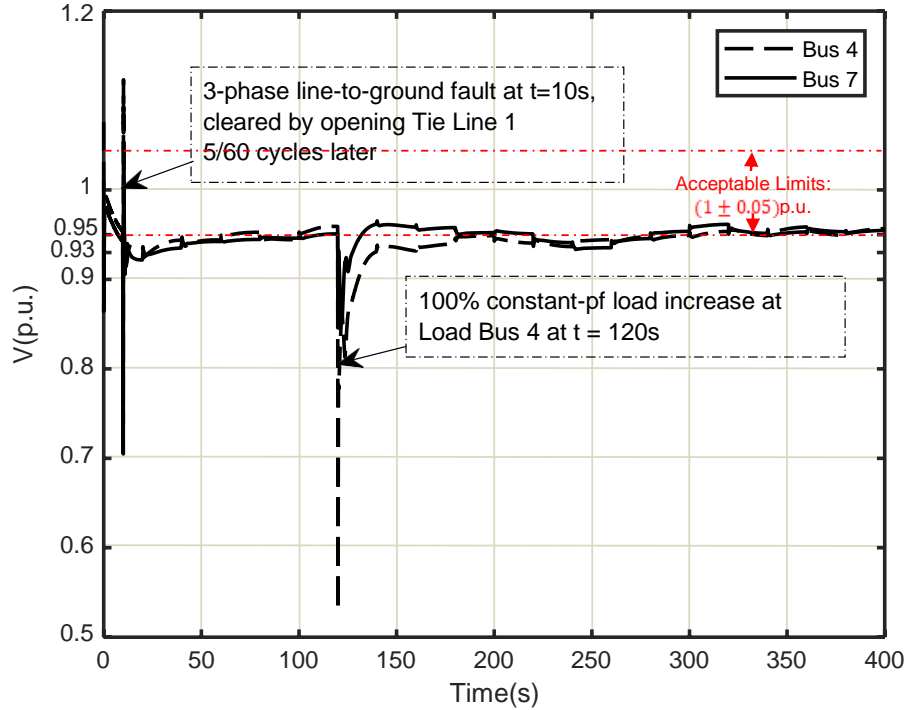

FIGURE 6.18: Case Study A: Voltage profile with SBPVC

The system is simulated for 400s with the controller providing secondary voltage level regulation to the AVRs and SVCs. After the application of the fault at $t = 10s$ and the clearance through the opening of the lines, the controller modulates the set-points as shown in Figures 6.19 and 6.20. The change in system conditions occurred in between controller sampling, and control inputs are applied on the next sampling instant. At first, the cheaper SVC references and the reference of the area increased to improve the voltage profile. The controller reduces the references of the relatively more expensive G_1 reference. Indeed, it can be noticed that there is a reluctance to modulate the G_1 AVR set-points at the initial stages before the load change occurred at $t = 120s$. However, the controller de-emphasised the focus on cheaper but less effective controls and increased the modulation of those relatively more expensive set-points.

In the previous scenario, without the SBPVC action, the load bus 4 voltage became relatively worse than that of load bus 7 after the loading was increased in Area 1 at $t = 120s$. At the new reference points provided by the controllers, the voltage at bus 7 was more inclined to recover to a more desirable voltage level post-loading than in the absence of controls. However, load bus 4 voltage remained outside the acceptable limits. In order to drive the voltage to the desired band, the controller modulates more of the references in Area 1, and sought to reduce the use of Area 2 controls.

6.7.3 Case Study A: Effect of model order on the SBPVC performance

The SBPVC described so far has been based on a 10th-order internal model. Even though the voltage is driven back to the desired bands, the erratic nature of the control inputs resulted in
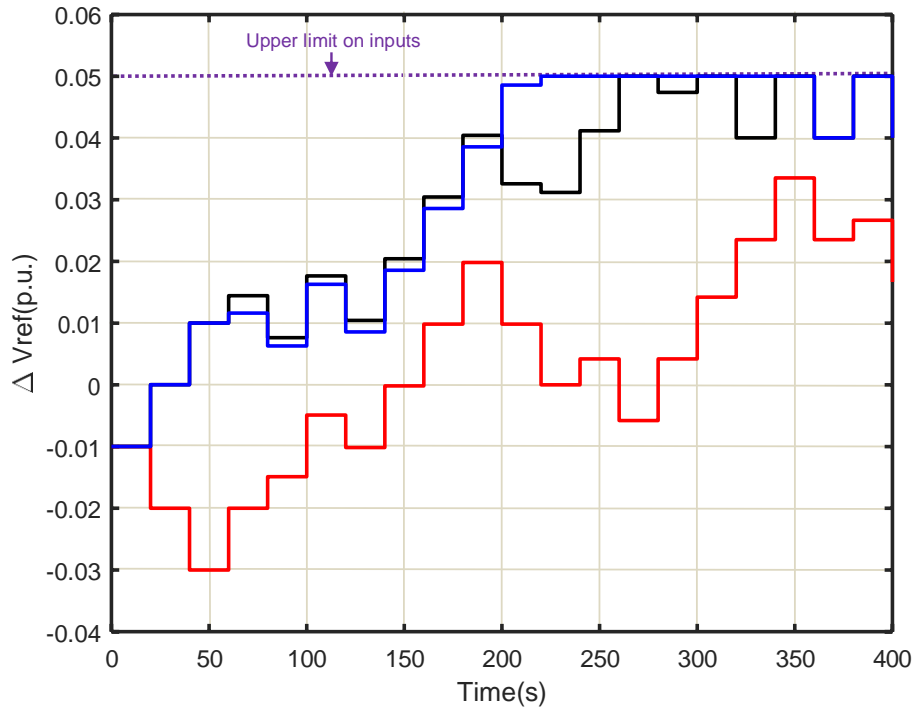
FIGURE 6.19: Case Study A: SBPVC control inputs in Area 1, (red- G_1, black-G_2, blue-SVC at load bus 4), (*Limits on ΔV_{ref}(p.u.) is $\pm 0.05 p.u$*)
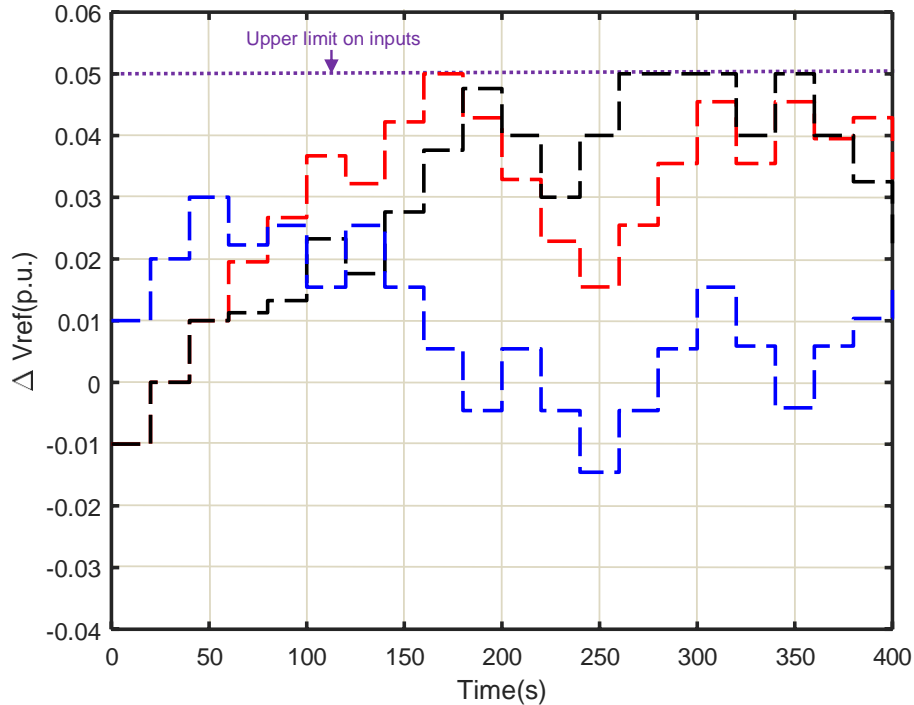

FIGURE 6.20: Case Study A: control inputs in Area 2, (red- G_3, black-G_4, blue-SVC at load bus 7), (*Limits on ΔV_{ref}(p.u.) is $\pm 0.05 p.u$*)

a less than desirable smoothness of the controlled inputs. However, it is possible to improve its performance by increasing the model order. Higher-order models capture the behaviour of the

systems more accurately and enable more accurate state predictions. This can be illustrated by the response shown in Figure 6.21 when the model order was increased from 10 to 15. Compared to the 10th-order model, the voltage response is steadier after the events as a result of a more assured control input estimation, compared to the response in Figure 6.18.
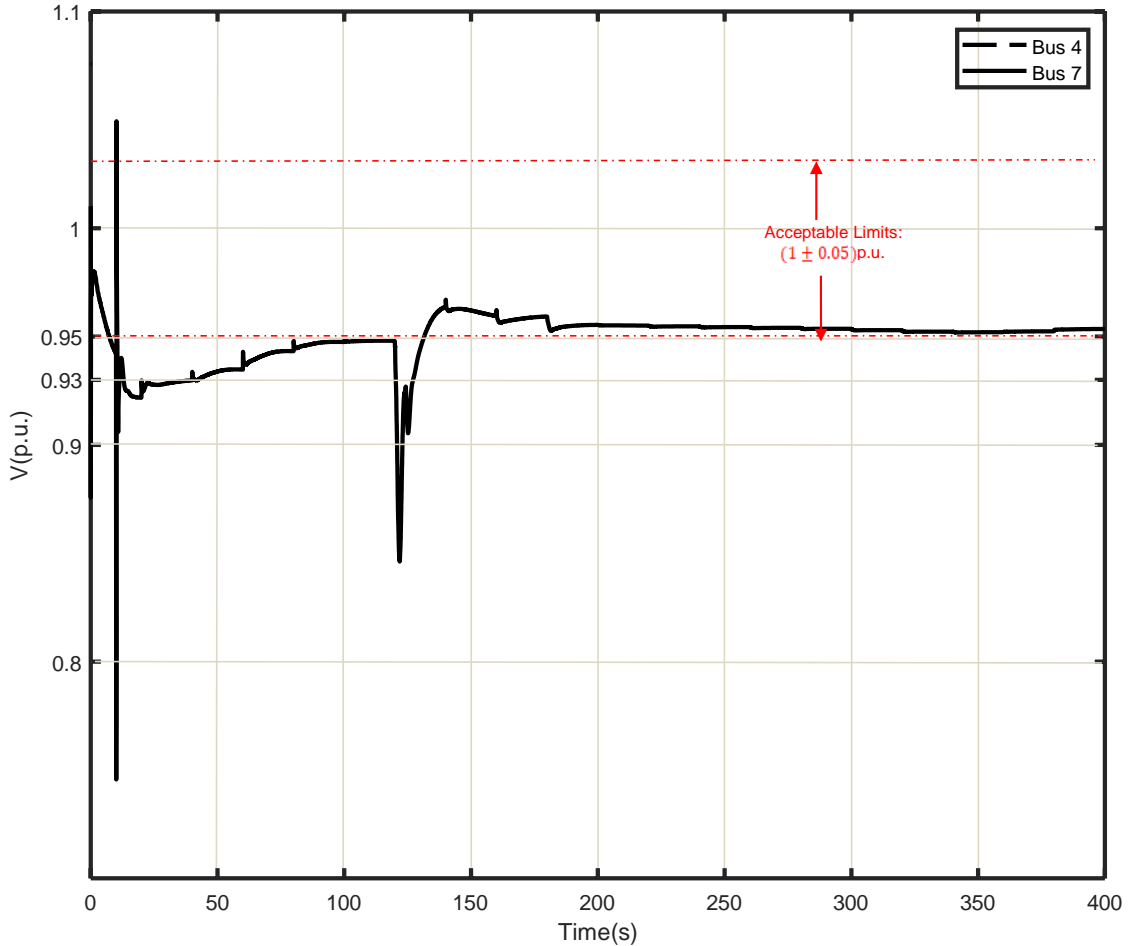
FIGURE 6.21: Case Study A: Voltage profile with SBPVC based on model with order
$n = 15$, (*Limits on V(p.u.) is $\pm 0.05 p.u$ of unity*)

From Figure 6.22, it is clear that the control inputs estimated by the 15th-order-model-based predictive controller are less erratic than those obtained by the 10th-order SBPVC of Figures 6.19 and 6.20. This is because more eigenvalues corresponding to system dynamics have been captured in the state-space model. On account, the controller is more efficient in the anticipation of system's future changes, and is better positioned to the provision of more accurate predictions that do not need to be corrected in the future. As can be seen from Figure 6.22, bigger control steps are taken at the sampling instants immediately following the events to drive the outputs back to acceptable limits, and smaller steps are taken towards the end of the simulation after the constraints have been obeyed. The pattern is more discernible than can be inferred from the 10th-order-model-based SBPVC .
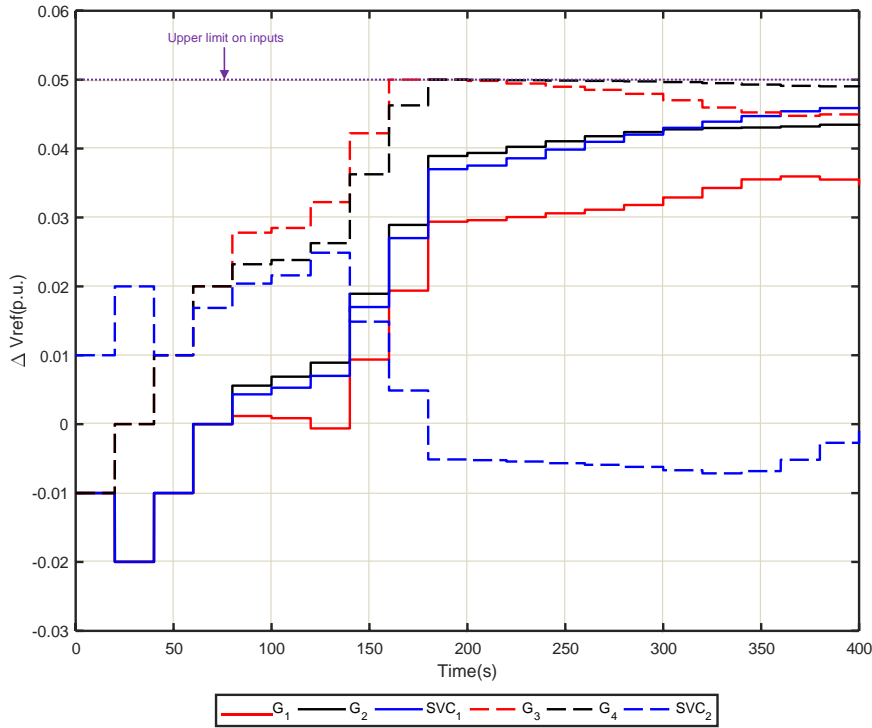
FIGURE 6.22: Case Study A: Reference modulations with SBPVC based on model
with order $n = 15$

6.7.4   Case Study B: 39-Bus New England test network

Next, we test the SBPVC performance on the Modified 39-Bus New England test network earlier
described in Section 6.5.2 and shown in Figure 6.8 of the same section. The set-up with and without
the feedback control was implemented on the Simscape PowerSystems platform using Artemis and
RT-LAB blocks. The network was simulated in the discrete-time domain with a fixed sampling time
$T_s = 25\mu s$. The loads are constant-PQ dynamics whose PQ inputs are fed from an external source,
lending, at once the flexibility to increase and shed load. Each generator was equipped with a static
exciter and a turbine governor models but only Generator 1 has a PSS to dampen oscillation.

6.7.5   Case Study B: Scenario

A loss of line 21 -22 without fault occurs at time $t = 20s$, resulting in the loss of a direct connection
of Bus 21 with Generator 6, and with it a reduced potential for reactive power support from this
generator. The loss of Line 21-22 was followed by a continuous ramping up of loads in the Eastern
zones 1 and 2 from $t = 40s$, as shown in Figure 6.23, for 80s (until $t = 120s$) at constant power
factor.

Although only the Eastern zones loads were increased, the voltages in other parts of the net-
work followed the same pattern as the East zones 1 and 2, decreasing continuously, albeit at differ-
ent rates to those areas of direct load perturbations, as shown in Figures 6.24, 6.25, and 6.26.

Figure 6.27 shows the increase in reactive power outputs of generators as they respond counter-
act the increased loading effect on the voltages. It can be observed that each generator's response
depends on the proximity and electrical connection to the load bus as well as their respective capac-
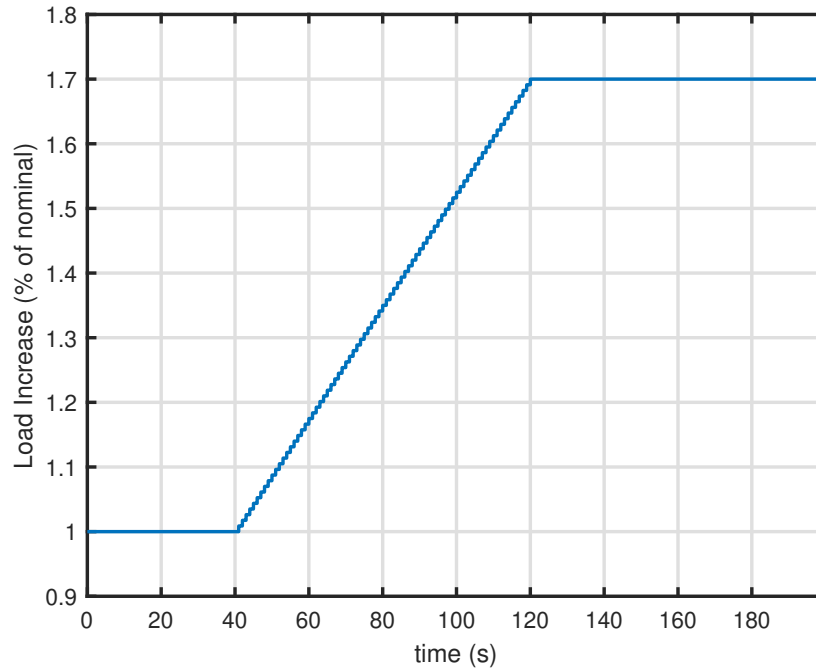ities. The increase in reactive power output from the generators was accompanied by an increases

FIGURE 6.23: Case Study B: Load ramp up in the Eastern Zone (percentage of nominal loads)

in respective generator's field currents. In practice, sustained increase in reactive power could potentially activate the OELs and cause the generators to cease further voltage regulation actions. In this case, OEL effects are not considered.

After the load ramp-up had stopped at $t = 120s$, some of the generators reduce their reactive powers, mostly by slight amounts,and then maintained a constant outputs, from around $t = 140s$. In the absence of further controls, it can be seen that load bus voltages increased after 120s but maintained steady-state profiles which were different from pre-event values. In the Eastern zones especially, most of the voltages remained out of the regulated bands. Most notably, the under-voltages occurred at all load bus voltages in the East zone (except at Bus 23 which is directly connected to Generator 7), at buses 4, 8, 39, and 7 in the West zone, but only at Bus 18 in the North Zone.

Case Study B: Performance of the SBPVC in non-viable voltage regulation

The SBPVC performance on the regulation of non-viable voltages is again examined here, this time on the modified 39-bus New England test network, following from the line loss and load ramp-up scenario described in Section 6.7.5. PMUs are assumed to be selectively placed at the load buses, and up to 60 samples of voltage measurements are fed from the PMUs to a comparator every second. Load bus voltage values are compared to a nominal value and then fed to a centralised controller at the PMU rate. Generators' AVR references, which are assumed to be the main control inputs in this case, are modulated every 30s by the controller. Weights R on the inputs and R_Δ on the rate of change of the inputs are 0.01 and 0.1 p.u. respectively for each control variable. Generator 10 is not allowed to participate in the secondary voltage control, and therefore its references are not modulated. However, this does not preclude the generator from participating in primary voltage control within the limits of its set terminal voltage. Since the controller is only fed
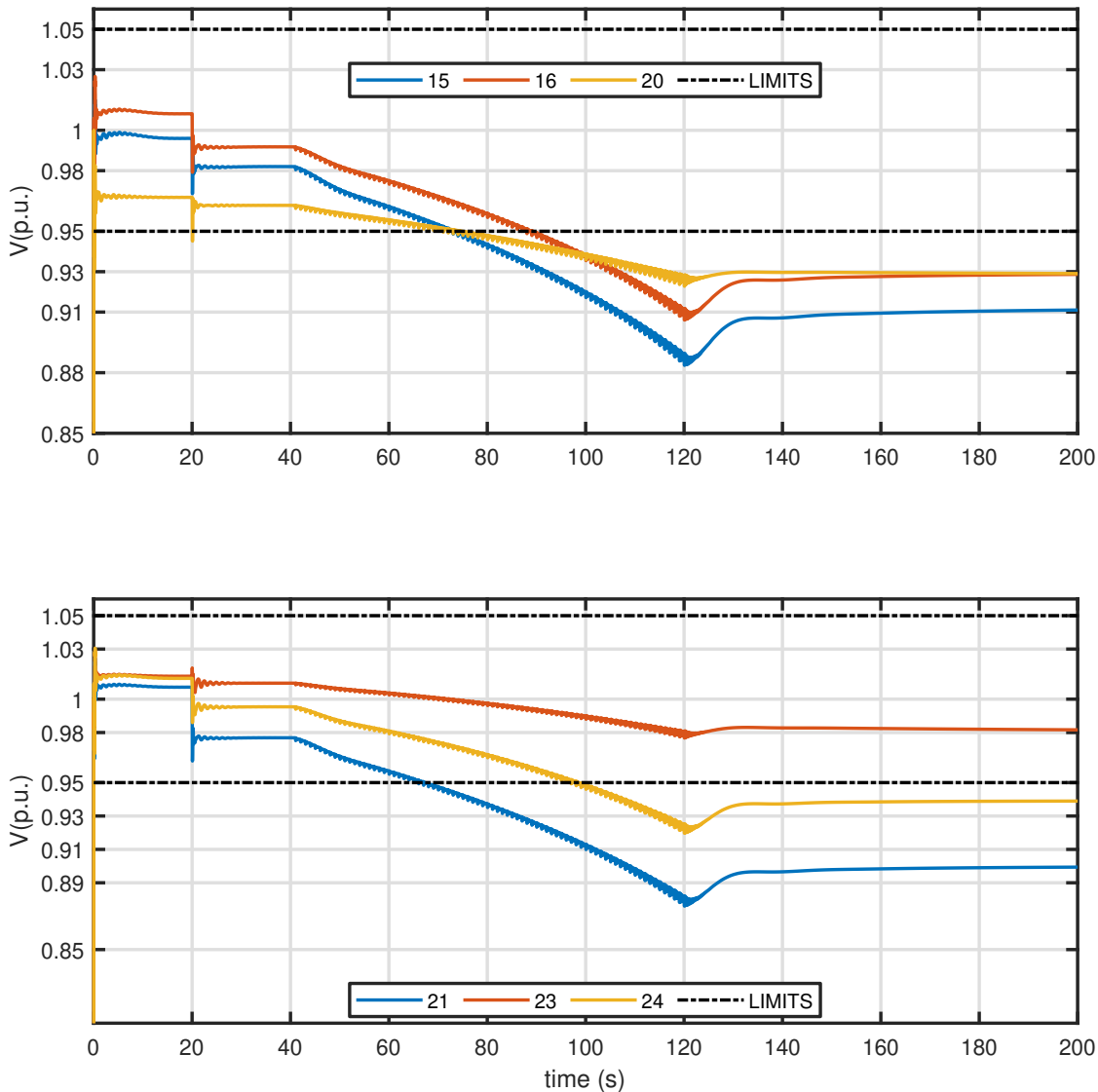
FIGURE 6.24: Case Study B: East Zones 1 and 2 load voltages with primary controls only

voltage deviations measurements, input constraints are ± 0.05p.u. deviations from nominal. The input constraints are hard and uniform over the prediction and control horizons. However, voltage deviation constraints (also $\pm 0,05$p.u. of nominal) are relaxed by a very small amount to allow the controller to find a feasible solution within the bounds of admissible control inputs. An 18th-order internal model was used in the design, and all load bus voltages, except at bus 31, are controlled from a central location.

The voltage profiles across the zones with 18th-order SBPVC are shown in Figures 6.29, 6.30, and 6.31. It can be observed that the SBPVC successfully regulated the voltage profiles of all the network load bus voltages to within the admissible bands after the contingencies of Section 6.7.5.

This was implemented by modulating the references of Generators G_1 to G_9 as shown in Figure 6.32. The large controller sampling time of 30s meant that a lot of voltage events happening in the system may be not detected by the controller. Therefore, even with frequent measurement updates, some of the voltages are well out of the regulated bands especially during the load ramp-up period.
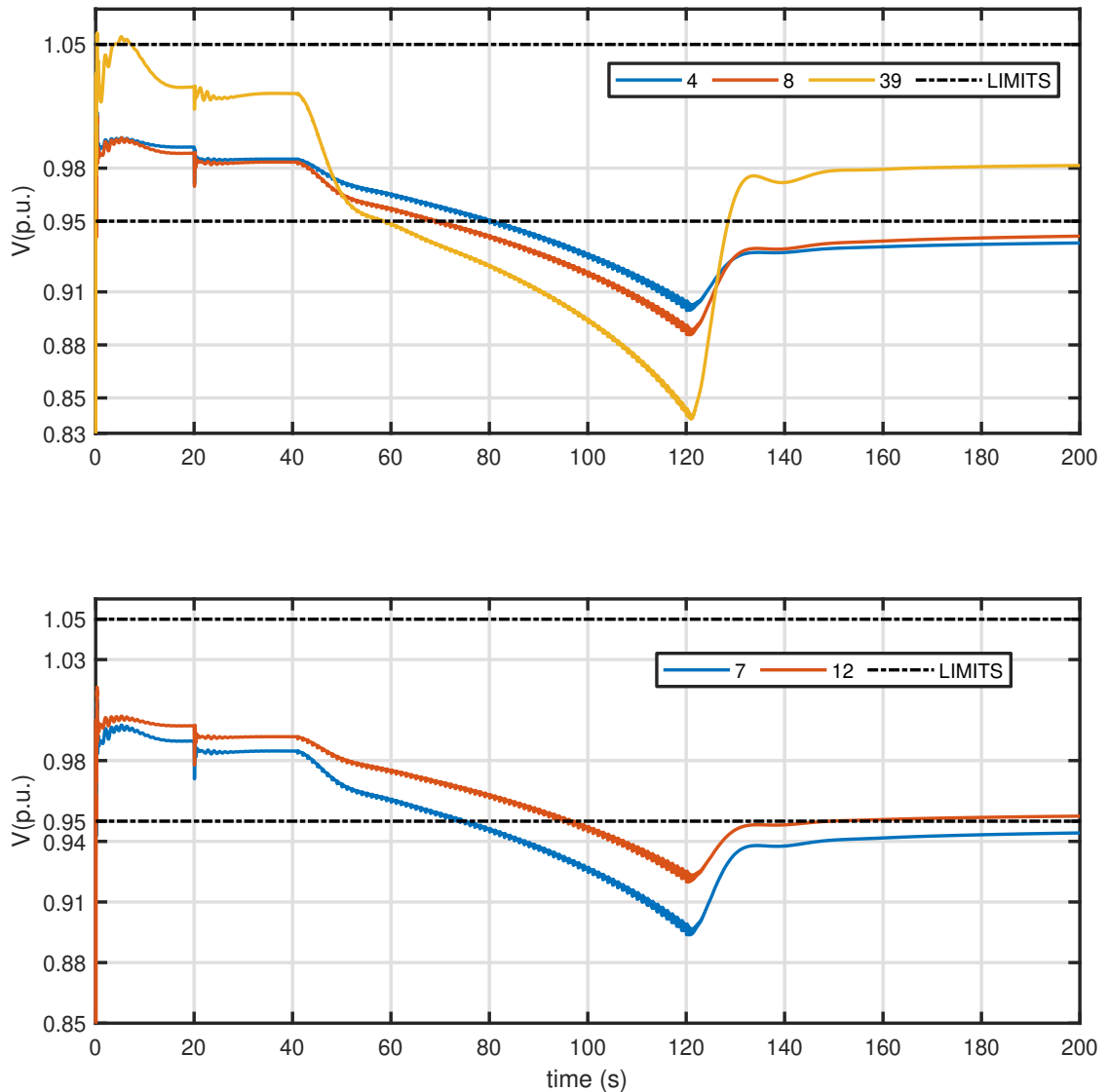
FIGURE 6.25: Case Study B: West Zones 1 and 2 load voltages with primary controls only

Too frequent control changes to AVR set-points may however be impractical as it constitutes a nuisance to operators. However, AVR reference modulations intervals of 10s are used in practical systems, such as the Italian grid [72].

The SBPVC performance can be improved by reducing the sampling time to 10s, and using a control and prediction horizons of 50s and 100s respectively. Even with a reduced internal model order $n = 10$, Figure 6.33 shows that voltage restoration of the most recalcitrant load bus 21 is faster than in the previous case. Consequently, all voltages are driven to the acceptable time in less than 200s of simulation time. The SBPVC with sampling time of 10s was able to apply control inputs to the changes in system's condition faster compared to the sampling time of 30s. On account, voltage regulation was faster and better than in the previous case.

The control inputs estimated by the with the internal model $n = 10$ are also shown in Figure 6.34. Faster sampling times enables the feedback and control application process to be faster. Consequently, the controller is able to detect that the modulations of AVR reference 6 may not have the
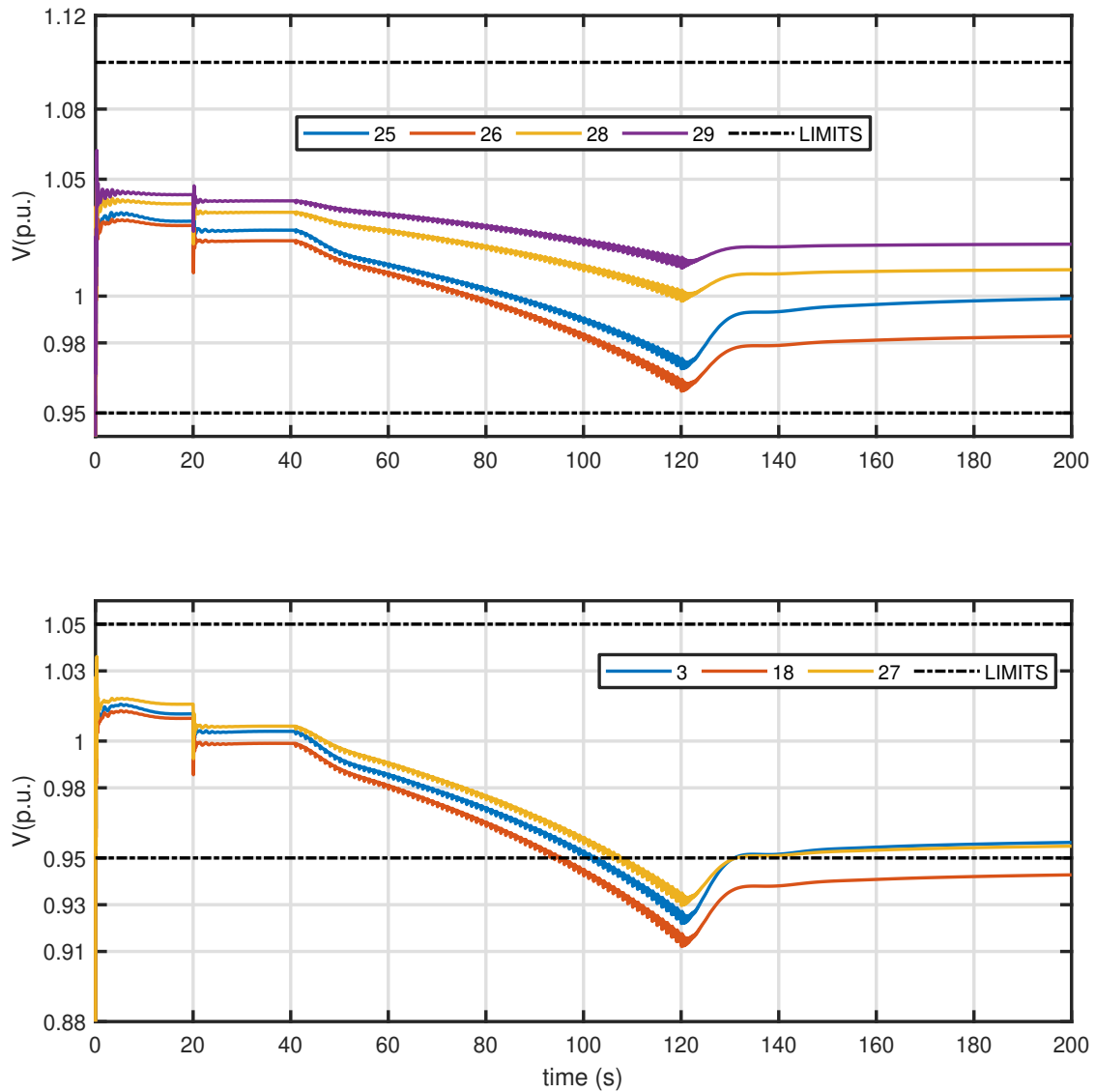
FIGURE 6.26: Case Study B: North Zones 1 and 2 load voltages with primary controls
only

desired effects on the voltage regulation and therefore this reference was not modulated until other
controls had been used. Although a reduction in the controller's sampling time may improve the
SBPVC performance, smaller control intervals would be impractical. In both cases of Figures 6.32
and 6.34, the linear SBPVC was able to successfully implement voltage regulation. However, this
was done by maximising the set-points of most of the control plants. However, any further events
could drive the system into undesirable operating regions without the control resources needed
to forestall this happen-stance. The lack of available required to prevent emergency situation can
happen in practice if other control avenues, such as capacitor bank switching, have been exhausted.
A well-designed system prevents this by expanding the range of control variables available to the
controller for a number of contingencies. A maximisation of available control resources would usu-
ally result in load shedding. A method of improving the performance of the SBPVC in emergency
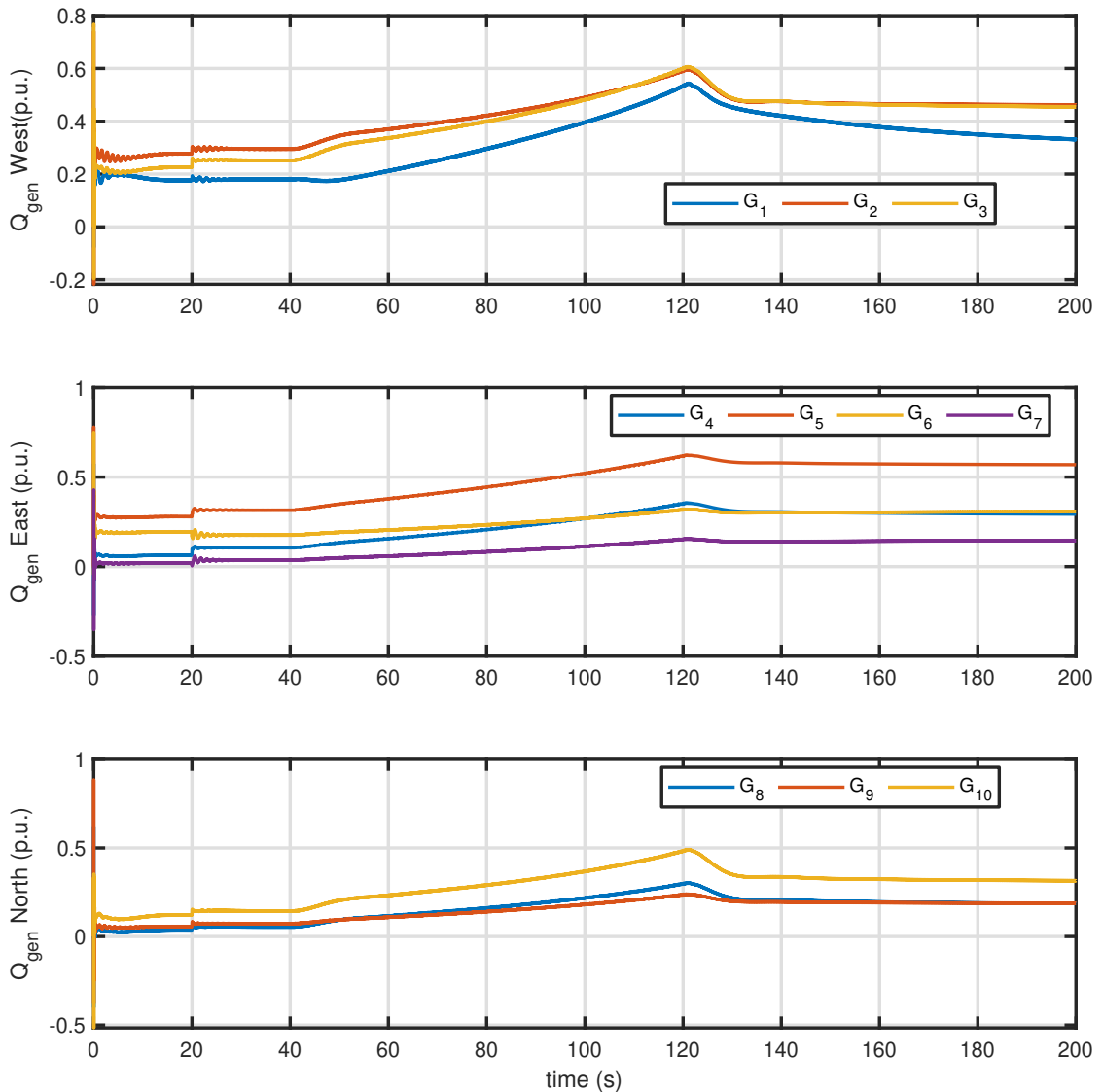
FIGURE 6.27: Reactive power outputs from generators with primary controls only

situations is described in the next section.

6.8 Improving SBPVC performance for emergency voltage situations

It can be seen that the use of AVR references for SVR is influenced by the practicalities of how often these controls may be applied, and the resulting degeneration of system conditions into undesirable states between control intervals. In addition, most of the generator AVR set-points are modulated to their maximum limits. In emergency situations, it becomes pertinent to review the sufficiency of the exclusive use of AVR set-point modulations for voltage regulation or stabilisation. In view of the foregoing, and in spite of the eventual success of the SBPVC in voltage regulation in both implementation cases, more control variables, which can be used more quickly and more frequently are needed. For normal situations, the use of capacitor banks is usually prioritised before generator AVR reference modulation or load curtailment. However, for the present analysis, only
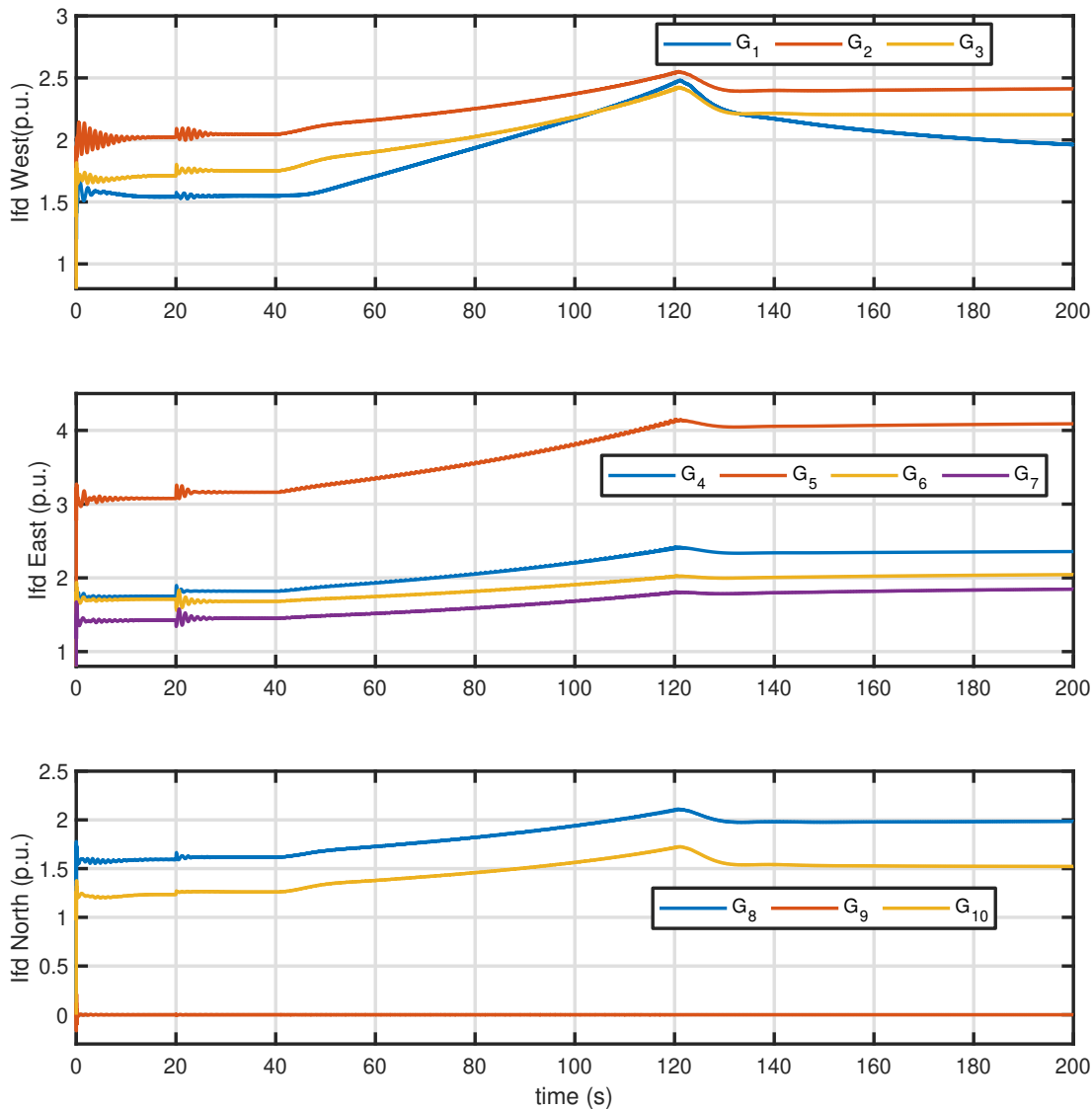
FIGURE 6.28: Field current with primary controls

the control variables which are present in the system as-is are assumed to be available for use. This section discusses how the SBPVC performance may be improved for emergency voltage situation by using AVR reference modulations and load shedding.

6.8.1 Voltage Stability Indicators (VSI)

It is widely recognised, especially following from the experience of the August 14 2003 blackout and reports on the event [63], that without continuous monitoring, a power system is a disaster-in-waiting. To prevent or mitigate voltage collapse situations, it is reasonable to devise strategies which can be used to assess the proximity of the system to undesirable working conditions. The singularity of the load flow Jacobian, [176]–[178] has been used as an indicator of the distance of a power system under consideration to voltage instability. However, this is based on a critical assumption of generators with negligible internal reactances and infinite capabilities of these generators to maintain constant terminal voltages[179]. The assumption has been widely neglected
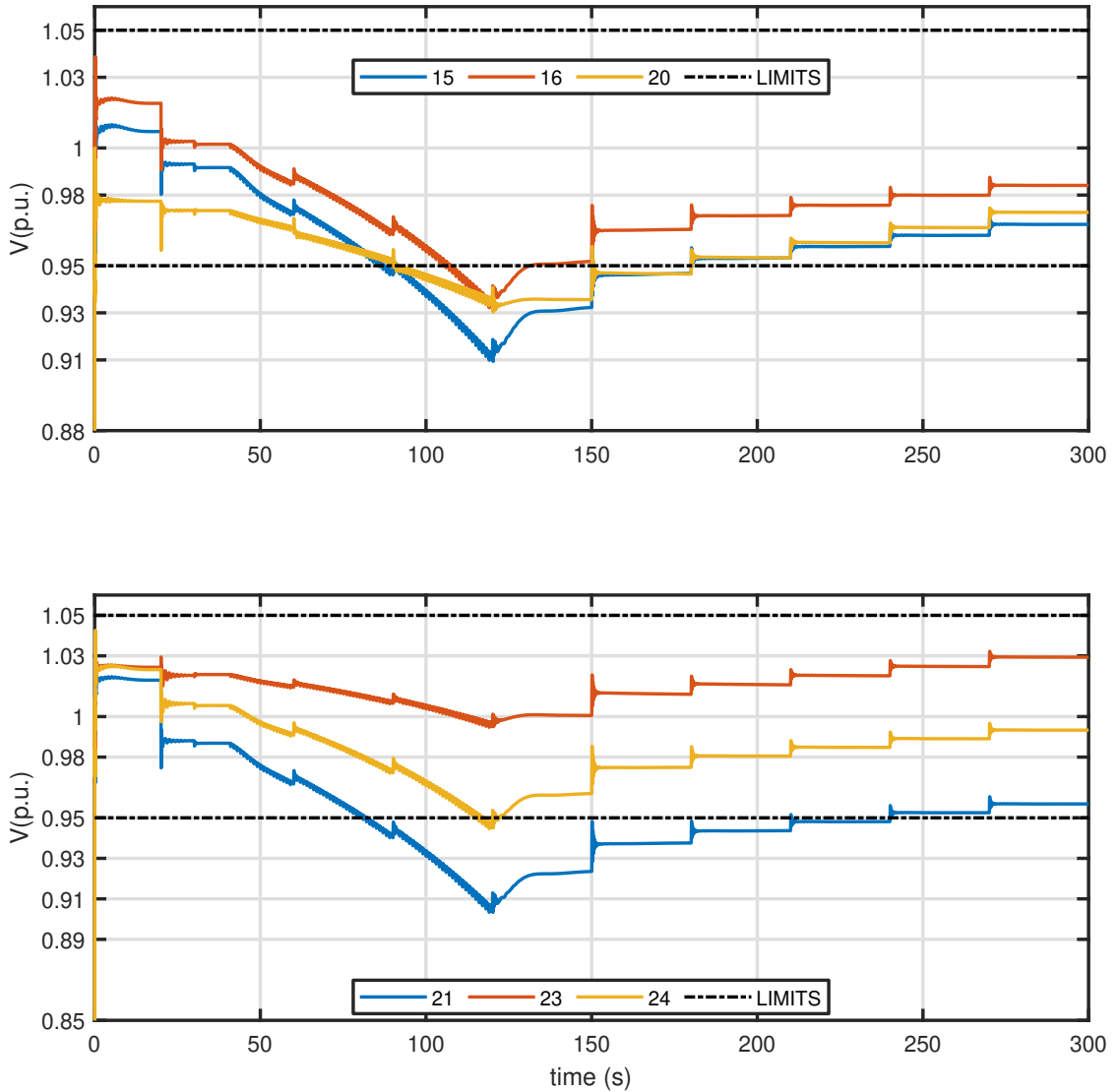
FIGURE 6.29: East Zones 1 and 2 load voltages with SBPVC of model order $n = 15$, $N_p = 10, N_c = 5$

in VSI literature and consequently, generator dynamics have been neglected in a number of VSI studies. On account of increasing WAMS proliferation, a number of PMU-based voltage monitoring schemes [54]–[57], [180]–[185] have been developed. With the the availability of real-time data, online WAMS-based schemes have the advantage of accounting for dynamic behaviours of some components and the changes in system behaviours with time.

Some VSIs are used to detect sudden or abrupt changes in system conditions by using WAMS measurements of fundamental power system quantities such voltage and current phasors and their derivatives to trigger a set of control actions. For appreciable faults or non-ambient changes in load conditions, the change in these indices are significant. Such VSIs are often designed using differences, at successive time instances, in system conditions or derivatives of system parameters such as rates of changes of frequency(ROCOF) and voltage angles (ROCOA). They are classified as *triggers* here because the large change in the index can be likened to an impulse signal of magnitude $|M_{tr}|$. If $|M_{tr}|$ over a pre-defined threshold β persists over a sufficiently long duration Δt_{tr}, then
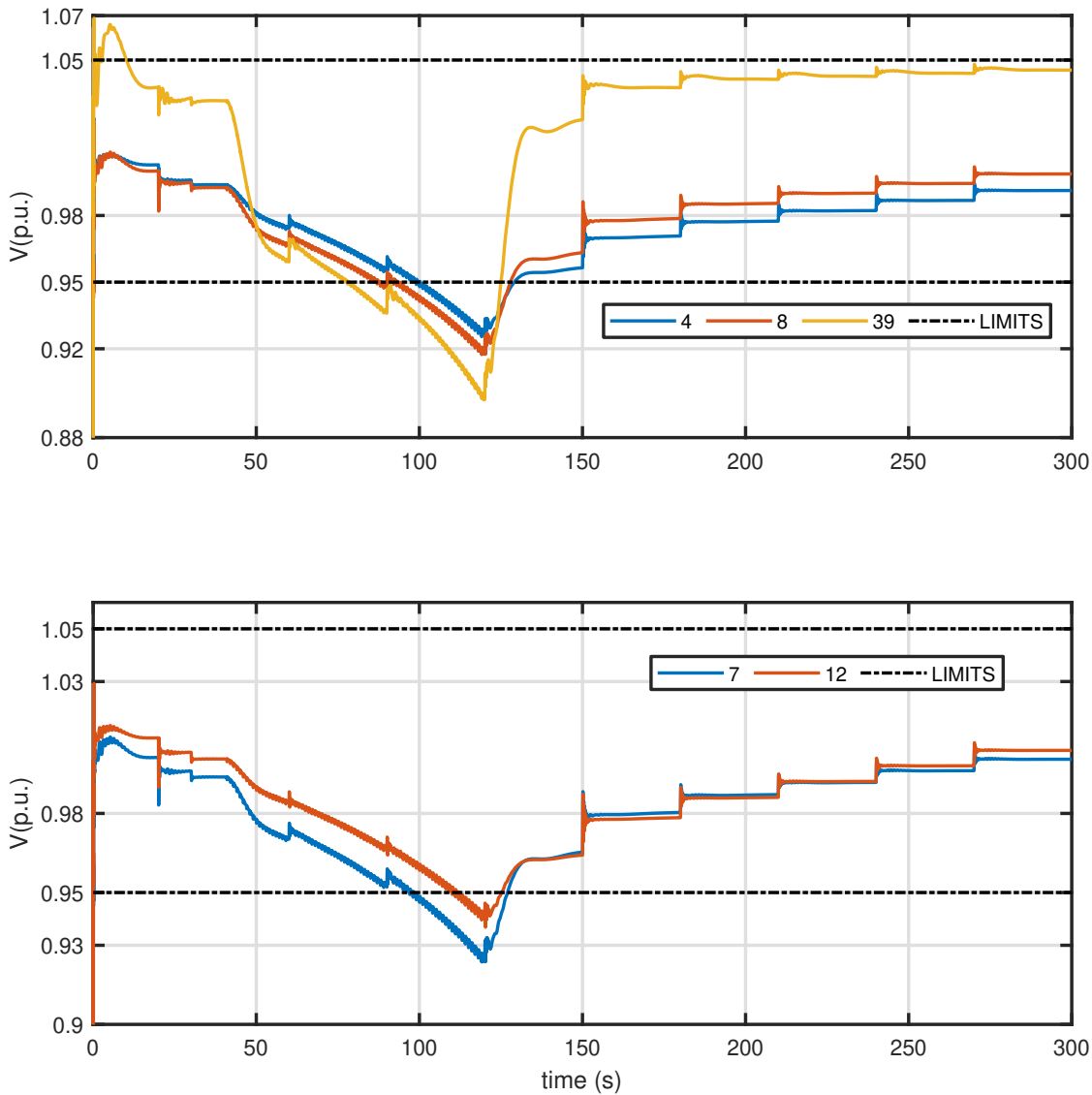
FIGURE 6.30: West Zones 1 and 2 load voltages with SBPVC of model order $n = 15$, $N_p = 10, N_c = 5$

corrective actions must be taken to mitigate voltage conditions. The magnitude of trigger-VSIs are usually maximum at fault locations and in the regions where changes in grid loads are maximum. This serves to emphasise the regions or buses where the bulk of control efforts may be directed. It is especially important to monitor, identify, and correct all possible local sources of voltage instability early enough, in order to prevent cascading disasters.

Monitor VSIs are those whose non-zero indices are a continuous measure of the relative conditions of the system compared to a nominal. For instance, a $+0.1$ frequency deviations in an area frequency relative to a nominal would indicate that the area of the electric power system which was previously supplying power to other regions in the grid has lost synchronisation leading to an islanding, while a -0.1 deviation is an indication of that the area was formerly importing power from another part of the grid. For instance, the loading in Case Study B resulted in a progressively decreasing frequency, as shown in Figure 6.35.
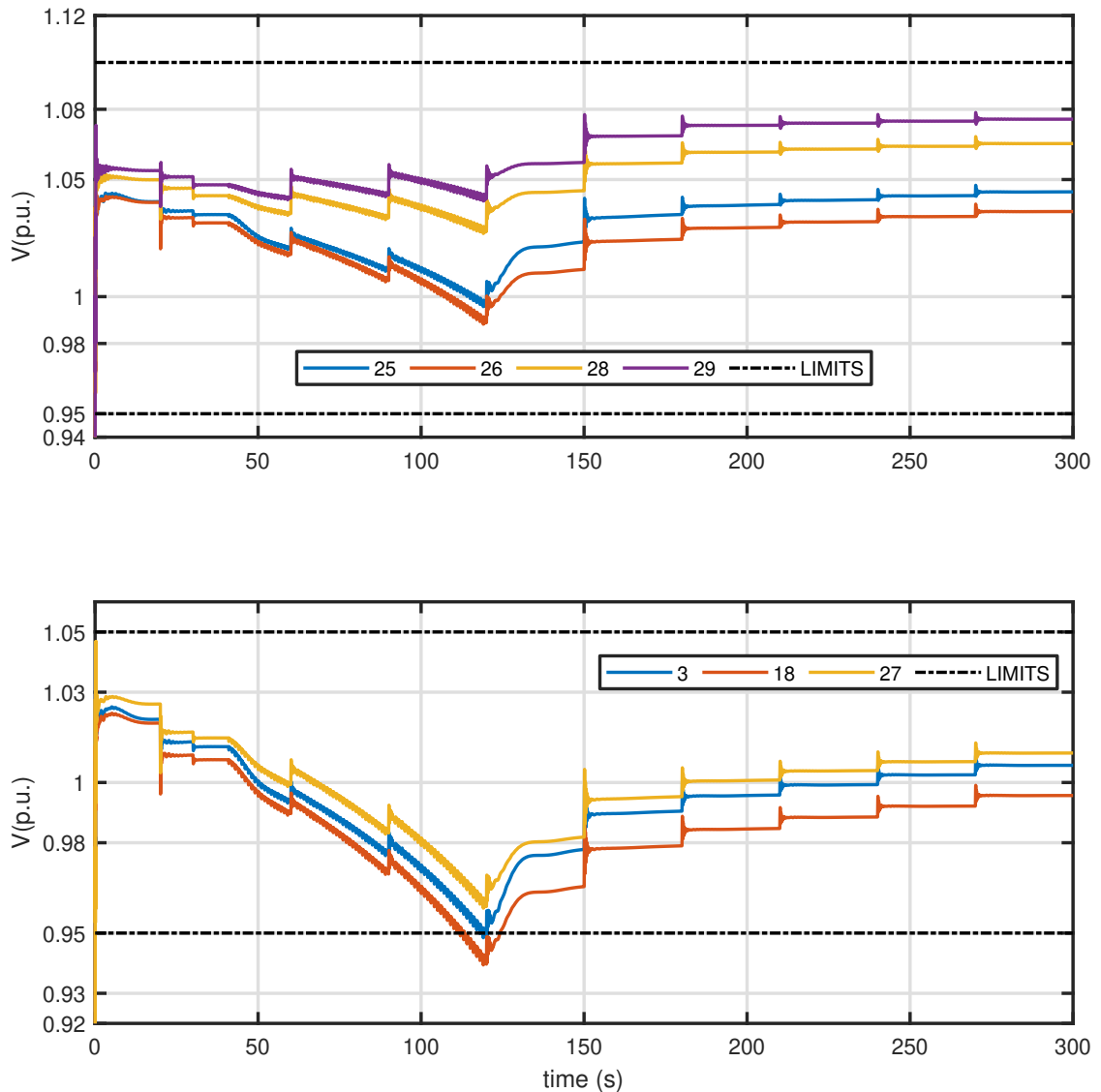
FIGURE 6.31: North Zones 1 and 2 load voltages with SBPVC of model order $n = 15$,
$N_p = 10, N_c = 5$

Rate of Change of Frequency

A region of the electric power grid under stress will sometimes witness a frequency deviation from the nominal whose sign would depend on whether the area was supplying or importing power before the fault. Such frequency changes are usually indicative of machine angle separation and the rate of change of the frequency (ROCOF) is a good indicator of how fast system conditions might be changing pre-fault.

To illustrate, consider how the derivation of the ROCOF proceeds from the measured phase angle, of (2.40), (2.41) and (2.41). Note that the phase angle provides an indication of system stress, as described in 2. This follows that being a second derivative, the ROCOF is an indication of how fast the system stress rate is changing. Sudden system events, such as islanding and loss of generators, that require prompt protection tripping or load shedding actions may be detected faster with ROCOF with a measure of operating frequency deviation from the nominal. However,
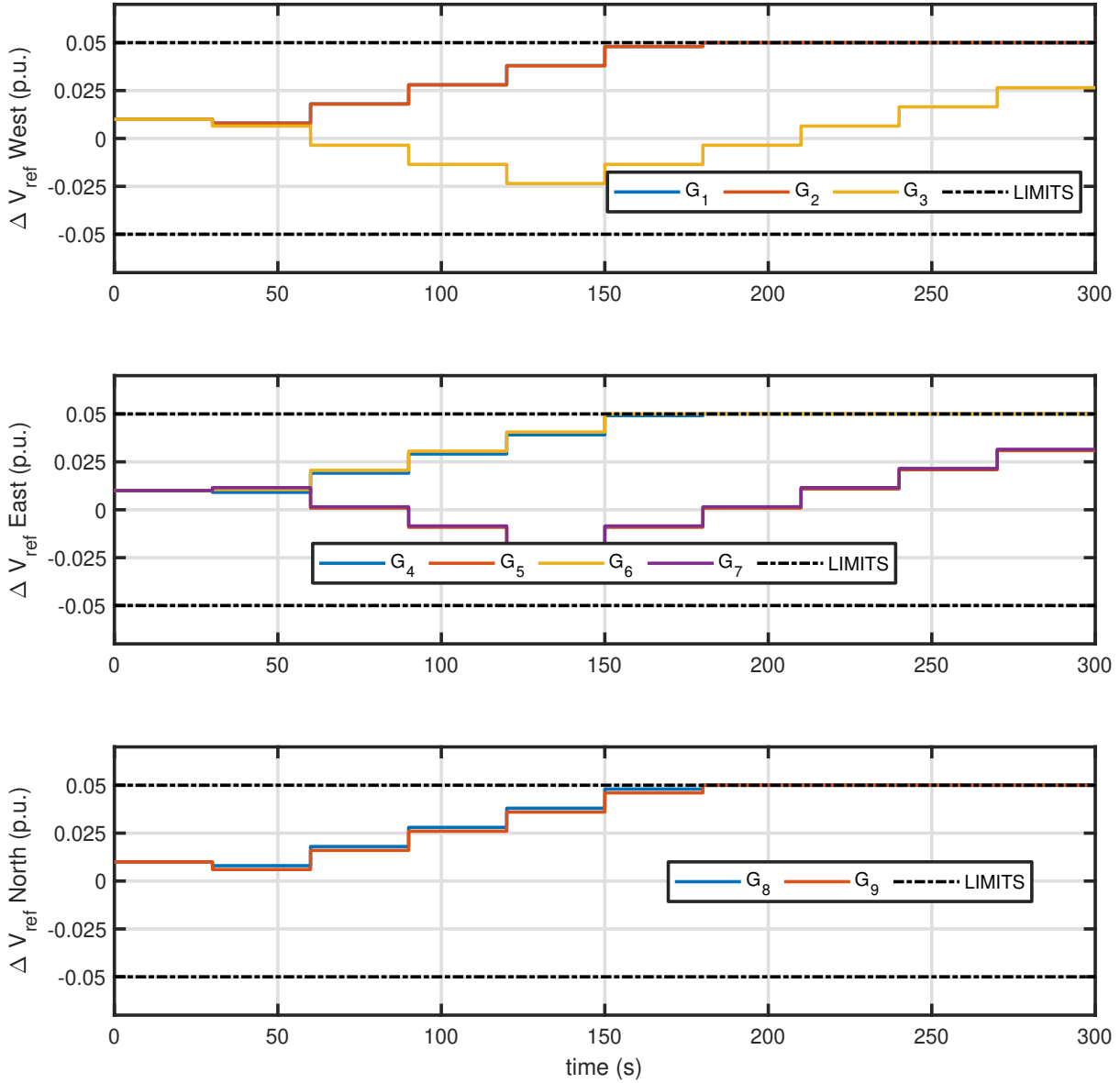
FIGURE 6.32: Case Study B: SBPVC control inputs with SBPVC of model order $n = 15, N_p = 10, N_c = 5$

for slowly-deteriorating system conditions, especially for long-term SVR, loading margins, reactor power reserve of generators, and frequency deviations are much better indicators of system conditions than ROCOF. In addition, it can be used to estimate changes in the real power of the system [74].

The mathematical expression for estimating the ROCOF has been stated in Section 2.5.6. For the simulation, the discrete-time ROCOF can be estimated from the measured frequency over a fixed time step $t_R = \frac{1}{f_R}$ using the different finite difference equation (6.37).

$$\text{ROCOF} = K\frac{f[k] - f[k-1]}{t_R} \tag{6.37}$$

where $f[k], f[k-1]$ are the frequencies at time step k and $k-1$, K is the gain and f_R is the PMU reporting rate.
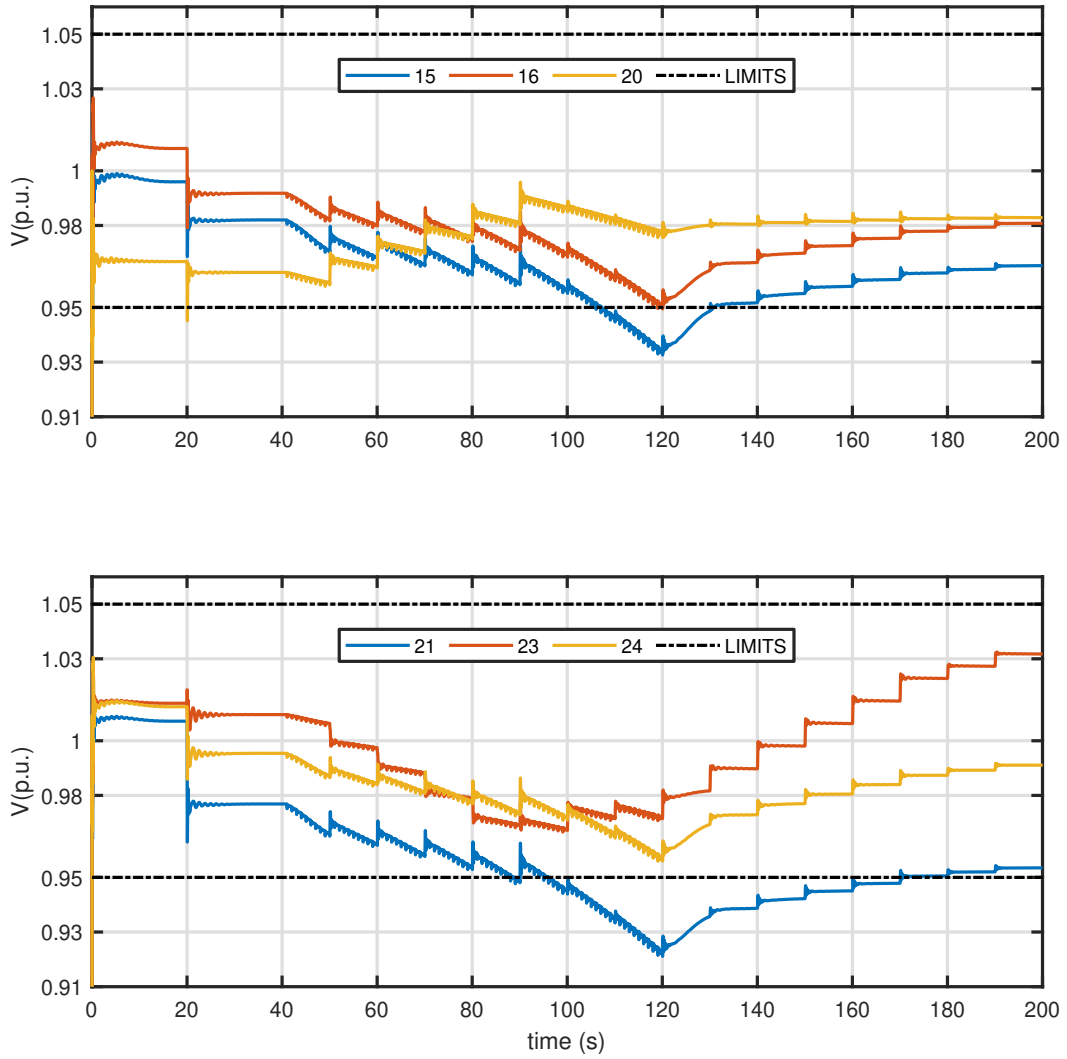
FIGURE 6.33: East Zones 1 and 2 load voltages with SBPVC of model order $n = 10$,
$N_p = 10, N_c = 5$

Reactive Power Reserves of Generators and Voltage Compensation Devices(VCDs)

Apart from desiring the knowledge of the margin to voltage instability or collapse, operators are also interested in the quantity of the reactive power left for voltage support in the network. It is assumed that Q-capacity (Q_{max}^i) of each generator and VCDs are known and define the Q-reserve at each generator simply as,

$$Q_{res}(t) = Q_{max}^i - \int_0^t Q^i(t)dt$$

6.8.2   Load shedding logic

Load shedding is a last-resort emergency control measure which is proven to be effective in the alleviation of undesirable voltage conditions. Traditionally, load may be shed manually in the face of an impending catastrophe. However, experience with the southern part of Hellenic system in the blackout of July 2004 showed that automatic load shedding based on a set of rules or advanced
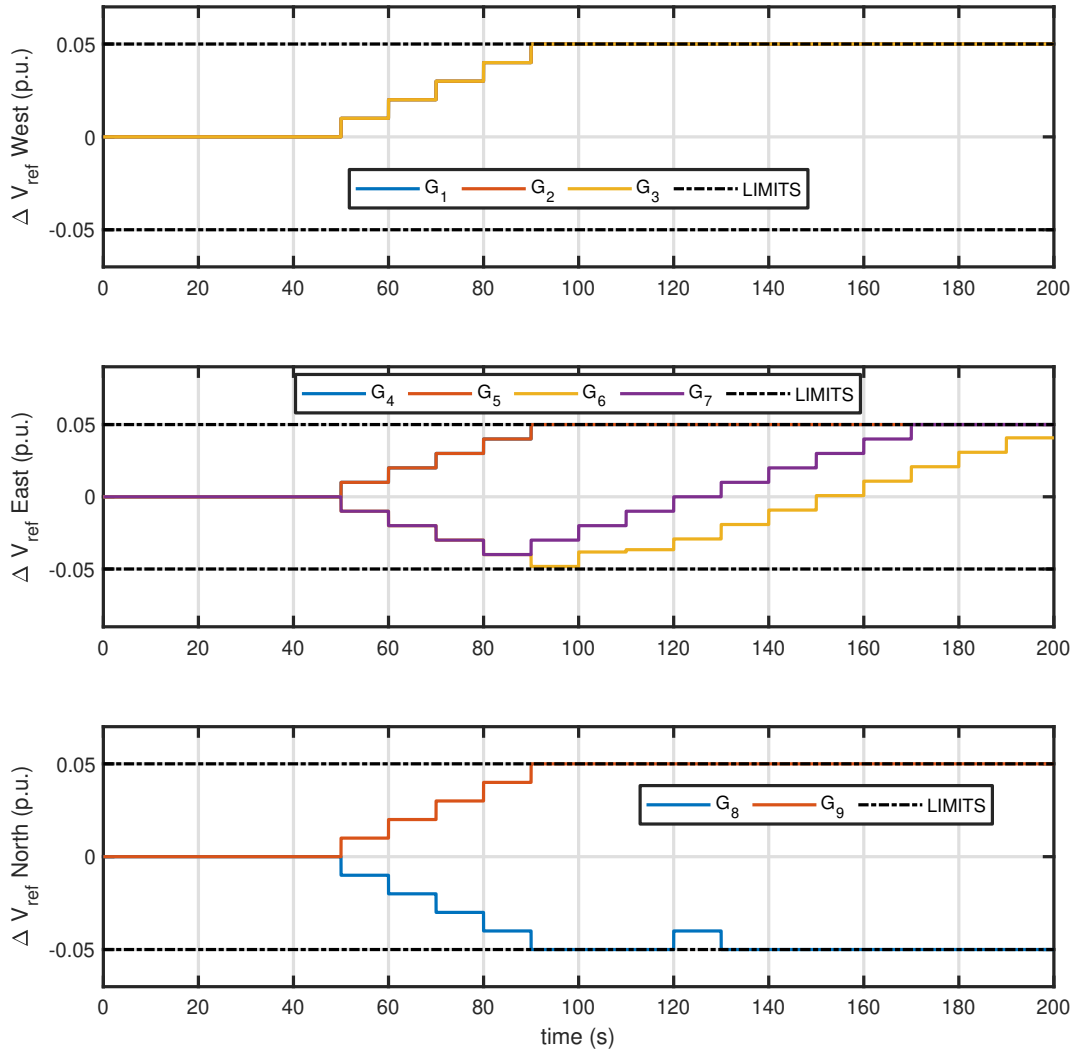
FIGURE 6.34: Case Study B: SBPVC control inputs with SBPVC of model order $n = 10, N_p = 10, N_c = 5$

model-based control is more effective [64]. The identification of an emergency situation may provide improved insight into the amount, location, and time in which load shedding may be applied. If the action is not timely, more load may be shed than is necessary in the situation [186]. A correct automatic load shedding scheme is timely, location-specific, and amount-specific.

Load may be shed based on the range of deviations of frequency and voltage to the respective nominal values, using a set of rules, as found in under-voltage or under-frequency load shedding schemes. Alternatively, an automatic load-shedding control algorithm such as [21], [23]. An under-voltage load shedding scheme is predicated on the increased reactive demand at a load bus, with an insufficient supply of reactive power from generators or reactive power compensation devices such as SVCs or capacitor banks. In the Hydro-Québec system [187] for example, a typical under-voltage rule-based load shedding would be:

1. Shed 400 MW of load after 11s at $V < 0.94$,.

2. After 9s time delay and at at $V < 0.92$,, shed another 400MW of load,
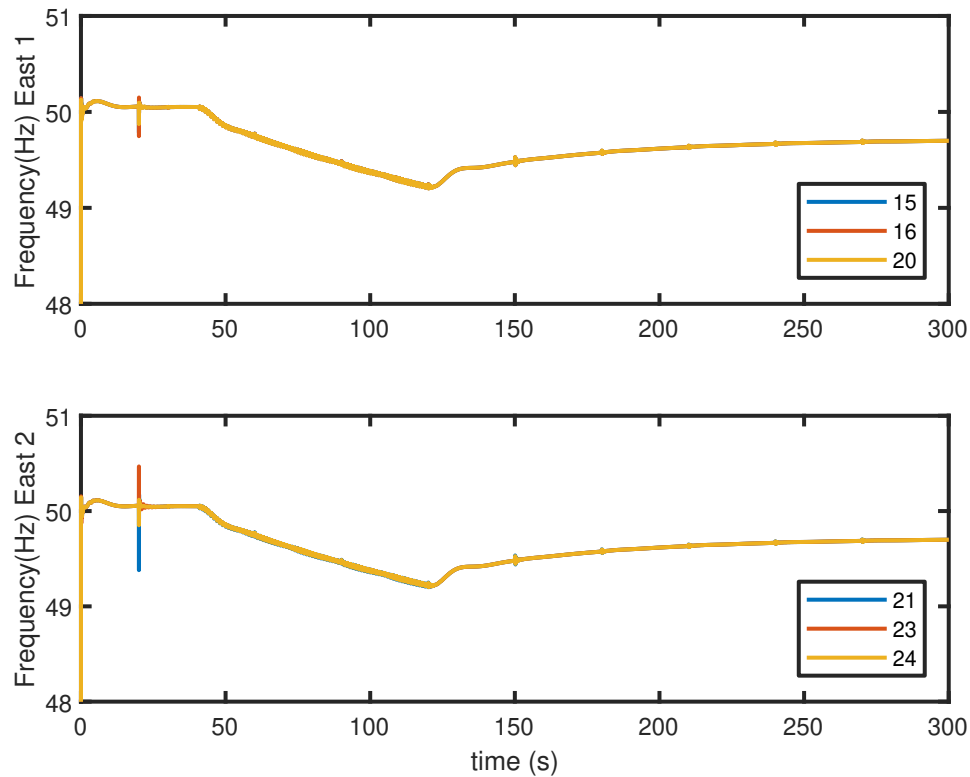
FIGURE 6.35: Case Study B: Frequency deviation in the East zone

3. After 6s delay, and shed 700M of load at $V < 0.90$

   Under-frequency load shedding follows from the observation of deteriorating frequency conditions when the generated power supplied to an area is less than the load demand in the area, which may be relieved by balancing load with the available generation in the absence of spinning reserves. The actual locations and amounts of loads to be shed based on under-frequency values has been described in [74] and [75], for instance based on an analytical derivation of load power sensitivities to frequency. In a similar manner to under-voltage load shedding, curtailment may also based on the extent of frequency deviations from the nominal using a set of rules as in Table 6.2.

TABLE 6.2: Undefrequency load shedding based on a pre-determined amount of loads

Frequency (Hz)	48	48.1	48.2	48.4	48.6	48.8	49
Load Shed (% of original)	50	45	35	25	15	5	0

   Since voltage and frequency measurements can be obtained from PMUs, stability measurements can be compared to the nominal values and the extent of deviation can be directly estimated in a simple manner. However, while frequency control is closely aligned with voltage control in the maintenance of normal power systems operation, voltages beyond regulated bands beyond reasonable lengths of time are consequences of reactive powers having reached their limits. Usually, a sequence of controls are activated by Transmission System Operators (TSO). These include

capacitor switching, OLTC actions, and generator reference modulation, typically in that order. If the generator Q-reserves or capacitor Q-capacities are exhausted, Load shedding is a drastic and disruptive emergency control measure that may be used to prevent voltage collapse, and may not be used unless it is absolutely necessary to do so. The logic in Figure 6.36 may be used to activate a load-shedding scheme.

A subspace-based load shedding scheme

Rule-based load shedding shed a pre-determined amount of loads at certain voltage values. These rules would usually vary from one system to another, and are normally derived from experience. As an alternative to rule-based load curtailment, a subspace-based control scheme based on the synthesis of models from known load perturbations, following the steps outlined in Section 6.5.2. The inputs would be small step changes (ideally of a constant power factor) in curtail-able loads, and the response would be the voltage outputs at buses of interest, as measured from the PMU. The load-shedding model can then be synthesised using the flow chart of Figure 6.4. A load-shedding SBPVC using this synthesised model can be designed with a much smaller sampling time than those used in AVR reference modulations in the preceding case studies. A good value for the sampling time for load shedding SBPVCs would be 3-5s in order to allow quick but sufficiently spaced-out control actions and avoid unnecessary curtailments.

Load shedding may be activated using the logic of Figure 6.36. System conditions are identified using PMU-measurable quantities and/or their derivatives. Slowly-deteriorating conditions are frequency and voltage deviations resulting from slow changes in loads or OLTC dynamics as well as the depletion of generators' and VCD reactive power outputs. Fast changes would result in sudden changes to frequency deviations, or the rise of ROCOF above a set maximum value. In order to prevent spurious activations of load-shedding signals, undesirable system conditions may be allowed to persist over a certain time duration. If a condition is true after a maximum allowable time period, load shedding signal is activated and further load increases are prevented if possible.

In contrast to rule-based load shedding approaches where the amount of load to be shed is pre-determined, load curtailing SBPVC determines the amount automatically and issues curtailment signals only if the logic in Figure 6.36 is high. The complete load shedding SBPC set-up has two SBPC controllers with different sampling times. The one SBPVC used AVR set-point modulation and is used for normal operating conditions, with high sampling time T_c^1. The other is designed for emergency system conditions and is only activated if load shedding signals are received from the logic in Figure 6.36. A graphical illustration is presented in Figure 6.37.

Blocking load signals during load shedding

In practice, it may be necessary that no additional load be added while load shedding is in progress, or if an alarm is triggered on account of frequency falling below the nominal value for a given period of time. This prevents further aggravation of frequency conditions, and allows for load shedding control signals to be effective. This rule is implemented by blocking any further loading at the load buses, and then proceeding to prioritise the use of load shedding, rather than reference modulation, in the control algorithm. In practice, blocking load increase may be possible only if there is an previous agreement with the point of demand. If this is not possible, more curtail-able loads must be shed in order to achieve desired voltage regulations. This is also synonymous to blocking load restoration in the previously-shed load to prevent long-term voltage instability [8].
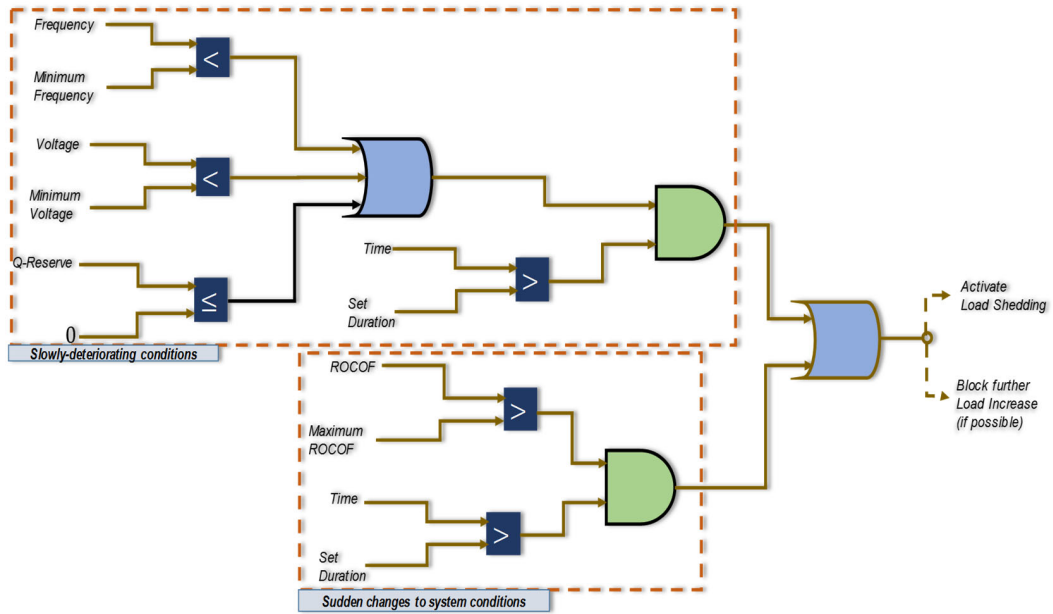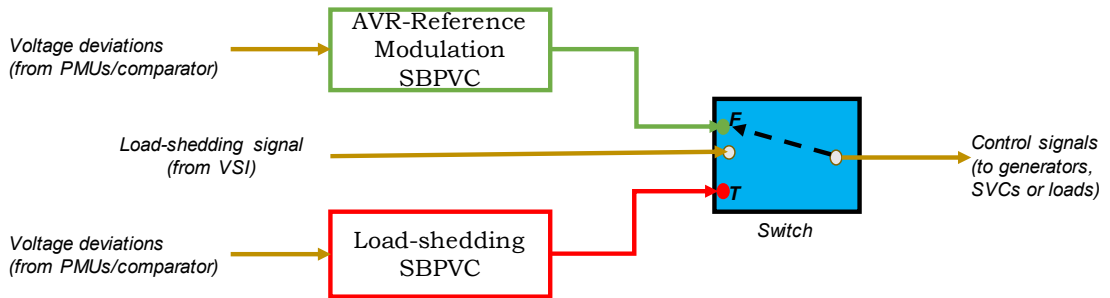
FIGURE 6.36: Load shedding logic based on VSI

FIGURE 6.37: A robust SBPVC scheme

6.9 Discussion

The controller is able to drive load voltages to within acceptable in spite of the changes in system topology. This was achieved through a system of feedback and continuous improvements in the control inputs estimated by the controller over given prediction and control horizons. Furthermore, in spite of the linearity of the internal models, effective automatic control was achieved through AVR reference coordination.

This study has presumed that only AVR reference modulation is available for the SVR, since the focus has been to show the effectiveness of a model-free control design. Therefore, the scenarios used in the case studies have been rather conservative, focusing on the control of non-viable voltage profiles. However, for more drastic voltage situations in the electric grid, better controllability can be achieved using a wider range of reactive power sources. A small-signal model can be synthesised for these controls using the procedures outlined in Section 6.5.2. Using capacitor banks for example, it is possible to specify smaller sampling intervals $T_s = 5s$ in the design of the

controller, and to persist with the sampling time used in the implementations of the case studies of Section 6.7. In essence, two SBPVC controllers of different sampling times for voltage control as it were; the one using estimating capacitor reactive power input for every 5s, and the other, more conservative in the dispatch of AVR references, at 30s intervals.

The test networks used as case studies in Section 6.7 have load buses whose voltages are at 230kV and above. Although the actions of OLTCs should be simulated in such cases, it may be sufficient to presume that tap operations have been locked in order to prevent the dynamics of downstream distribution networks from affecting the transmission system. This is a common practice for TSOs in continental Europe when available controls are limited.

In order to be suitable for practical application, it is necessary to consider some implementation issues which may affect the SBPVC performance. These are discussed in the following sections.

6.9.1 Impact of measurement noise on the SBPVC's performance

The SBPVC schemes described in the previous section depend on a measurement of voltage states or outputs as feedback in order to calculate, over prediction and control horizons, the amount of control inputs to apply in the next step. Fo the desktop-based simulation, the inherent assumption is that the measured signals are noise-free and accurate, and are summarily without any issues which may affect the performance of the controller. However, in practice, measured signals may be highly corrupted with noise. In addition, issues with measurement devices may affect signal accuracy or result in a failure to fetch data in the next measurement cycle. If these happen, large controller gains —which may improve the controller's speed of response —may amplify the noise measurements and this may be fed into the controlled system, leading to spurious variations in the control signals and controlled voltage states. Consequently, the system may become unstable. In the same vein, missing data and measurement errors may lead to inaccurate control estimation and hence an inefficient control process.

Measurement noise, bad or missing data and other issues with measured data are usually handled, in practice, through state estimation methods [37] —introduced in Section 1.1.1 and described succinctly in Section 2.5.8. This includes preprocessing, detection, filtering, and error minimisation, which are mentioned as an important part of the modelling process and included in the flow chart of Figure 6.4. For the present purpose, the setup of Figure 6.3 of Section 6.5.2, which incorporates the state estimation process, may be used for a more practical implementation of the SBPVC.

6.9.2 Communication delays

The control inputs estimated by the SBPVC were assumed to be applied at the right time without any delay. The performance of the controller deteriorates considerably if measured and/or control signals are not applied or transmitted in a timely manner. In practice, communication medium, through which control signals are sent and over which feedback measurements are received by the controller introduce some amount of delay into the system. To deal with this problem, delay compensators may be added to the forward and/or feedback paths. Alternatively, mathematical and statistical modelling methods for delay estimation (such as described in [188]) may be incorporated into the systems identification process to account for a finite amount of delay in the communication medium. A standard P-class PMU would be the recommended and practical choice for the control.

6.9.3   Handling changes in operating conditions

Changes in operating condition for a linear controller may put the robustness of the controller to test. The robustness of a controller may be roughly defined as its ability to handle changes to operating conditions, for which it has been designed, without a considerable change in its performance. The robustness of the feedback SBPVC system would depend on the accuracy of its measured state, the timeliness of state measurements, the timeliness of control signal application, and the availability of controls. On the last count, the sufficiency of available control is particularly critical in the SBPVC performance should the operating region vary widely from the nominal operating point. For example, it has been shown that the controller was effective in the regulation of non-viable but stable voltage operation, simply by modulating its AVR set-points. However, for large disturbances such as the loss of a generator or a critical line, changing AVR set-points only will not be sufficient. For this, the two-level SBPVC of Section 6.8.2 may be more robust.

Alternatively, a time-varying SBPVC may provide more robustness with rapidly or widely changing operating conditions. For this, the systems identification process is carried out online and the model described the power system is continually updated based on more recent measurements. It is important to note, however, that this requires considerable computational resources so that the timeliness of control estimation is not compromised.

6.9.4   Selection of measurement units for control

In order to deploy PMUs, care must be taken that they conform to the desired level of performance required, in terms of response times, latency, frequency, ROCOF and phasor measurement fidelity. Appropriate levels of filtering required must be verified before the unit is chosen. The dynamic performance of a PMU is important in its selection for control purposes. Some of the tests were discussed in Section 2.5.7 under the C37.118.1-2011 standard. Laboratory and practical tests to evaluate degree of compliance of PMUs with standards can be found in literature [189], [190]. In contrast to the IEEE C37.118-2005 standard, stringent requirements for ROCOF estimation were specified in the IEEE C37.118.1-2011. Based on the faster response requirements as well as other more stringent requirement in the C37.118.1-2011 standard, P-class PMUs would be more suitable for control systems than would M-class.

6.9.5   Impact of using the rate of change of frequency as an indicator

The use of the ROCOF as an indicator of impending undesirable system situation was described for the two-level SPBVC scheme. It is easy to see from (2.42) that the ROCOF is a first derivative of frequency. In the discrete-time domain, this relationship may be expressed as a first-order finite difference equation over a fixed time step. The use of the ROCOF has some advantages over the use of frequency in a warning system, especially for emergency load shedding or islanding detection. One of these is that the ROCOF enables faster detection, even with time delay, of critical situations before they degenerate. This means that, in load shedding application for example, smaller amount of loads are shed.

However, it is important to note that there are a number of issues with using ROCOF. First, it cannot discriminate between frequency decrease or spurious fault in the system. In terms of

estimating ROCOF from a PMU, the reliability and accuracy of measurements may be compromised under transients. This is because the synchrophasor model does not behave perfectly with time-varying conditions of a signal.

The estimation of ROCOF as a second derivative of angle amplifies the noise or error already present in the angle and frequency measurements [102], [190]–[193]. This makes ROCOF very noisy even in the steady-state. To illustrate, consider the plots of Figure 6.38, obtained from a simulation of a line loss following a $\frac{1}{12}$th cycle fault on the tie line 3-13 of Figure 6.5. The increased stress in the system phase can be observed from the frequency plot. The frequency and ROCOF plots shown are those of the boundary bus of Area 1. The sudden surge in the frequency is reflected in the ROCOF measurements at a higher scale. The second subplot of Figure 6.39 shows an enlarged
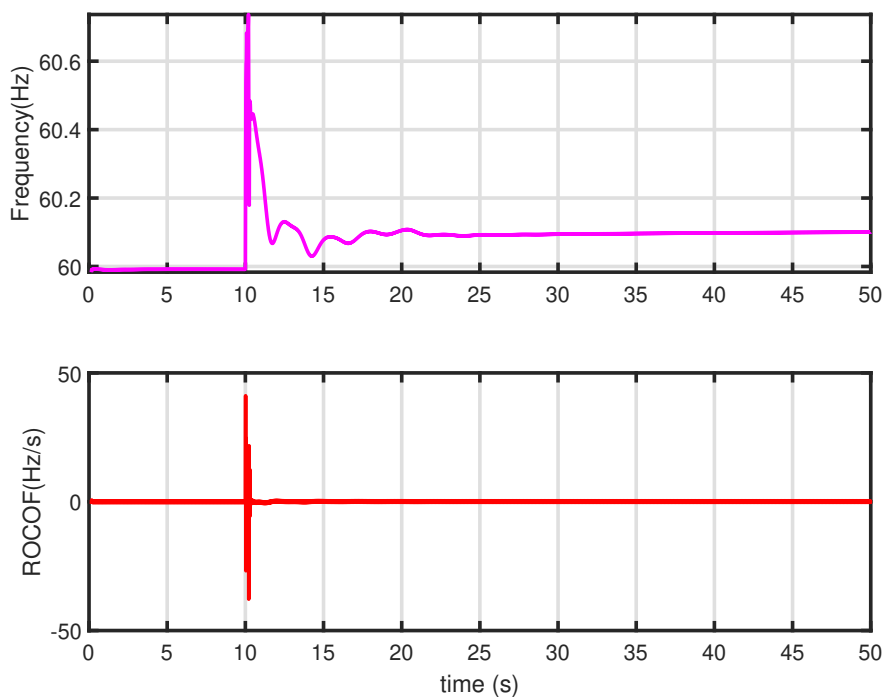

FIGURE 6.38: Frequency and ROCOF plots

plot of the ROCOF subplot of Figure 6.38. Noisy ROCOF measurements may be unsuitable for use in control applications, especially with high-gain controllers and/or communication media, like the PLC, which have low signal-to-noise ratio (SNR). System instability may proceed from this, as described in Section 6.9.1. In a similar vein, noisy ROCOF measurements will not give accurate values. Consequently, stability indicators using ROCOF may give false alarms which lead to wasteful control efforts.

However, the noise can be reduced by using highly-correlated phasor values computed at point-on-wave rate [102]. An alternative method is to fit a polynomial over a number of consecutively-measured point [192]. In [191], a low-pass filter was designed to meet the more stringent ROCOF requirements in the steady state according to the scheme in Figure 6.40. A set of logic are designed to identify transient conditions and to cease to apply low-pass filtering to the signal during the transient.
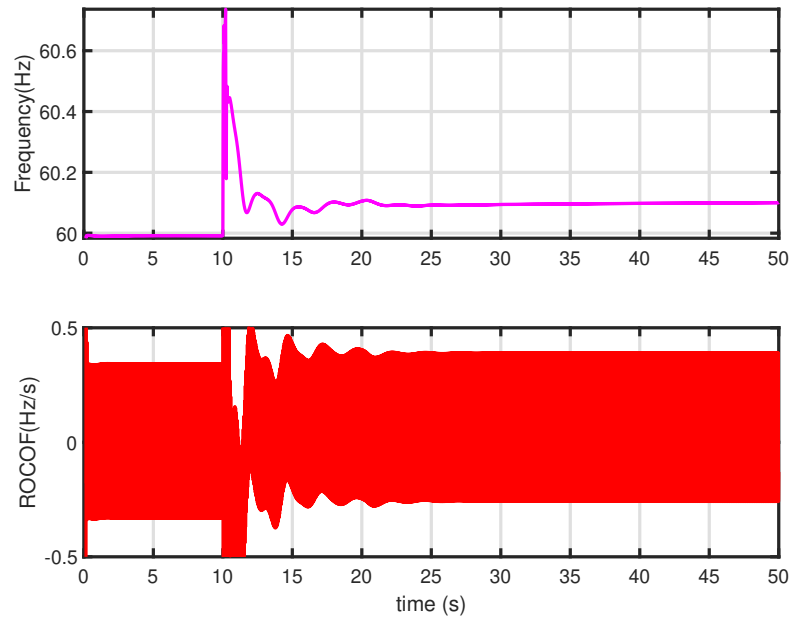
FIGURE 6.39: Frequency and ROCOF (enlarged) plots, showing the *noisy* nature of ROCOF measurements
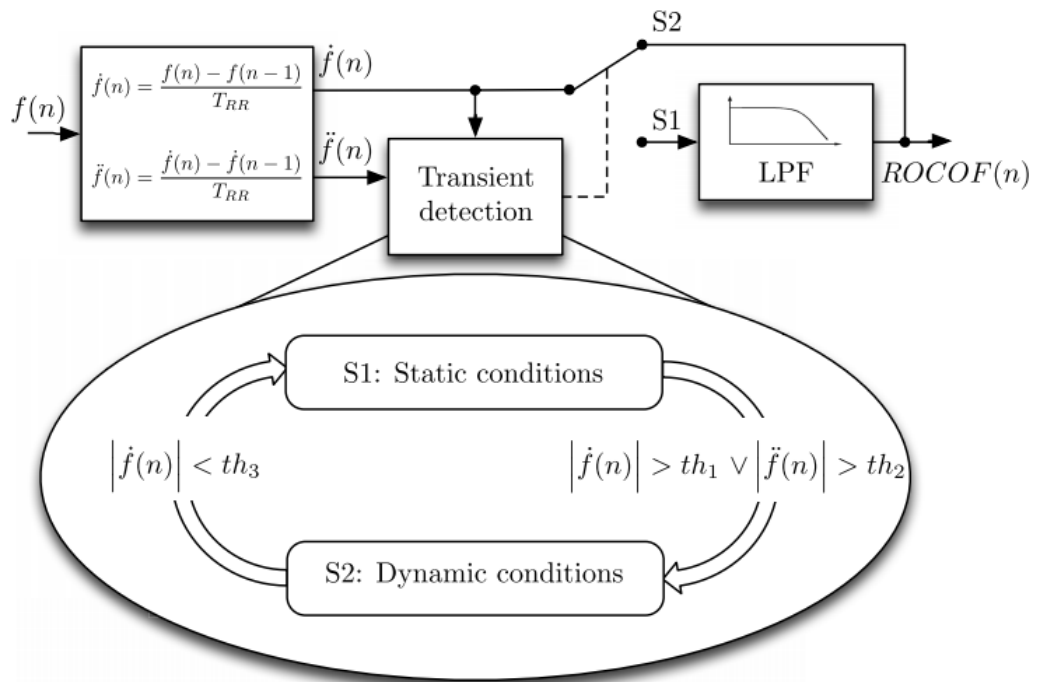

FIGURE 6.40: A ROCOF estimation scheme with a low-pass filter at steady state
[191]

6.10   Summary

A linear predictive controller has been designed using subspace algorithm on measurement data. The phasor measurements were obtained from simulated PMUs at 60 positive-sequence samples per second. The PMUs were assumed to have been selectively placed at load or pilot buses. The

chapter describes a method of synthesising models from measured response from simulated PMUs following from perturbations of known magnitude. The synthesised models form the basis of the proposed Subspace-based Predictive voltage controller. The measurement-based approach that has been used here does not depend on an explicit mathematical model of the system, compared to methods using static power-flow solutions and those attempting to linearise a complete model of the system. The SBPVC's performance was implemented on the OPAL-RT's real-time platform using various types of standard test networks which mimic the behaviour of wide-area power systems. Results showed that, subject to proper tuning of controller's design parameters, the performance of the proposed controller is satisfactory and effective in regulating non-viable voltages in undesirable voltage situations. A more robust scheme of the controller was also proposed. This considered a two-level controller, the one considering the use of mainly load-shedding in emergency situations, and the other mainly AVR set-point modulations. Both operate at different sampling time, with switching between the controllers achieved at different operating conditions by described voltage stability indicators.

The impact of the events which are likely to affect the performance of the SBPVC in practical applications are identified and discussed. These include the effect of communication lag inherent in the use of feedback controls, measurement noise, and changes in the operating conditions. Some of this effect, such as communication delays can be studied on a RT-HIL-ready platform —similar to the one used for the simulation in this chapter —by incorporating a PMU hardware in the control loop.

Chapter 7

Conclusion and Future Work

7.1 Thesis Summary

This thesis has described strategies for WAMS placements and WAMS-based secondary voltage control of the electric power network. In essence, the projects consists of two parts; the first describes viable methods for cost-effective placement of WAMS devices using extensive modelling of many practical and the second model-free control strategies using numerical derivatives, receding horizon and systems identifications concepts.

In Chapter 2, the general background to modelling, measurement and control have been presented in this chapter. The efforts required to completely model the power system in a linear form that would be suitable for power systems analysis was presented and shown to be impractical for a control algorithm which was intended for a real-time application. The use of WAMS was an alternative approach to comprehensive modelling, and model-free methods were more promising to real-time control. A background to the standards and processes involved in the use of measurements, such as state estimation, and various standards required for the measurement devices were also presented. In the next chapter, novel optimal measurement placement methods were introduced, in preparation for the use of measurement-based predictive control designs in the later chapters.

Chapter 3 describes a multi-objective, multi-vendor, multichannel placement algorithm was proposed for the deployments of WAMS in the electric power grid. The formulation considered practical costs identified from reports of the actual costs, as obtained from power utilities, of WAMS installations. In the reports [13], [49], labour and communication, not unit procurement, costs were identified as major factors contributing to the PMU installation costs. A topology defragmentation and channel-capacity minimisation approach to PMU co-placements with communication infrastructure has been described in this paper. Using the proposed method, the optimal PMU solutions include the bus, branch(es), PMU channel capacities, the optimal PDC location to connect to, and the vendors to buy from. These were more detailed than can be obtained from existing methods and the performance was demonstrated for a range of IEEE test networks. The setup enable the economically-desirable option of deploying multiple PMUs at a single bus.

In Chapter 4, a novel multi-stage placement algorithm has been described using a two-step multi-objective PMU ILP optimisation formulation. The first step involved the planning of the optimal PMU locations and the second was concerned with the implementation of the plan over a period of time depending on the financial capability of the utility. In addition to the description of the multi-stage budget-constrained algorithm, the chapter also included a discussion of the effect of inflation costs on planned installations, the effect of maintenance and repair costs on already-installed components, changes in network topology, and the prioritisation of the observability of some buses during the multi-stage placements. The algorithm returns an optimal solution which

compares favourably with existing work in literature. The performance was demonstrated on the IEEE 14-bus and the IEE 118-bus test networks across a number of scenarios using a simplified versions and subsequently, a complete model, considering, essentially, the presence of multiple vendors, multiple PMU capacities, and co-placement with PDCs.

A number of PMU placement algorithms was described in Chapter 5 for application-sensitive PMU placements by extending the OPP 3.16 of Chapter 3. For secondary voltage control application where the observability of certain *pilot* or boundary buses were critical, proposed solutions for full and selective observability was shown to be superior to other voltage control deployment algorithms, even with a simplified form of the algorithm. In addition, for SVR applications, it was shown that a better strategy for utilities would be to maximise the number of observed buses without the enforcement of direct PMU placement, as found in some practice, on pre-identified pilot buses. This would translate to increased observability of more buses, a better use of resources and does not compromise the observability of pilot buses.

To extend to applications such as oscillation detection, state estimation, voltage control, islanding detection, and voltage instability prediction which may be offered as add-on incentives by vendors, the multi-objective multi-vendor OPP 3.16 was reformulated to account for the range of add-on applications. The new formulation not only sought to minimise the cost of deployment, as done in the old, but also to maximise the range of applications by using an adjusted cost which accounted for the benefits offered by each additional application. A number of hypothetical scenarios was used to illustrate the validity of the proposed algorithms.

In Chapter 6, two methods of obtaining models from measurements were described. The first involved an estimation of sensitivities to inputs, and the second a subspace state-space identification using voltage response to known input perturbations. For the second approach, a linear predictive controller was designed using subspace algorithms on measurement data. The phasor measurements were obtained from the simulated PMUs at 60 positive-sequence samples per second. The PMUs were assumed to have been selectively placed at load or pilot buses. The chapter described a method of synthesising models from measured response from simulated PMUs following from perturbations of known magnitude. The synthesised models form the basis of the proposed Subspace-based Predictive Voltage controller (SBPVC). The measurement-based approach that was used here does not depend on an explicit mathematical model of the system, compared to methods using static power-flow solutions and those attempting to linearise a complete model of the system. The SBPVC's performance was tested on the OPAL-RT's real-time platform using various types of standard test networks which mimic the behaviour of wide-area power systems. Results showed that, subject to proper tuning of controller's design parameters, the performance of the proposed controller was satisfactory and effective in regulating non-viable voltages in undesirable voltage situations. A more robust scheme of the controller was also proposed. This considered a two-level controller, the one considering the use of mainly load-shedding in emergency situations, and the other mainly AVR set-point modulations. Both operate at different sampling times, with switching between the controllers achieved at different operating conditions by described voltage stability indicators.

7.2 Thesis Statement

The thesis stated at the beginning of the project that it is possible to design an automated and affordable predictive secondary voltage controller. In Chapters 3, 4, and 5, cost-effective and practical

PMU placements strategies were proposed. The various methods of achieving affordable WAMS deployment ranged from spreading the installation costs over multiple stages to selective placements for application-specific purposes.

Following from that, given the challenges of using exhaustive mathematical models, two methods were proposed for model realisation from phasor data. The first was the numerical sensitivity-based model which provided a simple and viable alternative to exhaustive model-based trajectory-sensitivity evaluation. The second was based on a systems identification technique of model synthesises from measured data. Both approaches did not depend on the mathematical models of the systems, and were based only on input-output relationships, using responses from selectively-placed devices. A predictive controller was then designed using the synthesised model of the second approach. The performance of this controller was demonstrated on different test systems which were representative of practical wide-area networks. Results showed that the WAMS-based controller was able to regulate non-viable voltage situations by estimating control inputs without any explicit mathematical modelling. A two-stage multi-rate controller using WAMS-based VSIs was also proposed for emergency situations.

Consequently, it can be safely concluded that the thesis statement holds true.

7.3 Research Implications

This project particularly proposes novel cost-effective and optimal methods of deploying WAMS over a wide-area network in Chapters 3, 4, and 5. The compelling reason to use the proposed placement approaches of Chapters 3, 4, and 5 in general is that optimality is guaranteed without the need for algorithmic parameter tuning. This eliminates the need for meta-heuristic algorithms that have been previously applied to the co-placement problem. Furthermore, compared to existing methods, it is more practically applicable as real costs and a range of channel capabilities can be specified for distribution and transmission networks at different levels of observability. Consequently, it can be used for PMU deployments where full grid observability is desired and in applications like generator model validation and secondary voltage control which require data only from only a selected number of buses. For research endeavours seeking to employ limited-channel PMUs such as the OpenPMU endeavours [90], [194], the algorithm can be deployed to estimate the number of components needed for specified levels of network observability.

The modelling approaches proposed in this work provoke the need to shift focus from exhaustive mathematical modelling of the network into simple estimation procedures afforded by numerical and subspace methods. With the increasing availability of synchrophasor data, more algorithms from systems identification and other fields which were previously under-navigated can now be better explored.

7.4 Research Limitations

This research has proposed WAMS placement and WAMS-based control design for secondary voltage regulation. However, for the placement algorithms proposed, the project used some hypothetical scenarios which may not be the same in practice. This project has endeavoured to consider as many factors as possible in the cost modelling, but has been limited in getting access to real data. Therefore, the costs used in the models have proceeded from relative costs garnered from industrial reports. Although these do not detract from the veracity of the proposed methods, the results

may only be interpreted in the light of the factors that have been considered and the assumptions that have been made.

For SVR, the use of capacitor banks preceded the use of generator AVR reference modulation or load shedding. However, in order to implement the capacitors adequately in the simulation, capacitor would have to be connected using switches on the simulation platform. For the Artemis-based real-time simulation used in this project, too many switches may introduce discontinuities into the simulation. Therefore, the use of capacitor banks was not used in the model. It may be safe to assume that the number of modulation of AVR references by the controller would have been reduced in the simulation cases of 6 if they had been considered.

The use of PMUs to measure some power system quantities that are necessary for the effective performance of the two-level SPBVC may be limited under transient conditions. These quantities include reactive power and ROCOF. The stability indicator built around the ROCOF may lead to false alarm if the PMU is not properly calibrated according to the experience of events around the grid under study.

With respect to real-time simulation, the very limited number of cores on the real-time simulator also meant that the size of networks that could be used in the network is vastly reduced. In order to overcome some of the limitation, the number of subsystems used in the real-time implementation in the 39-Bus model of Chapter 6 was reduced from 7 to 2. Thus, no claim for real-time may be made on this case study.

7.5   Potential Impact of this Work

Given that the placement algorithms proposed in this work was based on a comprehensive modelling of costs involved in placements, it can be implemented on any practical network with a given topology. This would include electric power networks in a developed or developing country. The placement formulations should induce a paradigm shift in co-placement optimisations, in terms of the considerations of the number of cost factors, non-homogeneous channel capacities, multiple vendors, and in the manner with which the problem has been set up. The topology defragmentation approach described in 3 will dissuade further employment of less formal meta-heuristic algorithms in the co-placement problem. The discrepancy between the actual and modelled cases of the events leading to the UK August 9 blackout emphasises the need for increased WAMS deployments in the UK grid [4]. With more WAMS devices deployed, prompt control action could have been taken and the causes of blackout could have been easier to identify. The measurement-based controller designs also means that it is possible to automate voltage regulation tasks without depending on an exhaustive modelling of the electric power grid. With this possibility, huge volumes of data which are obtained from WAMS devices can be put to good use.

7.6   Recommendation for further works

7.6.1   Improved metric for placement algorithms

In Chapter 3, a novel co-placement formulation was introduced along with the novel consideration of multiple vendors. In order to provide a metric for choosing between vendors, a reliability index was also introduced. Another metric was also introduced to this end by considering the benefits offered by the add-ons offered by the vendors in Chapter 5. The reliability metric was defined loosely in Chapter 3 as the rate by which the vendor's products exceeded the standard TVE. A suggestion

for future research is to introduce more robust and more metrics to choose between vendors in the placement algorithms. Similarly, a more standard accounting method may be used to calculate the effect of inflation and the factors affecting multi-stage placements which were discussed in Chapter 4. A stochastic model for failure of the devices may be introduced into the multi-stage models.

7.6.2 Time-varying SBPVC and the effect of OLTC dynamics

The SBPVC was effective in voltage regulation for a number of contingencies. However, this was based on linear time-invariant model following from an offline synthesis. A future work could be to examine how the performance of the controller may be improved by considering time-varying models in the feedback control set-up. OLTCs have been assumed to be locked in this simulation. However, their dynamics can have a destabilising effect on system's operations. Future works could incorporate OLTC operations and examine their effect on the controller's performance.

7.6.3 Integration of control variables from renewable energy sources

With the increasing proliferation and integration of RES and the attendant complexity in obtaining adequate models for increasingly complex electric power grids, future works could focus on exploiting the additional controllability offered by the RES, and design a measurement-based controller for the downstream distribution grid using the methods outlined in this project. Improved observability can be obtained by deploying μPMUs [1] using the placement algorithms proposed in this work.

7.6.4 Consideration of communication and feedback delays

Like all positive-sequenced estimation of PMUs characteristics, the actual natures of PMUs are usually well represented. Although this project has implemented the proposed controller in a real-time-ready environment, future works could consider the effects of communication delays on the data sent from the PMUs to the controllers as well as the loss of data, on the SBPVC performance. It might be necessary to consider in addition, the effect of controller delays. To this end, a substantial part of this project has been dedicated to developing a laboratory-based RT-HIL environment which considers these effects.

7.6.5 Performance of a hybrid combination of model-based and model-free control

It may happen that the operating condition for which the SPBVC has been designed may change rapidly, in such a way that the single-layer SPBVC, which performed well for non-viable voltage regulation, no longer gives satisfactory performance. The two-level SPBVC has been designed to handle such situations. However, a suggestion for a future research would be an investigation of how well the controller, based on a hybrid combination of mathematical and measurement-synthesised model, performs under the similar operating conditions. Note that the mathematical model is composed of the synchronous machine equations and others, as detailed in Chapter 2.

---

[1]It is important to state that this was earlier defined as being so named on account of its micro-second accuracy

Appendix A

Definitions of OPP (3.22) Matrices

This appendix describes the actual form of the matrices of the optimisation formulation (3.22) in Section 3.7. Recall that these (3.22) is the compact form of the OPP (3.16) in Section 3.5.

$$
\boldsymbol{B}_d = \left[\left[\overbrace{\left[\overbrace{\begin{bmatrix} b_{1111} & \cdots & b_{1n11} \\ \vdots & \ddots & \vdots \\ b_{n111} & \cdots & b_{nn11} \end{bmatrix}}^{r=1} \ddots \overbrace{\begin{bmatrix} b_{111r_s} & \cdots & b_{1ni1r_s} \\ \vdots & \ddots & \vdots \\ b_{n1i1r_s} & \cdots & b_{nni1r_s} \end{bmatrix}}^{r=r_s} \right]}^{l=1} : \overbrace{\left[\overbrace{\begin{bmatrix} b_{11L1} & \cdots & b_{1nL1} \\ \vdots & \ddots & \vdots \\ b_{n1L1} & \cdots & b_{nnL1} \end{bmatrix}}^{l=1} \ddots \overbrace{\begin{bmatrix} b_{11Lr_s} & \cdots & b_{1nLr_s} \\ \vdots & \ddots & \vdots \\ b_{n1Lr_s} & \cdots & b_{nnLr_s} \end{bmatrix}}^{r=r_s} \right]}^{l=L} \right]
$$
$$(A.1)$$

For D number of PDCs, each vendor v's containment matrix is defined by,

$$\boldsymbol{B}_v = \begin{bmatrix} \boldsymbol{B}_d & \cdots & \boldsymbol{B}_D \end{bmatrix} \tag{A.2}$$

And the containment matrix $\boldsymbol{B}$ over all n buses, L non-homogeneous channels, D PDCs, and V vendors may be summarised as,

$$\boldsymbol{B} = \begin{bmatrix} \boldsymbol{B}_v & \cdots & \boldsymbol{B}_V \end{bmatrix} \tag{A.3}$$

The process of formulating $\boldsymbol{B}$ in (A.3) holds true for matrices $\boldsymbol{H}, \boldsymbol{F}$ and $\boldsymbol{G}$. The entries of the elements are somehow different. For instance,

$$
\boldsymbol{H}_d = \left[\left[\overbrace{\left[\overbrace{\begin{bmatrix} I_{n\times n} \end{bmatrix}}^{r=1} \ddots \overbrace{\begin{bmatrix} I_{n\times n} \end{bmatrix}}^{r=r_s} \right]}^{l=1} \cdots \overbrace{\left[\overbrace{\begin{bmatrix} I_{n\times n} \end{bmatrix}}^{l=1} \ddots \overbrace{\begin{bmatrix} I_{n\times n} \end{bmatrix}}^{r=r_s} \right]}^{l=L} \right] : \overbrace{\left[\overbrace{\begin{bmatrix} I_{n\times n} \end{bmatrix}}^{r=1} \ddots \overbrace{\begin{bmatrix} I_{n\times n} \end{bmatrix}}^{r=r_s} \right]}^{l=1} \cdots \overbrace{\left[\overbrace{\begin{bmatrix} I_{n\times n} \end{bmatrix}}^{l=1} \ddots \overbrace{\begin{bmatrix} I_{n\times n} \end{bmatrix}}^{r=r_s} \right]}^{l=L} \right]
$$
$$(A.4)$$

$$\boldsymbol{X}_d = \begin{bmatrix} [x_{111} & \cdots & x_{n11}] & \cdots & [x_{11r_s} & \cdots & x_{n1r_s}] & \cdots & [x_{nL1} & \cdots & x_{nL1}] & \cdots & [x_{nLr_s} & \cdots & x_{n1r_s}] \end{bmatrix}^T \tag{A.5}$$

$$\boldsymbol{X}_v = \begin{bmatrix} \boldsymbol{X}_d^T & \cdots & \boldsymbol{X}_D^T \end{bmatrix}^T \tag{A.6}$$

$$\boldsymbol{X} = \begin{bmatrix} \boldsymbol{X}_v^T & \cdots & \boldsymbol{X}_V^T \end{bmatrix}^T \tag{A.7}$$

$$\boldsymbol{C}_{v_i} = \begin{bmatrix} [C_{111} & \cdots & C_{n11}] & \cdots & [C_{11r_s} & \cdots & C_{n1r_s}] & \cdots & [C_{niL1} & \cdots & C_{nL1}] & \cdots & [C_{nLr_s} & \cdots & C_{n1r_s}] \end{bmatrix}^T \tag{A.8}$$

$$\boldsymbol{C} = \begin{bmatrix} \boldsymbol{C}_d^T & \cdots & \boldsymbol{C}_D^T \end{bmatrix}^T \tag{A.9}$$

$$\boldsymbol{C}_v = \begin{bmatrix} \boldsymbol{C}_d^T & \cdots & \boldsymbol{C}_D^T \end{bmatrix}^T \tag{A.10}$$

$$\boldsymbol{C} = \begin{bmatrix} \boldsymbol{C}_v^T & \cdots & \boldsymbol{C}_V^T \end{bmatrix}^T \tag{A.11}$$

$$\boldsymbol{R}_d = \log \left(\begin{bmatrix} [R_{111} & \cdots & R_{n11}] & \cdots & [R_{11r_s} & \cdots & R_{ni1r_s}] & \cdots & [R_{nL1} & \cdots & R_{nL1}] & \cdots & [R_{nLr_s} & \cdots & R_{n1r_s}] \end{bmatrix}^T \right) \tag{A.12}$$

$$\boldsymbol{R}_v = \begin{bmatrix} \boldsymbol{R}_d^T & \cdots & \boldsymbol{R}_D^T \end{bmatrix}^T \tag{A.13}$$

$$\boldsymbol{R} = \begin{bmatrix} \boldsymbol{R}_v^T & \dots & \boldsymbol{R}_V^T \end{bmatrix}^T \tag{A.14}$$

TABLE A.1: Detailed Case: Assumed Costs for PMU Placements

	Costs(Units)										
	Labour						Others				
Wages	Communi-cation	Training	Travel Allowance	Instrument Transformer	Commun-ication	Cyber-security	Commi-ssioning	Swit-ches	Repe-aters	GPS
Charge Per Extra Channel	*Wages (per km)*	*Flat (per bus)*	*(per km)*	*(per piece per bus)*	*(per km length)*	*Flat (per bus)*	*Flat (per bus)*	*per piece*	*per piece*	*per piece*
0.083	0.05	0.083	0.017	3	0.667	0.667	0.667	0.667	0.667	0.033

Base Wage 0.667

Appendix B

Additional results from Chapter 5

The result in the following tables may be interpreted using this example. $54\text{-}l_4, [E] - [1]$ means to install a 4-channel PMU device on Bus 4 and connect to PDC E. The total number of PMUs connected from a particular vendor to a a particular PDC are indicated in square parentheses.

TABLE B.1: Full observability: Maximisation of benefits with reliability considera-
tion

Vendors	h = 1	
	R = 0	R = 1
v_1		
v_2	1-l_2, 5-l_4 [A]-[2]	1-l_2, 3-l_1, 5-l_4, 6-l_2 [A]-[4]
	26-l_2, 27-l_4, 32-l_4 [B]-[3]	22-l_1, 24-l_2, 25-l_2, 26-l_2, 27-l_4, 32-l_4,115-l_1 [B]-[7]
	10-l_1, 12-l_4, 15-l_4, 19-l_4, 31-l_2 [C]-[5]	9-l_2, 10-l_1, 11-l_2, 12-l_5, 15-l_4, 17-l_4, 19-l_4, 21-l_2, 29-l_1, 31-l_2, 117-l_1 [C]-[11]
	34-l_4, 36-l_4, 40-l_4 [D]-[3]	34-l_4, 36-l_2, 37-l_4, 40-l_4, 43-l_1 [D]-[5]
	56-l_4, 59-l_4 [E]-[2]	54-l_4, 56-l_4, 59-l_4, 63-l_1 [E]-[4]
	61-l_4, 62-l_4 [F]-[2]	61-l_4, 62-l_4 [F]-[2]
	65-l_4, 66-l_4, 45-l_2, 49-l_4 [G]-[4]	65-l_4, 66-l_4, 51-l_2, 48-l_1, 52-l_2, 50-l_1, 49-l_5, 45-l_2 [G]-[8]
	70-l_4, 77-l_4, 69-l_4, 85-l_4, 89-l_4, 76-l_2 116-l_1, 71-l_2 [H]-[8]	69-l_4, 76-l_2, 77-l_4, 116-l_1, 83-l_2, 75-l_2, 85-l_4, 71-l_2, 68-l_2, 86-l_1, 70-l_4, 87-l_1, 89-l_4, 73-l_1 [H]-[14]
	105-l_4, 100-l_4, 180-l_4, 110-l_4, 92-l_4 [I]-[5]	79-l_1, 105-l_4, 112-l_1, 106-l_1, 92-l_4, 100-l_5, 96-l_2, 110-l_4, 101-l_2, 94-l_2, 80-l_6, 108-l_2, 111-l_1, 91-l_2 [I]-[14]
v_3	22-l_1 [B]-[1]	
	52-l_1 [G]-[1]	41-l_1 [D]-[1]
	86-l_1 [H]-[1]	
	96-l_1 [I]-[1]	

TABLE B.2: Full observability: Maximisation of benefits without reliability consideration

Vendors	h = 1		
	R = 0	R = 1	R = 2
v_1	1-l_2 [A]-[1] 26-l_2 [B]-[1] 31-l_2 [C]-[1] 36-l_2 [D]-[1] 45-l_2 [G]-[1] 71-l_2, 76-l_2 [H]-[2]	1-l_2 [A]-[1] 22-l_1, 26-l_2, 27-l_2 [B]-[3] 10-l_1, 19-l_2, 31-l_2, 31-l_2 [C]-[4] 34-l_2, 36-l_2, 40-l_2 [D]-[3] 45-l_2, 52-l_1 [G]-[2] 71-l_2, 76-l_2, 116-l_1 [H]-[3] 96-l_1 [I]-[1]	3-l_2, 5-l_5, 11-l_2, 12-l_5, 16-l_2, 27-l_2, 29-l_1, 37-l_6, 39-l_2, 41-l_1, 45-l_1, 48-l_2, 49-l_4, 55-l_2, 56-l_2, 59-l_6, 63-l_1, 69-l_2, 69-l_3, 75-l_3, 88-l_2, 93-l_2, 100-l_3, 106-l_2, 108-l_1, 117-l_1 [A]-[26] 15-l_2, 17-l_2, 27-l_2, 52-l_2, 53-l_1, 54-l_1, 56-l_1, 57-l_1, 58-l_1, 62-l_2, 63-l_1, 66-l_1, 70-l_2, 74-l_2, 86-l_2, 107-l_1, 110-l_2, 113-l_1, 118-l_2 [B]-[19] 39-l_2, 50-l_3, 60-l_3, 61-l_2, 62-l_2, 64-l_2, 67-l_1 78-l_1, 80-l_4, 85-l_3, 105-l_1, 109-l_1 [C]-[12] 19-l_2, 28-l_2, 34-l_2, 59-l_6, 65-l_3, 66-l_2, 67-l_1, 71-l_2, 74-l_2, 94-l_2, 106-l_2, 111-l_1, 115-l_2 [D]-[13] 9-l_2, 15-l_2, 51-l_2, 52-l_2, 70-l_3, 77-l_1, 80-l_4, 87-l_1, 95-l_1, 112-l_1 [E]-[10] 2-l_1, 28-l_2, 38-l_2, 46-l_2, 68-l_2, 72-l_1, 108-l_1 [F]-[7] 10-l_1, 44-l_2, 51-l_2, 84-l_2, 88-l_2, 89-l_2, 94-l_2, 98-l_2, 99-l_2 [G]-[9] 19-l_2, 95-l_1 [H]-[2] 21-l_1, 22-l_2, 23-l_2, 26-l_1, 60-l_3, 73-l_1, 78-l_1, 82-l_1 116-l_1 [I]-[9]
v_2	5-l_4 [A]-[1] 27-l_4, 32-l_4 [B]-[2] 12-l_4, 15-l_4, 19-l_4 [C]-[3] 34-l_4, 40-l_4 [D]-[2] 56-l_4, 59-l_4 [E]-[2] 61-l_4, 62-l_4 [F]-[2] 49-l_4, 65-l_4, 66-l_4 [G]-[3] 77-l_4, 70-l_4, 69-l_4, 89-l_4, 85-l_4 [H]-[5] 92-l_4, 100-l_4, 80l_4, 105-l_4, 110-l_4 [I]-[5]	1-l_2, 5-l_4, l_4 [A]-[3] 26-l_2, 27-l_4, 32-l_4, 32-l_4 [B]-[4] 12-l_4, 12-l_4, 15-l_4, 15-l_4, 19-l_4 [C]-[5] 34-l_4, 36-l_4, 40-l_4 [D]-[3] 56-l_4, 56-l_4, 59-l_4, 59-l_4, 61-l_4 [E]-[5] 62-l_4, 61-l_4 [F]-[2] 49-l_4, 49-l_4, 65-l_4, 45-l_2, 66-l_4 [G]-[5] 85-l_4, 110-l_4, 85-l_4, 69-l_4, 70-l_4, 70-l_4, 71-l_2 65-l_4, 76-l_2, 89-l_4, 69-l_4, 77-l_4, 77-l_4 [H]-[13] 92-l_4, 89-l_4, 92-l_4, 100-l_4, 105-l_4, 110-l_4 180-l_1, 180-l_4, 100-l_4, 105-l_4 [I]-[10]	22-l_2, 29-l_1, 36-l_2, 47-l_1, 100-l_3 [A]-[5] 24-l_1, 75-l_3, 104-l_2 [B]-[3] 8-l_2, 40-l_3, 43-l_1, 64-l_2, 76-l_1, 90-l_2, 115-l_2 [C]-[7] 14-l_2, 18-l_1, 30-l_2, 36-l_2, 57-l_1, 77-l_1 [D]-[6] 20-l_2, 25-l_2, 35-l_2, 45-l_1, 46-l_2, 82-l_1, 113-l_1, 93-l_2, 83-l_3,91-l_1 [E]-[11] 10-l_1, 81-l_2, 4-l_2, 2-l_2, 32-l_4, 8-l_2, 97-l_1, 38-l_2, 20-l_2, 65-l_3, 1-l_2, 114-l_2 [F]-[12] 98-l_2, 21-l_1, 61-l_2, 11-l_2, 49-l_4, 91-l_1, 85-l_3, 32-l_4, 92-l_3 [G]-[9] 89-l_2, 17-l_2, 12-l_5, 105-l_1, 84-l_2, 68-l_2, 73-l_1 58-l_1, 26-l_1, 101-l_1 [H]-[10] 42-l_2, 79-l_1, 50-l_1, 102-l_2, 79-l_1, 5-l_5, 96-l_4 [I]-[7]
v_3	22-l_1 [B]-[1] 10-l_1 [C]-[1] 52-l_1 [G]-[1] 86-l_1, 116-l_1 [H]-[2] 96-l_1 [I]-[1]	22-l_1 [B]-[1] 10-l_1 [C]-[1] 52-l_1 [G]-[1] 116-l_1, 86-l_1 [H]-[2] 86-l_1, 96-l_1 [I]-[2]	6-l_1, 33-l_2, 99-l_2, 103-l_4, 112-l_1 [A]-[5] 79-l_1, 1-l_2, 6-l_1, 90-l_2, 7-l_1, 7-l_2, 81-l_2 [B]-[7] 96-l_4, 35-l_2, 102-l_2, 101-l_1, 33-l_2 [C]-[5] 76-l_1, 37-l_6, 103-l_3, 43-l_1, 110-l_1, 31-l_2, 4-l_2 [D]-[7] 3-l_2, 13-l_1, 40-l_3, 114-l_2, 47-l_1, 116-l_1, 104-l_2 40-l_3, 14-l_2, 24-l_2, 83-l_3, 31-l_2, 117-l_1, 111-l_1 [E]-[14] 16-l_2, 92-l_3,30-l_2, 48-l_2, 41-l_1, 71-l_1 [F]-[6] 53-l_1, 13-l_1, 34-l_2, 44-l_2, 25-l_2, [G]-[5] 118-l_2, 86-l_2, 9-l_2, 55-l_2, 109-l_2, 18-l_1, 42-l_2 42-l_2, 9-l_2, 55-l_2, 109-l_1, 18-l_1, 107-l_1 [H]-[13] 23-l_2, 87-l_1, 97-l_1, 72-l_1, 54-l_1 [I]-[5]

TABLE B.3: Selective observability: maximisation of benefits without reliability consideration

Vendors	h = 1			h = 2		
	R = 0	R = 1	R = 2	R = 0	R = 1	R = 2
v_1		1-l_2 [A]-[1]	1-l_2 [A]-[1] 24-l_2 [B]-[1] 81-l_2 [I]-[1]			1-l_2 [A]-[1] 37-l_1 [D]-[1]
v_2	32-l_4 [B]-[1] 12-l_4, 15-l_4 [C]-[2] 34-l_4, 40-l_4 [D]-[4] 59-l_4 [E]-[1] 61-l_4, 62-l_4 [F]-[2] 65-l_4, 66-l_4 [G]-[2] 69-l_4, 85-l_4 [H]-[2] 80-l_4, 100-l_4 [I]-[2]	32-l_4 [B]-[1] 12-l_4, 15-l_4 [C]-[2] 34-l_4, 40-l_4 [D]-[2] 56-l_4, 59-l_4 [E]-[2] 61-l_4, 62-l_4 [F]-[2] 65-l_4, 66-l_4 [G]-[2] 70-l_4, 77-l_4, 69-l_4, 85-l_4, 89-l_4 [H]-[4] 103-l_4, 100-l_4, 80-l_4 [I]-[3]	32-l_4 [B]-[1] 12-l_4, 15-l_4, 19-l_4 [C]-[3] 34-l_4, 40-l_4 [D]-[2] 54-l_4, 56-l_4, 59-l_4 [E]-[3] 61-l_4, 62-l_4 [F]-[2] 65-l_4, 66-l_4 [G]-[2] 70-l_4, 85-l_4, 89-l_4, 77-l_4, 69-l_4 [H]-[5] 105-l_4, 100-l_4, 80-l_4, 103-l_4 [I]-[4]	32-l_4 [B]-[1] 12-l_4, 15-l_4, 15-l_4 [C]-[3] 34-l_4, 40-l_4 [D]-[2] 59-l_4, 59-l_4, 61-l_4 [E]-[3] 61-l_4, 62-l_4 [F]-[2] 65-l_4, 66-l_4 [G]-[2] 69-l_4, 65-l_4, 85-l_4, 69-l_4 [H]-[4] 100-l_4, 80-l_4, 80-l_4 [I]-[3]	32-l_4, 32-l_4 [B]-[2] 12-l_4, 12-l_4, 15-l_4, 15-l_4 [C]-[4] 34-l_4, 40-l_4 [D]-[2] 59-l_4, 59-l_4, 61-l_4 [E]-[3] 61-l_4, 62-l_4 [F]-[2] 65-l_4, 66-l_4 [G]-[2] 65-l_4, 85-l_4, 85-l_4, 69-l_4, 69-l_4 [H]-[5] 80-l_4, 100-l_4, 80-l_4, 100-l_4 [I]-[4]	32-l_4, 32-l_4 [B]-[2] 12-l_4, 12-l_4, 15-l_4, 15-l_4 [C]-[4] 34-l_4, 40-l_4 [D]-[2] 56-l_4, 59-l_4, 59-l_4, 61-l_4 [E]-[4] 61-l_4, 62-l_4 [F]-[2] 65-l_4, 66-l_4 [G]-[2] 65-l_4, 69-l_4, 69-l_4, 70-l_4, 77-l_4, 85-l_4, 85-l_4, 89-l_4 [H]-[8] 100-l_4, 100-l_4, 103-l_4, 80-l_4, 80-l_4 [I]-[5]
v_3		115-l_1 [B]-[1] 37-l_1 [D]-[1]	2-l_1 [A]-[1] 114-l_1, 115-l_1 [B]-[2] 37-l_1, 39-l_1 [D]-[2] 88-l_1 [H]-[1]			115-l_1 [B]-[1] 37-l_1 [D]-[1]

Bibliography

[1] M. E. V. Segatto, H. R. de Oliveira Rocha, J. A. L. Silva, M. H. M. Paiva, and M. A. do Rosário Santos Cruz, "Telecommunication Technologies for Smart Grids: Total Cost Optimization," *Advances in Renewable Energies and Power Technologies*, vol. 2, pp. 451–478, 2018. DOI: 10 . 1016/B978-0-12-813185-5.00007-3.

[2] National Grid ESO, "National Electricity Transmission System Security and Quality of Supply Standard," no. April, pp. 1–94, 2019.

[3] PSNH, "Final Report on the August 14, 2003 Blackout in the United States and Canada: Causes and Recommentations, April 2004, U.S.-Canada Power System Outage Task Force," no. April, 2003. [Online]. Available: https://www3.epa.gov/region1/npdes/merrimackstation/pdfs/ar/AR-1165.pdf.

[4] National Grid ESO, "Technical Report on the events of 9 August 2019," no. September, pp. 2–38, 2019.

[5] S. Wilde, "9 August 2019 Power Outage Report," no. August 2019, 2020.

[6] U.S. Energy Information Administration, *New technology can improve electric power system efficiency and reliability*. [Online]. Available: https://www.eia.gov/todayinenergy/detail.php?id=5630{\#}{\%}0D (visited on 10/2019).

[7] S. Supriya, M. Magheshwari, S. Sree Udhyalakshmi, R. Subhashini, and Musthafa, "Smart grid technologies: Communication technologies and standards," *International Journal of Applied Engineering Research*, vol. 10, no. 20, pp. 16 932–16 941, 2015, ISSN: 09739769.

[8] M. Glavic, D. Novosel, E. Heredia, D. Kosterev, A. Salazar, F. Habibi, and M. Donnelly, "See It Fast to Keep Calm," *IEEE Power & Energy Magazine*, vol. 10, no. july/august, pp. 43–55, 2012, ISSN: 1540-7977. DOI: 10.1109/MPE.2012.2196332.

[9] H. Y. Su and C. W. Liu, "An adaptive PMU-based secondary voltage control scheme," *IEEE Transactions on Smart Grid*, vol. 4, no. 3, pp. 1514–1522, 2013, ISSN: 19493053. DOI: 10.1109/TSG.2013.2272583.

[10] M. K. Neyestanaki and A. M. Ranjbar, "An Adaptive PMU-Based Wide Area Backup Protection Scheme for Power Transmission Lines," *IEEE Transactions on Smart Grid*, vol. 6, no. 3, pp. 1550–1559, 2015, ISSN: 19493053. DOI: 10.1109/TSG.2014.2387392.

[11] S. Y. Seyedi, "SYNCHROPHASOR DATA ANALYTICS FOR CONTROL AND PROTECTION APPLICATIONS IN SMART GRIDS," 2017.

[12] D. B. Arnold, C. Roberts, O. Ardakanian, and E. M. Stewart, "Synchrophasor data analytics in distribution grids," *2017 IEEE Power and Energy Society Innovative Smart Grid Technologies Conference, ISGT 2017*, 2017. DOI: 10.1109/ISGT.2017.8085979.

[13] U.S. Department of Energy Office of Electricity Delivery and Energy Reliability (DOE-OE), "Factors Affecting PMU Installation Costs," no. September, p. 12, 2014.

[14] F. Aminifar, M. Fotuhi-firuzabad, and A. Safdarian, "Optimal PMU Placement Based on Probabilistic Cost/Bene fi t Analysis," *IEEE Transactions on Power Systems*, vol. 28, no. 1, pp. 1–2, 2012.

[15] J. M. Maciejowski, *Predictive control: with constraints*. Pearson education, 2002, ISBN: 0201398230.

[16] E. F. Camacho and C. B. Alba, *Model predictive control*. Springer Science & Business Media, 2013, ISBN: 0857293982.

[17] M. Larsson, D. J. Hill, and G. Olsson, "Emergency voltage control using search and predictive control," *International Journal of Electrical Power {&} Energy Systems*, vol. 24, no. 2, pp. 121–130, 2002, ISSN: 01420615. DOI: 10.1016/S0142-0615(01)00017-5. [Online]. Available: http://www.sciencedirect.com/science/article/pii/S0142061501000175.

[18] M. Zima and G. Andersson, "Stability assessment and emergency control method using trajectory sensitivities," *2003 IEEE Bologna Power Tech Conference Proceedings*, vol. 2, 2003. DOI: 10.1109/PTC.2003.1304313.

[19] M. Larsson and D. Karlsson, "Coordinated system protection scheme against voltage collapse using heuristic search and predictive control," *IEEE Transactions on Power Systems*, vol. 18, no. 3, pp. 1001–1006, 2003, ISSN: 0885-8950. DOI: 10.1109/TPWRS.2003.814852.

[20] A. Panda, R. Mukherjee, A. De, and S. Chakraborty, "Model predictive control for power system dynamic security enhancement," *2016 National Power Systems Conference (NPSC)*, pp. 1–6, 2016. DOI: 10.1109/NPSC.2016.7858932. [Online]. Available: http://ieeexplore.ieee.org/document/7858932/.

[21] I. A. Hiskens and B Gong, "MPC-based load shedding for voltage stability enhancement," *Decis. Control. 2005 2005 Eur. Control Conf. CDC-ECC'05. 44th IEEE Conf.*, pp. 4463–4468, 2005. DOI: 10.1109/CDC.2005.1582865. [Online]. Available: http://ieeexplore.ieee.org/xpls/abs{_}all.jsp?arnumber=1582865.

[22] M. Zima and G. Andersson, "Model predictive control employing trajectory sensitivities for power systems applications," *Proceedings of the 44th IEEE Conference on Decision and Control, and the European Control Conference, CDC-ECC '05*, vol. 2005, no. 5, pp. 4452–4456, 2005. DOI: 10.1109/CDC.2005.1582863.

[23] B. G. B. Gong and I. Hiskens, "Two-stage model predictive control for voltage collapse prevention," *2008 40th North American Power Symposium*, pp. 1–7, 2008. DOI: 10.1109/NAPS.2008.5307302.

[24] T Amraee, A. M. Ranjbar, and R Feuillet, "Adaptive under-voltage load shedding scheme using model predictive control," *Electr. Power Syst. Res.*, vol. 81, no. 7, pp. 1507–1513, 2011, ISSN: 03787796. DOI: 10.1016/j.epsr.2011.03.006. [Online]. Available: http://dx.doi.org/10.1016/j.epsr.2011.03.006.

[25] M. Glavic, M. Hajian, W. Rosehart, and T. Van Cutsem, "Receding-horizon multi-step optimization to correct nonviable or unstable transmission voltages," *IEEE Transactions on Power Systems*, vol. 26, no. 3, pp. 1641–1650, 2011, ISSN: 08858950. DOI: 10.1109/TPWRS.2011.2105286.

[26] G. Valverde and T. Van Cutsem, "Model predictive control of voltages in active distribution networks," *IEEE Transactions on Smart Grid*, vol. 4, no. 4, pp. 2152–2161, 2013, ISSN: 19493053. DOI: 10.1109/TSG.2013.2246199.

[27] M Farina, A Guagliardi, F Mariani, C Sandroni, and R Scattolini, "Model predictive control of voltage profiles in MV networks with distributed generation," *Control Eng. Pract.*, vol. 34, pp. 18–29, 2015, ISSN: 09670661. DOI: 10.1016/j.conengprac.2014.09.010. [Online]. Available: http://dx.doi.org/10.1016/j.conengprac.2014.09.010.

[28] M. Hajian, W. Rosehart, M. Glavic, H. Zareipour, and T. Van Cutsem, "Linearized Power Flow Equations Based Predictive Control of Transmission Voltages," *2013 46th Hawaii International Conference on System Sciences*, pp. 2298–2304, 2013, ISSN: 15301605. DOI: 10.1109/HICSS.2013.385. [Online]. Available: http://ieeexplore.ieee.org/document/6480121/.

[29] S. Talukdar, Dong Jia, P. Hines, and B. Krogh, "Distributed Model Predictive Control for the Mitigation of Cascading Failures," *Proceedings of the 44th IEEE Conference on Decision and Control*, no. July 1996, pp. 4440–4445, 2005. DOI: 10.1109/CDC.2005.1582861. [Online]. Available: http://ieeexplore.ieee.org/xpls/abs{_}all.jsp?arnumber=1582861{\%}5Cnhttp://ieeexplore.ieee.org/lpdocs/epic03/wrapper.htm?arnumber=1582861.

[30] M. R. Almassalkhi and I. A. Hiskens, "Model-Predictive Cascade Mitigation in Electric Power Systems With Storage and Renewables—Part I: Theory and Implementation," *IEEE Transactions on Power Systems*, vol. 30, no. 1, pp. 67–77, 2015, ISSN: 0885-8950. DOI: 10.1109/TPWRS.2014.2320982. [Online]. Available: http://ieeexplore.ieee.org/lpdocs/epic03/wrapper.htm?arnumber=6824273.

[31] ——, "Model-Predictive Cascade Mitigation in Electric Power Systems With Storage and Renewables—Part II: Case-Study," *IEEE Transactions on Power Systems*, vol. 30, no. 1, pp. 78–87, 2015, ISSN: 0885-8950. DOI: 10.1109/TPWRS.2014.2320982. [Online]. Available: http://ieeexplore.ieee.org/lpdocs/epic03/wrapper.htm?arnumber=6824273.

[32] A. N. Venkat, I. A. Hiskens, J. B. Rawlings, and S. J. Wright, "Distributed MPC strategies with application to power system automatic generation control," *IEEE Trans. Control Syst. Technol.*, vol. 16, no. 6, pp. 1192–1206, 2008, ISSN: 10636536. DOI: 10.1109/TCST.2008.919414.

[33] C. Trabert, A. Ulbig, and G. Andersson, "Model Predictive Frequency Control employing stability constraints," *Proceedings of the American Control Conference*, vol. 2015-July, pp. 5678–5685, 2015, ISSN: 07431619. DOI: 10.1109/ACC.2015.7172229. arXiv: arXiv:1405.6744v1.

[34] P. Mc Namara, R. R. Negenborn, B. De Schutter, G. Lightbody, and S. McLoone, "Distributed MPC for frequency regulation in multi-terminal HVDC grids," *Control Engineering Practice*, vol. 46, pp. 176–187, 2016, ISSN: 09670661. DOI: 10.1016/j.conengprac.2015.11.001. [Online]. Available: http://dx.doi.org/10.1016/j.conengprac.2015.11.001.

[35] L. Papangelis, M.-S. Debry, P. Panciatici, and T. Van Cutsem, "Coordinated Supervisory Control of Multi-Terminal HVDC Grids: A Model Predictive Control Approach," *IEEE Transactions on Power Systems*, vol. 32, no. 6, pp. 4673–4683, 2017, ISSN: 0885-8950. DOI: 10.1109/TPWRS.2017.2659781. [Online]. Available: http://ieeexplore.ieee.org/document/7835265/.

[36] F. Aminifar, M. Fotuhi-Firuzabad, and A. Safdarian, "Optimal PMU placement based on probabilistic cost/benefit analysis," *IEEE Transactions on Power Systems*, vol. 28, no. 1, pp. 566–567, 2013, ISSN: 08858950. DOI: 10.1109/TPWRS.2012.2198312.

[37] A. Abur and A. G. Exposito, *Power system state estimation: theory and implementation*. CRC press, 2004, ISBN: 0203913671.

[38] V. Madani, D. Novosel, K. Martin, R. Carroll, H. Huang, V. Centeno, V. Tech, Y. Hu, R. Hayes, J. Stenbakken, T. Weekes, and M. Hydro, "A Guide for PMU Installation, Commissioning and Maintenance," 2007.

[39] B. Gou, "Optimal Placement of PMUs by Integer Linear Programming," *IEEE Transactions on Power Systems*, vol. 23, no. 3, pp. 1525–1526, 2008, ISSN: 0885-8950. DOI: 10.1109/TPWRS.2008.926723.

[40] B. Mohammadi-Ivatloo and S. H. Hosseini, "Optimal PMU placement for power system observability considering secondary voltage control," *Canadian Conference on Electrical and Computer Engineering*, pp. 365–368, 2008, ISSN: 08407789. DOI: 10.1109/CCECE.2008.4564558.

[41] R. Sodhi, S. C. Srivastava, and S. N. Singh, "Optimal PMU placement to ensure system observability under contingencies," *2009 IEEE Power and Energy Society General Meeting, PES '09*, 2009, ISSN: 1944-9925. DOI: 10.1109/PES.2009.5275618.

[42] M. Korkali and A. Abur, "Placement of PMUs with channel limits," *2009 IEEE Power and Energy Society General Meeting, PES '09*, pp. 1–4, 2009, ISSN: 1944-9925. DOI: 10.1109/PES.2009.5275529.

[43] A. Biswal and H. Mathur, "Optimized PMU Stationing for Wide Area Monitoring of Power Grid," *Procedia Technology*, vol. 21, pp. 2–7, 2015, ISSN: 22120173. DOI: 10.1016/j.protcy.2015.10.002. [Online]. Available: http://linkinghub.elsevier.com/retrieve/pii/S2212017315002303.

[44] J. Aghaei, A. Baharvandi, A. Rabiee, and M. A. Akbari, "Probabilistic PMU Placement in Electric Power Networks: An MILP-Based Multiobjective Model," *IEEE Transactions on Industrial Informatics*, vol. 11, no. 2, pp. 332–341, 2015, ISSN: 15513203. DOI: 10.1109/TII.2015.2389613.

[45] Z. H. Rather, Z. Chen, P. Thogersen, P. Lund, and B. Kirby, "Realistic approach for phasor measurement unit placement: Consideration of practical hidden costs," *IEEE Transactions on Power Delivery*, vol. 30, no. 1, pp. 3–15, 2015, ISSN: 08858977. DOI: 10.1109/TPWRD.2014.2335059.

[46] O. Gomez, C. Portilla, and M. A. Rios, "Reliability analysis of substation monitoring systems based on branch PMUs," *IEEE Transactions on Power Systems*, vol. 30, no. 2, pp. 962–969, 2015, ISSN: 08858950. DOI: 10.1109/TPWRS.2014.2330736.

[47] V. S. S. Kumar and D. Thukaram, "Approach for Multistage Placement of Phasor Measurement Units Based on Stability Criteria," *IEEE Transactions on Power Systems*, vol. 31, no. 4, pp. 2714–2725, 2016, ISSN: 08858950. DOI: 10.1109/TPWRS.2015.2475164.

[48] S. L. Ramírez-P and C. A. Lozano, "Comparison of PMU Placement Methods in Power Systems for Voltage Stability Monitoring," *Ingenieria y Universidad*, vol. 20, no. 1, pp. 41–61, 2016, ISSN: 01232126. DOI: 10.11144/Javeriana.iyu20-1.cppm.

[49] N. R. Guideline, "PMU Placement and Installation," *NERC, Atlanta, GA, USA*, no. June, 2016.

[50] M. T. Jelodar and A. S. Fini, "Probabilistic PMU placement considering topological change in high voltage substations," *International Journal of Electrical Power and Energy Systems*, vol. 82, pp. 303–313, 2016, ISSN: 01420615. DOI: 10.1016/j.ijepes.2016.03.022. [Online]. Available: http://dx.doi.org/10.1016/j.ijepes.2016.03.022.

[51] M. Ghamsari-Yazdel and M. Esmaili, "Reliability-based probabilistic optimal joint placement of PMUs and flow measurements," *International Journal of Electrical Power and Energy Systems*, vol. 78, pp. 857–863, 2016, ISSN: 01420615. DOI: 10.1016/j.ijepes.2015.11.106. [Online]. Available: http://dx.doi.org/10.1016/j.ijepes.2015.11.106.

[52] Z. Wu, X. Du, W. Gu, P. Ling, J. Liu, and C. Fang, "Optimal micro-PMU placement using mutual information theory in distribution networks," *Energies*, vol. 11, no. 7, 2018, ISSN: 19961073. DOI: 10.3390/en11071917.

[53] O. Sun and N. Fan, "Solving the multistage PMU placement problem by integer programming and equivalent network design model," *Journal of Global Optimization*, 2018, ISSN: 0925-5001. DOI: 10.1007/s10898-018-0672-8. [Online]. Available: http://link.springer.com/10.1007/s10898-018-0672-8.

[54] M. Parniani, J. H. Chow, L. Vanfretti, B. Bhargava, and A. Salazar, "Voltage stability analysis of a multiple-infeed load center using phasor measurement data," *2006 IEEE PES Power Systems Conference and Exposition, PSCE 2006 - Proceedings*, pp. 1299–1305, 2006. DOI: 10.1109/PSCE.2006.296493.

[55] S. Dasgupta, M. Paramasivam, U. Vaidya, and V. Ajjarapu, "PMU-based model-free approach for short term voltage stability monitoring," *IEEE Power and Energy Society General Meeting*, 2012, ISSN: 19449925. DOI: 10.1109/PESGM.2012.6345522.

[56] R. Leelaruji, L. Vanfretti, U. Kjetil, and J. O. Gjerde, "Computing sensitivities from synchrophasor data for voltage stability monitoring and visualization," *Iranian Journal of Science and Technology - Transactions of Electrical Engineering*, vol. 36, no. E1, pp. 933–947, 2015, ISSN: 22286179. DOI: 10.1002/etep.

[57] J. M. Lim and C. L. DeMarco, "SVD-Based Voltage Stability Assessment From Phasor Measurement Unit Data," *IEEE Transactions on Power Systems*, vol. 31, no. 4, pp. 2557–2565, 2016. DOI: 10.1109/TPWRS.2015.2487996.

[58] L. Chu, R. Qiu, X. He, Z. Ling, and Y. Liu, "Massive Streaming PMU Data Modelling and Stability Analysis of Large Scale Power System," pp. 1–12, 2016. arXiv: 1609.03301. [Online]. Available: http://arxiv.org/abs/1609.03301.

[59] J. D. Nieto and J. M. Mauricio, "Power system optimal wide area control based on identified models," *2015 IEEE Eindhoven PowerTech, PowerTech 2015*, no. february 2011, 2015. DOI: 10.1109/PTC.2015.7232742.

[60] K. Máslo and M. Vrba, "Using WAMS for HVDC Control," *IFAC-PapersOnLine*, vol. 49, no. 27, pp. 395–399, 2016, ISSN: 24058963. DOI: 10.1016/j.ifacol.2016.10.765. [Online]. Available: http://dx.doi.org/10.1016/j.ifacol.2016.10.765.

[61] R. Yousefian and S. Kamalasadan, "Design and real-time implementation of optimal power system wide-area system-centric controller based on temporal difference learning," *IEEE Transactions on Industry Applications*, vol. 52, no. 1, pp. 395–406, 2016, ISSN: 00939994. DOI: 10.1109/TIA.2015.2466622.

[62] M. Monadi, H. Hooshyar, and L. Vanfretti, "Design and real-time implementation of a PMU-based adaptive auto-reclosing scheme for distribution networks," *International Journal of Electrical Power and Energy Systems*, vol. 105, no. May 2018, pp. 37–45, 2019, ISSN: 01420615. DOI: 10.1016/j.ijepes.2018.07.064. [Online]. Available: https://doi.org/10.1016/j.ijepes.2018.07.064.

[63] B Liscouski and W. Elliot, "U.S.-Canada Power System Outage Task Force," *System*, vol. 40, no. April, p. 238, 2004. [Online]. Available: https://reports.energy.gov/BlackoutFinal-Web.pdf.

[64] C. D. Vournas, V. C. Nikolaidis, and A. A. Tassoulis, "Postmortem analysis and data validation in the wake of the 2004 Athens blackout," *IEEE Transactions on Power Systems*, vol. 21, no. 3, pp. 1331–1339, 2006, ISSN: 0885-8950.

[65] P. Kundur, *Power_System_Stability_and_Control_Kundur.pdf*, 1994.

[66] National Grid Electricity System Operator, "The Grid Code (Uk)," no. 5, pp. 0–1014, 2020.

[67] D. K. Molzahn, "A Survey of Distributed Optimization Algorithms for Optimal Power Flow Problems," *IEEE Transactions on Smart Grid*, vol. 8, no. 6, pp. 2941 –2962, 2017.

[68] P. N. Vovos, A. E. Kiprakis, A. R. Wallace, and G. P. Harrison, "Centralized and distributed voltage control: Impact on distributed generation penetration," *IEEE Transactions on Power Systems*, vol. 22, no. 1, pp. 476–483, 2007, ISSN: 08858950. DOI: 10.1109/TPWRS.2006.888982.

[69] J Van Hecke, N Janssens, J Deuse, and F Promel, "Coordinated voltage control experience in Belgium," *CIGRE Session Report 38*, vol. 111, 2000.

[70] J. P. Piret, J. P. Antoine, M Stubbe, and N Janssens, "The study of a centralized voltage control method applicable to the Belgian system," in *INTERNATIONAL CONFERENCE ON LARGE HIGH VOLTAGE ELECTRIC SYSTEMS*, vol. 2, 1992, pp. 39–201, ISBN: 1016-2437.

[71] S Corsi, M Pozzi, U Bazzi, M Mocenigo, and P Marannino, "A simple real-time and on-line voltage stability index under test in Italian secondary voltage regulation," in *Proc. CIGRE Conf*, 2000, pp. 38–115.

[72] S. Corsi, M. Pozzi, C. Sabelli, and A. Serrani, "The coordinated automatic voltage control of the Italian transmission grid - Part I: Reasons of the choice and overview of the consolidated hierarchical system," *IEEE Transactions on Power Systems*, vol. 19, no. 4, pp. 1723–1732, 2004, ISSN: 08858950. DOI: 10.1109/TPWRS.2004.836185.

[73] M. D. Ili, C. Vialas, X. Liu, G. Leung, M. Athans, and P. Pruvot, *Improved Secondary and New Tertiary Voltage Control*, 1995. DOI: 10.1109/59.476050.

[74] V. V. Terzija, A. Derviskadic, Y. Zuo, G. Frigo, and M. Paolone, "Under Frequency Load Shedding based on PMU Estimates of Frequency and ROCOF," *Proceedings - 2018 IEEE PES Innovative Smart Grid Technologies Conference Europe, ISGT-Europe 2018*, vol. 21, no. 3, pp. 1260–1266, 2018, ISSN: 08858950. DOI: 10.1109/ISGTEurope.2018.8571481. arXiv: arXiv:1805.00744v1.

[75] C. P. Reddy, S. Chakrabarti, and S. C. Srivastava, "A sensitivity-based method for under-frequency load-shedding," *IEEE Transactions on Power Systems*, vol. 29, no. 2, pp. 984–985, 2014, ISSN: 08858950. DOI: 10.1109/TPWRS.2013.2288005.

[76] A. Derviskadic, Y. Zuo, G. Frigo, and M. Paolone, "Under Frequency Load Shedding based on PMU Estimates of Frequency and ROCOF," *Proceedings - 2018 IEEE PES Innovative Smart Grid Technologies Conference Europe, ISGT-Europe 2018*, pp. 1–6, 2018. DOI: 10.1109/ISGTEurope.2018.8571481. arXiv: arXiv:1805.00744v1.

[77] J. S. Thorp, M. Ilic-Spong, and M. Varghese, "An optimal secondary voltage-VAR control technique," *Automatica*, vol. 22, no. 2, pp. 217–221, 1986, ISSN: 00051098. DOI: 10.1016/0005-1098(86)90083-X.

[78] T. Gomez, A. Conejo, J. la Fuente, F. Pagola, and C. Rehn, "Decentralized secondary voltage control and pilot bus selection," *IFAC Symposia Series*, no. 9, 1992, ISSN: 09629505. DOI: 10.1016/S1474-6670(17)50473-5.

[79] A. Conejo, "COMPARISON OF ALTERNATIVE ALGORITHMS TO SELECT PILOT BUSES FOR SECONDARY VOLTAGE CONTROL IN ELECTRIC POWER NETWORKS," *Methods*, pp. 1–4, 1994.

[80] P. O. Gatta, J. A. Filho, and J. L. Pereira, "Comparison among methodologies for identification of pilot buses and its impact on the steady state secondary voltage control," *2014 11th IEEE/IAS International Conference on Industry Applications, IEEE INDUSCON 2014 - Electronic Proceedings*, 2014. DOI: 10.1109/INDUSCON.2014.7059434.

[81] F. Milano, *Power system modelling and scripting*. 2010, vol. 54, pp. 1–550, ISBN: 9783642136689. DOI: 10.1007/978-3-642-13669-6. arXiv: arXiv:1011.1669v3.

[82] P. W. Sauer, M. A. Pai, and J. H. Chow, *Power System Dynamics and Stability: With Synchrophasor Measurement and Power System Toolbox 2e*. 2017, ISBN: 9781119355793. DOI: 10.1002/9781119355755.

[83] R. Tomovic and M. Vukobratovic, "General sensitivity theory," 1972.

[84] P. M. Frank and M Eslami, "Introduction to system sensitivity theory," *IEEE Transactions on Systems, Man, and Cybernetics*, vol. 10, no. 6, pp. 337–338, 1980, ISSN: 0018-9472.

[85] I. A. Hiskens, "Trajectory sensitivity analysis of discontinuous differential-algebraic systems," *Department of Electrical and Computer Engineering, The University of Newcastle, Tech. Rep. EE9717*, 1997.

[86] I. A. Hiskens and M. A. Pai, "Sensitivity analysis of power system trajectories: Recent results," in *ISCAS'98. Proceedings of the 1998 IEEE International Symposium on Circuits and Systems (Cat. No. 98CH36187)*, vol. 3, IEEE, 1998, pp. 439–443, ISBN: 0780344553.

[87] H. K. Khalil, "Nonlinear systems," *Upper Saddle River*, 2002.

[88] M. J. Laufenberg and M. A. Pai, "A new approach to dynamic security assessment using trajectory sensitivities," in *Proceedings of the 20th International Conference on Power Industry Computer Applications*, IEEE, 1997, pp. 272–277, ISBN: 0780337131.

[89] J. H. Chow and K. W. Cheung, "A Toolbox for Power System Dynamics and Control Engineering Education and Research," *IEEE Transactions on Power Systems*, vol. 7, no. 4, pp. 1559–1564, 1992, ISSN: 15580679. DOI: 10.1109/59.207380.

[90] X. Zhao, D. M. Laverty, A. McKernan, D. J. Morrow, K. McLaughlin, and S. Sezer, "GPS-Disciplined Analog-to-Digital Converter for Phasor Measurement Applications," *IEEE Transactions on Instrumentation and Measurement*, vol. 66, no. 9, pp. 2349–2357, 2017, ISSN: 00189456. DOI: 10.1109/TIM.2017.2700158.

[91] W. J. Kim, S. R. Nam, and S. H. Kang, "Adaptive phasor estimation algorithm based on a least squares method," *Energies*, vol. 12, no. 7, 2019, ISSN: 19961073. DOI: 10.3390/en12071387.

[92] M. Gupta, R. Ganesan, and S. R. Bhide, "Comparative study of synchrophasor estimation algorithms under dynamic conditions for on-line transmission line parameter estimation," *2016 IEEE 6th International Conference on Power Systems, ICPS 2016*, pp. 1–6, 2016. DOI: 10.1109/ICPES.2016.7584109.

[93] D. L. Mills, "Internet Time Synchronization: The Network Time Protocol," *IEEE Transactions on Communications*, vol. 39, no. 10, pp. 1482–1493, 1991, ISSN: 00906778. DOI: 10.1109/26.103043.

[94] T. Committee, *IEEE Std 1588-2008, IEEE Standard for a Precision Clock Synchronization Protocol for Networked Measurement and Control Systems*, July. 2008, vol. 2008, pp. c1 –269, ISBN: 9780738154008. DOI: 10.1109/IEEESTD.2008.4579760.

[95] T. G. R. C. Council, "TELEMETRY GROUP TELEMETRY STANDARDS IRIG STANDARD 106-04 Part I," 2004.

[96] B. Hofmann-Wellenhof, H. Lichtenegger, and E. Wasle, *GNSS – Global Navigation Satellite Systems GPS, GLONASS, Galileo, and more*. SpringerWienNewYork, 2008, ISBN: 9783211730126. DOI: 10.1192/bjp.112.483.211-a.

[97] IEEE Power & Energy Society, *IEEE Standard for Synchrophasor Measurements for Power Systems IEEE Power & Energy Society*, December. 2011, ISBN: 9780738168111. DOI: 10.1109/IEEESTD.2011.6111219.

[98] P. Castello, C. Muscas, P. A. Pegoraro, and S. Sulis, "Active Phasor Data Concentrator performing adaptive management of latency," *Sustainable Energy, Grids and Networks*, vol. 16, pp. 270–277, 2018, ISSN: 23524677. DOI: 10.1016/j.segan.2018.09.004. [Online]. Available: https://doi.org/10.1016/j.segan.2018.09.004.

[99] IEEE Power and Energy Society, *IEEE Guide for Phasor Data Concentrator Requirements for Power System Protection, Control, andMonitoring*, May. 2013, pp. 1 –65, ISBN: 978-0-7381-8260-5. DOI: 10.1109/IEEESTD.2013.6514039.

[100] K. E. Martin, G. Benmouyal, M. G. Adamiak, M. Begovic, R. O. Burnett, K. R. Carr, A. Cobb, J. A. Kusters, S. H. Horowitz, G. R. Jensen, G. L. Michel, R. J. Murphy, A. G. Phadke, M. S. Sachdev, and J. S. Thorp, *IEEE standard for synchrophasors for power systems*, 1. 2005, vol. 13, pp. 73–77, ISBN: 0738148202. DOI: 10.1109/61.660853.

[101] I. Power and E. Society, *C37.118.1-2011 - IEEE Standard for Synchrophasor Measurements for Power Systems*, December. 2011, vol. 2011, p. 61, ISBN: 9780738168111. DOI: 10.1109/ieeestd.2011.6111219.

[102] K. E. Martin, A. R. Goldstein, M. G. Adamiak, G. Antonova, M. Begovic, G. Benmouyal, G. Brunello, B. Dickerson, Y. Hu, M. Jalali, H. Kirkham, M. Kezunovic, A. Kulshrestha, R. Midence, M. Patel, J. Murphy, K. Narendra, D. Ouellette, G. Stenbakken, V. Skendzic, E. Udren, and Z. Zhang, "Synchrophasor measurements under the IEEE standard C37.118.1-2011 with amendment C37.118.1a," *IEEE Transactions on Power Delivery*, vol. 30, no. 3, pp. 1514–1522, 2015, ISSN: 08858977. DOI: 10.1109/TPWRD.2015.2403591.

[103] K. E. Martin, D. Hamai, M. G. Adamiak, S. Anderson, M. Begovic, G. Benmouyal, G. Brunello, J. Burger, J. Y. Cai, B. Dickerson, V. Gharpure, B. Kennedy, D. Karlsson, A. G. Phadke, J. Salj, V. Skendzic, J. Sperr, Y. Song, C. Huntley, B. Kasztenny, and E. Price, "Exploring the IEEE standard C37.118-2005 synchrophasors for power systems," *IEEE Transactions on Power Delivery*, vol. 23, no. 4, pp. 1805–1811, 2008, ISSN: 08858977. DOI: 10.1109/TPWRD.2007.916092.

[104] C. I. Budeanu, "Reactive and fictitious powers," *Rumanian National Institute*, vol. 2, 1927.

[105] S. Svensson, "Power measurement techniques for non-sinusoidal conditions," *Philosophy*, vol. 21, p. 153, 1999, ISSN: 1346-718X.

[106] Power Systems Instrumentation and Measurements Committee, *IEEE Standard Definitions for the Measurement of Electric Power Quantities Under Sinusoidal, Nonsinusoidal, Balanced, or Unbalanced Conditions*. 2010, p. 50, ISBN: 9780738160580.

[107] A. Abur, "State Estimation Operating States of a Power System," 2014.

[108] P. Whittle, *Optimization over time*. John Wiley & Sons, Inc., 1982, ISBN: 0471101206.

[109] W. H. Kwon and S. H. Han, *Receding horizon control: model predictive control for state models*. Springer Science & Business Media, 2006, ISBN: 1846280176.

[110] S. Joe Qina and h. Badgwell, "A survey of industrial model predictive control technology," *Control Engineering Practice*, vol. 11, pp. 733–764, 2003.

[111] B. Marinescu, "Robust predictive control for the flexible coordinated secondary voltage control of large-scale power systems," *IEEE Transactions on Power Systems*, vol. 14, no. 4, pp. 1262–1268, 1999, ISSN: 08858950. DOI: 10.1109/59.801882.

[112] M. Glavic and T. V. Cutsem, "Some Reflections on Model Predictive Control of Transmission Voltages," *2006 38th North American Power Symposium*, pp. 625–632, 2006. DOI: 10.1109/NAPS.2006.359637.

[113] J. Licheng and R Kumar, "Coordinated dynamic voltage stabilization based on model predictive control," *Power Systems Conference and Exposition, 2009. PSCE '09. IEEE/PES*, pp. 1–8, 2009.

[114] M. N. Zeilinger, C. N. Jones, D. M. Raimondo, and M. Morari, "Real-time MPC - Stability through robust MPC design," *Proceedings of the IEEE Conference on Decision and Control*, pp. 3980–3986, 2009, ISSN: 01912216. DOI: 10.1109/CDC.2009.5400903.

[115] R. R. Negenborn, S Leirens, B De Schutter, and J Hellendoorn, "Supervisory nonlinear MPC for emergency voltage control using pattern search," *Control Eng. Pract.*, vol. 17, no. 7, pp. 841–848, 2009, ISSN: 09670661. DOI: 10.1016/j.conengprac.2009.02.003.

[116] A. G. Beccuti, T. H. Demiray, G. Andersson, and M. Morari, "A lagrangian decomposition algorithm for optimal emergency voltage control," *IEEE Transactions on Power Systems*, vol. 25, no. 4, pp. 1769–1779, 2010, ISSN: 08858950. DOI: 10.1109/TPWRS.2010.2043749.

[117] L. Jin, R. Kumar, and N. Elia, "Model predictive control-based real-time power system protection schemes," *IEEE Transactions on Power Systems*, vol. 25, no. 2, pp. 988–998, 2010, ISSN: 08858950. DOI: 10.1109/TPWRS.2009.2034748.

[118] M. Almassalkhi, "Optimization and Model-predictive Control for Overload Mitigation in Resilient Power Systems," *Thesis*, p. 157, 2013.

[119] B. Otomega, M. Glavic, and T. Van Cutsem, "A two-level emergency control scheme against power system voltage instability," *Control Engineering Practice*, vol. 30, pp. 93–104, 2014, ISSN: 09670661. DOI: 10.1016/j.conengprac.2013.10.007. [Online]. Available: http://dx.doi.org/10.1016/j.conengprac.2013.10.007.

[120] Fengda Xu, Qinglai Guo, H. Sun, Bin Wang, and Qiuwei Wu, "A secondary voltage control method for an AC/DC coupled transmission system based on model predictive control," *2015 IEEE Power & Energy Society General Meeting*, pp. 1–5, 2015. DOI: 10.1109/PESGM.2015.7286354. [Online]. Available: http://ieeexplore.ieee.org/document/7286354/.

[121] J. A. Martin and I. A. Hiskens, "A Model-Predictive Control Strategy for Alleviating Voltage Collapse," *IREP Symposium : X Bulk Power Systems Dynamics and Control Symposium*, pp. 1–15, 2017.

[122] A. Morattab, O. Akhrif, and M. Saad, "Decentralised coordinated secondary voltage control of multi-area power grids using model predictive control," *IET Generation, Transmission and Distribution*, vol. 11, no. 18, pp. 4546–4555, 2017, ISSN: 17518687. DOI: 10.1049/iet-gtd.2016.2054.

[123] H. Yassami, A. Rabiee, A. Jalilvand, and F. Bayat, "Model predictive control scheme for coordinated voltage control of power systems at the presence of volatile wind power generation," *IET Generation, Transmission and Distribution*, vol. 12, no. 8, pp. 1922–1928, 2018, ISSN: 17518687. DOI: 10.1049/iet-gtd.2017.1422.

[124] I. A. Hiskens and M. A. Pai, "Trajectory sensitivity analysis of hybrid systems," *IEEE Transactions on Circuits and Systems I: Fundamental Theory and Applications*, vol. 47, no. 2, pp. 204–220, 2000, ISSN: 10577122. DOI: 10.1109/81.828574.

[125] Y. Gong, A. Guzmán, and S. E. Laboratories, "Synchrophasor-based online modal analysis to mitigate power system interarea oscillation," *Analysis*, vol. 2, no. 1, pp. 1–6, 2008.

[126] B. Appasani and D. K. Mohanta, "A review on synchrophasor communication system: communication technologies, standards and applications," *Protection and Control of Modern Power Systems*, vol. 3, no. 1, 2018, ISSN: 23670983. DOI: 10.1186/s41601-018-0110-4.

[127] B. Naduvathuparambil, M. C. Valenti, and A. Feliachi, "Communication delays in wide area measurement systems," *Proceedings of the Annual Southeastern Symposium on System Theory*, vol. 2002-Janua, pp. 118–122, 2002. DOI: 10.1109/SSST.2002.1027017.

[128] S. Chakrabarti and E. Kyriakides, "Optimal placement of phasor measurement units for power system observability," *IEEE Transactions on Power Systems*, vol. 23, no. 3, pp. 1433–1440, 2008, ISSN: 08858950. DOI: 10.1109/TPWRS.2008.922621.

[129] Z. Jin, P. Dattaray, P. Wall, J. Yu, and V. Terzija, "A Screening Rule-Based Iterative Numerical Method for Observability Analysis," *IEEE Transactions on Power Systems*, vol. 32, no. 6, pp. 4188–4198, 2017, ISSN: 08858950. DOI: 10.1109/TPWRS..2660068.

[130] A. Pal, A. K. S. Vullikanti, and S. S. Ravi, "A PMU Placement Scheme Considering Realistic Costs and Modern Trends in Relaying," *IEEE Transactions on Power Systems*, vol. 32, no. 1, pp. 552–561, 2017, ISSN: 08858950. DOI: 10.1109/TPWRS.2016.2551320.

[131] Z. Miljanić, I. Djurović, and I. Vujošević, "Multiple channel PMU placement considering communication constraints," *Energy Systems*, vol. 4, no. 2, pp. 125–135, 2013, ISSN: 18683967. DOI: 10.1007/s12667-012-0069-6.

[132] M. Shahraeini, M. S. Ghazizadeh, and M. H. Javidi, "Co-optimal placement of measurement devices and their related communication infrastructure in wide area measurement systems," *IEEE Transactions on Smart Grid*, vol. 3, no. 2, pp. 684–691, 2012, ISSN: 19493053. DOI: 10.1109/TSG.2011.2178080.

[133] F. Haghighatdar Fesharaki, R. A. Hooshmand, and A. Khodabakhshian, "Simultaneous optimal design of measurement and communication infrastructures in hierarchical structured WAMS," *IEEE Transactions on Smart Grid*, vol. 5, no. 1, pp. 312–319, 2014, ISSN: 19493053. DOI: 10.1109/TSG.2013.2260185.

[134] M. B. Mohammadi, R. A. Hooshmand, and F. H. Fesharaki, "A new approach for optimal placement of PMUs and their required communication infrastructure in order to minimize the cost of the WAMS," *IEEE Transactions on Smart Grid*, vol. 7, no. 1, pp. 84–93, 2016, ISSN: 19493053. DOI: 10.1109/TSG.2015.2404855.

[135] B. Appasani and D. K. Mohanta, "Co-optimal placement of PMUs and their communication infrastructure for minimization of propagation delay in the WAMS," *IEEE Transactions on Industrial Informatics*, vol. 14, no. 5, pp. 2120–2132, 2018, ISSN: 15513203. DOI: 10.1109/TII.2018.2799659.

[136] N. Abbasy and H. Ismail, "A unified approach for the optimal PMU location," vol. 24, no. 2, pp. 1–1, 2009. DOI: 10.1109/pes.2009.5275803.

[137] J. J. Yu, A. Y. Lam, D. J. Hill, and V. O. Li, "A unified framework for wide area measurement system planning," *International Journal of Electrical Power and Energy Systems*, vol. 96, pp. 43–51, 2018, ISSN: 01420615. DOI: 10.1016/j.ijepes.2017.09.032. arXiv: arXiv:1711.07652v1.

[138] N. Fan and J. P. Watson, "On integer programming models for the multi-channel PMU placement problem and their solution," *Energy Systems*, vol. 6, no. 1, pp. 1–19, 2014, ISSN: 18683975. DOI: 10.1007/s12667-014-0132-6.

[139] O. Gomez, G. Anders, and M. A. Rios, "Reliability-based phasor measurement unit placement in power systems considering transmission line outages and channel limits," *IET Generation, Transmission & Distribution*, vol. 8, no. 1, pp. 121–130, 2014, ISSN: 1751-8687. DOI: 10.1049/iet-gtd.2013.0251. [Online]. Available: http://digital-library.theiet.org/content/journals/10.1049/iet-gtd.2013.0251.

[140] M. Mouwafi, R. A. El-Sehiemy, A. Abou El-Ela, and A. Kinawy, "Optimal placement of phasor measurement units with minimum availability of measuring channels in smart power systems," *Electric Power Systems Research*, vol. 141, pp. 421–431, 2016, ISSN: 03787796. DOI: 10.1016/j.epsr.2016.07.029. [Online]. Available: http://linkinghub.elsevier.com/retrieve/pii/S0378779616303091.

[141]   M. Esmaili, M. Ghamsari-Yazdel, and R. Sharifi, "Enhancing observability in MILP-based optimal joint allocation of PMU channels and conventional measurements with new security concepts," *Energy Systems*, pp. 1–29, 2018, ISSN: 1868-3967. DOI: 10.1007/s12667-018-0289-5. [Online]. Available: http://link.springer.com/10.1007/s12667-018-0289-5.

[142]   F. Aminifar, A. Khodaei, M. Fotuhi-Firuzabad, and M. Shahidehpour, "Contingency-constrained PMU placement in power networks," *IEEE Transactions on Power Systems*, vol. 25, no. 1, pp. 516–523, 2010, ISSN: 08858950. DOI: 10.1109/TPWRS.2009.2036470.

[143]   F. Aminifar, M. Fotuhi-Firuzabad, M. Shahidehpour, and A. Khodaei, "Observability enhancement by optimal PMU placement considering random power system outages," *Energy Systems*, vol. 2, no. 1, pp. 45–65, 2011, ISSN: 18683967. DOI: 10.1007/s12667-011-0025-x.

[144]   H. B. Püttgen, "Computational cycle time evaluation for steady state power flow calculations," *Rep. Thomson-CSF, Div. Simulateurs, School Elect. Eng., Georgia Inst. Technol.*, no. December, 1985.

[145]   Y. Wang, C. Wang, W. Li, J. Li, and F. Lin, "Reliability-based incremental PMU placement," *IEEE Transactions on Power Systems*, vol. 29, no. 6, pp. 2744–2752, 2014, ISSN: 08858950. DOI: 10.1109/TPWRS.2014.2310182.

[146]   F. Aminifar, M. Fotuhi-Firuzabad, M. Shahidehpour, and A. Khodaei, "Probabilistic multistage PMU placement in electric power systems," *IEEE Transactions on Power Delivery*, vol. 26, no. 2, pp. 841–849, 2011, ISSN: 08858977. DOI: 10.1109/TPWRD.2010.2090907.

[147]   D. Dua, S. Dambhare, R. K. Gajbhiye, and S. A. Soman, "Optimal multistage scheduling of PMU placement: An ILP approach," *IEEE Transactions on Power Delivery*, vol. 23, no. 4, pp. 1812–1820, 2008, ISSN: 08858977. DOI: 10.1109/TPWRD.2008.919046.

[148]   et al. Bills, G.W, "On-line Stability Analysis Study," Tech. Rep., 1970, pp. 1–20 –1–35.

[149]   R. J. Zimmerman, Ray Daniel and Murillo-S{\'a}nchez, Carlos Edmundo and Thomas, "MATPOWER: Steady-state operations, planning, and analysis tools for power systems research and education," *IEEE Transactions on power systems*, vol. 26, no. 1, pp. 12–19, 2010.

[150]   L. Mili, T. Baldwin, and R. Adapa, "Phasor measurement placement for voltage stability analysis of power systems," *29th IEEE Conference on Decision and Control*, no. December, 3033–3038 vol.6, 1990. DOI: 10.1109/CDC.1990.203341. [Online]. Available: http://ieeexplore.ieee.org/document/203341/.

[151]   P. Ye, B. Yao, and J. Song, "Coordinated secondary voltage control among zones based on grey prediction controllers," *Proceedings of the IEEE Power Engineering Society Transmission and Distribution Conference*, vol. 2005, pp. 1–4, 2005. DOI: 10.1109/TDC.2005.1546902.

[152]   C. Zhang, Y. Jia, and Z. Xu, "Optimal PMU placement for voltage control," *2016 IEEE International Conference on Smart Grid Communications, SmartGridComm 2016*, pp. 747–751, 2016. DOI: 10.1109/SmartGridComm.2016.7778851.

[153]   H. P. Hong, "An efficient point estimate method for probabilistic analysis," *Hong, H. P.*, vol. 59, no. 3, pp. 261–267, 1998, ISSN: 0951-8320. DOI: 10.1016/S0951-8320(97)00071-9.

[154]   C. B. Hsu YY, Ho KL, Liang CC, Lai TS, Chen KK, "Voltage control using a combined integer linear programming and rule-based approach," *IEEE transactions on power systems*, vol. 7, no. 2, pp. 744–752, 1992. DOI: 10.1109/59.141781.

[155]   L Ljung, "System Identification, Theory for the User, Information and System Science Series," *Englewood Cliffs*, 1987.

[156]   P. Stoica and T. Söderström, "On reparametrization of loss functions used in estimation and the invariance principle," *Signal processing*, vol. 17, no. 4, pp. 383–387, 1989, ISSN: 0165-1684.

[157]   . L. Ho and R. E. Kálmán, "Effective construction of linear state-variable models from input/output functions," *at-Automatisierungstechnik*, vol. 14, no. 1-12, pp. 545–548, 1966, ISSN: 2196-677X.

[158]   W. E. Larimore, "Canonical variate analysis in identification, filtering, and adaptive control," *Proceedings of the IEEE Conference on Decision and Control*, vol. 2, pp. 596–604, 1990, ISSN: 01912216.

[159]   P Van Overschee and B. De Moor, "Two subspace algorithms for the identification of combined deterministic-stochastic systems," in *Proceedings of the 31st IEEE Conference on Decision and Control*, IEEE, 1992, pp. 511–516, ISBN: 0780308727.

[160] P. Van Overschee and B. De Moor, "Subspace algorithms for the stochastic identification problem," *Automatica*, vol. 29, no. 3, pp. 649–660, 1993, ISSN: 0005-1098.

[161] ——, "N4SID: Subspace algorithms for the identification of combined deterministic-stochastic systems," *Automatica*, vol. 30, no. 1, pp. 75–93, 1994, ISSN: 00051098. DOI: 10.1016/0005-1098(94)90230-5.

[162] V Overchee and B. L. Moor, "Subspace identification for linear systems," *Dordrecht, Holanda: Kluwer Academic Publishers*, 1996.

[163] M. Verhaegen, "Application of a subspace model identification technique to identify LTI systems operating in closed-loop," *Automatica*, vol. 29, no. 4, pp. 1027–1040, 1993, ISSN: 00051098. DOI: 10.1016/0005-1098(93)90104-2.

[164] ——, "Identification of the deterministic part of MIMO state space models given in innovations form from input-output data," *Automatica*, vol. 30, no. 1, pp. 61–74, 1994, ISSN: 00051098. DOI: 10.1016/0005-1098(94)90229-1.

[165] M. Viberg, "Subspace-based methods for the identification of linear time-invariant systems," *Automatica*, vol. 31, no. 12, pp. 1835–1851, 1995, ISSN: 00051098. DOI: 10.1016/0005-1098(95)00107-5.

[166] J.-N. Juang, *Applied system identification*. Prentice-Hall, Inc., 1994, ISBN: 013079211X.

[167] J. J. Sanchez-Gasca, "Computation of power system low-order models from time domain simulations using a hankel matrix," *IEEE Transactions on Power Systems*, vol. 12, no. 4, pp. 1461–1467, 1997, ISSN: 08858950. DOI: 10.1109/59.627842.

[168] K. E. Bollinger and W. E. Norum, "Time series identification of interarea and local generator resonant modes," *IEEE Transactions on Power Systems*, vol. 10, no. 1, pp. 273–279, 1995, ISSN: 15580679. DOI: 10.1109/59.373950.

[169] I. Kamwa and L. Gérin-Lajoie, "State-space system identification-toward MIMO models for modal analysis and optimization of bulk power systems," *IEEE Transactions on Power Systems*, vol. 15, no. 1, pp. 326–335, 2000, ISSN: 08858950. DOI: 10.1109/59.852140.

[170] R. Eriksson and L. Soder, "Wide-area measurement system-based subspace identification for obtaining linear models to centrally coordinate controllable devices," *IEEE Transactions on Power Delivery*, vol. 26, no. 2, pp. 988–997, 2011, ISSN: 08858977. DOI: 10.1109/TPWRD.2010.2094628.

[171] S. Berhausen and S. Paszek, "Synchronous Generator Model Parameter Estimation Based on Noisy Dynamic Waveforms," *Journal of Electrical Engineering*, vol. 67, no. 1, pp. 21–28, 2016, ISSN: 13353632. DOI: 10.1515/jee-2016-0003.

[172] E. T. Hale and S. J. Qin, "Subspace model predictive control and a case study," *Proceedings of the 2002 American Control Conference IEEE Cat NoCH37301*, vol. 6, no. Ic, pp. 4758–4763, 2002, ISSN: 07431619. DOI: 10.1109/ACC.2002.1025411. [Online]. Available: http://dx.doi.org/10.1109/ACC.2002.1025411.

[173] IEEE Task Force, *Identification of Electromechanical Modes in Power Systems*, June 2012. 2012, pp. 1–282, ISBN: 9781479913039.

[174] N. Zhou, J. W. Pierre, and J. F. Hauer, "Initial results in power system identification from injected probing signals using a subspace method," *IEEE Transactions on Power Systems*, vol. 21, no. 3, pp. 1296–1302, 2006, ISSN: 08858950. DOI: 10.1109/TPWRS.2006.879292.

[175] P Van Overschee and B. De Moor, "Subspace algorithms for the stochastic identification problem," *Automatica*, vol. 29, no. 3, pp. 649–660, 1993, ISSN: 00051098. DOI: 10.1016/0005-1098(93)90061-W.

[176] V. A. Venikov, V. A. Stroev, V. I. Idelchick, and V. I. Tarasov, "Estimation of electrical power system steady-state stability in load flow calculations," *IEEE Transactions on Power Apparatus and Systems*, vol. 94, no. 3, pp. 1034–1041, 1975, ISSN: 00189510. DOI: 10.1109/T-PAS.1975.31937.

[177] A. Tiranuchit and R. J. Thomas, "A posturing strategy against voltage instabilities in electric power systems," *IEEE Transactions on Power Systems*, vol. 3, no. 1, pp. 87–93, 1988, ISSN: 15580679. DOI: 10.1109/59.43177.

[178] M. M. Begovic and G. Britain, *Power Systems*, 4. 1990, vol. 5, pp. 1529–1534, ISBN: 9783642136689. DOI: 10.1007/978-3-642-13669-6.

[179] V. A. Venikov, *Transient processes in electrical power systems*. Mir Publishers, 1977.

[180] S. Corsi and G. Taranto, "A Real-Time Voltage Instability Identification Algorithm Based on Local Phasor Measurements," *IEEE Transactions on Power Systems*, vol. 23, no. 3, pp. 1271–1279, 2008, ISSN: 0885-8950. DOI: 10.1109/TPWRS.2008.922586. [Online]. Available: http://ieeexplore.ieee.org/document/4512044/.

[181] M. Glavic and T. Van Cutsem, "Wide-area detection of voltage instability from synchronized phasor measurements. Part I: Principle," *IEEE Transactions on Power Systems*, vol. 24, no. 3, pp. 1408–1416, 2009, ISSN: 08858950. DOI: 10.1109/TPWRS.2009.2023271. arXiv: arXiv:1312.2598v2. [Online]. Available: http://ieeexplore.ieee.org/lpdocs/epic03/wrapper.htm?arnumber=6345154.

[182] M. Vaiman, M. Vaiman, S. Maslennikov, E. Litvinov, and X. Luo, "Calculation and Visualization of Power System Stability Margin Based on PMU Measurements Calculation and Visualization of Power System Stability Margin Based on PMU Measurements," no. November, pp. 1–6, 2010. DOI: 10.1109/SMARTGRID.2010.5622011.

[183] E. P. R. I. (EPRI), "Real-Time Applications of Phasor Measurement Units (PMU) For Visualization, Reactive Power Monitoring and Voltage Stability Protection," vol. 3, no. 3, pp. 58–62, 2010.

[184] F. Hu, K. Sun, A. Del Rosso, E. Farantatos, and N. Bhatt, "An adaptive three-bus power system equivalent for estimating voltage stability margin from synchronized phasor measurements," *IEEE Power and Energy Society General Meeting*, vol. 2014-Octob, no. October, 2014, ISSN: 19449933. DOI: 10.1109/PESGM.2014.6939177.

[185] ——, "Measurement-Based Real-Time Voltage Stability Monitoring for Load Areas," *IEEE Transactions on Power Systems*, vol. 31, no. 4, 2016, ISSN: 08858950. DOI: 10.1109/TPWRS.2015.2477080.

[186] T. Van Cutsem and C. D. Vournas, "Emergency voltage stability controls: An overview," *2007 IEEE Power Engineering Society General Meeting, PES*, pp. 1–10, 2007, ISSN: 1932-5517. DOI: 10.1109/PES.2007.386089.

[187] D. Lefebvre, S. Bernard, and T. Van Cutsem, "Undervoltage load shedding scheme for the Hydro-Québec system," in *IEEE Power Engineering Society General Meeting, 2004.*, IEEE, 2004, pp. 1619–1624, ISBN: 0780384652.

[188] R. Dhand, G. Lee, and G. Cole, "Communication Delay Modelling and its Impact on Real-Time Distributed Control Systems," *ADVCOMP 2010, The Fourth International ...*, no. c, pp. 39–46, 2010. [Online]. Available: http://www.thinkmind.org/index.php?view=article{\&}articleid=advcomp{_}2010{_}3{_}10{_}20046.

[189] Z. Huang, J. F. Hauer, and K. E. Martin, "Evaluation of PMU dynamic performance in both Lab environments and under field operating conditions," *2007 IEEE Power Engineering Society General Meeting, PES*, pp. 1–6, 2007. DOI: 10.1109/PES.2007.385992.

[190] P. V. Brogan, D. M. Laverty, X. Zhao, J. Hastings, D. J. Morrow, and L. Vanfretti, "Technique for pre-compliance testing of phasor measurement units," *International Journal of Electrical Power and Energy Systems*, vol. 99, no. December 2017, pp. 323–330, 2018, ISSN: 01420615. DOI: 10.1016/j.ijepes.2018.01.031. [Online]. Available: https://doi.org/10.1016/j.ijepes.2018.01.031.

[191] P. Romano and M. Paolone, "Enhanced interpolated-DFT for synchrophasor estimation in FPGAs: Theory, implementation, and validation of a PMU prototype," *IEEE Transactions on Instrumentation and Measurement*, vol. 63, no. 12, pp. 2824–2836, 2014, ISSN: 00189456. DOI: 10.1109/TIM.2014.2321463.

[192] A. G. Phadke and T. Bi, "Phasor measurement units, WAMS, and their applications in protection and control of power systems," *Journal of Modern Power Systems and Clean Energy*, vol. 6, no. 4, pp. 619–629, 2018, ISSN: 21965420. DOI: 10.1007/s40565-018-0423-3. [Online]. Available: https://doi.org/10.1007/s40565-018-0423-3.

[193] P. V. Brogan, R. J. Best, D. J. Morrow, K. McKinley, and M. L. Kubik, "Effect of BESS Response on Frequency and RoCoF During Underfrequency Transients," *IEEE Transactions on Power Systems*, vol. 34, no. 1, pp. 575–583, 2019, ISSN: 08858950. DOI: 10.1109/TPWRS.2018.2862147.

[194]   M. A. Donolo, V. A. Centeno, I. Power, E. Society, D. M. Laverty, L. Vanfretti, R. J. Best, D. J. Morrow, L. Nordstrom, M. Chenine, P. V. Brogan, I. Al Khatib, L. Vanfretti, D. J. Morrow, R. Khan, K. McLaughlin, D. M. Laverty, S. Sezer, X. Zhao, D. M. Laverty, A. McKernan, D. J. Morrow, K. McLaughlin, S. Sezer, P. V. Brogan, D. M. Laverty, X. Zhao, J. Hastings, D. J. Morrow, and L. Vanfretti, "The OpenPMU platform for open-source phasor measurements," *IEEE Transactions on Instrumentation and Measurement*, vol. 62, no. 4, pp. 701–709, 2017, ISSN: 00189456. DOI: 10.1109/TIM.2013.2240920.